KABUL POLYTECHNIC UNIVERSITY

INTERNATIONAL JOURNAL OF ENGINEERING & TECHNOLOGY

(KPU - iJET)

VOLUME 02 ISSUE 02 Dec. 2022

E - ISSN : 2790 - 0819
P - ISSN : 2790 - 0800

Picture: KPU Campus

VISIT US AT: KPU Campus, 5th District, Kabul City, Afghanistan.
www.kpu-ijet.af AND www.kpu-ijet.com

بسم الله الرحمن الرحيم

Kabul Polytechnic University
Vice-Chancellor in Academic Affairs

KPU International Journal of Engineering & Technology (KPU-iJET)

KPU Press, KPU Campus, 5th District, Kabul City, Afghanistan.

Chief Editor: Associate Prof. A. J. Niazi
Managing Director: Prof. A. Faqiri
Cover & Page Designer: Associate Prof. A. J. Niazi

Email Address: ijet@kpu.edu.af / kpuijet2@gmail.com
Website: www.kpu-ijet.af

Messages

Message from Editor in Chief

I am truly honored to announce the Volume 02, Issue 02 of the KPU-iJET. This is the first accredited International Journal by Ministry of Higher Education of Afghanistan. I am also very proud to be working with an outstanding team of KPU officials and members of the Editorial Board and reviewer's panel. This is a team that is fully engaged and committed to the success of this outstanding journal. In this new issue of the KPU-iJET has a new printed size that has been approved by MoHE regulations, that aims to becoming a standard publication.

KPU-iJET represents the work and research being conducted in all regions of the world, and at the same time also highlights key issues critical to Science & Technology not only in Afghanistan and developing countries but also in developed countries. KPU-iJET is an international platform for academicians, researchers across the globe to address the challenges related to science and technology. I want to encourage all those who are interested in being part of this energetic team to contact us, as we will welcome your contribution. We invite colleagues working with KPU-iJET.

As Editor-in-Chief, I wish to express my gratitude to all the authors of this publication for contributing of their research works. I would also like to thank Dr. H. Muzamel the Director of Research, Compilation & Translation Department of MoHE for their efforts to the growth of the journal. In addition, I would like to thank our Publication Department at KPU, and their devoted team, for their outstanding work. Thank you all once again for your amazing support and continued efforts aimed at development of the KPU-iJET.

In summary, we want our journal to be your primary source of information in science & technology. We also believe that this forum will move the imagination of intellectuals toward taking up more research for betterment of human life. I'm thankful to all the people who have worked very hard and made this volume possible.

Sincerely,

Associate Prof. A. J. Niazi, Ph.D.

Editor in Chief, KPU-iJET

Message from the Chancellor of KPU

Kabul Polytechnic University is proud of conducting and playing a significant role and brining positive impacts in all its three targeted areas of Teaching, Research and Social Development within Afghan Society despite of various turbulence, conflicts and problems in different period in this country.

I am Pleased to hear about the publishing of the second issue of second volume of Kabul Polytechnic University International Journal of Engineering & Technology (KPU-iJET). This achievement is indeed pride and honored which brings together academicians, scientists, and researchers from different walks of life on a single platform to present their innovative ideas and research findings concerning different spheres of engineering & technology.

With the dedicated efforts of the Editor-in-chief and other staff of KPU-iJET, I am certain that KPU-iJET will have great successes in their future initiative steps.

Regards,
Professor Abdul Rashid Iqbal
Chancellor of KPU

Message from the
Vice-Chancellor in Academic Affairs

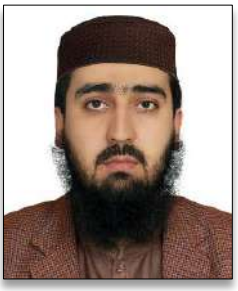

Academic interaction is one of the most efficient way within universities and educational institutions in order to accomplish their expectations of high standards. Universities in all over the globe are mandated to undertake the three main tasks Teaching, Research, and social services & development. Research and studies are brought about, and outcomes of the findings are presented with the world as a means of contributing to the bulk of knowledge.

Kabul Polytechnic University is also not an exclusion in the act of the above three mentioned goals where the International Journal of Engineering & Technology is one of its major initiatives which sees as an address for better interaction, collaboration and cooperation among researchers, professors, and professionals both locally and internationally, meanwhile it paved the way to present the result of researches finding with the world through this high-principled platform.

I would like to take this opportunity to applaud this achievement to the leadership of the KPU-iJET, and officials of KPU, right from the pioneer to the current and also to the Editorial team for their efforts reaching this level.

Regards,
Engineer Rohullah Rohani
KPU Vice-Chancellor in Academic Affairs

Members of Editorial Board and Reviewer's Panel

Editor in Chief

Ahmad Jawad NIAZI, Ph.D.
Associate Professor, Kabul Polytechnic University (KPU)

Managing Director

Amanullah Faqiri, Ph.D.
Professor, Kabul Polytechnic University (KPU)

No	*Name*	*Affiliation*
1	Hafizullah Wardak, Ph.D.	Former Professor at KU, Washington, USA
2	Sifatullah Bahij, Ph.D.	Assistant Professor, Kabul Polytechnic University (KPU)
3	Zakeria Shnizai, Ph.D.	Professor, Kabul Polytechnic University (KPU)
4	Zahra Nazari, Ph.D.	Professor, Kabul Polytechnic University (KPU)
5	Fatima Rezaye, Ph.D.	Professor, Kabul Polytechnic University (KPU)
6	Khojesta Kawish, Ph.D.	Professor, Herat University, Afghanistan.
7	Khadija Rahmani, Ph.D.	Professor, Herat University, Afghanistan.
8	Mohammad Assem Mayar, Ph.D.	Assistant Professor, Kabul Polytechnic University (KPU)
9	Aminullah Mahmood, Ph.D.	Former Professor at Kabul University (KU).
10	Ahmad Naqi, Ph.D.	Professor, Toyohahsi University of Technology (TUoT)
11	Mohammad Wali Salari, Ph.D.	Professor, Kabul University (KU)
12	Abdul Wasay Najimi, Ph.D.	Former Professor, Kabul University (KU)
13	Ghulam Hazrat Aimal Rasa, Ph.D.	Professor, Kabul Educational University (KEU)
14	Mohammad Hassan Mudaber, Ph.D.	Professor, Kabul Educational University (KEU)
15	Mujtaba Amin, Ph.D.	Professor, Kabul Polytechnic University (KPU)
16	Sekandar Zadran, Ph.D.	Professor, Kabul Polytechnic University (KPU)
17	Tawfiqullah Ayoubi, Ph.D.	Professor, Kabul Educational University (KEU)
18	Abdul Wasim Noori, Ph.D.	Assistant Professor, Kabul Polytechnic University (KPU)
19	Mohammad Nazir Nejabi, Ph.D.	Professor, Kabul Polytechnic University (KPU)
20	Abdulellah Rasooli, M.Sc.	Professor, Kabul Polytechnic University (KPU)
21	Saleh Mohammad Yari, M.Sc.	Professor, Kabul Polytechnic University (KPU)
22	Jan Aqa Satar, M.Sc.	Professor, Kabul Polytechnic University (KPU)
23	Mohammadullah Ebrahimi, M.Sc.	Professor, Kabul Polytechnic University (KPU)

24	Noor Ahmad Khalidi, Ph.D.	Researcher, Educator, Queensland, Australia
25	Muhammad Zeeshan Khan, M.Sc.	Islamiyah College University, Pakistan.
26	Qareeb Ullah Anwari, M.Sc.	Assist. Prof. Kardan University, NUST, Islamabad, Pakistan
27	Zekrullah kochai, Ph.D.	Researcher, Parul University (PU), Gujarat, India
28	Ahmad Javeed Faizi, M.Sc.	Researcher, Parul University (PU), Gujarat, India
29	Jami Osmanyar, M.Sc.	Assistant Professor, Kabul Polytechnic University (KPU)
30	Izatmand Halimzai, M.Sc.	Assistant Professor, Kabul Polytechnic University (KPU)

Disclaimer

The views expressed in the manuscript/text by the author(s) are their own and KPU-iJET, KPU or Editor or Publishers do not take any responsibility for the same.

In this issue, texts are copied from the soft copies provided by the author(s). hence printing errors/omissions if any are regretted.

Editorial Committee
KPU-iJET, 2023

Contents

KPU International Journal of Engineering & Technology
Volume 2, Issue2, Dec. 2022
e-ISSN:2790-0819, p-ISSN:2790-0800

Date Received: 2022-06-21
Date Accepted: 2022-12-21
Date Published: 2022-12-30

Improved Prediction Method of Lateral Girder Response of Footbridges Induced by Pedestrians

AHMAD SHOAIB KOHESTANI[1*], SHUNICHI NAKAMURA[2]

[1*]Assistant Professor, Dept. of Building Construction Management, Kabul Polytechnic University, KPU Campus, 5th District, Kabul, Afghanistan. E-mail: s.kohestani@kpu.edu.af

[2]Professor Emeritus, Tokai University, Kitakaname 1117, Hiratsuka, Japan 259-1292. E-mail: snakamu@tsc.u-tokai.ac.jp

Abstract

Besides having structural rationality and elegant feature, cable-supported bridges are flexible and often suffer from dynamic problems. On the T-bridge, a pedestrian cable-supported footbridge, the girder vibrated laterally with a frequency of 0.93 Hz, the natural frequency of first lateral mode, when a large number of pedestrians crossed the bridge. The zigzag movement of pedestrians caused the bridge girder to vibrate laterally. When the frequency of this dynamic force is close to the bridge's natural frequency, it makes a resonance which results in a big response. The same vibration occurred on the London Millennium Bridge. The response of the London Millennium Bridge was much larger than that of the T-bridge and the bridge was closed for 20 months until the vibration was suppressed by viscous and tuned mass dampers. Nakamura proposed a simplified model to predict girder responses by introducing non-linear pedestrian behaviors. When the vibration amplitude becomes large, some of the pedestrians feel unsafe and stop walking or change their walking pace. Therefore, the pedestrian-induced forces do not increase proportionally with deck vibration at the large girder amplitude. Nakamura's method includes this non-linear behavior but it assumes that this lateral vibration only occurs when the bridge's natural frequency is around 0.9-1.0Hz. In this paper, the improved method is proposed for the bridge's natural frequencies. However, the authors have found that lateral vibration could occur on the bridge with a frequency far less than 0.9Hz. The authors have proposed the new
The prediction method covers the resonant frequencies outside 0.9-1.0Hz and the new method is verified by comparing with the field-measured data.

Keywords: Lateral vibration, Cable-stayed bridge, Dynamic model, Resonance, Pedestrians

* Corresponding Author

1. Introduction

Although cable-supported bridges have structural rationality and elegant feature, they are flexible and often suffer from dynamic problems. The T-bridge (Figure.1), a pedestrian cable-stayed bridge located in Japan, suffered strong lateral vibration induced by pedestrians. The bridge connects the motor boat race stadium and the bus terminal. The girder vibrated laterally with a frequency of 0.93Hz, the natural frequency of the first lateral mode when a large number of people crossed the bridge after the final race was over (Figure.2). This type of lateral vibration had not been reported before and research was conducted to clarify the mechanism [1-7].

Figure 1: T-Bridge

Figure 1: Pedestrians after the final race

The mechanism of this vibration was studied by Fujino et al. [1] and Nakamura et al. [2,3,6] and clarified. The gravity center of the human body moves laterally while they walk to their left and right foot in turn, which makes the girder vibrate laterally with a frequency of about 1.0Hz, this is called lateral dynamic force which is induced by pedestrians. When the frequency of this dynamic force is close to the bridge's natural frequency, it makes a resonance which results in a further response. Even though many people walk at the same frequency, their phases would be different and the induced forces could cancel out. This phase problem was solved by assuming that people synchronize their walking pace to the vibrating deck. However, the girder response reached about 10 mm and some pedestrians felt uncomfortable and unsafe. But, this was not considered to be too large and the bridge was not closed.

The same vibration problem occurred on the London Millennium Bridge in 2000. The lateral response of the London Millennium Bridge was much larger than that of the T-bridge, and the bridge was closed for 20 months until the vibration was suppressed by viscous and tuned mass dampers [4]. To clarify the mechanism of the vibration, field tests on the bridge and experiments at Imperial College were carried out. Then, a dynamic model based on the single degree of the dynamic equation was proposed by Dallard et al. [4,5], assuming that the external force induced by pedestrians is proportional to the girder lateral velocity.

Nakamura proposed a simplified model to predict girder responses by introducing non-linear pedestrian behaviors [7]. When the vibration amplitude becomes large, some

of the pedestrians feel unsafe and stop walking or change their walking pace. Therefore, the pedestrian-induced forces do not increase proportionally with deck vibration at the large girder amplitude. Nakamura's method includes this non-linear behavior but it assumes that this lateral vibration only occurs when the bridge's natural frequency is around 0.9-1.0Hz. In this paper, the improved method is proposed for the bridge's natural frequencies. However, the authors have found that lateral vibration could occur on the bridge with a frequency far less than 0.9Hz. The authors have proposed a new prediction method to cover the resonant frequencies outside 0.9-1.0Hz and the new method is verified by comparing it with the field-measured data.

2. Dynamic Model for The Lateral Vibration

2.1.The layout of the T-Bridge

The layout of the T-bridge is shown in Fig.3. The T-bridge is a cable-stayed footbridge with a main span length of 134 m, a side span length of 45m, two cable planes, and 11 stays per plane (Fig.3) Semi-parallel type cables with epoxy resin surface layer are used. The girder is a steel box girder with an orthotropic deck. The web height is 1.8m and the walkway width is 5.26m (Fig.4).

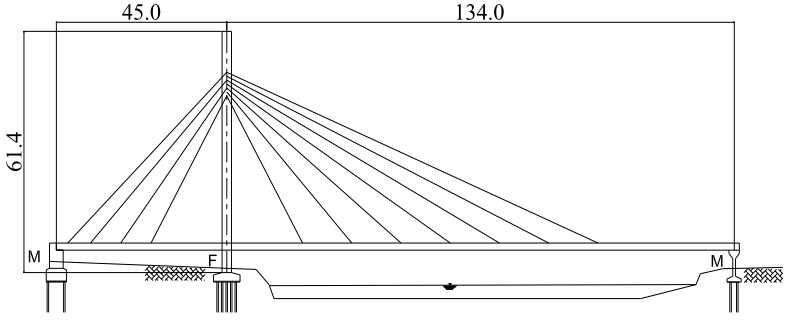

Fig.3 Layout of the bridge (m)

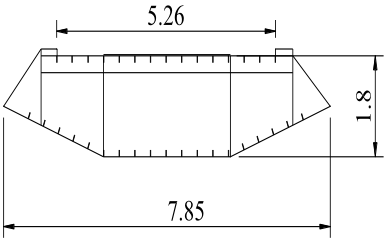

Fig.4 Girder cross-section (m)

$$M_B X''(t) + C_B X'(t) + K_B X(t) = Fp \quad \ldots\ldots\ldots\ldots\ldots\ldots (1)$$

$$Fp = k_1 k_2 H(X'_B) G(f_B) Mpg \quad \ldots\ldots\ldots\ldots\ldots\ldots\ldots\ldots (2)$$

$$H(X'_B) = \frac{X'_B(t)}{k_3 + |X'_B(t)|} \quad \ldots\ldots\ldots\ldots\ldots\ldots\ldots\ldots\ldots (3)$$

$$G(f_B) = \begin{cases} G_0 = 1 \quad \ldots\ldots\ldots\ldots\ldots\ldots\ldots\ldots\ldots\ldots (4) \\ G_1 = 1 - 20(f_B - 0.9)^4 \quad \ldots\ldots\ldots\ldots\ldots\ldots (5) \\ G_2 = 1 - 5(f_B - 0.9)^2 \quad \ldots\ldots\ldots\ldots\ldots\ldots (6) \end{cases}$$

The T-bridge connects the motor boat race stadium and the bus terminal. On a race day too many spectators entered the stadium through the bridge at a random time. When the final race was over, the spectators left the stadium and walked through the bridge to get to the bus terminal on the opposite side of the stadium. As the entrance areas to the

bridge were fairly large, the pedestrians could proceed on the bridge and were not forced to stop in this congested situation. At that time the bridge deck was overcrowded with pedestrians. In several minutes of this overcrowded situation, the girder and the cables started to vibrate. [2,3,6]

The field measurements were carried out on the T-bridge to find the mechanism of this vibration by Fujino et al. [1] and Nakamura et al. [2,3,6]. Accelerometers were attached to the girder and cables in vertical and lateral directions. By analyzing the obtained data, it was found that the girder vibrated laterally. It was also found that the zigzag movement of pedestrians was the exiting force and the synchronization of the pedestrian to the girder vibration was the phase problem.

Nakamura proposed the following method to predict the girder response induced by pedestrians [7]. The dynamic model for the lateral vibration can be modeled by a single-degree-of-freedom system. Eq. (1) shows the dynamic equation of motion; X_B is the modal displacement of the girder, X'_B the modal velocity of the girder, X''_B the modal acceleration of the girder, M_B is the modal mass, C_B is the modal damping coefficient and K_B the modal stiffness of the bridge.

The external force induced by pedestrians is key in this dynamic equation. Dallard et al. proposed that the dynamic force induced by a pedestrian is proportional to the girder velocity [4,5]. Based on the field test conducted on the Millennium Bridge, the coefficient is proposed to be 300 N.s/m. According to the Dallard method, if the lateral force FP is larger than the damping force CBX', there is no upper limit for the girder response and it increases linearly. This does not seem correct because some pedestrians feel unsafe and hold handrails or stop walking when the vibration amplitude becomes large. Therefore, the exciting force must saturate at a certain level. The right side of Eq. (1) is the external force induced by pedestrians. Nakamura assumed that the pedestrian force is proportional to the modal self-weight of pedestrians, Mpg, multiplied by two coefficients, k1 and k2, and two functions, H (X'B) and G (fB), as shown in Eq.(2). The coefficient k1 is the ratio of the lateral force to the pedestrian`s weight and is assumed to be 0.0987 in this study. The coefficient k2 is the percentage of pedestrians who synchronized to the girder vibration and is assumed to be 0.2.

H (X'B) is a function to describe the pedestrian' synchronization nature. It is assumed that the pedestrians synchronize proportionally with the girder velocity X'_B at low velocities. When the girder velocity becomes large, the pedestrians feel uncomfortable or unsafe and they decrease their walking paces. Therefore, the girder response does not increase infinitely but is limited at a certain level. The denominator of Eq.(3) expresses this saturation phenomenon. The saturation rate depends on coefficient k3[8]. The pedestrian forces proposed by Dallard and Nakamura are shown in Fig.5. The one by the Dallard method is linear and no upper limit exists. Whereas, the one by the Nakamura method is linear only in the small girder velocity range and saturates at a certain level. This seems more appropriate to explain the pedestrian's walking attitude on the vibrating deck.

G (fB) is the function to describe how pedestrians synchronized with the girder response. It was originally thought that the lateral vibration only occurred at the bridge frequency of 0.8-1.0 Hz and, therefore, the value of G (fB) was assumed to be 1.0, as

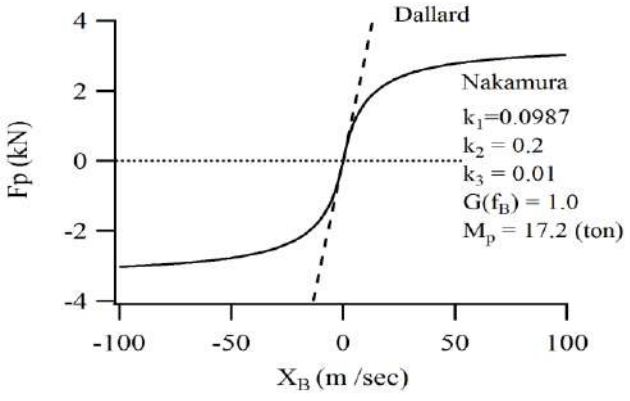

Fig.5 Lateral force induced by pedestrians

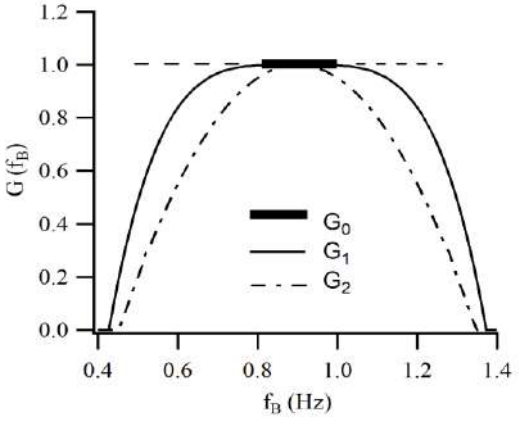

Fig.6 G-function

shown in Eq.(4). This is shown as G_0 in Fig.6. However, the authors have recently found on another bridge that the lateral vibration could occur with the bridge natural frequency outside this range.

The authors have proposed the two improved G (fB) functions, as shown as G1 and G2 in Eq. (5) and Eq. (6). Both functions have peaks at 0.9 Hz and Eq. (6) have a sharper shape. These three G-functions are shown in Fig.5. In this study the effect of these new G-functions is compared and studied.

Field measurements were conducted in 1989 and two data were used in this study: Data T1 with a pedestrian density of 0.8 person/m2 and data T2 with a pedestrian density of 0.6 person/m2. Fig.7 and Fig.8 show the girder lateral displacements of these two cases. Both show clear sinusoidal waves with a natural frequency of 0.93 Hz. This indicates that resonance occurred between the pedestrians and the girder in both cases. The maximum amplitude of T1 is 13.1mm and that of T2 is 8.4mm. These differences are caused by the number of pedestrians, in other words, the pedestrian density. In the T1 data, the bridge was more overcrowded than in the T2.

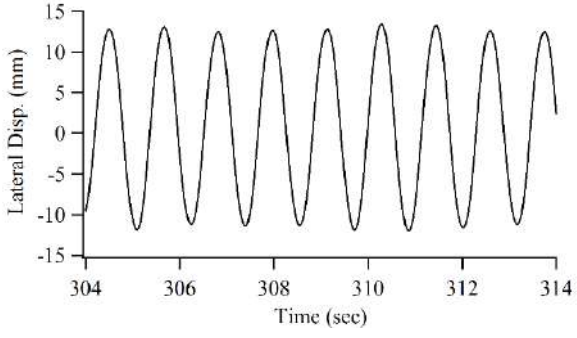

Fig.7 Measured girder displacement (T_1)

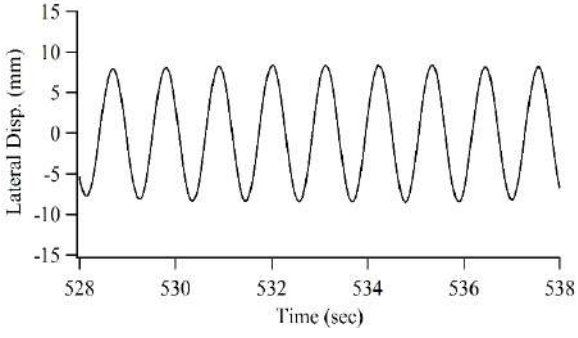

Fig.8 Measured girder displacement (T_2)

The eigenvalue analysis was conducted by FEM. The natural frequency of the first lateral mode of the T-bridge fB is 0.93Hz, which is the same as the measured natural

frequency of T1 and T2. It is therefore clear that resonance occurred in the first lateral mode. The mode shape is shown in Fig.9. The modal mass MB is 185.2 tons.

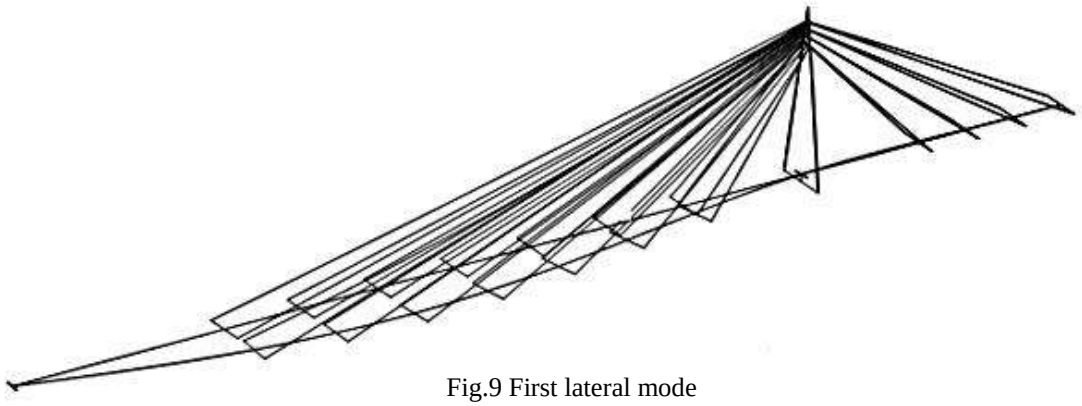

Fig.9 First lateral mode

3. Parametric Studies

The dynamic responses of the girder were obtained for T1 and T2 data by the proposed dynamic model. Eqs. (1)-(6) were solved numerically by Runga-Kutta method [2,3,6,7]. Parametric studies were conducted to clarify the effects of pedestrian density, girder mass, and bridge natural frequencies on the girder responses.

Fig.10 shows the girder response with different pedestrian densities. In this calculation girder, modal mass is kept at 185.2 tons, and the girder's natural frequency of 0.93Hz. The girder response increases with pedestrian density. This tendency is easily understood: the vibration amplitude of the girder becomes larger as more people walk on the bridge. The measured data, T1 and T2, are also shown in this figure and agree with the calculated values, which validate the proposed method.

Fig.11 shows the girder response with different girder masses. In this calculation, pedestrian density is kept at 0.8 person/m2 and the girder natural frequency of 0.93Hz. The girder response decreases with girder mass, showing that the lighter girder has more likely to have a vibration problem. The measured data T1 is also shown in this figure.11, corresponding to the calculated value.

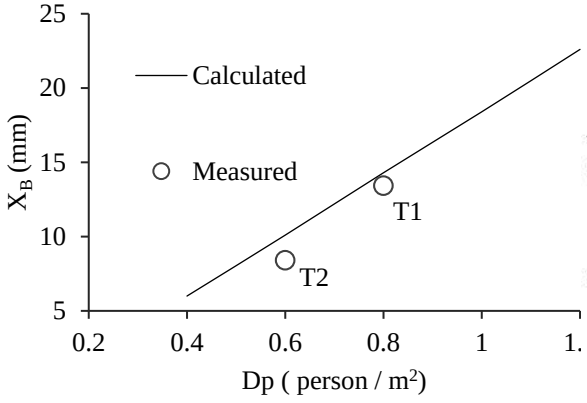

Fig.10 Effect of density of pedestrian

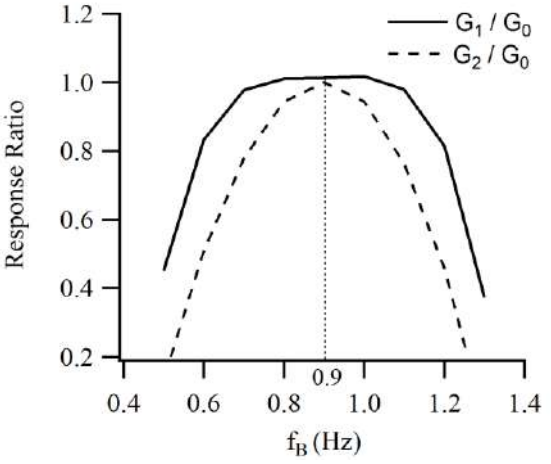

Fig.12 Response ratio due to G_1 and G_2

Fig.12 shows the girder response ratio; the response is calculated by G_1-function over that by G_0-function. The response ratio calculated by G_2-function over that by G_0-function is also shown in this figure. Both response ratios have a peak at 0.9Hz and they decrease as the bridge's natural frequency becomes further away from 0.9Hz. This decreasing ratio with G_2-function is sharper than that with G_2-function.

The improved method with G_1-function and G_2-function is useful to Fig.11 shows the girder response ratio; the response calculated by G_1-function over that by G_0-function. The response ratio calculated by G_2-function over that by G_0-function is also shown in this figure. Both response ratios have a peak at 0.9Hz and they decrease as the bridge's natural frequency becomes further away from 0.9Hz. This decreasing ratio with the G_2 function is sharper than that with predicted responses when the bridge's natural frequency is away from the usual resonant frequency of about 0.9Hz. However, further study is necessary to decide which is more suitable for practical bridges.

4. Conclusions

The lateral vibration problem induced by the pedestrian was first observed on the T-bridge and it has then been widely known in the world. This is mainly because many footbridges suffer from this type of vibration. After all, footbridges have become lighter and more flexible. The mechanism of this vibration has almost been clarified but the prediction method and the design criteria have not been established yet.

Nakamura proposed a simple method to predict the response induced by pedestrians which seems useful for practical bridge designers and engineers. One of his assumptions is that this problem only occurs for bridges with a natural frequency of about 0.9Hz (0.8-1.0Hz). However, this vibration has been observed with a natural frequency outside of this range.

This paper has proposed an improved method to cover a wide range of bridge natural frequencies by introducing the distribution function, G_1-function, and G_2 function. The

predicted girder responses generally agree with the measured values obtained on the T-bridge. Parametric studies were conducted with the proposed method. The girder response increases with pedestrian density. The girder response decreases with girder mass, showing that the lighter girder has more likely to have a vibration problem.

The girder response ratio has a peak at 0.9Hz, and it decreases as the bridge's natural frequency becomes further away from this peak frequency. This decreasing ratio with G_2-function is sharper than that with G_1-function. The improved method with G_1 and G_2 functions is useful to predict responses when the bridge's natural frequency is away from the usual resonant frequency of about 0.9Hz. However, further study is necessary to decide which is more suitable for actual bridges.

5. Acknowledgements

The first author would like to thank JICA for providing him the opportunity to study at Tokai University through the PECE program.

6. Abbreviations

X_B:	**modal displacement**
X'_B:	modal velocity
X''_B:	modal acceleration:
M_B:	modal mass
C_B:	modal damping coefficient
K_B:	modal stiffness
$M_p g$:	modal self-weight of pedestrians
F_P:	the lateral force of pedestrians
F_b:	natural frequency of the first lateral mode of the bridge
K_1:	ratio of the lateral force to the pedestrian`s weight
K_2:	percentage of synchronized pedestrians
K_3:	Saturation rate

7. References

[1] Fujino Y, Pacheco B, Nakamura S, Warnitcahi P. Synchronization of human walking observed during lateral vibration of a congested pedestrian bridge. Earthquake Engineering and Structural Dynamics 1993;22:741–58.

[2] Nakamura S, Fujino Y. Lateral vibration on a pedestrian cable-stayed bridge. Structural Engineering International, IABSE 2002;12(4):295–300.

[3] Nakamura S, Kawasaki T. Lateral vibration of footbridges by synchronous walking. Journal of Constructional Steel Research, Elsevier 2006;62(11): 1148–60.

[4] Dallard P, Fitzpatrick A, Flint A, Le Bourva S, Low A, Smith R. The London Millennium Footbridge. The Structural Engineer 2001;79(22):17–35.

[5] Dallard P, Fitzpatrick A, Flint A, Low A, Smith R, Willford M. London Millennium Footbridge, pedestrian induced lateral vibration. Journal of Bridge Engineering, ASCE 2001;6(6):17–35.

[6] Nakamura S. Field measurements of lateral vibration on a pedestrian suspension bridge. The Structural Engineering 2003;81(22):22–6.

[7] Nakamura S. Dynamic model for lateral vibration. Journal of Structural Engineering, ASCE 2004;130(1):32–7.

[8] Nakamura S, Kawasaki T. Lateral vibration of footbridges by synchronous walking.Journal of Construction Steel Research, Elsevier 2006;62(11):1148-60.

Authors Profile:

Ahmad Shoaib Kohestani received his B.Sc. degree in Civil and Industrial Construction from Kabul Polytechnic University in 2009 and M.Sc. degree in Civil Engineering from Tokai University, Japan in 2015.Started work with Care International Organization in 2009 for two years, then worked in City and Implementation Directorate of Kabul Municipality till late 2015. Presently he is working as assistant professor in the Department of Building Construction Management, Faculty of Construction of Kabul Polytechnic University, Kabul Afghanistan. His research interest is seismic evaluation of RC structures.

Shunichi Nakamura received his B.Eng. and M.Eng. From Kyoto University, and PhD. from Imperial College London. He worked for Nippon Steel Corporation as a bridge engineer for 21 years, and was involved in design and construction of many bridges including the Tokyo Aqua-line Bridge and the Akashi Kaikyo Bridge Cable Work. He then moved to Tokai University, where he taught and studied Bridge and Structural Engineering for 25 years. He supervised seven Afghan students in the master course. He is now the vice president of IABSE (International Association of Bridge and Structural Engineering). He was conferred the best paper awards from JSCE, IABSE and Institution of Structural Engineers.

KPU International Journal of Engineering & Technology
Volume 2, Issue2, Dec. 2022
e-ISSN:2790-0819, p-ISSN:2790-0800
Date Received: 2022-07-12
Date Accepted: 2022-12-25
Date Published: 2022-12-30

Groundwater Prospective Zones and Precise Location Using Integrated Geological, Geomorphological, and Geophysical Methods in Sholgara District, Balkh Province

ZAKERIA SHNIZAI[1], ABDUL RASHID IQBAL[2*], MOHAMMAD WALID OMID[3]

[1]Associate Professor, Department of Oil and Gas Mines Engineering, Kabul Polytechnic University, KPU campus, 5th district, Kabul Afghanistan. Email: z.shnizai@kpu.edu.af

[2*]Professor, Department of Oil and Gas Mines Engineering, Kabul Polytechnic University, KPU campus, 5th district, Kabul Afghanistan. Email: rashidiqbal55@kpu.edu.af

[3]Assistant Professor, Department of Oil and Gas Mines Engineering, Kabul Polytechnic University, KPU campus, 5th district, Kabul Afghanistan. Email: walid.omid99@kpu.edu.af

Abstract

All over the world, studies of groundwater reserves are highly important. One of the best ways to identify groundwater reservoirs without negative impacts on the environment is to study geology and geomorphology based on remote sensing data and geophysical methods. The main purpose of this paper is to delineate the groundwater prospective zones and to determine the relative depth and thickness of layers that accumulate groundwater. The groundwater reservoir depends on several factors such as geology, geomorphology, land use, slope, and physical properties. Thus, the mapping and groundwater potential zones were identified in Sholgara District, and then geophysical methods were used in Qazel Kand village to find the water table depth and location. Exploration geophysical methods, especially electric, are one of the most important ways to study and solve the problems of drinking water in the study area Based on the VES investigations, at least five layers were identified with different lithology. The top three layers consist of clay, sand, and gravel, which are mostly dry. These rocks do not have many water resources but could recharge the aquifer, particularly in the wet season. The field data also show that water table depth ranges between 80 to 100 m with limestone and marl formations that mostly belong to Neogene. These are carbonate rocks having secondary porosity in the form of fractures and wreathing. The formations formed a karst aquifer to a maximum of 130 depths. The water in this aquifer seems fresh and suitable for drinking.

Keywords: Groundwater Prospective Zones, Remote Sensing and Geophysical Methods, Balkh Province.

* Corresponding Author

1. Introduction

In nature, water resources are divided into two parts: surface and underground. From a groundwater point of view, the earth's crust is divided into water-saturated and unsaturated zones. The water which has taken place in the porous media and voids of the upper layers of the crust is called underground water. All around the world, groundwater studies play a vital role in human beings. Therefore, groundwater investigations and management are getting increased day by day all around the world. One of the very important investigation methods is the integrated geological, geomorphological, and geophysical methods which do not affect badly on the environment. Using Remote Sensing together with geological, geomorphological, and geophysical methods is an easy and effective way to delineate groundwater zones and solve the drinking water problem in the study area. Using geophysical methods, we can measure the physical properties of underground rocks. Then we acquire important information using geophysical methods that we cannot sample or measure directly. Geological, geomorphological, and geophysical investigations are amongst the best tools for understanding the landform and physical context of the earth's surface.

The under-research area is located in the Sholgara district southern part of Balkh Province – Afghanistan. Currently, in Sholgara including the study area, there is a depletion of the river and groundwater storage and an increase in concern of overdraft of groundwater due to over-abstraction, drought, low recharge, and high evaporation. The groundwater quality has progressively deteriorated with water hardness, salinity, nitrate and boron concentrations, etc., which become a real threat to the health of inhabitants and agricultural activities [1] .

The research method of this work is based on valid theoretical bases and practical experiences. Primary data for this research paper includes the geologic map, initial field data, and satellite imagery. A geological map was used to study the geology of the area in detail. Remote sensing and geographic information systems (GIS) are used to prepare geomorphological information and thematic maps from various satellite imageries. For the geomorphological study, different satellite images were used. The initial geophysical field data was collected during fieldwork by Danish Committee for Aid to Afghan Refugees (DACAAR) in 2013, includes of Vertical Electrical Sounding (VES). These methods are used to study, map and assess groundwater in Qazel Kand village, Sholgara District [2]

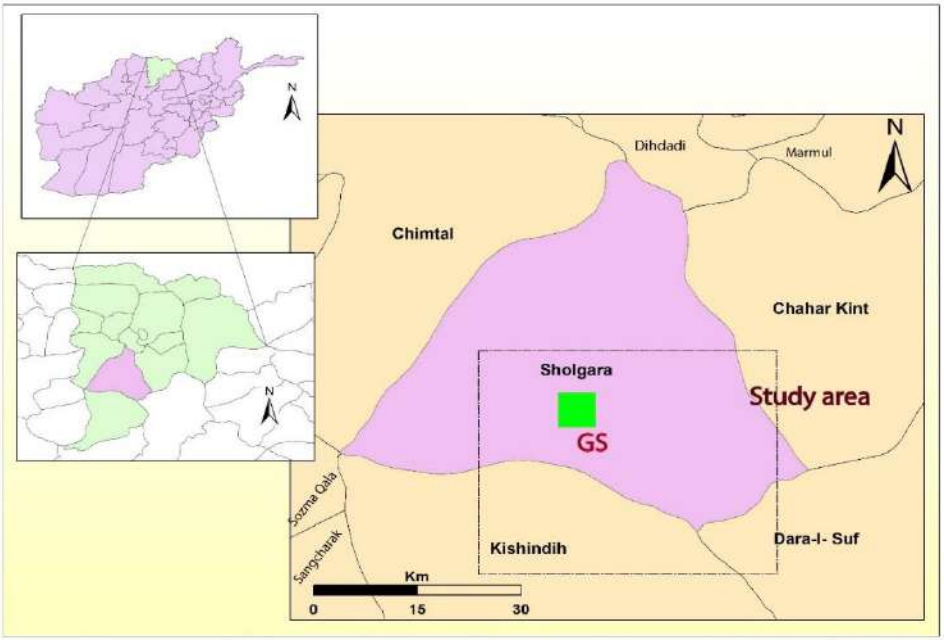

Figure 1: Location of the Sholgara District situated in the southern part of Balkh Province in Afghanistan. Hallow square with a black dash-line shows the location of the study area. Green-filled square with GS indicates the location of the geophysical survey shown in figure 8.

The main concern of this study is: How to extract and evaluate geomorphological features such as slope, elevation, and drainage from remotely sensed data? What is the geology of the study area? Which geologic formations are located there? How to delineate groundwater potential zones? Can the location of drinking water be determined in the area to some extent? Is it possible to determine the position and thickness of aquifers using electrical methods? Hence, the overall goal of this paper is to interpret thematic maps and the graphs of the electrical method (VES) to determine the potential zones of groundwater, to study the geology and geomorphology of the area, and to find the boundary and depth of an aquifer as well as the water table in Sholgara District and specifically in the Qazel Kand Village.

2. Regional Setting of the Study Area

2.1. Geology of the study area and northern part of Afghanistan

Based on geophysics and borehole records in northern Afghanistan, shows clear boundaries between the associated layers. The pre-Palaeozoic, Palaeozoic, Mesozoic, and Cainozoic rocks form the geological structure of the platform. Northern Afghanistan has a Pre-Jurassic basement unconformably overlain by Jurassic and Paleogene sediments, which in turn overlain by Neogene and post-orogenic continental clasts [3] Relatively undeformed mostly clastic Jurassic to recent sediments overlay deformed Triassic and older age rocks. Also, the geophysical researches show a gradual passage into the Murghab and Tajik Basin, which is filled with dominantly clastic Mesozoic-Quaternary sediments [4]. In general, the platform formed a single Mesozoic to Paleogene

sedimentary basin, which existed until Neogene time [5,6]. According to [6,7] the Amu Darya and Afghan-Tajik Basins' Pre-Neogene history and stratigraphy consist of (1) Paleozoic to Triassic basement complex, (2) Jurassic to Paleogene sedimentary cover, and (3) Neogene to Holocene orogenic clastic. Neogene to Holocene orogenic clastic were deposited in Oligocene time as a result of tectonic deformation due to the Indian and Eurasian tectonic plates [5,6,7]

However, the geology of northern Afghanistan is studied particularly in the west and very limited research works have been done due to the unstable political situation in the country. Mostly Russian researchers worked and prepared maps of the study area. They mapped northern Afghanistan at a 1:500,000 scale [3,8,9,10,11,12] summarized the geology and tectonics of the area.

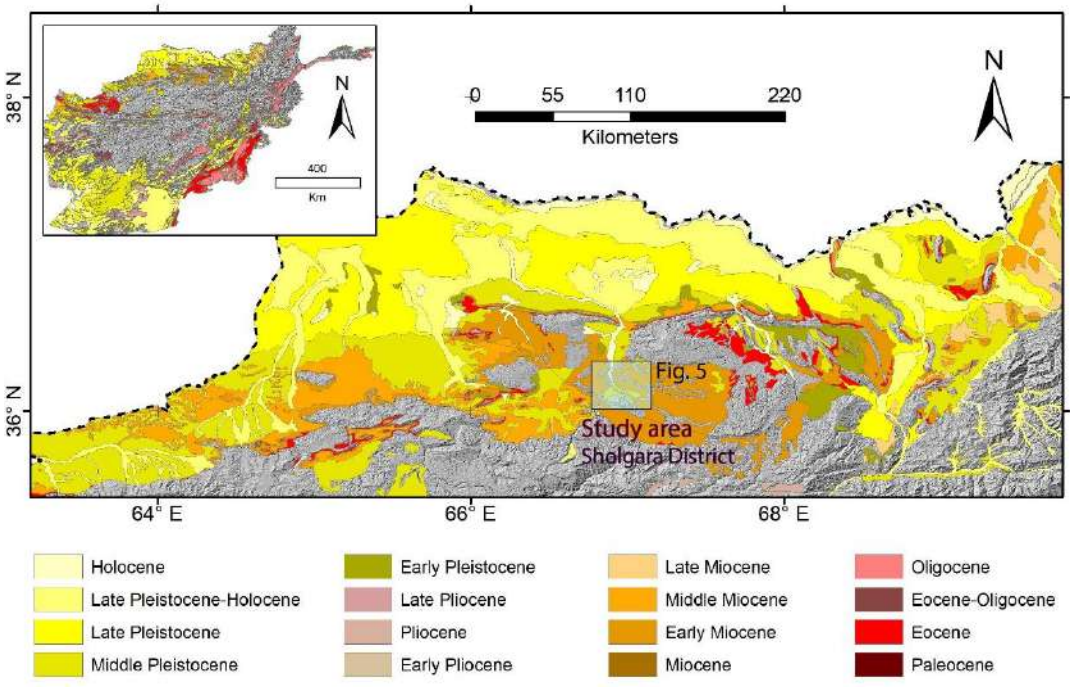

Figure 2: Geological map (Cainozoic) of northern Afghanistan. The map is modified from [13]

The lithology of the northern part of Afghanistan has similar sediments the same as the neighboring regions of Central Asian Countries (the southwestern area of the mount Hesar and Bukhara oil and gas fields). The lithology of the northern Afghan platform usually consists of bitumen graphite, tuff-andesite, sandstone, sand, conglomerates, calcite, dolomite, dense limestone, salt, anhydrite, gypsum, argillite with the remnants of coal, mud, and others . The formation of the underground geology of the study area is as follows: Quaternary sediments: sand, gravel, mud, and loess that have been deformed by climate. Medium quaternary sediments: sand, gravel, mud, loess, silt, and travertine or limestone. Miocene sediments: red muds, sandstones, siltstones, conglomerates, and calcites. Paleocene sediments: lime-stones, calcites, dolomites, conglomerates, sandstones, and siltstones [13,14,15] (Fig. 2).

The Northern Afghan platform is separated from the Turan platform of southern Eurasia by the Amu Darya and Afghan Tajik basins [3]. The ongoing collision of the

Indian plate with the Eurasian plate is accommodated by faults that have historically caused devastating earthquakes in the region. On the east and south, the North Afghan Platform is bordered by the Herat right-lateral and Darwaz left-lateral strike-slip and related faults (Shnizai, 2020b). The study area is located close to the Alburz-Marmul fault lies between the Northern Afghan High to the south and Afghan-Tajik Basin to the north (Figs. 3a, b). The Alburz-Mormul fault also separates the Tajikistan depression from the Parapamiz Bande-Turkistan uplift. The Dosi Mirzavalang fault has continuous and sub-linear scarps on middle and late Pleistocene alluvial deposits and bedrock [16,17] (Figs. 3a, b).

2.2. Geomorphic Setting

Generally, landscapes in Afghanistan are tectonically active due to vertical and horizontal crustal blocks motion as well as erosion and deposition process (Fig. 3a). Afghanistan is dominated by rugged mountainous terrains like the massive Hindu Kush Mountains, which form a barrier between the Northern Afghan Platform and the rest of the country. The Hindu Kush plays a watershed role between the northern Amu Darya and Afghan Tajik Basins to the north and Indus Basin to the south (Figs. 3a, 4). Northern Afghanistan is located in desert and semi-desert areas. Two big basins are located inside the platform, which encompasses approximately 87,000 square kilometers in those portions that lie within Afghanistan [6]. The Afghan-Tajik Basin is located to the east of the Afghan platform while the Amu Darya Basin is to the west. These two basins are separated from one another by a Gissar mega anticline called Gissar [6] (Fig. 4). In general, the northern Afghan occupies a narrow zone between Alburz-Marmul Fault North Afghan High and Bande Turkistan Rang to the south, and Amu

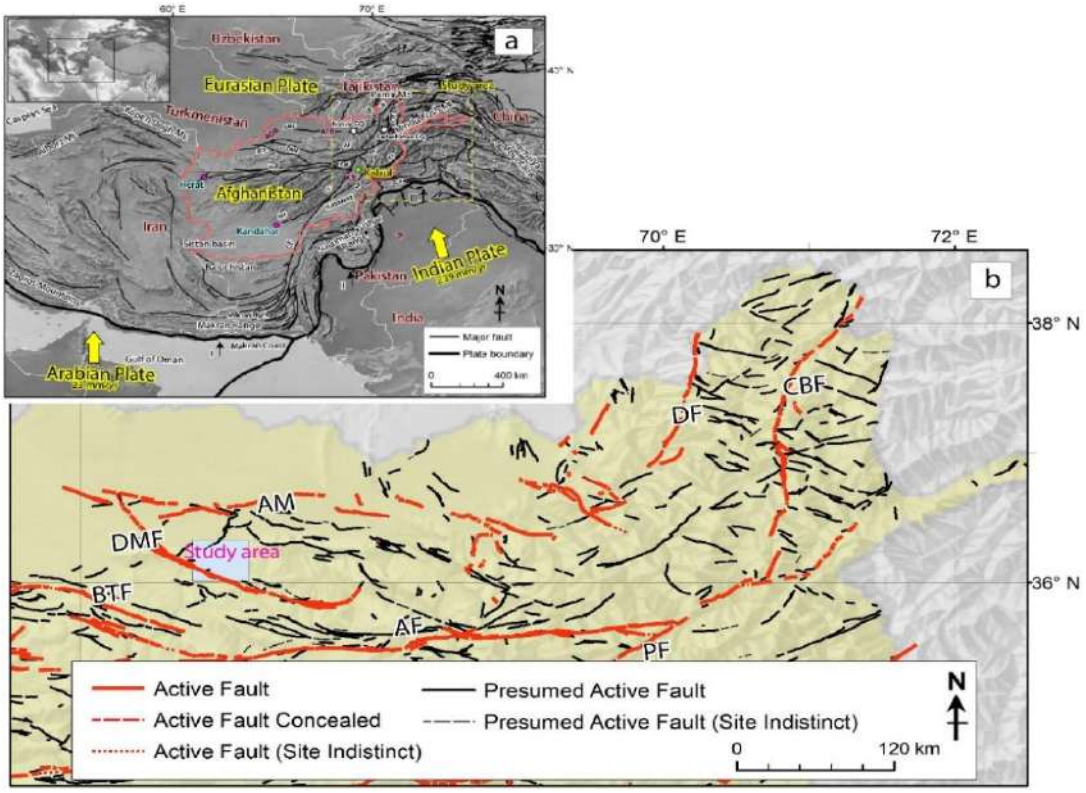

Figure 3. a) Tectonic setting of Afghanistan and the surrounding regions. Yellow-filled arrows show relative plate motion directions between the Arabian and Indian plates concerning the Eurasian plate (plate velocities from [18] and active faults are from [16] and [17]. The plate boundaries are marked with numbers: I) Makran subduction zone, II) fold-and-thrust belt east of the Chaman fault, and III) Himalaya collision zone. ATB, Afghan-Tajik Basin; ADB, Amu Darya Basin; IB, Indus Basin; KB, Kabul Basin. b) Active faults map of northern Afghanistan. Faults names in both figures: AMF, Alburz Marmul; AF, Andarab; BTF, Band-e Turkestan; CF, Chaman; CBF, Central Badakhshan; DF, Darvaz; DMF, Dosi Mirzavalang; GF, Gardez; HeF, Herat; HF, Henjvan; KF, Konar; MF, Mokur; PaF, Paghman; PF, Panjshir; SGF, Spinghar. The active fault maps is modified from Shnizai (2020)

3. Site description and research background

The district is located in the southern part of Balkh Province, just south of Mazari Sharif about 450 km north of the Capital Kabul. The main occupation of the residents here is agriculture and livestock. This district is the sole producer of industrial products in Balkh Province. The people generally use drinking water from wells, most of which are without hand pumps. In summer, the water of the pits and drilled wells dry out, and people cannot dig deeper wells due to the presence of hard rocks. Therefore, people use water from streams or ditches located a few hundred meters from their homes. These waters are muddy, polluted, and contain bacteria. Since the main problem of this village is the lack of healthy and safe water in terms of quantity and quality, it is necessary to provide safe drinking water by drilling deep wells and constructing a water supply system [2]

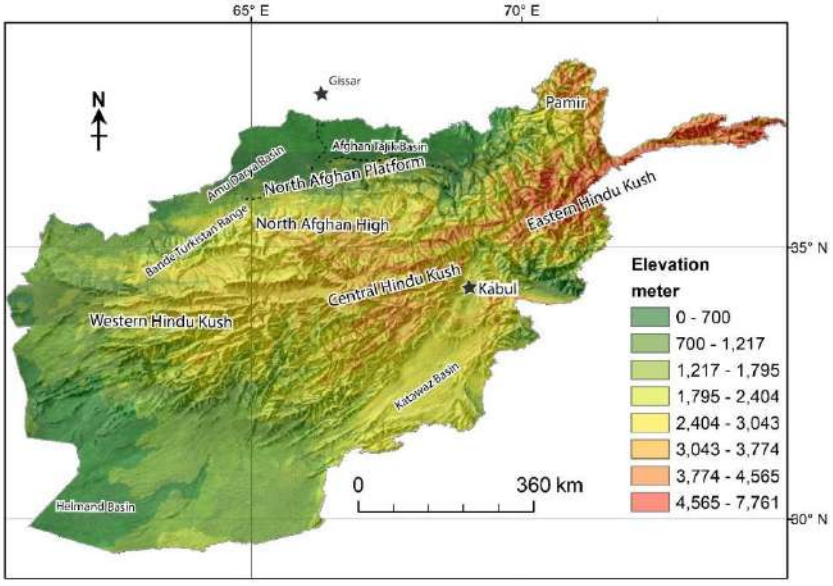

Figure 4. Geomorphology of northern Afghanistan.

4. Methods

The people's demand for water supply is met by surface and groundwater. The current drought and population growth have caused serious problems, particularly in groundwater pollution over abstraction. In shallow wells and streams within the research area, the water level drops and even completely dried particularly in the summer season. Thus, the residents of the area are faced with rapid decline and shortage in water for their livestock and even drinking. To identify groundwater conditions through surface and subsurface features, we have integrated geological, geomorphological, and geophysical methods. We have conducted geological and geomorphological research to map geomorphic features such as slope, landform, geology, watershed, and groundwater potential zones in the study area with the help of thematic maps prepared using a remote sensing geographical information system. We, therefore, analyzed the geology and geomorphology of the Qazel Kand Village and the surrounding region in the Sholgara District using several satellite images. Remote sensing and GIS together with Adobe Illustrator have proved to be important tools to prepare thematic maps from various satellite imageries. Application of GIS and Remote Sensing in geology and geomorphology for groundwater evaluation has been proven to be efficient [19,20].They are also used as a multi-criteria decision tool for analysis and rapid assessment of surface geologic formation, surface water drainage, groundwater, and other natural resources. However, after the delineation of groundwater zones, we focus on a small research area located in Qazel Kand village to estimate the water table. Therefore, DACAAR Institution conducted a geophysical survey for groundwater exploration in Qazel Kand village on the 23rd of November 2013 that was used as primary geophysical data in the research area.

Large-scale images were constructed from SPOT (Satellite Pour l' Observation de la Terre) earth observation satellite that is freely available from ESRI (Environmental Systems Research Institute) as a base map [17]. All the images were imported to ArcMap for geo-referencing into a global framework and manipulated to highlight the scenes to

map the critical geomorphic elements of the study area. Fieldwork was also conducted in the broader area, particularly along the riverside, to examine the details underground structure. So, DACAAR funded team did a Vertical Electrical Sounding (VES) survey using Schlumberger Electrodes Array to explore and prepare drinking water for the people in the Qazel Kand village [2]. Field measurements were done by the Syscal Pro Resistivity Meter and interpreted by IPI2 win software. Then the data were analyzed and interpreted to determine the location, depth, and boundary of the water table in the Qazel Kand Village.

5. Result and Discussion

Based on the availability of data and resources, this research is limited to the use of geology, geomorphology, and geophysics that focus on lithology, rock properties, slope, land use, and electrical properties of underground layers. The lithology and rock properties affect the early stage of erosion as well as water infiltration into the ground. The slope and land use are variables and have significantly influenced the geomorphological control of groundwater occurrence. The electrical properties of rocks and groundwater are measured by Vertical Electrical Sounding (VES) to obtain information about the aquifer.

5.1. Geology

The study area represents a clay steppe or semi-desert. The surface geological formation includes recent Quaternary (gravel, sand, clay, and loess), middle Quaternary (gravel, sand, clay loess, loam, and travertine), early Miocene (red clay, sandstone, siltstone, conglomerate, and limestone), and Palaeocene (sandstone, siltstone, conglomerate, marl, limestone, and dolomite) (Fig. 5).

In this region, the geological map [13] serves as a basis for the study of groundwater conditions (Fig. 5). The geological units play an important role in affecting the movement, accumulation, and quality of groundwater. The basement of the study area is constituted of granite and metamorphic rocks. They have very less porosity and are classified into low groundwater potential zones. The basement is cropped out in the south, east and west parts of the area. The stratigraphic sequence occurring in the area is listed in table 1. The Holocene, Late Pleistocene, and Middle and Early Miocene deposits have high porosity and seem to be good sources of groundwater. Among these deposits, the Holocene and Late Pleistocene have a high possibility of the occurrence of groundwater. These sediments have a high amount of porosity, so it has good groundwater potential. The stratigraphic sequence of Paleocene and Late Cretaceous in the study area are hard rock and located in a higher elevated area of this region. These rocks do not have much water resources but could be a good rechargeable region, particularly in the wet season (winter and spring) for the low elevated areas (Holocene and Late Pleistocene deposits) (Fig. 5).

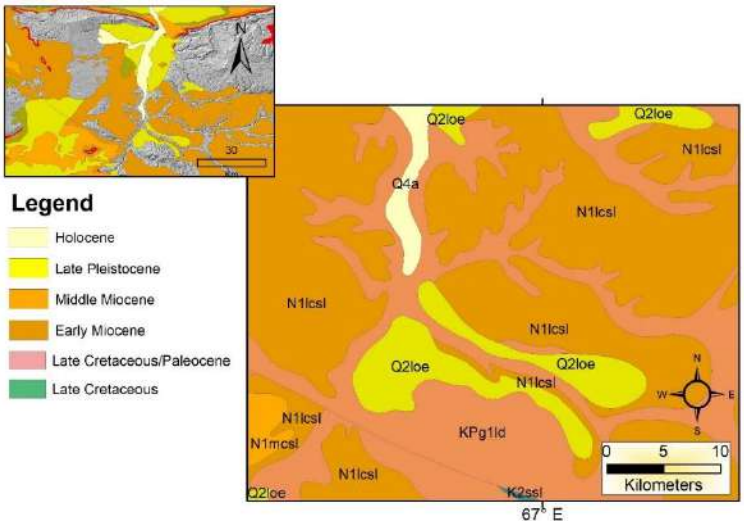

Figure 5. Geologic map of the study area simplified from [13]

Table 1: stratigraphic sequence of the study area (after [13]).

No	Unit Symbol	Lithology
1	Q4a	Conglomerate and sandstone (narrative: red clay, siltstone > sandstone, conglomerate, limestone)
2	Q2loe	Loess (narrative: Loess more abundant than sand, clay)
3	N1Lcsl	Clay and siltstone (narrative: red clay, siltstone > sandstone, conglomerate, limestone)
4	N1mosl	Clay and siltstone (narrative: brown clay, siltstone > sandstone, conglomerate, limestone)
5	Kpg1ld	Limestone and dolomite (narrative: limestone, marl, dolomite > sandstone, clay, siltstone, gypsum, conglomerate)
6	K2ssl	Sandstone and siltstone (narrative: sandstone, siltstone > clay, limestone, marl, conglomerate, gypsum (North Afghanistan); limestone)

5.2. Geomorphology

5.2.1. Land Use

The dependence on groundwater is determined by the land used in an area. The land use in the study area (Sholgara Drainage Basin) contains agricultural land (plantation, cropland, and fallow farmland), water bodies (steam and pound), and build-up area (Fig. 6). Based on the satellite imageries, irrigation in few areas is reliant on groundwater, while irrigation mainly is dependent on surface water. The Band-e Amir river nearly disappears in Balkh Province in the sands at the meeting place of desert and semi-desert without reaching the Amu Darya River (Figure 4).

5.2.2. Geomorphic features

The geomorphic features of different landforms are created by tectonic and geologic processes (temperature change, freezing, chemical reactions, water, and wind). Some active faults affect the landform such as the Alburz-Marmul fault and the Samangan fault. Foothill, linear ridges, peneplain, pediments, and valley fill are present in the area and can be identified from DEM and ESRI base-map (Figs. 6a, b). Weathering and erosion process create denudational hills, which reduce to infiltration of surface water [19,22]. Valley fill is developed due to the deposition of transported and weather materials, which mostly belongs to the Holocene and Late Pleistocene age (Figs. 5 and 6). The valleys are considered as having a very high groundwater potential as they are porous rock (conglomerates, sandstone, and siltstone) and have high infiltration. Linear ridges and residual hills are considered very low groundwater sources and have low infiltration due to high slopes and elevated areas particularly in the south (Figs. 6b, 7a).

Drainage area depends on the surface characteristics, topography, and slope (Fig. 7a). The Bande-e Amir River flows from the Sholgara District. This river is mostly seasonal and flows from south to north. Many pounds, springs, and small reservoirs are present in the depressed parts of the low topography. In some areas, a few wide-lined Kariz (canal networks) are dug for irrigation purposes.

5.2.3. Slope

From a hydrogeological point of view, the study area is located in the developed zone of seamed basins containing waters related to the northern slope of the western Hindu Kush. The slope of the study area has outstanding effects on the infiltration of surface water from the surface to the underground (Fig. 7). If the area has a low slope, the amount of infiltration of surface water will be in great amounts. Also, the precipitation has more time to remain on the earth's surface and penetrate the underground. If the ground has more slope, then the run-off is more rapid and greatly reduces the recharging potential of the groundwater. As the slope of an area greatly depends on the elevation, therefore it is good to know the topography of the area.

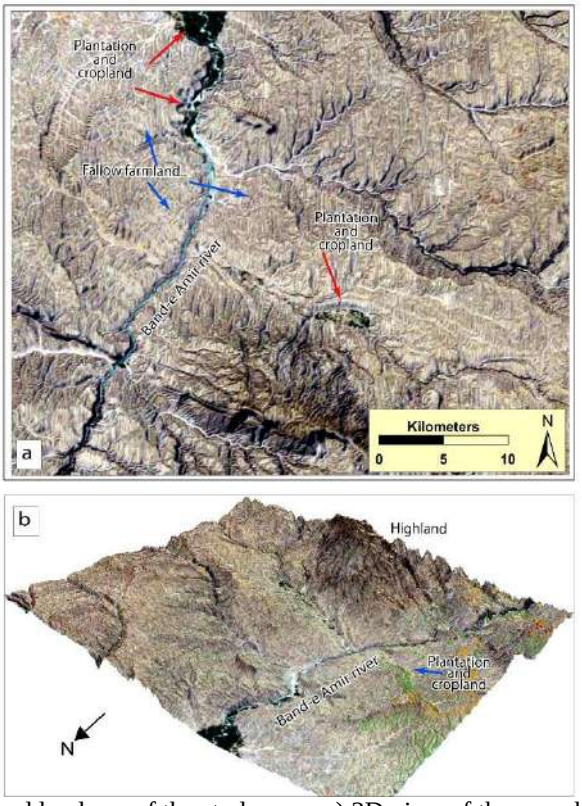

Figure 6. Geomorphology and land use of the study area. a) 2D view of the area. b) 3D view of the area. The satellite image is modified from the ESRI base map.

The highest elevation of the study is approximately 1800 m and the lowest is 575 meters above sea level. The ground surface slopes toward the river (Figs. 6b, 7a). For determining the slope, we used SRTM 1-arcsecond DEM. The slope of the area varies from 1^{o} to 73,6 degrees. Most of the region has a slope from 5.1^{o} - 20^{o} (Fig. 7b). The east and west areas have slopes ranging from 6 – 15 degrees. For the assessment of underground water, the area is classified into three zones based on the slope. A higher slope of 20^{o} - 73.6^{o} is giving a low rank of infiltration rate as well as accumulation [19,23]. The area with a slope of 0-5 has a higher rank as it increases the infiltration rate (Fig. 7b).

5.3. Geophysical survey

The geophysical survey helps us in determining the location and condition of groundwater in the study area. To achieve this goal, the electrical resistivity method was used. The method to obtain geophysical information is Vertical Electrical Sounding (VES) survey in the Qezel Kand village, Sholgara District (Figs. 1, 8). In this method, artificially-generated electric currents are transmitted into the ground and the resulting potential differences are measured at the surface. The resistivity of rocks is defined as the resistance in ohms between the opposite faces of a unit cube of the material [24]. Resistivity is one of the most variables of the physical properties of materials and rocks. Certain types of rocks and minerals conduct electricity through the passage of electrons, while most types

of minerals are insulators. On the other hand, the electrical current is carried through rocks/rock mainly by the passage of ions in pore waters. Thus, most rocks conduct electricity by electrolytic rather than electronic processes.

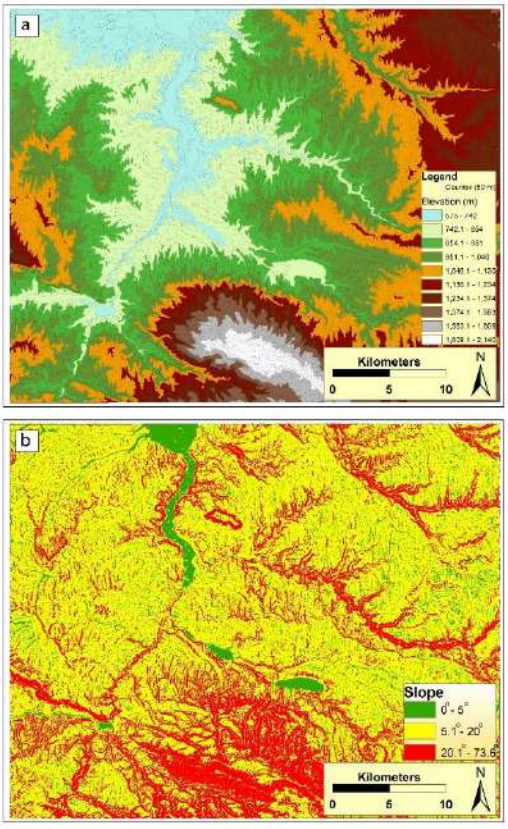

Figure 7. Geomorphic features. a) Topography of the study area. b) Slope characteristics

Many configurations of electrodes have been designed and are occasionally employed in specialized surveys. Here, the Schlumberger configuration method was used. In the Schlumberger configuration, potential electrodes have spaces which is a small proportion of that of the outer current electrodes. In Vertical Electrical Sounding surveys, the potential electrodes remain fixed and the current electrodes are expanded symmetrically about the center of the spread [24]. With a very large area, it is necessary to increase also the distance between current electrodes to maintain a measurable potential.

Figure 8: Location of electrical vertical sounding profiles on top of the google earth image in Qazel Kand village, Sholgara District (location of the geophysical survey is shown in figure 1).

The Schlumberger method was also used by introducing an electrical current into the ground from DC (direct current) or low-frequency sources by two electrodes (P1 and P2). The potential difference between a second pair of electrodes (C1 and C2) was measured (Fig. 9). This Schlumberger configuration is characterized by following up the vertical variations in the subsurface layers in each VES, together with horizontal variations through compiling and correlating the measured VES's along geoelectrical profiling [25].

During the process, first, we measure I_{P1P2} and Δu_{C1C2} for short distances P1P2/2, and later for long distances P1P2/2. Then the potential difference is calculated as follows:

$$\Delta u = I\rho C1C2/\Pi P1C1P1C2$$

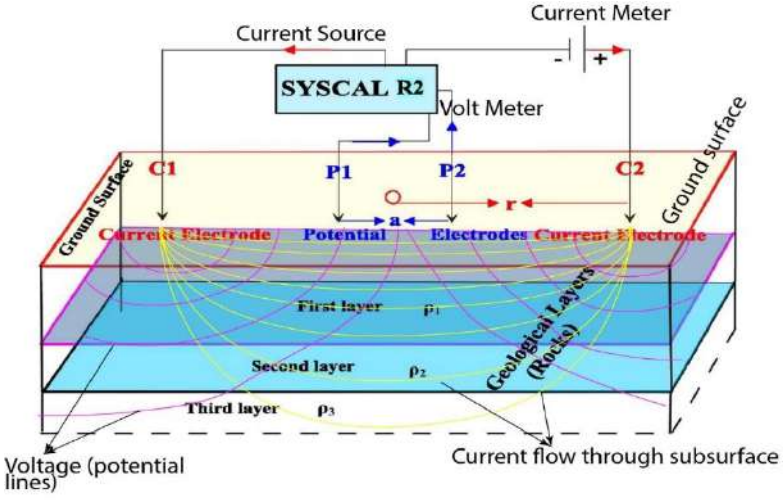

Figure 9: Schlumberger configuration for Vertical Electrical Sounding (VES) measurements. The figure is modified from [25]

From the above formula, calculate the specific electrical resistance as follow:
Here: ρ - apparent is electrical resistance, K- is the geophysical factor or coefficient of the device, Δu- is the potential difference between P1 and P2 electrodes, and the current intensity. Potential difference measure in millivolts (mV), current intensity in milliamperes (mA), and apparent electrical resistance in ohmmeters [25,26]. The values of apparent electrical resistance of water and some rocks are as follows: (Fig. 10):

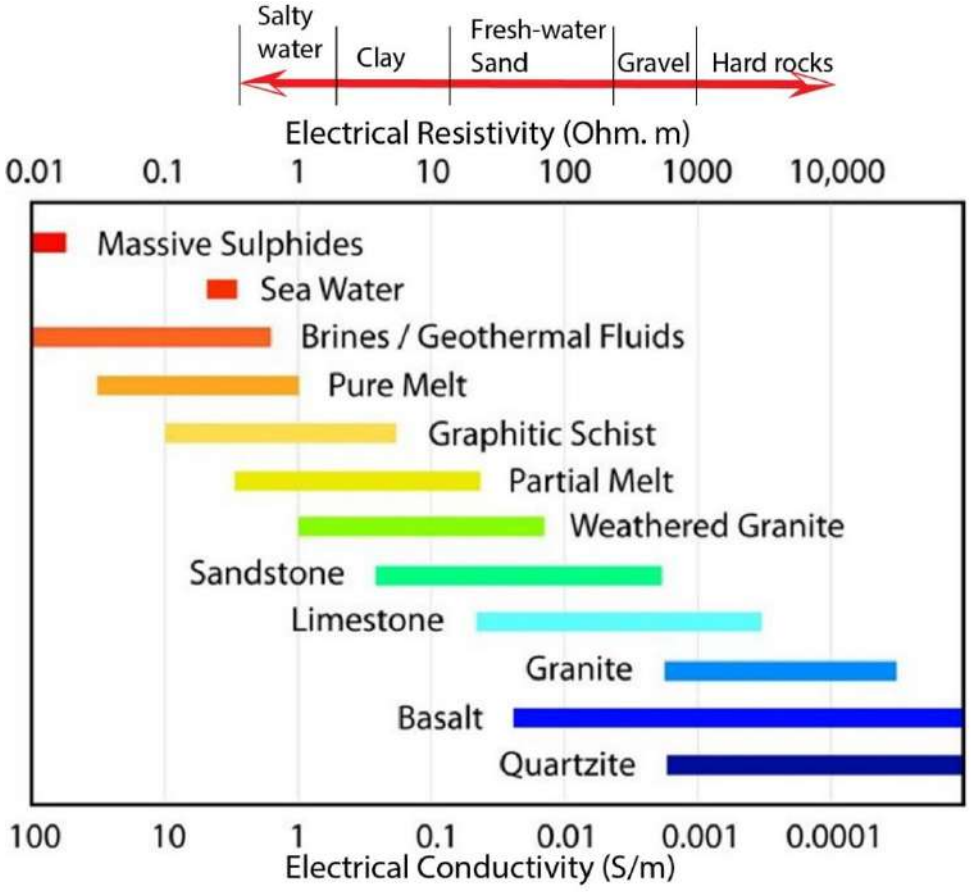

Figure 10: The electrical conductivity and resistivity values of water and different rock types. Ranges of values are shown as bars. Blue color shows high conductivity and low resistivity and red color shows high resistivity and low conductivity. The figure is modified from [27].

The value geophysical survey of vertical electric sounding (VES) conducted in Qazel Kand village such as absolute height, position, and length of vertical electrical sounding (VES) are listed in the tables 2 .

Table 2: Position and length of vertical electrical sounding

No	Location	Vertical Electric Sounding No.	Lat.	Lon.	VES Length (m)	Elev. (asl)
1	Qazel Kand village	1	66.89246	36.231613	600	-
2	-//-	2	66.89153	36.23494	600	648
3	-//-	3	66.89317	36.234443	600	643

Field data are measured by a Syscal Pro resistivity meter and their values are listed below (tables 3-5).

Table 3: Vertical Electrical Sounding values along the geophysical profile Number-1.

Distance between Current electrodes C1C2/2 (m)	Distance between Receiving electrodes P1P2/2 (m)	Apparent electrical resistance ρ_k (Ohm.m)	Potential differences Vp (mV)	Intensity of electric current in (mA)	Device coefficient K (m)
1	1	83.4769	1389.589	39.119	2.35
2	1	55.4316	158.276	33.693	11.8
3	1	55.007	93.498	46.743	27.5
4	1	57.1318	54.666	47.358	49.5
5	1	59.6179	18.678	24.343	77.7
6	1	61.82028	19.294	34.955	112
8	1	67.1214	9.396	27.997	200
10	1	72.4564	9.411	40.654	313
15	1	94.715	2.858	21.265	705
15	10	86.0596	29.134	21.262	1250
20	10	115.25	41.223	42.203	1960
20	1	123.47	4.168	42.194	62.8
25	1	142.95	2.679	36.732	118
25	10	135.77	26.434	36.601	188
30	10	157.35	14.274	24.946	275
35	10	176.55	16.021	34.209	377
40	10	196.117	25.353	63.991	495
50	10	230.73	9.64	32.588	780
60	10	259.1	2.886	12.475	1120
70	10	293.74	2.564	13.355	1530
80	10	332.68	2.464	14.813	2000
80	60	263.099	13.493	14.77	3130

100	60	296.102	16.866	27.056	4900
100	10	363.42	3.187	27.448	288
125	10	419.083	1.137	13.294	475
125	60	350.66	5.994	13.164	770
150	60	390.996	2.865	8.28	1130
175	60	415.21	3.186	11.97	1560
200	60	426.74	3.903	18.658	2040
250	60	446.231	1.573	11.386	3230
300	60	430.07	1.033	11.193	4660

Distance between Current electrodes C1C2/2 (m)	**Distance between Receiving electrodes P1P2/2 (m)**	**Apparent electrical resistance ρ_k (ohm.m)**	**Potential difference Vp (mV)**	**The intensity of electric current in (mA)**	**Device coefficient K(m)**
1	1	304.455	623.939	4.816	2.35
2	1	222.443	156.257	8.289	11.8
3	1	146.611	17.604	3.302	27.5
4	1	108.6682	11.251	5.125	49.5
5	1	84.34576	6.365	5.242	77.7
6	1	87.148.3	7.806	10.032	112
8	1	85.37498	9.13	21.388	200
10	1	95.22	3.65	11.998	313
15	1	112.101	6.234	39.204	705
15	10	109.48	68.346	39.203	1250
20	10	135.907	16.644	14.451	1960
20	1	135.011	4.813	44.561	62.8
25	1	156.27	2.825	35.431	118
25	10	158.024	29.886	35.555	188
30	10	179.0258	5.486	8.427	275
35	10	195.318	9.081	17.528	377
40	10	206.8685	3.317	7.937	495
50	10	231.576	6.746	22.722	780
60	10	245.929	1.893	8.621	1120
70	10	263.235	3.303	19.198	1530
80	10	264.8	3.789	28.617	2000
80	60	247.83	24.966	29.012	3130
100	60	230.07	42.276	87.282	4900
100	10	241.05	6.696	86.945	288
125	10	236.531	3.23	66.913	475
125	60	227.71	20.024	20.024	770

150	60	225.67	6.89	34.5	1130
175	60	254.529	4.412	27.041	1560
200	60	273.91	3.796	28.271	2040
250	60	236.55	3.882	53.006	3230
300	60	250.95	15.283	283.792	4660

Table 4: Vertical Electrical Sounding data along the geophysical profile Number-2.

Table 5: Vertical Electrical Sounding value along the geophysical profile Number-3.

Distance between Current electrodes C1C2/2 (m)	**Distance between Receiving electrodes P1P2/2 (m)**	**Apparent electrical resistance ρ_k (ohm/m))**	**Potential difference Vp (mV)**	**The intensity of electric current in (mA)**	**Device coefficient K (m)**
1	1	201.45	4843.389	56.498	2.35
2	1	240.34	1114.223	54.704	11.8
3	1	233.17	438.505	51.715	27.5
4	1	156.89	121.357	38.288	49.5
5	1	112.45	58.204	40.215	77.7
6	1	86.159	39.555	51.418	112
8	1	64.011	13.973	43.658	200
10	1	59.379	5.694	30.014	313
15	1	83.918	0.985	8.275	705
15	10	83.915	8.465	6.335	1250
20	10	118.369	7.685	7.661	1960
20	1	112.898	0.695	7.695	62.8
25	1	138.68	1.054	14.896	118
25	10	145.97	11.466	14.767	188
30	10	168.64	10.822	17.647	275
35	10	191.32	10.019	19.742	377
40	10	216.91	5.78	13.19	495
50	10	256.01	6.861	20.903	780
60	10	300.714	3.524	13.125	1120
70	10	327.898	0.394	1.843	1530
80	10	368.968	1.296	7.025	2000
80	60	351.969	8.831	7.226	3130
100	60	416.069	15.914	18.168	4900
100	10	424.06	2.457	18.135	288
125	10	443.1153	2.981	30.874	475
125	60	472.8989	9.754	15.882	770
150	60	488.59	21.731	50.258	1130
175	60	504.696	26.757	82.705	1560
200	60	484.6	4.331	18.232	2040

250	60	441.739	4	29.248	3230
300	60	357.05	6.052	78.987	4660

5.3.1. Geophysical Data Interpretation

The graphic interpretation of Vertical Electrical Sounding (VES) is shown in figures 11-13. Field data of the Vertical Electrical Sounding (VES-1, 2, 3) is interpreted with the win IPI2 software. Boundaries, thickness, and depth of rock layers are measured and calculated according to the apparent strength of the rocks. Thus the lithology of underground layers was determined. Apparent electrical resistance is determined on VES-1, VES-2, and VES-3 as shown in (tables 3, 4, and 5). The specific electrical resistivity evaluates the special image of the underground structure in the study area. With the increase in porosity and water content in the underground layer, there is a change in the specific resistance figures that leads us to detect and identify waterlogged strata. During this research work, the specific resistivity is always measured by giving current through the electrodes (C1C2) and measuring the potential difference between the potential electrodes (P1P2) (Fig. 9).

The VES-1 shows five different layers (table 3; Fig. 11). Apparent resistivity of the first layer is 133 ohmmeters. This layer is located at the shallow surface from the ground (0.5 m) with a thickness of 0.5 m. The expected lithology of this layer mostly contains clay with sand and gravel. The second layer has dry sand and gravel, which have apparent resistivity of 16.3 ohmmeters. At the depth of 0.676 m, the thickness of this layer is 0.18 m. Layer three has 58 ohmmeters of apparent resistivity. The boundary of this layer is from 0.17 to 7.403 m. The computed apparent resistivity of layer four is 529 ohmmeters. Layer five is unknown due to no data afterward. Based on the electrical resistivity of the various earth materials (Fig. 9), the lithology of this layer seems to be carbonate stones. As the computed apparent resistivity graph goes up, therefore we cannot identify the thickness, depth for layers 4 and 5, and expected lithology of layer 5 (Fig. 11).

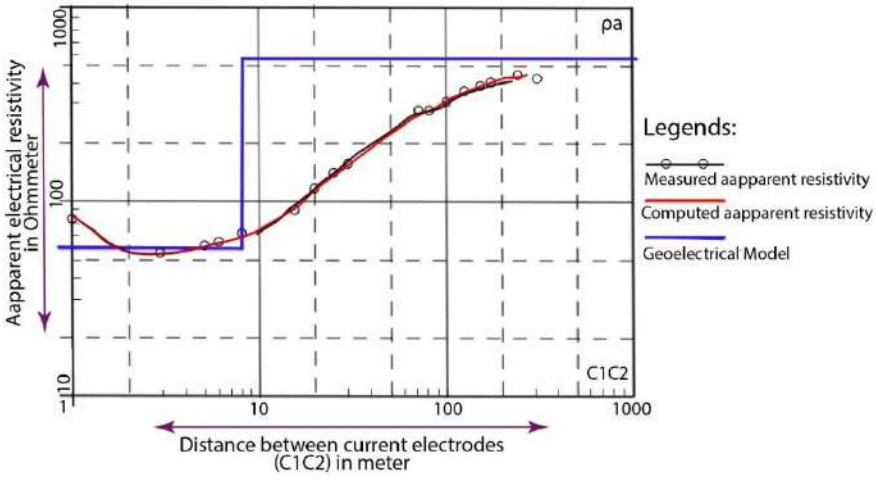

Figure 11: Graphic Interpretation of Vertical Electrical Sounding (VES-1) of table 3.

The VES-2 data shows about five layers having different resistivity, thickness, and depth. The expected lithology of each of these layers is different from the others. From surface to depth, the apparent electrical resistivity of the first layer is 327 ohmmeters. The depth of this layer is 1.27 m with the expected lithology of gravel, sand, and clay. The apparent resistivity of the second layer is 28.9 ohmmeters. With decreasing the apparent electrical resistivity, the electrical conductivity is getting increased, which seems to have wet clay with sand and gravel. The depth of this layer is 2.09 m with 0.86 m thickness. The third layer is located at the depth of 12.2 m with a thickness of ~10 m. The resistivity of this layer is 90 ohmmeters. This layer seems to have the potential of groundwater. In this regard, we can say that the water table is located at the depth of approximately 90 m. While the two the depth the apparent electrical resistivity is getting increased. For example, the fourth layer has apparent resistivity of 531 ohmmeters, while the rest of the layers are unknown due to raising the measured and computed apparent resistivity graphs with no data (Fig. 12).

VIS-3 graphical interpretation shows five distinct layers. The apparent resistance of the first layer is 200 ohmmeters with a depth of 1 m. The expected lithology of this layer is dried clay with some sand, silt, and gravel. The second layer has a depth of 1.8 m with a thickness of 0.8 m. The apparent resistivity of this layer is 412 ohmmeters, which seems to have carbonate rocks such as limestone and marl. These rocks have no primary porosity but can form fractures inside the rocks as secondary porosity, where water occurrence can be taken place. The third layer has a depth of 4 m, with a thickness of 2.8 m. This layer has very low resistivity and seems to have some water.

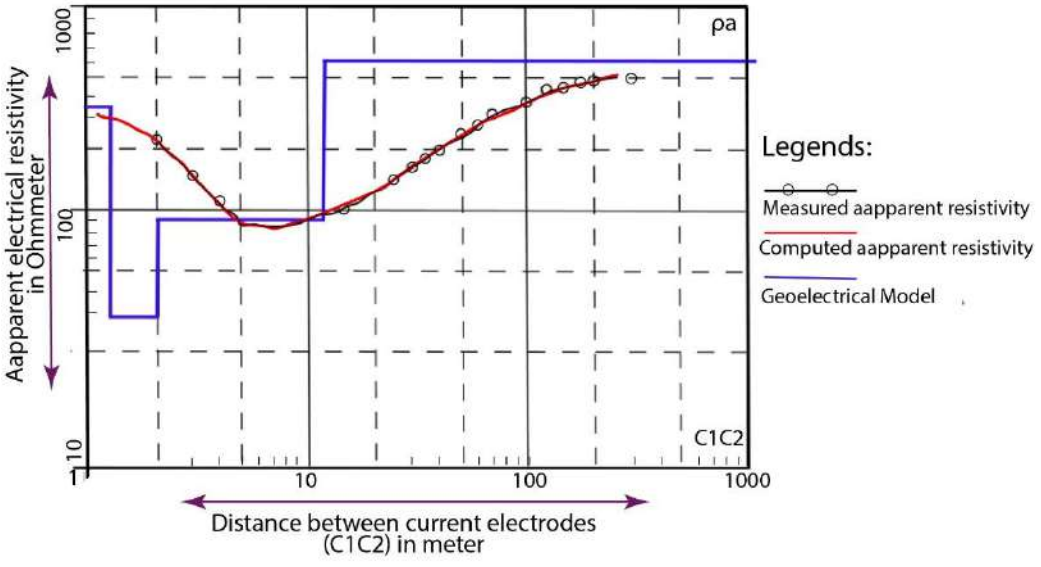

Figure 12: Graphic Interpretation of Vertical Electrical Sounding (VES-2) (table 4).

The expected lithology of this layer is clay with sand and silt. Again for the rest of the layer resistivity is getting increased, while we do not have VES-3 data to imagine the boundary and depth of the layers (Fig. 13; table 5).

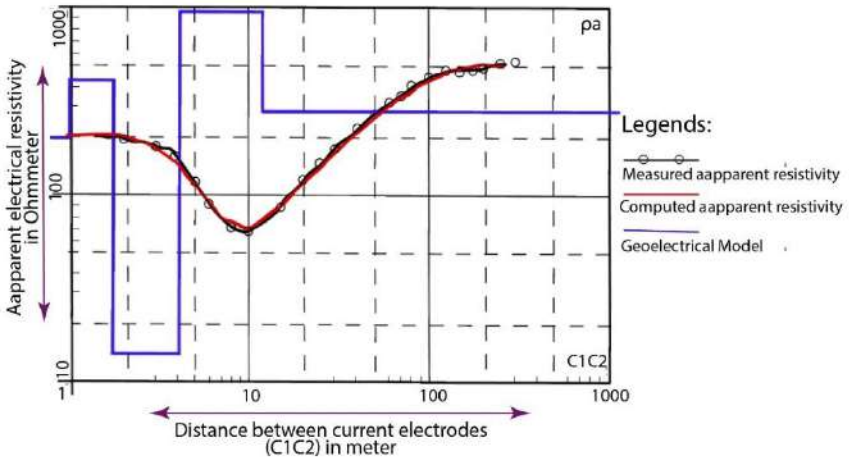

Figure 13: Graphic Interpretation of Vertical Electrical Sounding (VES-3)

Generally, after joining the three VES (VES-1, VES-2, and VES-3) data, the graphical interpretation of the Qazel Kand village, Sholgara District shows that the water accumulation is in carbonate rocks. These rocks have secondary fractures and can accumulate a large amount of groundwater and make a big reservoir. The secondary porosity in carbonate rocks (limestone and dolomite) can be formed by freshwater dissolution or dissolution by chemically aggressive subsurface fluid in the deep-burial environment. Also, the figures show that the water table depth ranges from 80 to 100 m in the study area. The water could be very clean and feasible for drinking.

This research is not enough in the study area. To better understand the area's geology, geomorphology, and physical properties, detailed fieldwork is needed to be done in the area. It is highly suggested to use high-resolution satellite images and increase the number of VESs in different parts of the study area, which can allow us to get more information about the thickness, depth, and lithology of the undersurface layer. To confirm the results of the geologic, geomorphic, and electric methods, it is necessary to drill several exploratory wells at least 120 m depth. It is also strongly recommended to take groundwater samples and analyze them quantitatively and qualitatively in a laboratory to know about groundwater contaminations.

6. Conclusion

Geological, geomorphological, and geophysical investigations provide a full description of the surface and underground. Satellite imagery examines landforms and hydrogeology in a remote area. As this method is reliable and cheap, and it gives the best result in detecting geomorphic features in Sholgara District. Geological maps and satellite images were used to prepare geomorphological and thematic maps. Geologically, Pre-Paleozoic, Paleozoic, Mesozoic, and Cainozoic rock form the structure of the north Afghan platform. Geophysical researches show that the central and northern side of the north Afghan platform (the Amu Darya and Afghan-Tajik Basins) consists of sedimentary rocks which gradually decrease their thickness toward the south and east. The Amu Darya and Afghan-Tajik Basins separate the northern Afghan platform from the Turan platform

of southern Eurasia. The landscape is tectonically active due to vertical and horizontal crustal blocks motion, and deposition and erosion process.

From the surface geological formation, the Holocene and late Pleistocene deposits have high porosity and seem to be a good source of groundwater. The Paleocene and late Cretaceous are hard rocks and mostly located in high elevation. The dependence on groundwater is determined by the land used in an area. The areas located close to the riverside or at a low elevation above sea level, have crops that spend more water. Thus, the cropping pattern depends on the availability of water resources and climatic conditions. On the other hand, the drainage of water depends on the characteristics, topography, and slope. The area with a slope of 5 degrees has a higher rate of infiltration. The valley developed due to the deposition of transported and weather rocks throughout the Holocene and Late Pleistocene times, which have high groundwater potential as having high porosity.

The geophysical survey helped us to determine the location and condition of groundwater in the Qazel Kand Village, Sholgara District. Boundaries, thickness, and depth of underlying layers were measured depending on the rock's apparent resistivity. Then the lithology was determined. Generally, based on the Vertical Electrical Sounding data five different layers are identified. From the surface to 15 m depth, the first 3 layers are located. The graphical interpretation shows that the water table ranges from 50 to 100 m in depth. The water mostly takes place in the karst aquifer with lithology of limestone and marl.

Acknowledgment.

We would like to thank DACAAR for providing the groundwater data.

References

[1] Shnizai, Z. and Iqbal, A.R. (2021) 'Physico-Chemical Properties of Groundwater In The Kabul Basin, Afghanistan', KPU INTERNATIONAL JOURNAL OF ENGINEERING & TECHNOLOGY, 1(1), pp. 61–79. , Saffi, M.H. (2011) Groundwater natural resources and quality concern in Kabul Basin, Afghanistan, Kabul: Afghanistan.

[2] Saffi, M.H. and Jawid, A. (2014) Geophysical Survey in Qezel Kand village, Sholgara District of Balkh Province.

[3] Brookfield, M.E. and Hashmat, A. (2001) 'The geology and petroleum potential of the North Afghan platform and adjacent areas (northern Afghanistan, with parts of southern Turkmenistan, Uzbekistan, and Tajikistan)', Earth-Science Reviews, 55(1–2), pp. 41–71. Available at: https://doi.org/10.1016/S0012-8252(01)00036-8.

[4] Kingston, J. and Clarke, J.W. (1995) 'Petroleum geology and resources of Afghanistan', International Geology Review, 37, pp. 111–127.

[5] Ulmishek, G.F. (2004) 'Petroleum geology and resources of the Amu-Darya Basin, Turkmenistan, Uzbekistan, Afghanistan, and Iran', U.S.

[6] Klett, B.T.R., et al. (2006) 'Assessment of Undiscovered Technically Recoverable Conventional Petroleum Resources of Northern Afghanistan'.

[7] Orudzheva, D.S. and Kornenko, G.Y. (1991) 'South Tadzhik depression', Petroleum Geology, 25(7/8), pp. 263–268.

[8] Sborshchikov, M.I. and Et, A. (1973) 'Geology and Minerals of Northern Afghanistan', Department of Geology and Mineral Survey [Preprint].

[9] Bratash, V.I. et al. (1970) 'Geologiya i neftegazonosnost severa Afghanistana Vsesyuznyi Nauchno-issledovatelskii Geolorazvedochnyii Neftiyanoi Trudy', Nedra, Moskva, 80, p. 106.

[10] Abdullah, S. and Chmyriov, V.M. (1977) 'Geologiya I poleznye iskopaemye Afganistana, Kniga 1', Nedra, Geologiy. Moscow [Preprint], (535).

[11] Abdullah, S., Chmyriov, V.M. and Dronov, V.I. (2008) Geology and Mineral Resources of Afghanistan. London: British Geological Survey.

[12] Shnizai, Z., Matsushi, Y. and Tsutsumi, H. (2020) 'Late Pleistocene slip rate of the Chaman fault based on 10Be exposure dating of offset geomorphic surfaces near Kabul, Afghanistan', Tectonophysics, 795, pp. 1–14. Available at: https://doi.org/10.1016/j.tecto.2020.228593.

[13] Doebrich, J.L. et al. (2006) 'Geologic and Mineral Resource Map of Afghanistan. 1:850,000', U.S. Geological Survey, No.2006-10. Available at: https://doi.org/https://doi.org/10.3133/ofr20061038.

[14] Iqbal, A.R. and Shnizai, Z. (2014) 'Interpretation and Analyzing of Vertical Electrical Sounding (VES) Data, in Kochi-abad Village, Bagrami

District, Kabul Afghanistan', Journal of Science and Technology, Kabul Polytechnic University, 52(64).

[15] Shnizai, Z. (2020a) Active Tectonics and Seismic Hazard Assessment of Afghanistan and Slip-rate Estimation of the Chaman Fault Based on Cosmogonic 10 Be Dating. Doshisha University. Available at: https://doi.org/10.14988/00027636.

[16] Shnizai, Z. (2020b) 'Mapping of active and presumed active faults in Afghanistan by interpretation of 1-arcsecond SRTM anaglyph images', Journal of Seismology [Preprint]. Available at: https://doi.org/10.1007/s10950-020-09933-4.

[17] Shnizai, Z. and Tsutsumi, H. (2020) 'Active Faults and Seismic Hazard in the Kabul Basin, Afghanistan', THE HARRIS SCIENCE REVIEW OF DOSHISHA UNIVERSITY, 61(2), pp. 96–107.

[18] Ruleman, C.A. et al. (2007) 'Map and Database of Probable and Possible Quaternary Faults in Afghanistan', U.S. Geological Survey. Open-File Report 2007-1103, (150), pp. 1–45. Available at: https://doi.org/10.3133/ofr20071103.

[19] Rajaveni, S.P., Brindha, K. and Elango, L. (2015) 'Geological and geomorphological controls on groundwater occurrence in a hard rock region', Applied Water Science [Preprint]. Available at: https://doi.org/10.1007/s13201-015-0327-6.

[20] Ndatuwong, L. and Yadav, G. (2014) 'Integration of hydrogeological factors for identification of groundwater potential zones using remote sensing and GIS techniques.', Journal Geosci Geomat, 2(1), pp. 11–16.

[21] Industries, M. of M. and (2008) Geological characteristics of oil-rich areas in northern Afghanistan, Ministry of Mines and Industries: Kabul, Afghanistan.

[22] Ramaiah, S.N. et al. (2012) 'Geomorphological mapping for identification of groundwater potential zones in hard rock areas using geo-spatial information—a case study in Malur Taluk, Kolar District, Karnataka, India.', Nat Environ Pollut Technol, 11(3), pp. 369–376.

[23] Bagyaraj, M. et al. (2013) 'Application of remote sensing and GIS analysis for identifying groundwater potential zone in parts of Kodaikanal Taluk, South India', Front Earth Sci, 7(1), pp. 65–75.

[24] Kearey, P., Brooks, M. and Hill, I. (2002) An Introduction to Geophysical Exploration. 3rd Editio. Blackwell Science.

[25] Helaly, A.S. (2017) 'Assessment of groundwater potentiality using geophysical techniques in Wadi Allaqi basin, Eastern Desert, Egypt – Case study', NRIAG Journal of Astronomy and Geophysics [Preprint]. Available at: https://doi.org/10.1016/j.nrjag.2017.09.003.

[26] Milsom, J. (2003) Field Geophysics (Resistivity Methods). Edited by 3rd. London: Willy.

[27] Comeau, M.J. (2015) Electrical Resistivity Structure of the Altiplano-Puna Magma Body and Volcan Uturuncu from Magnetotelluric Data. The University of Alberta. Available at: ttps://doi.org/10.13140/RG.2.2.10150.32329

Authors Profile:

Zakeria Shnizai born in Sayed Abad of Wardak province. He received his BSc in Oil and Gas Mines Engineering Department from Kabul Polytechnic University in 2007. He completed an MSc in environmental geology in 2012 and then a Ph.D. with a major in active tectonics in 2020. He is working as an associate professor at Kabul Polytechnic University-Kabul Afghanistan. His research area includes active tectonics, remote sensing and GIS, geophysics, and petroleum geology.

Abdul Rashidi Iqbal received an MSc degree in geophysical methods of exploration of mines in 1986 from the Azerbaijan State University of Oil and Industries. Started work at the Ministry of Mines and Industries of Afghanistan in 1986. Then worked with the Ministry of Water and Energy (WAPECA) and since 1989 tell now an assistant professor, associate professor, and professor at Kabul Polytechnic University-Kabul Afghanistan. His research area is prospecting and exploration of mines, water, and the use of full materials.

Mohammad Walid Omid received a B.Sc. degree in Oil and Gas Mines Engineering from Kabul Polytechnic University in 2014, and MTech (Master of Technology) degrees in Earth Sciences with a specialization in Petroleum Geoscience from the Indian Institute of Technology Bombay (IIT Bombay), Mumbai, India in 2020. He is working as an Assist. Prof. at the Department of Oil and Gas Mines Engineering, Geology and Mines Faculty, Kabul Polytechnic University, Kabul Afghanistan. His field of research includes Active Tectonics, Geology, Geophysics, Remote Sensing, and GIS.

KPU International Journal of Engineering & Technology
Volume 2, Issue2, Dec. 2022
e-ISSN:2790-0819, p-ISSN:2790-0800
Date Received: 2022-07-13
Date Accepted: 2022-12-20
Date Published: 2022-12-30

Urban Development Through Participatory Approach: Contemporary methods of Urban Planning in Kabul City

MOHAMMAD RAMIN AMIRYAR[1*], AHMAD JAWAD NIAZI[2], SHAHPERAI PERZAD SEDIQ[3]

[1*]Ph.D. Scholar, Toyohashi University, Japan. Email: mohammad.ramin.amiryar.gm@tut.jp

[2]Associate Professor, Department of Architecture, Kabul Polytechnic University, KPU campus, 5th District, Kabul, Afghanistan. Email: a.j.niazi@kpu.edu.af

[3]Assistant Professor, Department of Technical Drawing, Kabul Polytechnic University, KPU campus, 5th District, Kabul, Afghanistan. Email: sh.sediq@kpu.edu.af

Abstract

Since 2001, the urbanization trend is unprecedented, and both the government and the people have been making efforts to reconstruct Kabul city. More than 66 percent of Kabul's population lives in informal settlements. The urban planning projects (Detail Plans) are being prepared behind closed doors and are expected to be implemented on the site without the consent and agreement of the residents. The capacity to steer the planning and implementation process is very weak and most of these planners are not up to date. The existing situation of informal settlement and the trend of urban expansion implies that the public was not the main focus and residents were not involved in decision-making. The approach is one way, and the planning process (referred to as a top-down process) is of particular interest. On the other hand, participation is a process where public inclusion is a must for deciding on planning aspects that may benefit or affect a community. Kabul Municipality has introduced some novel methods that focus primarily on people, and decisions will be based on the opinions of affected residents. These methods are supposed to be used as alternatives to detailed planning and land acquisition methods. As it is clear, development is a process that increases choices. It means exploring options, diversifying, thinking about issues, and anticipating change. By involving multiple stakeholders, conflict can be resolved through consensus building and the plan's effectiveness is increased. The Holy Quran also mentions "and hold fast, all together, by the rope which Allah (stretches out for you and be not divided among yourselves". In this research study, the planning process stream, participatory structures, and the importance of participatory approaches to urban development will be examined. The main purpose of this paper is to encourage methods of planning through citizen participation.

Keywords: Participatory, informal settlement, Detail Plan, decision making, land acquisition

[*]Corresponding Author

1. Introduction

A significant amount of urbanization took place in Kabul after the 2000s, which is unprecedented for a capital city. Urbanization is not uniform, as a primate city contains approximately half of the country's urban population (1). More than 66 percent of Kabul's population lives in informal settlements (2). Urban central areas are increasingly characterized by rising poverty, vulnerability, environmental hazard, and health risk (3). In various parts of the city, residents experience insecurity and a lack of safety. However, urbanization offers opportunities for social development and economic growth too. There has been a concerted effort to rebuild Kabul city by the government and the people (4).

Excluding urban citizens from the planning and decision-making process casts doubt on the ability of the Kabul municipality and government. Governmental Agencies have prepared many urban projects without interference from residents. In the meantime, informal settlements have been expanded throughout Kabul city without compliance with these plans. The urban projects could be implemented based on master plans drafted with the participation and coordination of residents. As it is clear, participation is a process where public inclusion is a must for deciding on planning aspects that may benefit or affect a community (5). Kabul Municipality has introduced some novel methods that focus primarily on people, and decisions will be based on the opinions of affected residents. These methods are supposed to be used as alternatives to detailed planning and land acquisition methods. As it is clear, development is a process that increases choices. It means exploring options, diversifying, thinking about issues, and anticipating change (6). Additionally, Holy Quran mentions, "Hold fast, all of you, by the rope that Allah (stretches out for you) and don't split among yourselves"(7). It is therefore imperative that a close relationship between the government and the residents be fostered in order not only to collaborate but also to make decisions together. Because it is the right of residents to be informed in detail about the decisions that affect their lives (8).

1980 ***2018***

Fig1: A portion of Detail plan

Figure 1 depicts a section of the Wazir-Abad detail plan as a sports complex in the 1980s. During the plan's development, the residents were not informed and were not

involved in decision-making. The dilapidated state of the informal settlement areas that have grown without regard for the Master Plan and detailed plan is clear.

.

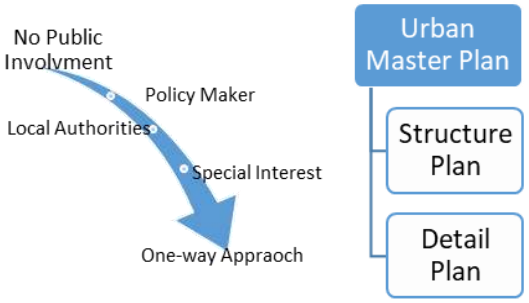

Fig2: Paradigm of Kabul Urban Planning Approach

In Kabul, a detailed planning method is a top-down approach to urban planning. The public was not involved, and the emphasis was on the special interest. In this method, not only is participation at stake but so is the speed with which detailed plans can be developed, which cannot keep up with the current rate of urbanization. This type of planning approach is appropriate for cities with low rates of growth and economic stability, not for Kabul, which has high population growth and economic instability. Depending on the Detail planning system, informal settlement expansion issues may worsen. In the current situation, not only is the government burdened with detailed planning, but residents also do not want to leave communities where they have lived for several years.

On the other hand, many countries have practiced participatory planning, which has led to greater success. In most countries, controversies over planning have been resolved through a participatory approach that directly involves residents in the planning process. To reach this milestone (engage and mobilize the citizens, gain their support and contribution through community organization, settlement regularization, and service delivery), proposed the Kabul Solidarity Program (9). Through KSP, a Neighborhood Development Council has been established by the election of representatives (one male and one female) of families that will be a forum for discussion and prioritization of needs and problems. It can be referred to as a traditional community governance structure such as the Gozer Assembly and Wakil Gozer. The management of KM recently embraced the participatory approach as well in their planning processes. Land Readjustment and Urban Redevelopment (LRUR) are now the two options as alternatives for land acquisition and Detail Planning, all of which require participatory planning.

Participatory approaches allow the public and authorities to reach a consensus, improve decision-making processes, and help a city move forward and improve its social structure. The primary goal of this paper is to promote planning methods that involve citizen participation.

To sum up, the Participatory approach has the ability that can build social capital, helps citizens and authorities reach a consensus regarding a certain matter, improve decision-making processes and finally help a city to move forward and improve social structure. The main purpose of this paper is to encourage the methods of planning through citizen participation.

1.1 Statement of Problems

Because of the influx of internal displacement persons (IDPs) and returning refugees in recent decades, central urban areas have been the primary focus of urban planning. Planning urban development accounts for a relatively small volume in comparison to urbanization. Many urban experts continue to employ the same urban planning methods and standards that they did in the 1970s and earlier. The planning process took one approach, and the implementation process was met with opposition. Even though some participatory methods are used in Kabul Municipality. However, no legally binding document to support the participatory approach has been prepared. The following are the major issues:

- Population growth
- outdated planning methods and standards
- Insufficient development capacity
- One-way approach
- No regulations or procedures for enacting and enforcing the policy

2. Method of Research

The methodology of this study includes a review of literature, records, and secondary data analysis regarding participatory approaches. A validated set of data was gathered from Kabul Urban Design Framework and JICA (Japan International Corporation Agency), as well as the literature and documents on the participation of civil society.

3. Research content

3.1 Reorientation of paradigms

It is necessary to mention the fact that during the last few years, the planning approaches have changed in Kabul city. The non-governmental organizations working in urban sectors mostly played key roles in the involvement of ordinary residents in their planning process and implementation stages. UN-Habitat and the World Bank are engaged in the betterment of informal settlement situations, maximally focusing on boosting social aspects. On the other hand, for a couple of years, Japan International Corporation Agency practicing contemporary Land Readjustment and Urban Redevelopment participatory is essential for the implementation of the projects. Over time, the notion of citizen participation and its designation in development projects is clear., the paradigm of participatory planning is changing from top-down to bottom-up approaches.

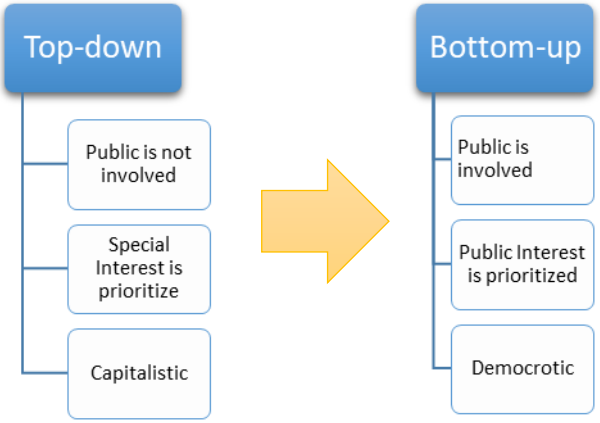

Fig 3: Two paradigm in public participation

Figure 3 shows that the top-down approach implies that public participation is not concentrated and that planners do all the things related to planning and decisions themselves. The outcome will be shared with the community and the implications of the decision will be contested by residents. On the other hand, the bottom-up approach emphasizes community involvement. Community members are involved in the process to get a more comprehensive understanding of the current state of affairs. The participation arrow distinguishes the level of participation in top-down and bottom-up approaches. In figure 4, the participation arrow demonstrates the engagement of the community from open-ended information exchange to exchanging information.

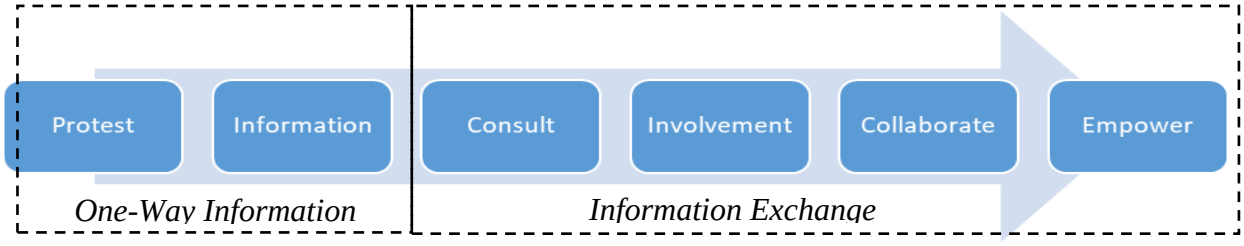

Fig 4: level of Engagement

Under the Empowerment Point, citizens and planners are equally involved in decision-making. Today, the process in Kabul is changing, but it is still struggling to move in the right direction. Planners and authorities are adamant about getting an early estimate of residents' willingness through workshops and meetings. Residents of the project met to discuss and debate the challenges they face and how they intend to address them. During this meeting, the residents frequently inquired about decisions that affect their quality of life and destinations. Following the meeting, the majority of residents provided positive feedback about the planning process, stating that their opinions would be considered and valued. The residents then requested a formal petition from Kabul Municipality, which they signed individually, for the projects to be implemented.

Fig 5: Willingness Evaluation Meeting in district 10

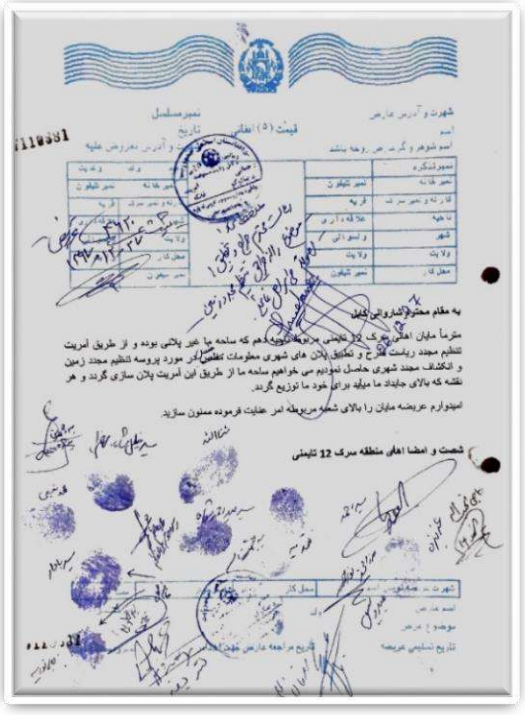

Fig 6: Group Petition from KM

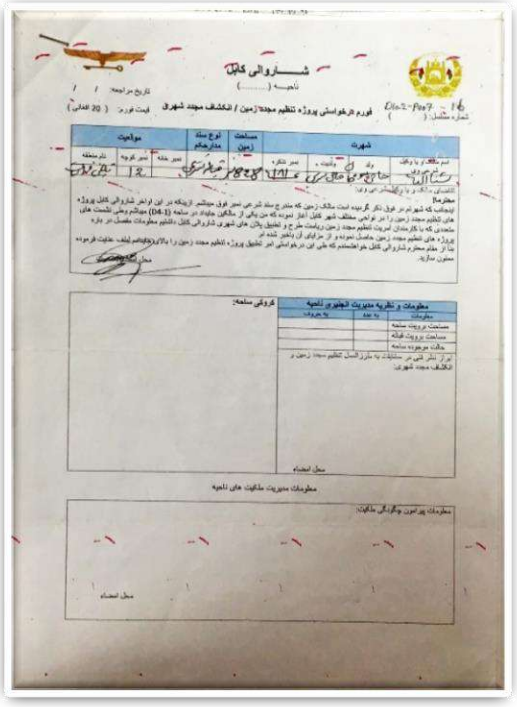

Fig 7: Individual Request Form

3.2 Common Participatory Forms in Kabul

Depending on the circumstances at the local level, participation forms may differ. Planning participation can take one of the following forms:

3.2.1 Direct-mass participation:

The resident is actively involved in a program, project, or decision-making process. Participation is open to all. Everyone in the community, regardless of age, gender, or socioeconomic status, is welcome to participate in the program (elders, youths, men, women, disabled, etc.).

3.2.2 Opinion leaders:

An opinion leader in this sense is a person or group of people who have more influence, ideas, and behaviors that can serve as models for others. Chiefs, religious preachers, businessmen, and district heads are examples of these leaders. Wakil Gozer, who coordinates all administrative and community affairs with the government and residents, is a popular model for the Afghan community's opinion leaders.

3.2.3 Representational:

Some residents divide their community based on various functions into different groups. Members are selected from related groups of matters to participate in the community and make decisions.

3.2.4 Self-Appointed Representatives:

This type of participation is more common in Kabul's local communities. A person or group of people imposes their point of view on the rest of the community. These are more radicals who want to be seen as intelligent. As is customary, they appear to be more knowledgeable and have a greater influence on the members of the community. For example, commanders or powerful individuals who act as the community's gods.

3.3 Advantages of a Participatory Approach

The participatory approach has the potential to provide significant support and contribution to reaching a new level of development, and social, and economic performance than the development approach used 50 to 60 years ago (8). This method can achieve goals that would be difficult to achieve in any other way. The fundamental feature of this approach is the inclusion of ordinary people in the process of change. More emphasis is placed on the process because many real benefits emerge when people collaborate, develop skills and confidence, and have individual and group capacity to address emerging issues and opportunities. The major benefits of involving ordinary people in the process are described below.

- **Creation of Shared Visions:** short and long-term strategies for a community's future must be developed.

- **Complex issues and problems** shall be resolved through discussion.
- **Increasing Consensus Building:** Building consensus among different interest groups leads to better and longer-term partnerships.
- **Raising Public Awareness:** An open forum discussion will raise residents' information and awareness.
- **Enhancement of Urban Design Quality:** Through participation, people will consider and reconsider their quality of life.
- **Act as a catalyst:** debates and exchanges of ideas will speed up the activation process.

Furthermore, civil participation will increase resources, social capital and cooperation, mutual aid and services, group learning, and volunteer work. Meanwhile, it will improve community-authority dialogue, the coherence and effectiveness of public policies, and the capacity of authorities, professionals, and experts to engage in communities. Finally, it breaks the community's isolation and brings them together.

3.4 Participatory Paradigm Shift from Real to Virtual-World

Community development is a requirement for long-term development. Since the planning approach is changing in Kabul, the number of meetings, workshops, and mutual discussions with citizens is increasing to reach a consensus. Authorities and planners make every effort to explain everything in weekly or monthly sessions. However, there are some questions and debates that need to be discussed and resolved after the session. Because meeting time is limited and residents are preoccupied with their businesses. As a result, a gap is still reasonable to reach mutual consent, or it takes more time to resolve a minor dispute or minor civil claim. Developed countries that have gained experience with the participatory approach through community development now engage in extensive online or digital participation. There are no time or location restrictions for the online sessions. Residents can log in at any time and from any location to discuss and debate a specific issue that was not addressed during the weekly or monthly session. Japan is one of the countries that is well-known for its participatory planning. The Internet-based discussion has received a lot of attention and will be one of the best methods of outreach for reaching consensus in Japan (10). COLLAGE is a system derived from the collective or collaborative agreement that is used in Nagoya. Residents actively participate in online workshops and discussions about issues affecting their communities. Figure 8 depicts the COLLAGREE consensus-building support system.

Fig 8: Image of consensus building support system on COLLAGREE,

Source, COLLAGREE

Another online participation experiment is taking place in Victoria, Canada, with online dispute resolution (ODR). "Through online dispute resolution, parties can have their issues resolved by enrolled members." Participants in the forum can share videos and documents from their own devices whenever they want, without regard to location" (11).

Kabul, as the capital city, must coordinate sessions in both real-time and online participation systems. Kabul Municipality has already seen widespread participation. It is now time to put online discussion methods into practice alongside in-person participation. The discussion tool can be used on social media platforms such as Facebook, Twitter, WhatsApp, or any academic forum. KM and Nagoya Institute of Technology recently signed a joint research agreement to put the online participatory approach into practice. The goal of this research agreement is to discuss a specific topic and obtain agreement from various parties in an online setting.

Finally, I propose comprehensive urban planning methods based on participatory approaches. Civil participation expands development options, and residents will be pleased that they are involved in decisions that affect their lives. As a result of the mutual agreement between planners and community members, sustainable development will be enhanced.

4. Conclusion:

Kabul is one of the world's fastest-growing cities. In recent decades, the city has experienced rapid urbanization. The approach to the planning process was capitalistic, and the public was excluded from the process. In closed-door offices, authorities and urban planners were attempting to prepare urban projects (Detail Plans). Residents protested the projects' implementation because they were excluded from the planning and decision-making processes.

On the other hand, the participatory approach has recently been recognized as an effective method of incorporating it into planning processes. In Kabul Municipality, some new methods are being used to ensure that citizen participation is essential from the start to the end of the project. These methods are intended to be alternatives to Detail Planning and land acquisition methods. Building consensus is a topic that requires discussion and agreement status. The paradigms of the participatory approach vary and can be located and time-dependent or limitless. Meetings or workshops can be held in a specific location with mass participation, or they can be held in online forums with discussions based on each individual's available time.

Acknowledgment

This paper is the result of an academic investigation into the literature on participatory approaches and Kabul urban data documents. I'd like to thank everyone who assisted me with my research. My co-authors did an excellent job by participating in all aspects of the article.

References

[1] MUDL, 2015, *Afghanistan country Report for Habitat 3*: the Islamic Republic of Afghanistan, managing rapid urbanization.

[2] Sasaki, Kabul Urban Design Framework, Executive Summary, A vision for sustainable and vibrant Kabul, Sasaki Company, USA.

[3] Joe Beall and Daniel Esser, 2005, shaping urban futures: challenges to governing and managing afghan cities, Afghanistan Research and Evaluation Unit, Afghanistan.

[4] Yachiyo Engineering Co. Ltd., 2011, Draft Kabul City Master Plan, RECS International Inc., Afghanistan.

[5] Jan-Hendrik LE ROUX, Elizelle Juaneé CILLIERS, 2013, the Participatory Planning Paradigm Shift: Comparing Disciplines and Methods, 49th ISOCARP Congress, North West University, South Africa, page 1.

[6] Jim Cavaye, 2015, Understanding Community Development. Cavaye Community Development.

[7]) Quran, Sura Al I-Imran, Ayah 103.

[8] Nick Wates, 2008, *the community Planning Event Manual*, UK (how to use Collaborative Planning and Urban Design Events).

[9] Kabul Municipality,2009, Kabul Solidary Program Document, KM, Kabul-Afghanistan.

[10] Takayuki Ito, 2018, COLLAGREE: Facilitator-mediated Large-scale Consensus Support System-Takayuki Ito, *The Ninth International Automated Negotiating Agent Competition, Nagoya, Japan.*

[11] VIVI TAN, 2019, Online Dispute Resolution for Small Civil Claims in Victoria: A New Paradigm in Civil Justice, Victoria, Canada.

Authors Profile:

Mohammad Ramin Amiryar received a B.Sc. degree in Architecture from Kabul Polytechnic University. He has got his master ‘degree in urban Environmental Planning and Policy Making from the Toyohashi University of Technology. He is currently a Ph.D. Candidate at the Toyohashi University of Technology majoring in Urban Environmental and Policy Making. He has worked as head of the Urban Planning Department in Kabul Municipality for many years. Besides, he is currently working as a consultant at Okumura Design Company

Ahmad Jawad Niazi received a B.S. degree in Architecture Engineering from Kabul Polytechnic University in 2010 an M.S. degree in Civil and Industrial Structures from KPU in 2013, M. Plan in Urban and Regional Planning from UoP. Presently, Ph.D. in Architecture & Ekistics from OPJS. He is working as an Associate Professor in Department of Architecture & Urban Planning, Kabul Polytechnic University, Kabul, Afghanistan. His areas of research include Ekistics, Urban Governance, Planning, Sustainable, and Islamic Architecture.

Shahpiri Pirzad Sediq is a resident of the Andar district of Ghazni province, she is working as an Assistant Professor at the Department of Technical Drawing of Construction Faculty of Kabul Polytechnic University.

She received her master’s degree in Industrial and Civil Engineering in 1367 from Kabul Polytechnic University.

KPU International Journal of Engineering & Technology
Volume 2, Issue2, Dec. 2022
e-ISSN:2790-0819, p-ISSN:2790-0800
Date Received: 2022-08-07
Date Accepted: 2022-12-23
Date Published: 2022-12-30

Seismic Performance of Tall Buildings with and Without Outrigger and Belt Truss Systems

EZATULLAH YAQUBI[1*], AHMAD JAWID RAHIMI[2], NASIBA FAKOR[3], PARWANA YAQUBI[4]

[1*]Assist. Professor, Department of Civil and Industrial Construction, Jawzjan University, Sheberghan, Afghanistan.
Email: ezatullahyaqubi651@gmail.com

[2]Assist. Professor, Department of Civil and Industrial Construction, Jawzjan University, Sheberghan, Afghanistan.
Email: jawidrshimi@gmail.com

[3]Assist. Professor, Department of Civil and Industrial Construction, Jawzjan University, Sheberghan, Afghanistan.
Email: Nasibafakor@gmail.com

[4]Lecturer, Department of Construction Engineering, Jawzjan Technical Institute, Sheberghan, Afghanistan.
Email: Parwanayaqubi1991@gmail.com

Abstract

The construction of tall buildings today is increasing all over the world to meet the needs and challenges of the construction industry. The intention to build tall buildings is due to population growth and insufficient horizontal space. The increase in height of tall buildings requires special attention to the lateral stiffness of the structure, where the introduction of outrigger sections and belt trusses plays an essential role. In this paper, an investigation has been performed to study the behavior of outrigger and belt trusses in different locations of the building using response spectrum analysis. For this analysis, a three-dimensional building model is developed for G + 16, G + 20, and G + 24 RC buildings with and without outrigger and belt truss systems to find out the performance of outrigger and belt trusses subjected to earthquake loading conditions. The analysis is done by dynamic analysis (Response spectrum method) in the zone (IV) as per IS code, using ETABS software, and the analysis results were compared among lateral displacements, story drift, and story stiffness to find out the optimal position of outriggers and an efficient reduction of story displacement and story drift in a tall building. It was observed that the introduction of outrigger and belt trusses at the middle stories reduces considerable story displacement and drift and enhances the stiffness of the structure. By providing outriggers and belt truss systems in middle stories, story displacement is reduced up to 60%, story drift is reduced by up to 50%, and story stiffness is increased by up to 10%.

Keywords: Outrigger and belt trusses, Response spectrum, Story displacement, Story drift, Story stiffness

* Corresponding Author

1. Introduction

Recent technological developments in several aspects related to building materials, construction methods and equipment, analysis, and structural design have allowed tall buildings to spread all over the world, especially in emerging economies. Tall buildings play a major role as important structures in urban and developed cities. High-rise buildings represent a potential solution from an economic, ecological, and social point of view [1], [6]. In addition, the lack of land in some cities has led to increasing demand for tall buildings in that cities [3], [9]. The race to the sky to build the tallest building is primarily associated with the development of innovative and innovative lateral load resistance systems. Over the past five decades, engineers have been able to develop several new framing options as structural systems (e.g. diagonal system, outrigger system, attached duct system) in many tall buildings to meet the criteria of aesthetics, ease of maintenance, and safety in addition to minimizing materials consumption [7],[13]. The outrigger and belt truss systems are one of the most effective structural systems for resisting lateral loads. The outrigger and belt truss systems consist of the central core of the brace or shear wall and the horizontal supports or deep beams connecting the central core to the perimeter columns. The loads are transferred from the core to the outer columns by two technical methods or in the other sense, there are two types of stable systems depending on the transmission, namely the conventional system and the virtual system [5],[15]. The conventional type of system means that the earthquake moment is transmitted directly from the inner core walls to the outer columns of the building through rigid supports. But this type of virtual system relies on inflexible dual-floor diaphragms to transmit seismic moments from the core to the building's outer columns. [11].

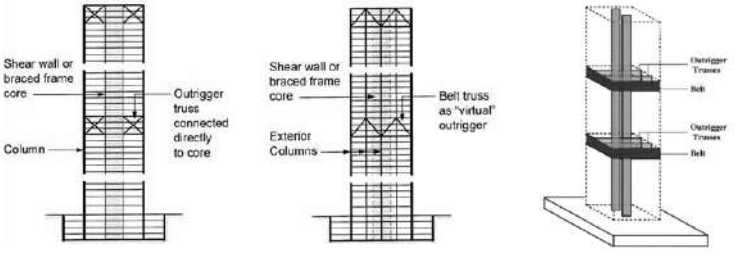

Figure 1. Conventional and virtual outrigger and belt truss system [11],[7].

As per (IS 16700-2017), A building of height greater than 50m, but less than or equal to 250m is called a tall building. In 1965, Fazlur Khan classified structural systems according to their ability to withstand lateral loads. This classification divides structural systems into four categories as shown in Figure 2.

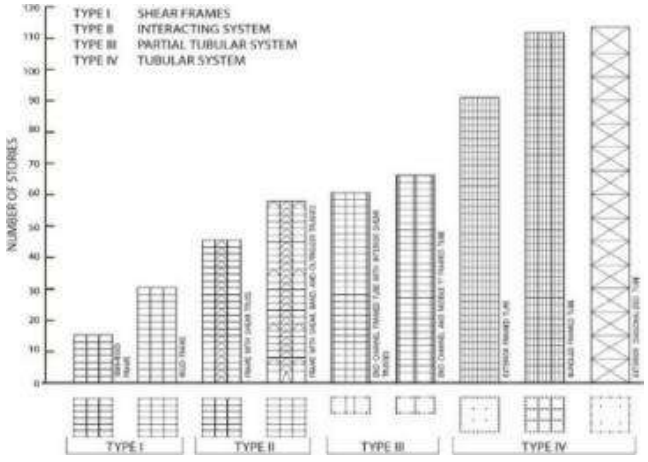

Figure 2. A structural system of tall buildings [5].

2. Literature Review

Amoussou et al. (2021) did an investigation on simplified modeling and analysis methods for skyscrapers with outrigger systems. The results of the simplified approach were verified with the analysis results of the detailed ETABS model, where static, modal, and dynamic analyses were performed. The applicability of the proposed method to different configurations of high-rise buildings with outrigger systems was also verified by a parametric study. A comparative study with several previous studies was performed to demonstrate the effectiveness of the proposed method. It was found that the applied simple modeling method has good accuracy in predicting the horizontal displacement and interstate deviation in linear and nonlinear analysis. As a result, the simplified modeling approach gives a deep understanding of the outrigger system behavior and its parameters. Wael Al Haddad et al. (2020) did a comprehensive research on the introduction of outrigger and belt truss systems in skyscrapers. The actual definition of outrigger and belt truss systems, different configurations and structural materials of the outrigger and belt truss system, the operation of the outrigger and belt truss system, and the advantages and disadvantages of the outrigger and belt systems were discussed. Ho, G. W. (2016) has evaluated the performance of the outrigger system in tall buildings. The concept of the outrigger system, optimum topology, design, and construction consideration was studied and presented. Lee, S., & Tovar, A. (2014) have done an investigation of the location of outriggers in high-rise buildings using topology optimization. The results showed that the outrigger placement problem was solved using topology optimization. The further method was used for the material penalty parameter to obtain the plane "0–1". The versatility of the proposed design method has been demonstrated using a realistic FEM model of a three-dimensional 201 m tall building. Kiran et al. (2012) have studied the static and dynamic behavior of outrigger systems for tall buildings. various alternative 3D models have been made using ETABS software for reinforced concrete structures with a central core with an outrigger and without an outrigger by varying the relative flexural stiffness from 0.25 to 2.0 with step 0.25. In addition, the position of the outriggers was modified along the height of the building by considering the relative height parameter of the outriggers

from 0.975 to 0.4. The results show that the performance of the outrigger is most effective for the relative height of the outrigger equal to 0.5.

This research focused on performing a comparison between RC framed irregular buildings with and without concrete outrigger and belt trusses structural systems as diagonal elements in different locations along the height of the buildings to find the suitable location which reduces the story displacement, story drift and increases the stiffness of the building under actual strong earthquakes by using ETABS software.

3. Objective of Study

In the present paper, the seismic performance of tall buildings with and without outrigger and belt truss systems are carried out in zone IV using Response spectrum analysis. Outrigger and belt trusses in two different locations are studied. Different characteristics like story displacements, the story drifts, and story stiffness of tall buildings with and without outrigger and belt trusses along X&Y directions are studied.

4. Methodology

In this research work modeling and analysis of the G+16, G+20, and G+24 buildings have been done in ETABS. The height of buildings (G+16=51m, G+20=63m, and G+24=75m) are greater than 15 m and are located in zone IV, a static analysis method is not applicable. Hence analysis of structures is carried out by linear dynamic analysis (Response spectrum method).

5. Modeling and Analysis

In this research, three buildings with different heights (G+16, G+20, and G+24), with and without outrigger and belt truss systems are considered. Outrigger and belt truss systems are introduced as RC diagonal members in ETABS. The exact dimension of the outrigger and belt trusses found after the design check-in ETABS. The necessary data for analyzing the buildings are given in Tables [1], [2], and [3] as follows:

Table 1: Geotechnical and Geological Data

S.No	*Variable*	*Type*	*Reference*
1	Type of soil	Medium soil	IS 1893(part 1):2016 [18]
2	Type of foundation	Raft footing	IS 2950(part1):1981 [19]
3	seismic zone	IV	IS 1893(part 1):2016 [18]
4	seismic zone factor	0.24	IS 1893(part 1):2016 [18]

Table 2: General data collection and condition assessment of the building

S.No	*Description*	*Information*	*Remarks*
1	Type of building usage	Residential	
2	Plan Size	30m×40m	
3	Building height	G+16=51m	
		G+20=63m	
		G+24=75m	
4	Building structure	Special moment frame with structural wall	IS 1893(part 1):2016 [18]
5	Open ground story	yes	

6	Horizontal floor system	Beams and slabs	IS 456: (2000) [22]
7	Grade of concrete	M30, M40	IS 10262: 2009 [20],[22]
8	Grade of steel	Fe 500	IS 431(part 1): 1982 [21]
9	Used software	ETABS 19.1.0	

Table 3: Dimension of the structural members

G+16		
S.No	*Member*	*Dimension (mm)*
1	Column	400×700
2	Beam	300×500
3	Central core shear wall	300
4	Exterior and Interior masonry walls	250&150
5	Slab thickness	150
G+20		
6	Column	400×900
7	Beam	300×500
8	Central core shear wall	300
9	Exterior and Interior masonry walls	250&150
10	Slab thickness	150
G+24		
11	Column	500×1000
12	Beam	300×500
13	Central core shear wall	400
14	Exterior and Interior masonry walls	250&150
15	Slab thickness	150

All the structural members which are shown In Table 3 are defined according to the design check of ETABS software, in which the column size, beams, and so on are taken differently by the change of the number of stories.

In this research paper, all frames are modeled as a special moment-resisting frame having central core shear walls. Columns and beams are modeled as frame elements and shear walls are modeled as shell elements. The test models are including two different types of models:

1. Conventional building.
2. Building with two different numbers and locations of outrigger and belt trusses systems.

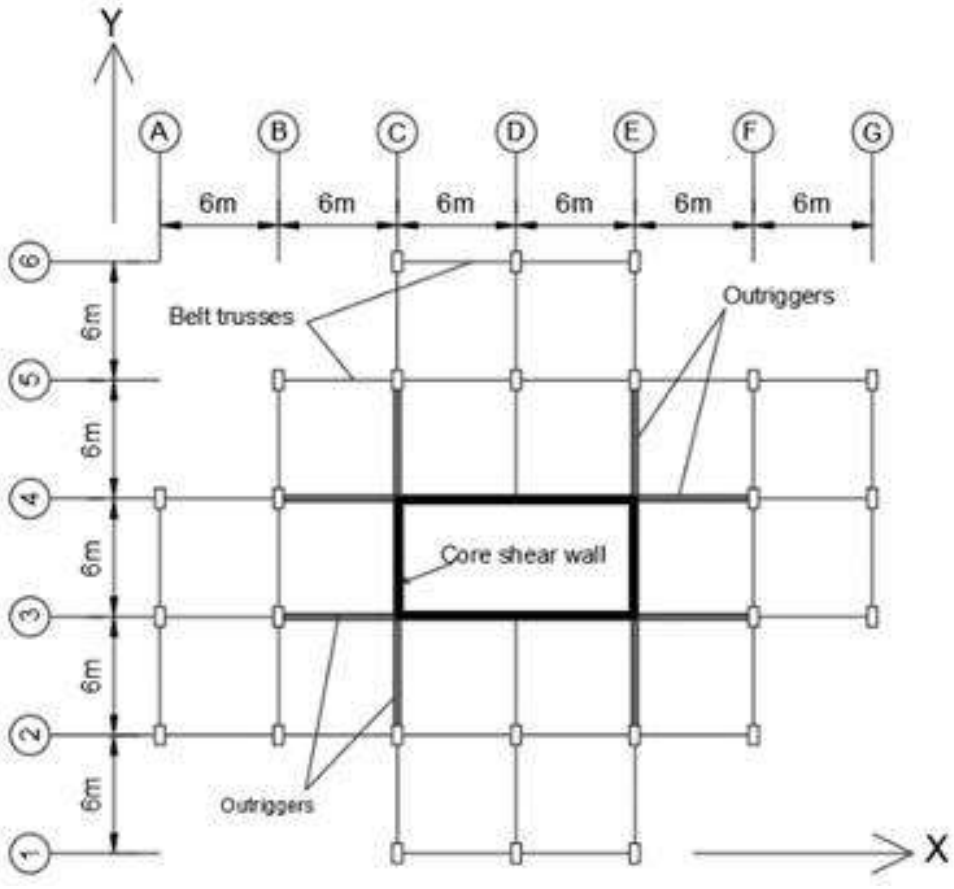

Figure 3. Plan of the building.

The designation of the test models is as follows:

1. MOB1-G+16 without outrigger and belt truss systems as presented in Figure 4a.
2. MOB2-G+16 with outrigger and belt truss systems in the 9th and 16th stories as presented in Figure 4b.
3. MOB3-G+16 with outrigger and belt truss systems in the 6th and 13th stories as presented in Figure 4c.
4. MOB4-G+20 without outrigger and belt truss systems as presented in Figure 4d.
5. MOB5-G+20 with outrigger and belt truss systems in the 10th and 20th stories as presented in Figure 4e.
6. MOB6-G+20 with outrigger and belt truss systems in 7th and 15th as presented in Figure 4f.
7. MOB7-G+24 without outrigger and belt truss systems as presented in Figure 4g.
8. MOB8-G+24 with outrigger and belt truss systems in the 14th and 24th stories as presented in Figure 4h.
9. MOB9-G+24 with outrigger and belt truss systems in 9th and 18th as presented in Figure 4i.

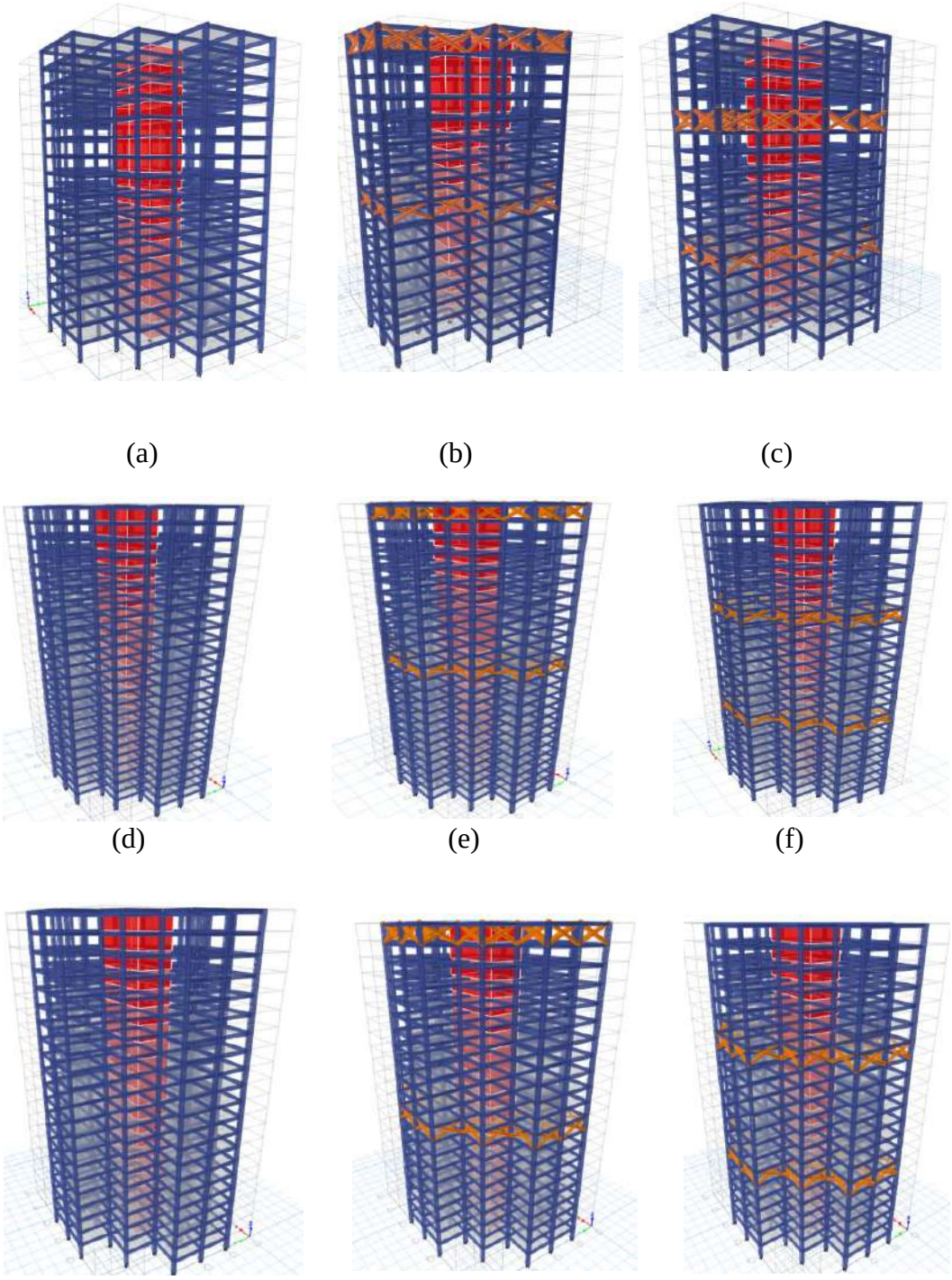

(a) (b) (c)

(d) (e) (f)

(g) (h) (i)

Figure 4. Buildings with and without outrigger and belt truss systems.

6. Results and Discussions

The results obtained from the analysis of models are compared and discussed as follows.

The variation of story displacements in tall buildings with and without outrigger and belt truss systems under seismic loads as indicated in Figure 5, is observed that in G+16 buildings the story displacement was reduced by 16.29% along the X-direction and 12.7% along the Y-direction by providing outriggers and built truss systems on 9th&last floors and reduced by 16.7% along X-direction and 13.8% along Y-direction by providing outriggers in 6th&13th floors. In G+20 buildings, the story displacement was reduced by 10.45% along the X-direction, and 12.4% along the Y-direction by providing outriggers and built truss systems on the 10th&last floors and reduced by 9.7% along the X-direction and 13.4% along Y-direction by providing outriggers and built truss systems on 7th&15th floors. In G+24 buildings, the story displacement was reduced by 10.14% along the X-direction, and 58.6% along the Y-direction by providing outriggers and built truss systems on the 14th& 24th floors and reduced by 11.4% along the X-direction and 58.5% along Y-direction by providing outriggers and built truss systems on 9th&18th floors.

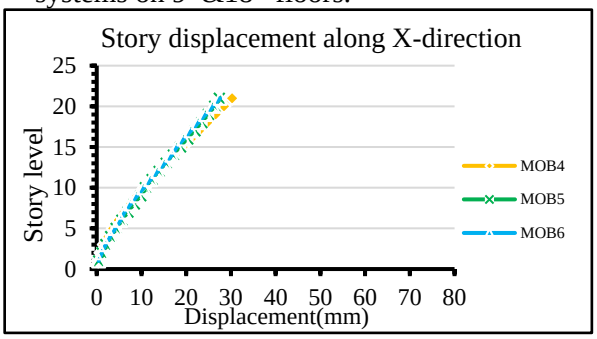

(a)

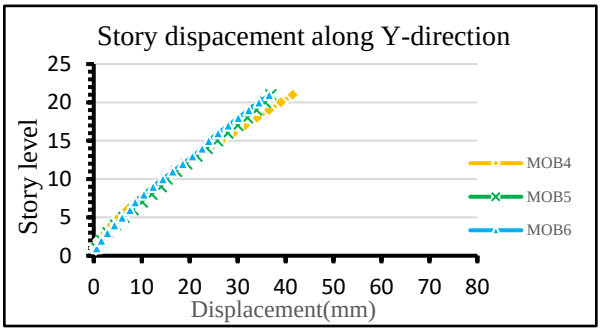

(b)

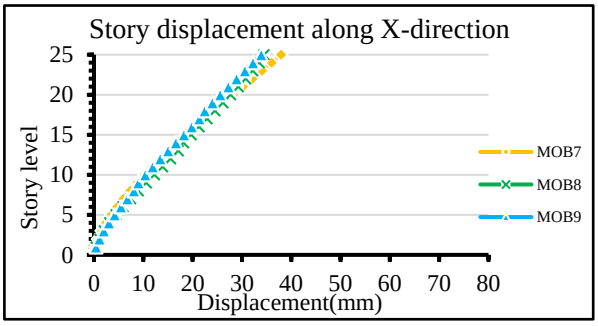

(c)

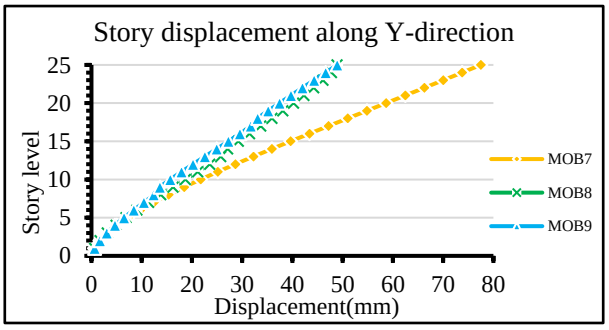

(d)

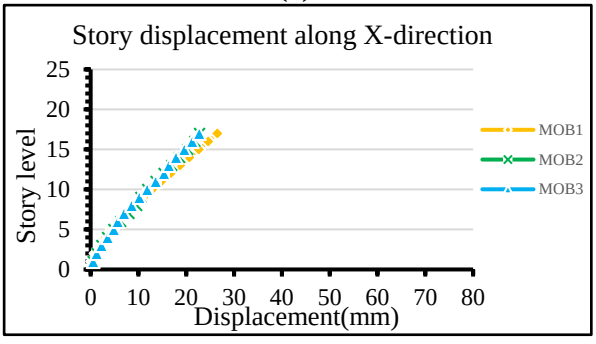

(e)

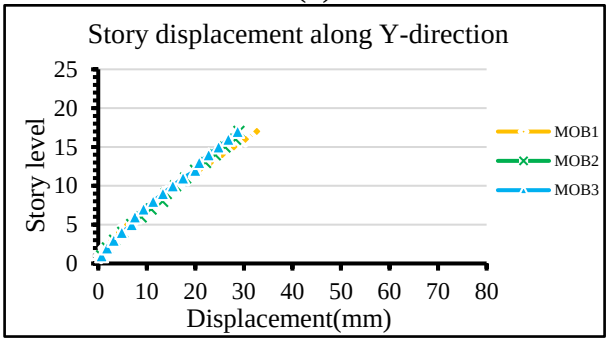

(f)

Figure 5. Story displacement (a) Story displacement along X-direction in G+16, (b) Story displacement along Y-direction in G+16, (c) Story displacement along X-direction in G+20, (d) Story displacement along Y-direction in G+20, (e) Story displacement along X-direction in G+24 and (f) Story displacement along Y-direction in G+24.

The variation of story drifts in tall buildings with and without outrigger and belt truss systems under seismic loads as indicated in Figure 6, clearly indicates the reduction of story drift in buildings with outrigger and belt truss systems. In G+16 buildings the story drift was reduced by 7.6% along the X-direction and 2.6% along the Y-direction by providing outriggers and built truss systems on the 9^{th}&last floors and reduced by 8.5% along the X-direction and 6.6% along Y-direction by providing outriggers in 6^{th}&13^{th} floors. In G+20 buildings, the story drifts were reduced by 12.3% along the X-direction, and 11.9% along the Y-direction by providing outriggers and built truss systems on the 10^{th}&last floors and reduced by 11.7% along the X-direction and 12.3% along Y-direction by providing outriggers and built truss systems on 7^{th}&15^{th} floors. In G+24 buildings, the story drifts were reduced by 16.5% along the X-direction, and 57.6% along the Y-direction by providing outriggers and built truss systems on the 14^{th}& 24^{th} floors and reduced by 12.9% along the X-direction and 55.8% along Y-direction by providing outriggers and built truss systems on 9^{th}&18^{th} floors.

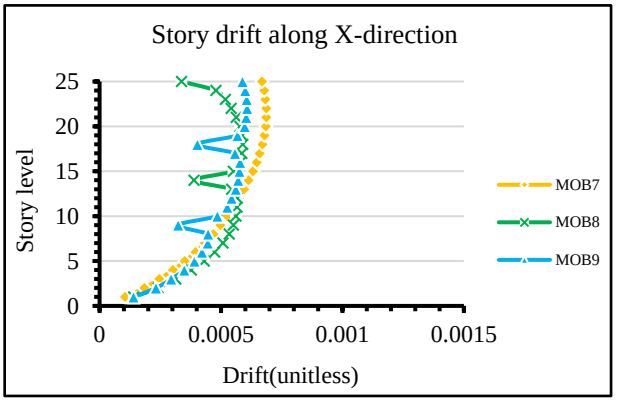

(a)

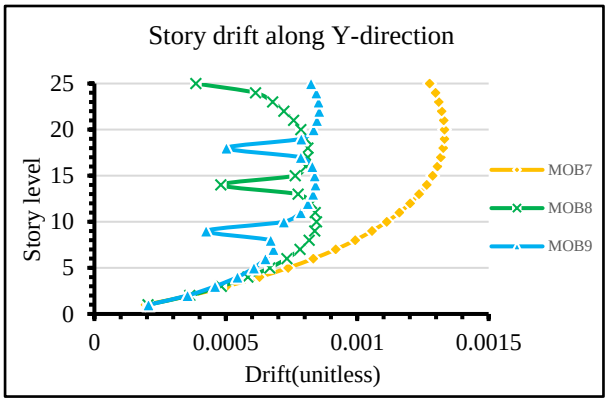

(b)

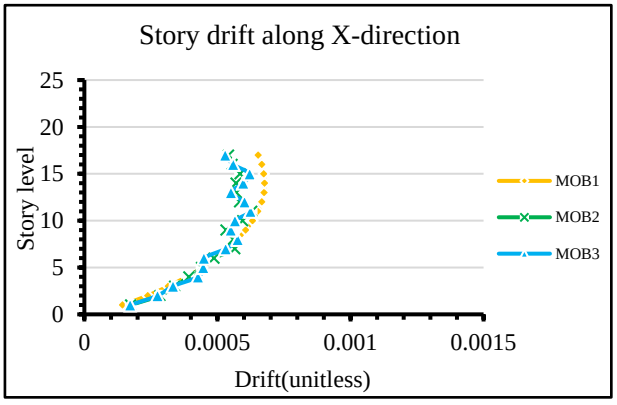

(c)

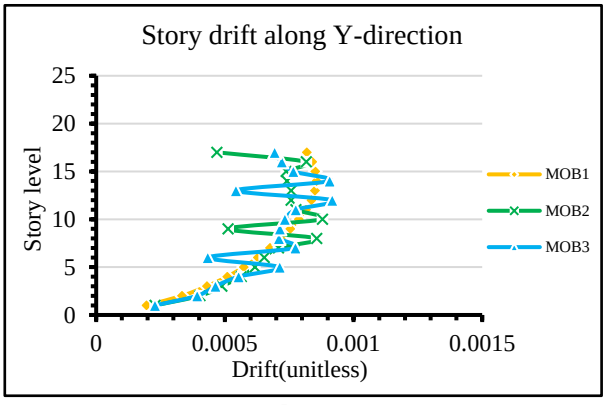

(d)

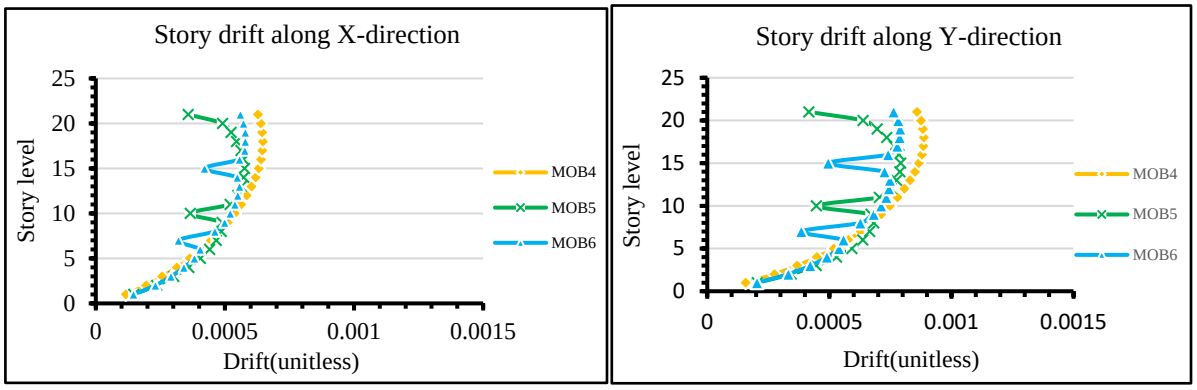

(e) (f)

Figure 6. The story drifts (a) Story drift along the X-direction in G+16, (b) Story drift along the Y-direction in G+16, (c) Story drift along the X-direction in G+20, (d) Story drift along the Y-direction in G+20, (e) Story drift along X-direction in G+24 and (f) Story drift along Y-direction in G+24.

The variation of story stiffness in tall buildings with and without outrigger and belt truss systems under seismic loads as indicated in Figure 7, clearly indicates the increase of story stiffness in buildings with outrigger and belt truss systems. In G+16 buildings the story stiffness increases by 3.1% along the X-direction and 2.7% along the Y-direction by providing outriggers and built truss systems on the 9th&last floors and increases by 5.6% along the X-direction and 5.8% along Y-direction by providing outriggers in 6th&13th floors. In G+20 buildings, the story stiffness increased by 27.9% along the X-direction, and 30.2% along the Y-direction by providing outriggers and built truss systems on the 10th&last floors and increase by 22.8% along the X-direction and 26.4% along Y-direction by providing outriggers and built truss systems on 7th&15th floors. In G+24 buildings, the story stiffness increases by 31.4% along the X-direction, and 16.9% along the Y-direction by providing outriggers and built truss systems on the 14th&24th floors and increases by 27.9% along the X-direction and 14.8% along Y-direction by providing outriggers and built truss systems on 9th&18th floors.

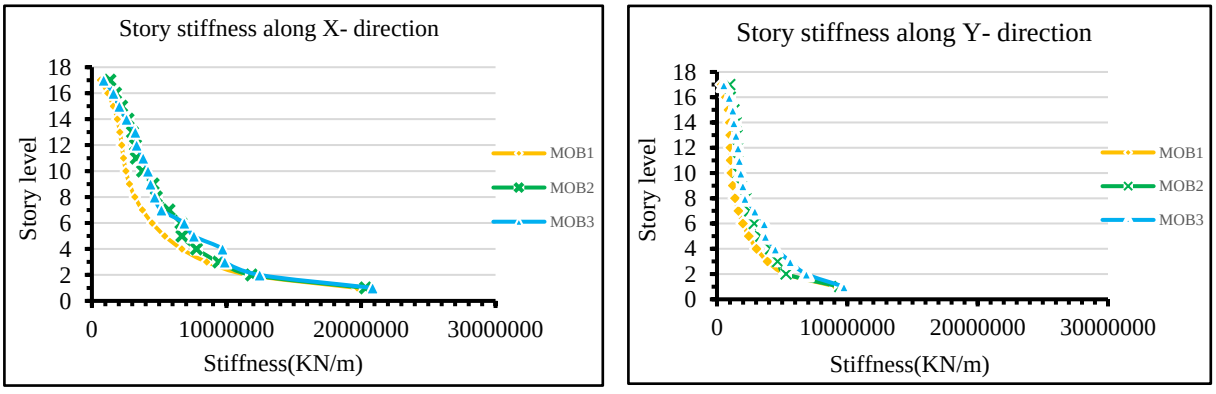

(a) (b)

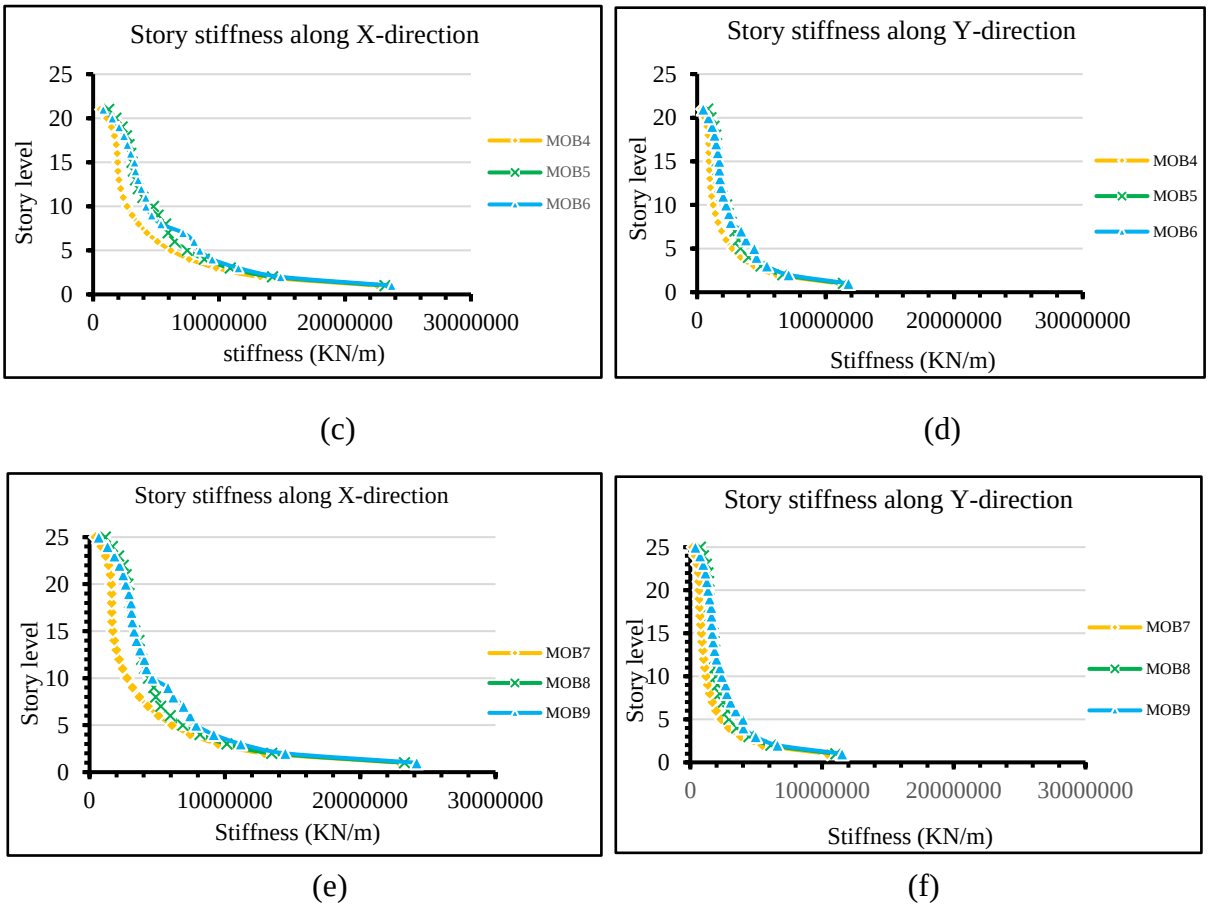

Figure 7. Story stiffness (a) Story stiffness along X-direction in G+16, (b) Story stiffness along Y-direction in G+16, (c) Story stiffness along X-direction in G+20, (d) Story stiffness along Y-direction in G+20, (e) Story stiffness along X-direction in G+24 and (f) Story stiffness along Y-direction in G+24.

7. Conclusion

The utilization of outriggers and belt trusses in tall buildings increases stiffness and reduces story displacement and story drift under lateral loads. Based on the results obtained from the analysis, the following conclusion was made:

- Outrigger and belt truss systems increase the performance of the building while subjected to earthquake loads by increasing the story stiffness and reducing the story displacement and story drift.
- The outrigger and belt truss systems at the top of the building are less efficient, the outrigger and belt truss systems are better to provide at mid-height, the benefits of placing at the middle stories resulting up to 50% reduction in story drift, and up to 60% reduction in story displacement.
- Providing the outrigger and belt truss systems increases the stiffness of the building under earthquake loads by up to 10%.

References

1. Al-Kodmany, K. (2018), "The sustainability of tall building developments," A conceptual framework. Buildings., vol.8, no. 1, pp. 1-31.
2. Alhaddad, W., Halabi, Y., Xu, H., and Lei, H. (2020), "A comprehensive introduction to outrigger and belt-truss system in skyscrapers," In Structures, Vol. 27, pp. 989-998. Elsevier.
3. Ali, M. M., and Moon, K. S. (2007), "Structural developments in tall buildings: current trends and prospects," Architectural science review, vol. 50, no. 3, pp. 205-223.
4. Amoussou, C. P. D., Lei, H., Alhaddad, W., and Halabi, Y. (2021), "Simplified modeling and analysis method for skyscrapers with outrigger system," In Structures, Vol. 33, pp. 1033-1050. Elsevier.
5. Choi, H. S., Ho, G., Joseph, L., & Mathias, N. (2017), "Introduction to Outrigger Systems. Outrigger Design for High-Rise Buildings. Routledge
6. Elbakheit, AR. (2012), "Why tall buildings," The potential of sustainable technologies in tall buildings. Int J High-Rise Build., vol. 1, no. 2, pp. 117-123.
7. Gunel, M. H., and Ilgin, H. E. (2007), "A proposal for the classification of structural systems of tall buildings," Building and Environment, vol. 42, no, 7, pp. 2667-2675.
8. Ho, G. W. (2016), "The evolution of outrigger system in tall buildings," International Journal of High-Rise Buildings, vol. 5, no. 1, pp. 21-30.
9. Kayvani, K. (2014), "Design of high-rise buildings: past, present and future," in ST Smith (ed.), 23rd Australasian Conference on the Mechanics of Structures and Materials (ACMSM23), vol. I, Byron Bay, NSW, 9-12 December, Southern Cross University, Lismore, NSW, pp. 15-20. ISBN: 9780994152008.
10. Kamath, K., Divya, N., and Rao, A. U. (2012), "A study on the static and dynamic behavior of outrigger structural system for tall buildings," Bonfring international journal of industrial Engineering and Management Science, vol. 2, no. 4, pp. 15-20.
11. Khandelwal, R., and Singh, S. (2020), "Optimum Shape and Position of Outrigger System for High Rise Building under Earthquake Loading," Regular Issue, vol. 9, no. 3, pp.3268–3275.
12. Khanorkar, A., Sukhdeve, S., Denge, S. V., and Raut, S. P. (2016), "Outrigger and belt truss system for a tall building to control deflection: A review," GRD Journals-Global Research and Development Journal for Engineering, vol. 1, no. 6, pp. 6-15.
13. Kowal, Z. (2011), "The formation of space bar structures supported by the system reliability theory," Archives of civil and mechanical engineering, vol. 11, no. 1, pp. 115-133.
14. Lee, S., and Tovar, A. (2014), "Outrigger placement in tall buildings using topology optimization," Engineering Structures, vol. 74, pp. 122-129.
15. Rathore, A., and Maru, S. (2017), "Dynamic Analysis of outrigger structural system in a tall building," International Journal of Modern Trends in Engineering & Research, vol. 4, no. 12, pp. 199–208.
16. Smith, B. S., Coull, A., and Stafford-Smith, B. S. (1991), "Tall building structures: analysis and design," Vol. 5. New York: Wiley.
17. Taranath, B.S. (2016), "Structural analysis and design of a tall building," New York: The William Byrd Press.
18. IS 1893 part 1 (2016): Criteria for Earthquake Resistant Design of Structures.
19. IS 2950 part 1(1981): Code of Practice for Design and Construction of Raft Foundation.
20. IS 10262 (2019): Concrete Mix Proportioning – Guidelines.
21. IS 431 part 1(1982): Mild Steel and Medium Tensile Steel Bars and Hard-Drawn Steel Wire for Concrete Reinforcement.
22. IS 456 (2000): Plain and Reinforced Concrete - Code of Practice.
23. IS 875 part 1 (1987): Code of Practice for Design Loads (Other than Earthquake) for Buildings and Structures.

24. IS 875 part 2 (1987): Code of Practice for Design Loads (Other than Earthquake) for Buildings and Structures.

Authors Profile:

Ezatullah Yaqubi received a B. Eng. degree in Civil and Industrial Engineering from Kabul Polytechnic University, Kabul Afghanistan in 2014 and M. Tech in Structural engineering from Osmania University, Hyderabad, Telangana, India in 2022. Currently, he is working as a lecturer in the Department of Civil and industrial engineering of the Construction Faculty of Jawzjan University. His area of research includes Structural Analysis, Structural Dynamics, Concrete structures, and Earthquake Engineering.

Ahmad Jawid Rahimi received a B. Eng. degree in Civil and industrial engineering from Jawzjan University, Jawzjan Afghanistan in 2014 and M. Tech in Structural Engineering from Amity University, Noida, Delhi NCR, and India in 2019. Currently, he is working as a lecturer in the Department of Civil and industrial engineering of the Construction Faculty of Jawzjan University. His area of research includes Structural Analysis, Concrete and steel structures, Construction management, and Earthquake Engineering.

Nasiba Fakor received a B. Eng. degree in Civil and industrial engineering from Jawzjan University, Jawzjan Afghanistan in 2014 and M. Tech in Civil and Industrial Engineering from KPU, Kabul Afghanistan in 2020. Currently, she is working as a lecturer in the Department of Civil and industrial engineering of the Construction Faculty of Jawzjan University. Her area of research includes Construction Technology, Construction Management, and Earthquake Engineering.

Parwana Yaqubi received a B. Eng. degree in Civil and industrial engineering from Jawzjan University, Jawzjan Afghanistan in 2015. Currently, she is working as a lecturer in the Department of Construction Engineering of Jawzjan Technical Institute. Her area of research includes Structural Analysis, Construction Technology, Construction Management, and Earthquake Engineering.

KPU International Journal of Engineering & Technology
Volume 2, Issue2, Dec. 2022
e-ISSN:2790-0819, p-ISSN:2790-0800

Date Received: 2022-08-13
Date Accepted: 2022-12-24
Date Published: 2022-12-30

Combined Tapered Optical Fiber and FBG Sensor for Temperature and Strain Measurement

HAMEEDULLAH ZAHIN[1*], FAZALULLAH MARUFI[2]

[1]Teaching Assistant, Department of physics, Education Faculty, Urozgan University, Khayro kariz, Tarinkot, Afghanistan. Email: zhameedullah12@gmail.com

[2]Teaching Assistant, Department of Physics, Education Faculty, Urozgan University, Khayro kariz, Tarinkot, Afghanistan. Email: fmarufi1@gmail.com

Abstract

Fiber Bragg Grating (FBG) sensors have found more usages in the industry to diagnose the safety of mechanical structures due to their high sensitivity, non-exposure to the electromagnetic field, linearity, and lightness. A limitation of the application of FBG sensors is the inability to distinguish the effects of temperature and strain in the simultaneous measurement. For this purpose, we must somehow discriminate the effect of temperature on the strain. In this Article, by designing a tapered fiber-FBG composite sensor we have provided a solution for this problem. Studies performed on the designed composite sensor show that no sensitivity interference will occur in the sensor. In the composite sensor, a tapered fiber optic sensor with a temperature sensitivity of $-932.8\frac{pm}{℃}$ *and an FBG sensor with a temperature and strain sensitivity of* $9.89\frac{pm}{℃}$ *and* $0.92\frac{pm}{\mu\varepsilon}$*, respectively, are used.*

Keywords: Tapered fiber, Temperature sensor, FBG sensor, Strain, Structural health monitoring.

* Corresponding Author

1. Introduction

There are different types of optical fiber sensors, of which the thinned optical fiber sensor is one of the most important. In a standard optical fiber, the intensity of the wave field on the outer surface is almost zero. To make the optical fiber sensitive to the external environment, it is thinned. By tapering the optical fiber due to the reduction of the diameter of the optical fiber and the increase of the numerical aperture, the amount of penetration depth and the intensity of the attenuation wave field can be significantly increased [1,2].

This causes the output to show significant sensitivity to changes in the refractive index of the surrounding environment. Different parts of tapered optical fiber are shown in figure (1).

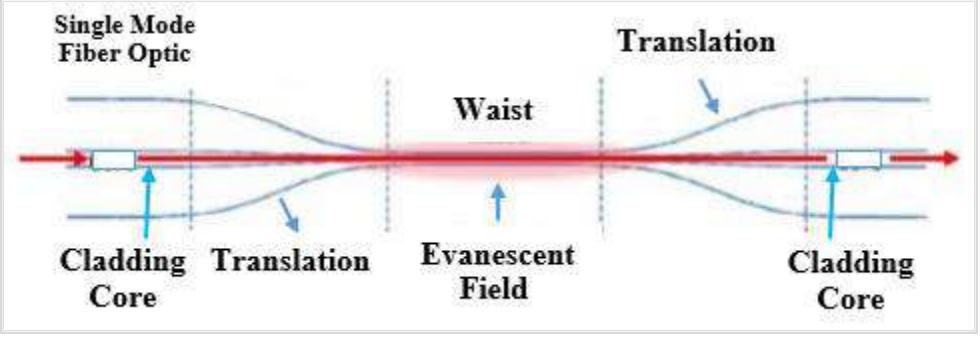

Figure (1). Schematic of tapered optical fiber and its different regions [3].

The performance of a tapered fiber optic-based temperature sensor relies on a sensitive laminated coating (absorber layer) on the surface of the optical fiber. In this situation, when the temperature of the surrounding environment changes, the physical and chemical properties of the tapered fiber change, and these changes change the properties of the light inside the fiber. Changes in the properties of the light beam inside the optical fiber include changes in the intensity, wavelength, or phase of the transmitted light; Therefore, by measuring the parameters of the transmitted light, the temperature value can be calculated (Figure (2)).

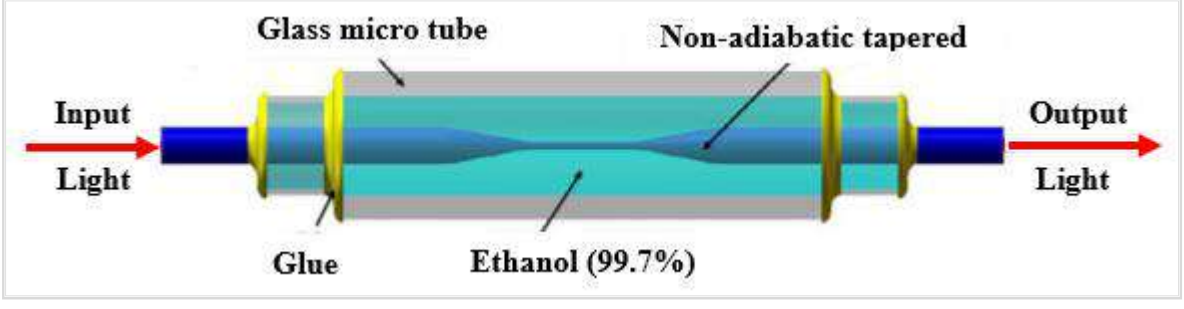

(Figure 2). Schematic diagram of temperature sensor based on thinned optical fiber [4].

Another type of fiber optic sensor is the Fiber Bragg Grating sensor. With the discovery of optical sensitivity in optical fibers, it became possible to make optical fiber Bragg Gratings. These gratings simply consist of periodic modulation of the refractive index inside the fiber optic core. Grid-like structures are very important in waveguide optics. Surface-enhanced lattice structures are used in flat waveguide optics for light refinement and coupling [5]. Optical fiber Bragg gratings have been considered a good sensor for measuring dynamic and static fields such as temperature and strain. One of the most important advantages of sensors made using optical fiber Bragg gratings is their wavelength-coding nature. This feature makes the Bragg grating sensors act as a self-reference, independent of the fluctuations of the light level and insensitive to changes in the light intensity of the source and losses caused by the connectors. Due to the low substitution loss and narrow bandwidth reflection wavelength, they can be easily wavelength multiplexed along a single-mode optical fiber [5]. Interferences of the refractive index lead to the reflection of light (propagated along the optical fiber) in a very small range of wavelengths, which is called the reflection wavelength of the Bragg grating or λ_B (Figure (3)). In addition to the periodicity of the Bragg grating, the reflected Bragg wavelength is dependent on temperature, strain, and other environmental factors, and by applying the smallest change in the said factors, we will have a shift in the reflected wavelength [6]. The intensified wavelength is reflected toward the source and the rest of the wavelengths pass through the part without change or attenuation. The reflection wavelength of an optical fiber Bragg grating is given as follows:

$$\lambda_B = 2n_{eff}\,\Lambda$$

Whereλ_B, n_{eff} and Λ is the Bragg wavelength (reflection wavelength), effective refractive index, and grating period, respectively.

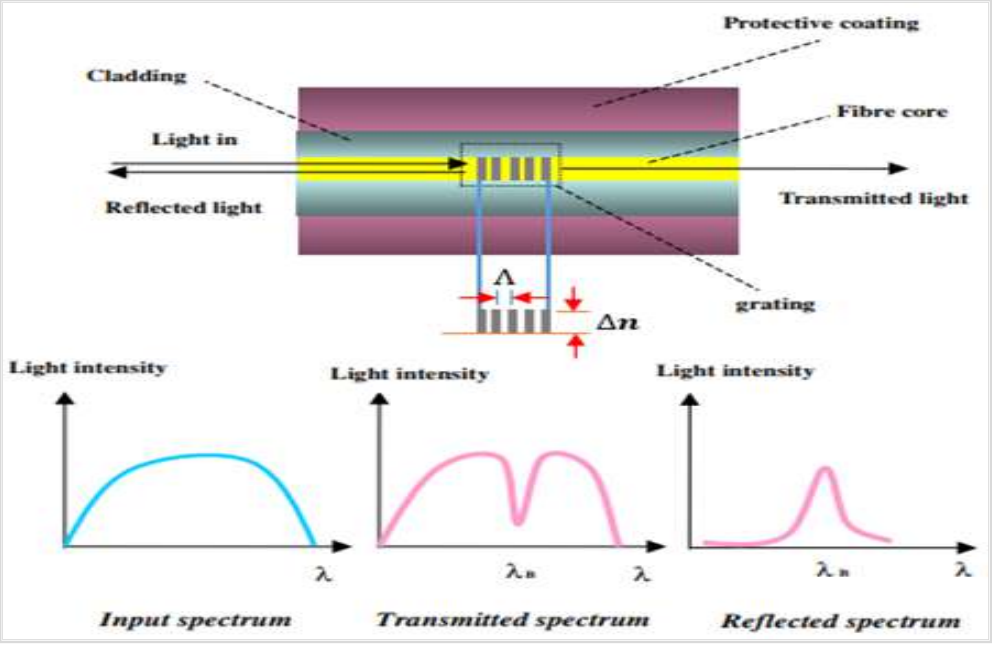

Figure (3). The general structure of optical fiber Bragg grating [7]

2. Research Methods

In this research, to Discrimination, the interference of temperature and strain in FBG sensors, a combined sensor design of tapered optical fiber (sensitive to temperature) and fiber optic Bragg grating sensor (sensitive to temperature and strain) was used to measure temperature and strain simultaneously and to separate We act on the effect of temperature and strain. By using the relationships between wavelength changes with strain and temperature, as well as measuring the amount of wavelength changed by each of the tapered optical fiber and the optical fiber Bragg grating, it is possible to determine the temperature and strain at the target point. To illustrate the proposed central idea, we use the experimental results of two types of sensors made by other groups. In reference [4], a temperature sensor based on tapered fiber has been tested. Temperature changes from 24°C to 38°C are considered with a step of 2°C. The wavelength range is from 1520 nm to 1620 nm, the waist diameter of the tapered area is about 8 micrometers and its length is about 20 mm. Also, the refractive index of 1.36 is considered. The value of the wavelength decreases almost linearly with increasing temperature, and the temperature sensitivity of -932.8 pm/°C has been obtained [4]. The diagram of the temperature relationship with wavelength changes for the temperature sensor based on non-adiabatic tapered optical fiber is given in figure (4).

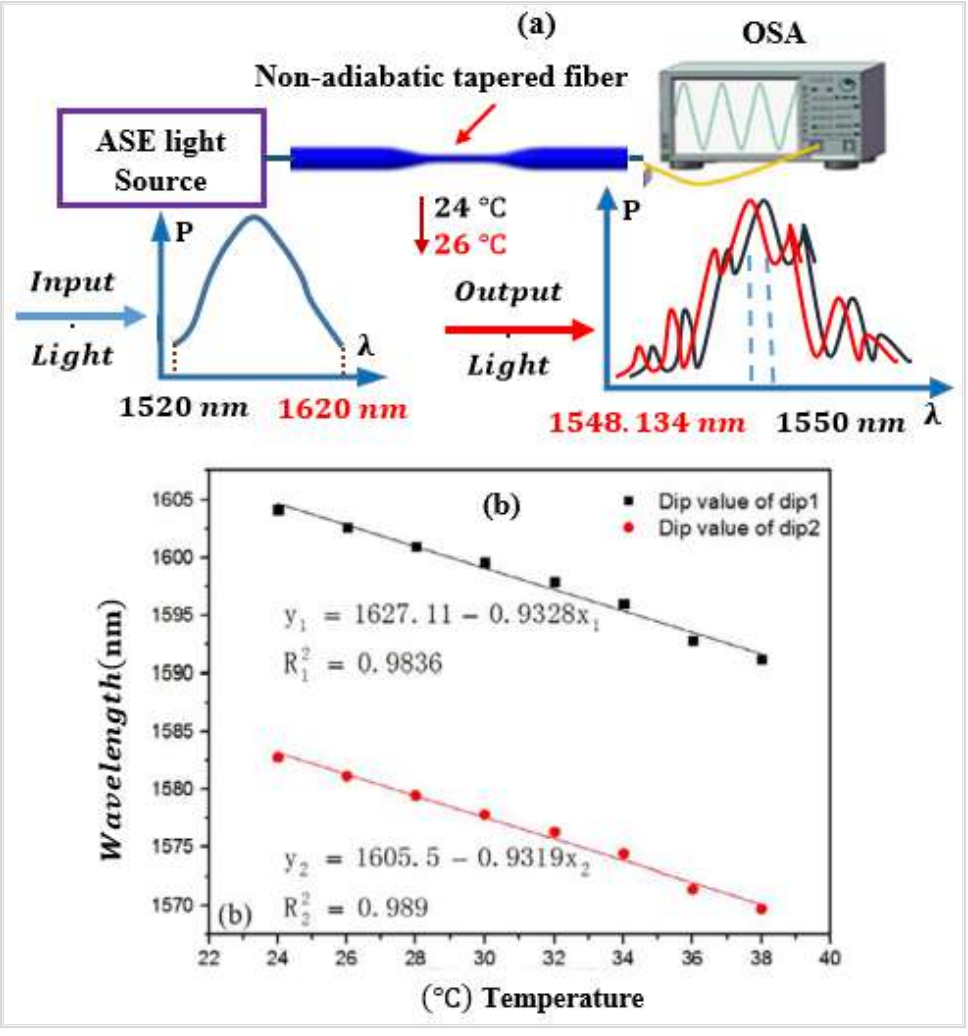

Figure (4). (a) Schematic diagram of tapered optical fiber-based temperature sensor arrangement which was designed by the author and (b) Wavelength change in the thinned optical fiber-based sensor due to temperature changes [4].

For the Bragg grating sensor, we use the laboratory results of reference [11]. The Bragg wavelength is 1530 nm, the effective refractive index is 1.444, and the temperature and strain sensitivity is $\frac{\Delta\lambda_B}{\Delta T} = 9.89\,{}^{pm}/_{°C}$ and $\frac{\Delta\lambda_B}{\Delta\varepsilon} = 0.92\,{}^{pm}/_{\mu\varepsilon}$ respectively, The temperature around the optical fiber Bragg grating was changed from 20°C to 80°C with a step of 20°C and the position of the reflection peak was measured. Wavelength changes in terms of temperature changes for the fiber Bragg grating are plotted in Figure (5).

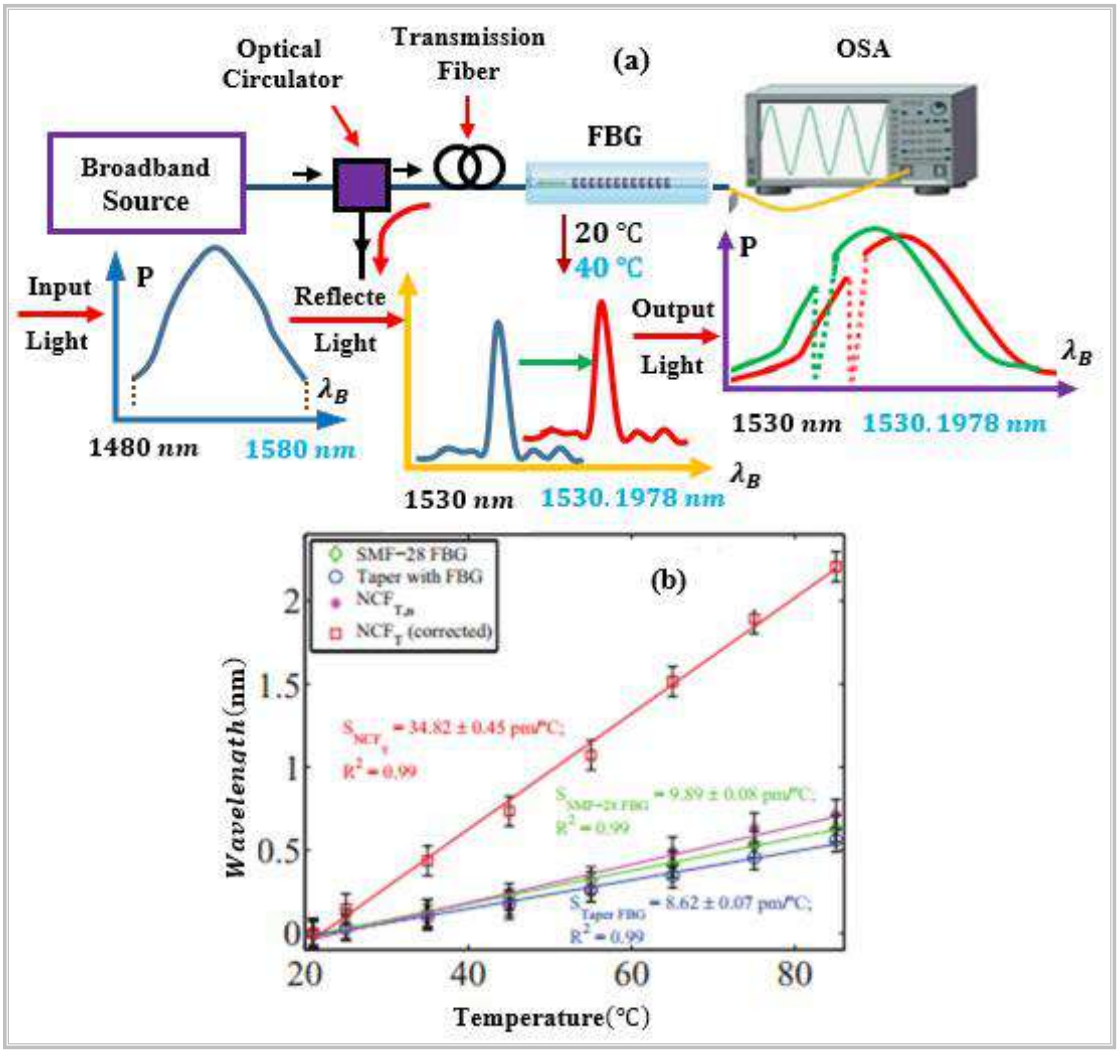

Figure (5). (a) Schematic diagram of Bragg grating sensor arrangement to measure temperature change which was designed by the author and (b) Change in wavelength at the peak of the reflection spectrum of FBG due to temperature changes [11].

To measure the strain, the amount of strain has been changed from zero to 1500($\mu\varepsilon$) microstrain with a step of 100($\mu\varepsilon$) microstrain [11]. Wavelength changes in terms of strain changes for optical fiber Bragg grating are plotted in Figure (6)

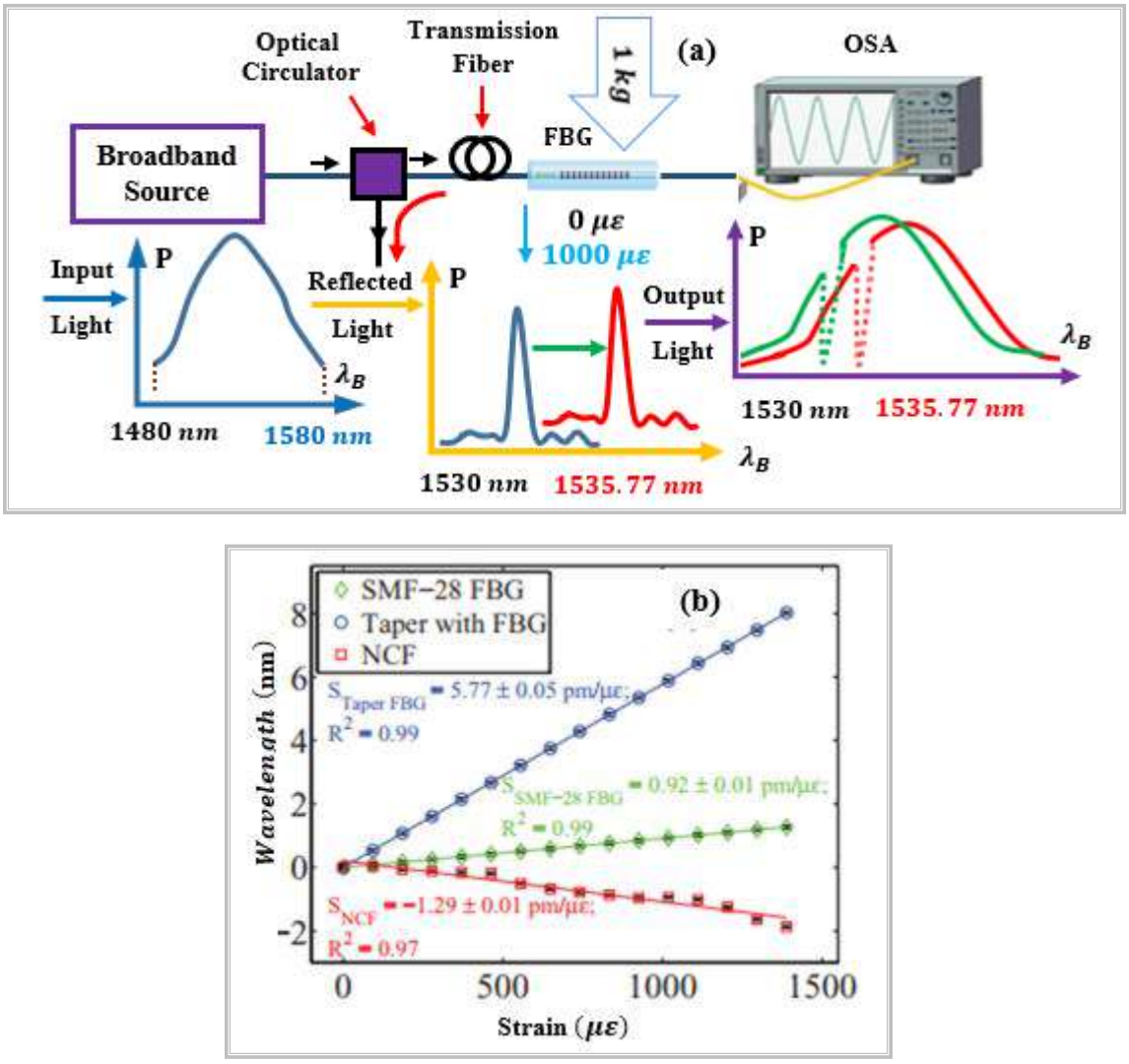

Figure (6). (a) Schematic diagram of Bragg grating sensor arrangement for strain change which was designed by the author and (b) Wavelength change in FBG due to strain change [11].

Now, we investigate the optical fiber Bragg grating sensor under the simultaneous influence of temperature and strain. This issue is shown schematically in Figure (7).

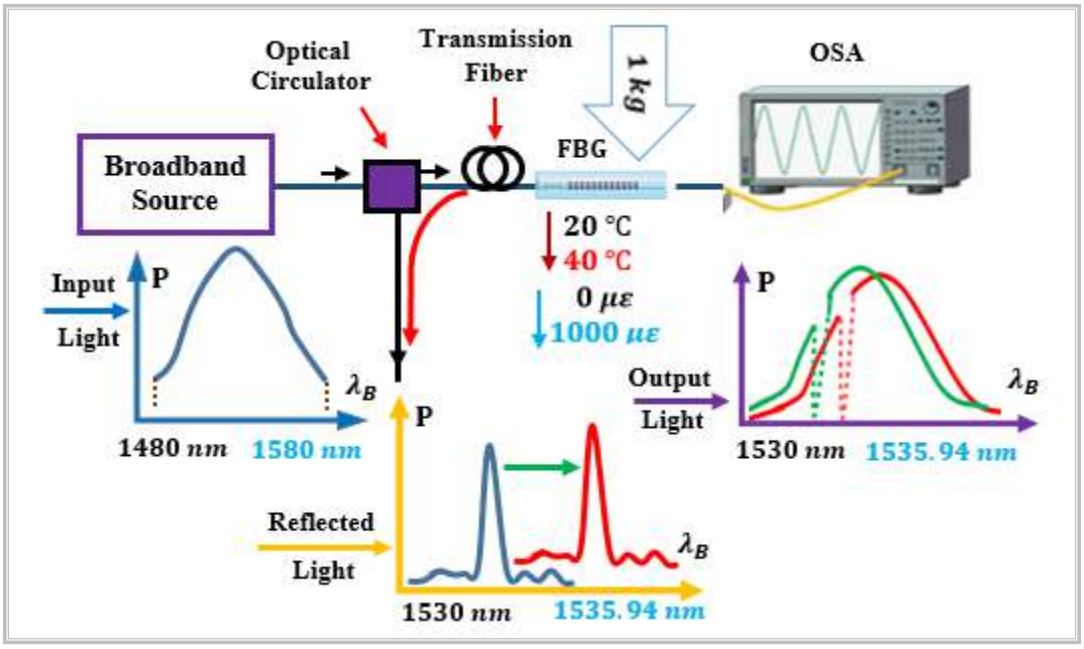

Figure (7). Schematic diagram of Bragg grating sensor arrangement due to a simultaneous change of temperature and strain designed by the author.

As it is clear in Figure (7), using the FBG sensor to measure temperature and strain simultaneously will cause sensitivity interference; and we cannot measure strain and temperature at the same time using this sensor. To eliminate the interference of temperature and strain, we investigate the design of a combined sensor of tapered optical fiber and FBG to measure temperature and strain simultaneously. The proposed sensor and the expected shift in the spectrum are schematically drawn in Figure (8).

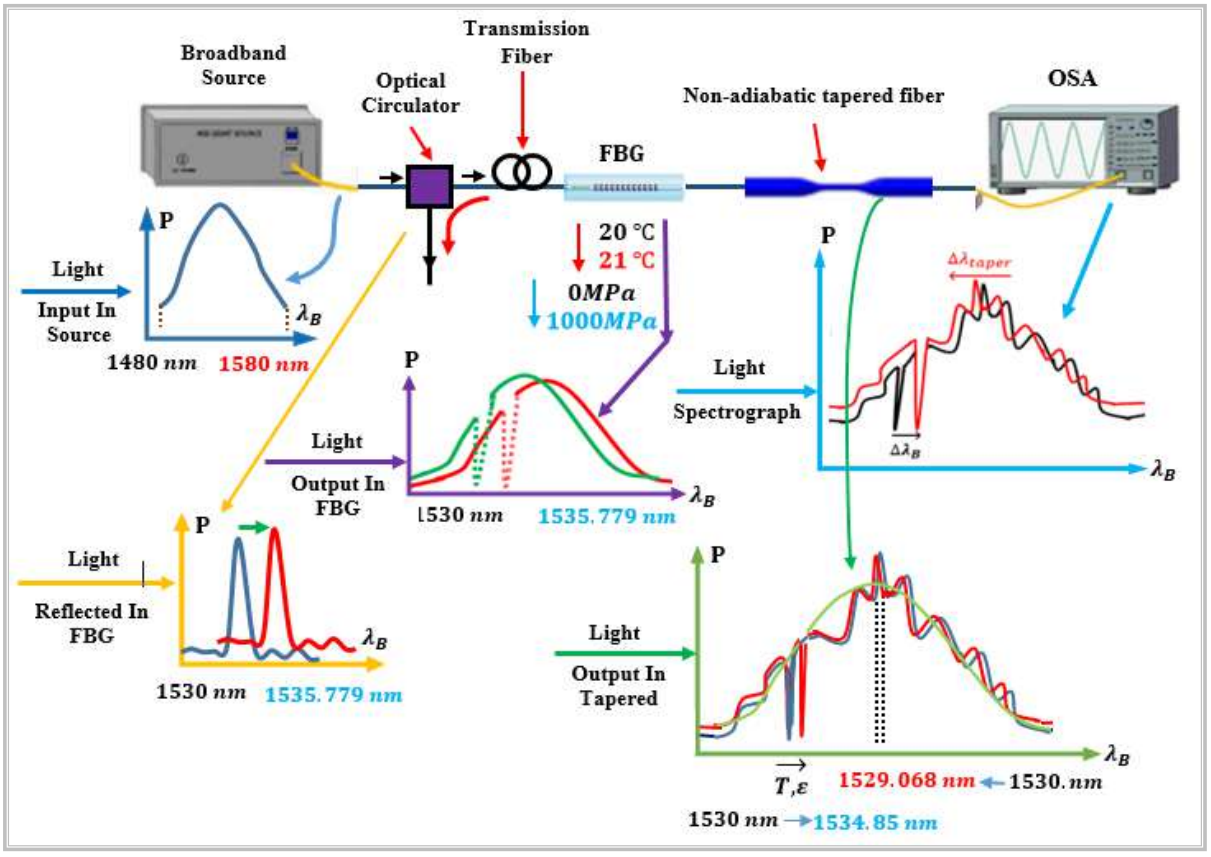

Figure (8). Schematic diagram of tapered optical fiber and FBG composite sensor arrangement due to temperature and strain changes designed by the author.

3. Results and Discussion

The temperature sensitivity of optical fiber Bragg gratings is calculated by the following equation [5]:

$$\frac{\Delta\lambda_B}{\lambda_B} = (\alpha + \xi) \cdot \Delta T \qquad (1)$$

Also, the axial strain sensitivity of an optical fiber Bragg grating is obtained by the following equation [12]:

$$\frac{\Delta\lambda_B}{\lambda_B} = (1 - P_e)\varepsilon_z \qquad (2)$$

By combining equations (1) and (2), the overall sensitivity to temperature and strain is obtained.

$$\frac{\Delta\lambda_B}{\lambda_B} = (1 - P_e) \cdot \varepsilon_z + (\alpha + \xi) \cdot \Delta T \qquad (3)$$

Equation (3) shows that the displacement of the Bragg grating is caused by two factors, strain, and temperature. To detect which factor the displacement is related to, a combined tapered optical fiber and FBG sensor can be used. The temperature-specific thinned fiber optic sensor and the FBG sensor examine both factors, which are obtained by comparing the temperature response of the thinned fiber sensors and the Bragg grating sensor and finally subtracting the result of both sensors from each other, the number of strain changes.

We rewrite equation (3) as follows:

$$\Delta\lambda_B = K_{\varepsilon B} \times \Delta\varepsilon + K_{TB} \times \Delta T \qquad (4)$$

Also, for the thinned fiber optic sensor which is sensitive to temperature, we have:

$$\Delta\lambda_{taper} = K_{T\,taper} \times \Delta T \qquad (5)$$

The values of $\Delta\lambda_B$ and $\Delta\lambda_{taper}$ can be seen in Figure (8), which can be determined in the laboratory. Now we perform an example of calculations for the proposed sensor. For example, let's suppose that in the laboratory we have measured the wavelength changes for the thinned optical fiber Δ and the Bragg wavelength changes separately and we want to determine the temperature and strain values. For example, let's suppose that in the laboratory we have measured the wavelength changes for the thinned optical fiber $\Delta\acute{\lambda}_{taper}$ and the Bragg wavelength changes $\Delta\acute{\lambda}_B$ separately and we want to determine the temperature and strain value. Assume that the values obtained for the wavelength change in the laboratory method for the thinned optical fiber sensor and FBG are $\Delta\acute{\lambda}_{taper} = -0.823\ nm$ and$\Delta\acute{\lambda}_B = 0.751\ nm$, respectively. Now we want to obtain the temperature and strain ($\Delta\acute{T}\ and\ \Delta\acute{\varepsilon}$) using these values.

$$\Delta\acute{T} = \frac{\Delta\acute{\lambda}_{taper}}{K_{T\,taper}} \implies \Delta\acute{T} = \frac{-0.823\ nm}{-0.9328^{nm}/_{\circ\mathrm{C}}} = 0.883\ ^{\circ}\mathrm{C} \qquad (6)$$

$$\Delta\acute{\varepsilon} = \frac{\Delta\acute{\lambda}_B - K_{TB}\times\Delta\acute{T}}{K_{\varepsilon B}} \implies$$

$$\Delta\acute{\varepsilon} = \frac{0.751\ nm - 0.00989^{nm}/_{\circ\mathrm{C}} \times 0.858\ ^{\circ}\mathrm{C}}{0.00092^{nm}/_{\mu\varepsilon}} = 807\ \mu\varepsilon$$

This shows that by using the adiabatic thinned optical fiber sensor and FBG in a combined form, the sensitivity interference will not be created in the said sensor, and strain and temperature can be measured simultaneously at any desired point. By using the relationship between wavelength changes with strain and temperature, as well as measuring the value of the changed wavelength by thinned optical fiber and optical fiber Bragg grating, it is possible to use the value of temperature and strain at any desired point. According to the measurements made in the references used in this article [4, 11], the

sensitivity for the said combined sensor for temperature and strain was obtained at 0.882 $^{pm}/_{\circ C}$ and 807 $^{pm}/_{\mu\varepsilon}$ respectively.

4. Conclusion

The limitation of using optical fiber Bragg grating sensors is that the response of the sensor to measure temperature and strain simultaneously can cause errors in strain measurement in different structures. For this purpose, we have to somehow separate the temperature effect from the strain effect, and various methods have been proposed for this task. In this paper, the design of thinned optical fiber hybrid sensor (sensitive to temperature) and an optical fiber Bragg grating sensor (sensitive to temperature and strain) was done to separate the effect of temperature and strain. Investigations conducted on the designed combined sensor showed that sensitivity interference will not occur in the said combined sensor. According to the sensors used as examples in this paper, the sensitivity for the combined sensor was obtained for temperature, 0.882 $^{pm}/_{\circ C}$ and for strain807 $^{pm}/_{\mu\varepsilon}$.

5. Acknowledgment:

The authors would like to thank Iran University of science and technology physics for providing research facilities.

6. Conflicts of Interest

All authors declare that they have no conflicts of interest to disclose.

7. References

[1] A. M. Valadez, C. A. Lana, S. I. Tu, M. T. Morgan, and A. K. Bhunia, “Evanescent wave fiber optic biosensor for Salmonella detection in food,” Sensors, vol. 9, no. 7, pp. 5810–5824, 2009.

[2] J. D. Love and W. M. Henry, “Quantifying loss minimization in single-mode fiber tapers,” Electronics Letters, vol. 22, no. 17, pp. 912–914, 1986.

[3] Zibaii, M. I., et al. "Non-adiabatic tapered optical fiber sensor for measuring the interaction between α-amino acids in aqueous carbohydrate solution." Measurement Science and Technology 21/1 (2010): pp. 105-801.

[4] Zhou, Tianjin, et al. "Low cost non-adiabatic tapered fiber for high-sensitive temperature sensing." Optical Fiber Technology 45 (2018): pp53-57.

[5] A. Othonos and K. Kyriako’s, "Fiber Bragg Grating: fundamentals and applications in telecommunications and sensing,” Artech House, Boston, 1999.

[6] F. T. S. Yu, SH. Yin,” In-Fiber Grating Optic Sensors”, Fiber Optic Sensors, New York, M. Dekker, paper, 2002: pp. 123-171.

[7] Ling, Hang-yin, et al. "Embedded fiber Bragg grating sensors for non-uniform strain sensing in composite structures." Measurement science and technology 16.12 (2005): 2415.

[8] Liu, Qiang, et al. "High-sensitivity plasmatic temperature sensor based on photonic crystal fiber coated with Nanoscale gold film." Applied Physics Express 8/4 (2015): 46701.

[9] Drusová, Sandra, et al. "Possibilities for Groundwater Flow Sensing with Fiber Bragg Grating Sensors." Sensors 19/7 (2019): pp. 1730.

[10] Ye XW, Su YH, Han JP Structural health monitoring of civil infrastructure using optical fiber sensing technology: a comprehensive review. Scientific World Journal. 2014; 11. Article ID 652329.

[11] Oliveira, Ricardo, et al. "Simultaneous measurement of strain, temperature and refractive index based on multimode interference, fiber tapering, and fiber Bragg gratings." Measurement Science and Technology 27/7 (2016): 75107.

[12] Hill, Kenneth O., and Gerald Meltz. "Fiber Bragg grating technology fundamentals and overview." Journal of lightwave technology 15/8 (1997): pp. 1263-1276.

Authors Profile:

Hameedullah zahin received the BSc. degree in general physics from Nangarhar University in 2009 and 2013, he completed his MSc. degree in physics – Optics & Laser from the University of Science and Technology of Iran in Iran. Currently, He is working as a teaching assistant in the Department of physics, at Urozgan University, Tarincot, Afghanistan. His areas of research include optics physics.

Fazalullah Marufi received the BSc. degree in general physics from Nangarhar University in 2009 and 2013, he completed his MSc. degree in condensed matter physics from the University of Science and Technology of Iran in Iran. Currently, He is working as a teaching assistant in the Department of physics, at Urozgan University, Tarincot, Afghanistan. His areas of research include nanophysics.

KPU International Journal of Engineering & Technology
Volume 2, Issue2, Dec. 2022
e-ISSN:2790-0819, p-ISSN:2790-0800
Date Received: 2022-08-21
Date Accepted: 2022-12-25
Date Published: 2022-12-30

Forecasting Monthly Electricity Consumption Using Machine Learning and Statistical-Based Models: A Case Study

ABDUL JALIL NIAZAI [1*], MOHAMMAD AKBAR SHAHPOOR [2,] ABDULLAH ZAHIRZADA [3], ABDUL RAHMAN SAFI [4], NOOR AHMAD NOORI [5]

[1]Assistant professor, Department of Software Engineering, Computer science Faculty, Kunduz Universit,1[the] District, Kunduz, Afghanistan. Email: ab.niazai@gmail.com

[2]Assistant professor, Department of Software Engineering, Computer science Faculty, Kunduz University, 1[the] District, Kunduz, Afghanistan. Email: akbarshshpoor@gmail.com

[3]Assistant professor, Department of Information Systems, Computer science Faculty, Kunduz University, 1[the] District, Kunduz, Afghanistan. Email: ab.zahirzada95@gmail.com

[4]Assistant professor, Department of Information Systems, Computer science Faculty, Kabul University, 3[the] District, Kabul, Afghanistan. Email: abrahman.safi@gmail.com

[5]Assistant professor, Department of Information Technology, Computer science faculty, Kandahar University, 9[the] District, Kandahar, Afghanistan. Email: noorah.kdr@gmail.com

Abstract

Forecasting electricity consumption demand plays a vital role in short-term load balancing and long-term planning for having secure power systems, new energy generation, and transmission infrastructures. Knowing the consumption demand is also essential in preparing the power system according to the anticipated load status. In this research paper, we conducted a time series forecasting analysis on the monthly electricity consumption data of Kunduz province gathered from April 2011 to July 2022 to predict the consumption demand in this province. For this purpose, we employed two well-known forecasting methods: Multilayer perceptron (MLP) from machine learning and ARIMA from statistics. The MAPE and MAE metrics were used to measure and compare the predictive performance of developed MLP and ARIMA models. The comparison result found that MLP outperforms ARIMA in model forecasting accuracy. We believe that the outcomes of this research work significantly help Kunduz's regional electricity authorities in better energy management and allow them to make effective decisions regarding electrical energy cost and efficiency.[*]

Keywords: Forecasting, Electricity consumption demand, MLP, ARIMA, Kunduz province.

[*] Corresponding Author

1. Introduction

The rapid increase in human population, insistence on large-scale industrialization, technology adoption, rise in energy cost, and the need to keep the country's economic growth positive have caused to drive the global demand for electricity consumption [1]. Indeed, electrical energy nowadays is considered one of the critical factors that can highly affect a country's economic growth and human living standards. The global demand for this energy increased by 4.5%, with over 1000 TWH in 2021. This upsurge was almost five times greater than the downfall in demand for electrical energy in 2020. Nearly 80 percent of the increase in demand was in emerging markets and developing economies [2]. Fulfilling the demand for electrical energy can be achieved from different sources, including wind, solar, hydro, coal, gas, and others. In 2021, the world's electrical energy production sources comprised 36% coal, 22% gas, and 38% clean electricity, including solar, wind, hydro, nuclear, and bioenergy [3].

Electricity consumption demand is steadily growing, and we are required to have statistical knowledge about this growth, which involves a predictive mathematical model of electricity consumption to foresee future demands. Forecasting electricity consumption demand plays a vital role in short-term load balancing and long-term planning for having secure power systems, new energy generation, and transmission infrastructures. Knowing the energy demand is also essential in preparing the power system according to the anticipated load status. Moreover, an accurate forecasting result enables authorities to better energy management and allows them to make effective decisions in terms of energy cost and efficiency. Hence, this paper proposes a mathematical model that predicts the electricity consumption demand in Kunduz. Kunduz province, located in northeast Afghanistan, shares a long international border with Tajikistan. With around 1,136,677 population, including 34% living in rural areas and 66% in urban areas, it is considered one of Afghanistan's largest provinces. Approximately 70% of the Kunduz population, including 95% of households in the city and 60% in a rural areas, have access to electricity. The total acquired electricity of Kunduz is supplied by imported power, and the consumption demand increased from 121,261,205 kWh equivalent in 2010 to 184,772,152 kWh in 2021, as per Kunduz regional electricity organization report.

Although the accessibility of households to the electricity grid has significantly improved, load shedding is common in most areas of Kunduz province. The reasons are weak transmission infrastructure, lack of generation capacity, unreliable power systems, and no precise knowledge about electricity demand growth in the upcoming years. Hence, we believe the outcome of this research significantly helps Kunduz's regional electricity organization make an effective energy strategy for solving the prevenient electricity supply shortage in the next three years. The rest of this research paper is organized as follows. Section 2 discusses the related literature review. Section 3 presents the data and research methodology used. The model development and discussions on results are given in section 4. Finally, section 5 concludes this research paper.

2. Related Work

Increases in electricity costs caused energy modeling and forecasting to become a hot topic for academic and research scholars [4]. Researchers employed different techniques to predict the electrical energy consumption demand. For instance, S. L. Lai *et al.*[5] adopted artificial neural network (ANN) and Auto-regressive moving average (ARIMA) models to predict the electricity consumption demand in Hong Kon. As a comparison result, ANN has been found acceptable regarding forecasting accuracy when considering a single predictor. J. Miao used the ARIMA model to forecast China's energy consumption demand for formulating economic policies [6]. C. Hamzacebi and H. A. Es [7] employed an optimized Gray model to predict Turkey's electric energy demand from 2013 to 2025. A. Bagnasco *et al.*[8] implemented ANN-based multilayer perceptron algorithm to forecast the electrical consumption of the Cellini medical hospital in Turin. The model was proved with satisfactory forecasting accuracy. S. Mishra and V. K. Singh [9] applied the ANN-based Windowed Momentum algorithm to three years of monthly consecutive consumed energy data and weather information to predict monthly energy consumption. S. G. Yoo and H.-Á. Myriam [10] used neural networks and information from other variables such as the overall population and the elderly population to forecast the electricity consumption demand of residential areas in Seoul city. A. Camara *et al.*[11] deployed seasonal ARIMA and Multilayer perceptron approaches to predict U.S. energy consumption. As an empirical evaluation result, they found that the MLP (ANN) model slightly outperforms the seasonal ARIMA model in forecasting accuracy.

3. Methodology

Researchers unanimously agree with the forecasting literature that any single model may not always capture the distinctive patterns in the data equally well since data-analytic problems are frequently dynamic and complicated. Hence, based on the literature conducted above, two well-known forecasting approaches, Multilayer Perceptron (ANN) and ARIMA, are employed to predict the electricity consumption demand in Kunduz province for the next three years.

3.1 Data Collection

The monthly electricity consumption data of Kunduz province used in this research was obtained from Kunduz regional electricity organization over the period from April 2011 to July 2022. The dataset consists of 124 observations with two features (i.e., consumed electricity and corresponding month). Each observation in the collected data represents the monthly kWh consumed electricity in Kunduz province. In the data preprocessing stage, a total of 6 observations founded as missing values and handled through the Python Skylearn preprocessing library. The data distribution and description of our dataset are given in Table 1. Also, fig. 1 shows the time series plot of Kunduz's consumed electricity amount.

Table 1. The statistical description of the dataset.

Observations	*Mean*	*Std*	*Min*	*25%*	*50%*	*75%*	*Max*
124	12894330	4127101	582394	10452600	13212750	15593910	21400540

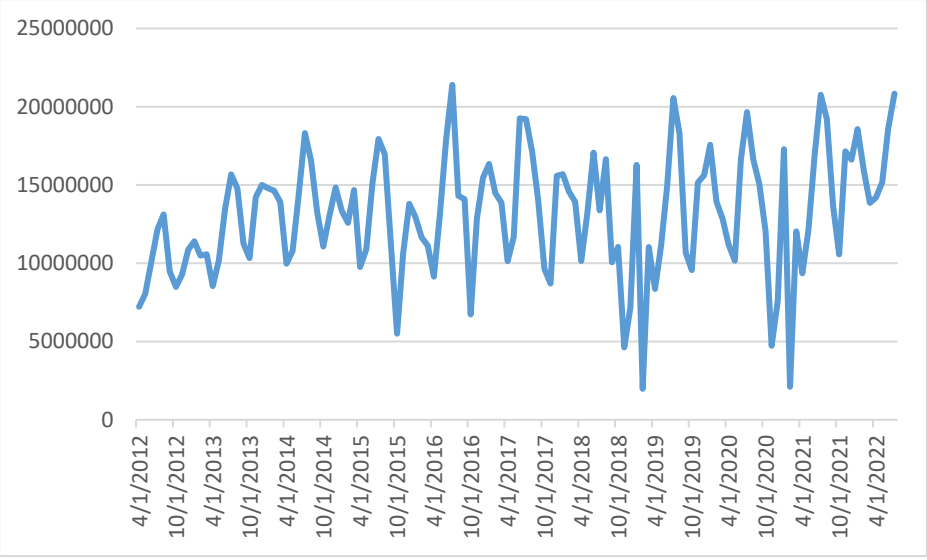

Fig. 1 Time series plot of electricity consumption in Kunduz.

As shown in Table 1, the minimum amount of electricity consumption is 582394 kWh, and the maximum consumption is 21400540 kWh. The average consumption is 12894330 kWh, whereas 50% of this province's monthly consumption is above 13212750 kWh.

Also, in the above plot graph, the x-axis represents the date, and the y-axis indicates the consumed electricity per month. As seen in Fig.1, consumption shows a steadily linear growth. In March and April, the plot marked a decrease in consumption, probably due to the cool weather in these months. However, the plot shows a sharp increase in consumption between July and August, probably due to summer air and intensive agricultural and industrial activities, as presented in Fig.1.

3.2 Proposed Models

Time series forecasting models' primary objective is to make future value predictions using data collected over a specific period. This research study employed two famous and most common time series forecasting models, Multilayer Perceptron (MLP) and Autoregressive Integrated Moving Average (ARIMA), to estimate and predict Kunduz's electricity consumption demand. The following phases summarize the development of the proposed models:

1. Developing an ARIMA model that includes the phases of model identification, model parameters estimation, and model diagnosis.
2. Constructing a Multilayer Perceptron model with optimum neural network architecture.
3. Evaluating proposed developed models utilizing various accuracy criteria.

3.3 ARIMA Model

Autoregressive Integrated Moving Average (ARIMA), also known as Box & Jenkins method, is one of the most popular models to forecast future values [12]. It predicts the future value of time series data as a linear combination of its previous values and forecast errors [13]. Unlike ordinary predictive models that involve explanatory variables, the ARIMA model is an utterly univariate method that uses its previous information in the series to forecast future value. Hence, the model is beneficial when little information, such as predictors, can be retrieved from the underlying data generation process and the variable to be forecasted is unknown. Three key components make up the ARIMA model: the autoregressive (AR) term, the Integrated (I) part, and the Moving Average (MA) part. For simplicity, each of these components is symbolized as parameters p,d, and q in the ARIMA model. Here, p represents the order of autoregressive term, d indicates the order of differencing to make the series stationary, and parameter q represents the size of the moving average process [14]. When parameter d=0, the series is stationary, and the ARIMA model is transformed into the ARMA model. Mathematically it can be written as follow:

$$y_t = c + \varepsilon_t + \sum_{i=1}^{p} \alpha_i \, y_{t-i} + \sum_{j=1}^{q} \beta_j \, \varepsilon_{t-j} \qquad (1)$$

Where yt is the actual value of series y at period t, c is the constant value in the series, and p and q denote the order of autoregressive and moving average terms, respectively. Building the ARIMA model with time series data is detailed: (1) Determining the stationarity of the original sequence. Apply differencing transformation on the original series to stabilize the mean and variance before applying the ARIMA model to the data. (2) Estimate order for parameters p and q using statistical functions, i.e., calculating auto-correlation and partial auto-correlation of the data series. (3) perform a diagnostic check for the developed model to confirm that the model is well-fitted to the data and that the residuals are random errors. The three phases are repeated until an ARIMA model with the fewest generated errors is developed.

3.4 MLP model

Artificial Neural Network (ANN) is a category of learning algorithms that mimic the human brain system to discover patterns in the data. Multilayer Perceptron (MLP), also known as a feed-forward neural network, is one of the ANN algorithms used most

frequently in time series forecasting [15]. The MLP typically comprises three layers an input layer, a hidden layer or core processing layer of the network, and an output layer, as illustrated in Fig. 2.

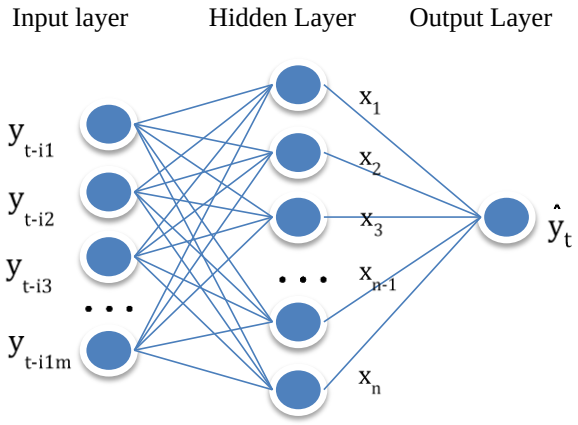

Fig. 2 Multilayer perceptron (MLP) neural network

The neural network of MLP iteratively learns by adjusting the weights of the neurons' connections based on the discrepancy between the actual and expected output. Initially, weights are assigned to neurons' connections with a random value between 0 and 1. The error estimated at the output layer is propagated back to the hidden layer, and weights are updated for subsequent iterations. This process continues until a minimum amount of errors is produced [9]. The equation below describes how MLP is trained for time series prediction.

$$y_t = w_0 + \sum_{i=1}^{n} w_i f\left(\beta_{0i} + \sum_{j=1}^{m} \beta_{ji}\, y_{t-j}\right) \qquad (2)$$

In the equation, w_0 (i = 0, 1, 2,3,…,n) and B_{ji} (j =0,1,2,3,…,n) are coefficients also referred to as the network's connection weights. Where n and m represent the number of input and hidden nodes, respectively.

4. Proposed predictive model development

This study employed Multilayer Perceptron (ANN) and ARIMA, two well-known time series forecasting techniques, to model and predict electricity consumption demand in Kunduz province. All model development has been carried out by splitting the original electricity consumption data into two sets of training and testing, each containing 90% (112 data points) and 10% (12 data points) of the data, respectively. Python's data analysis library, called Pandas, was employed to split the dataset. The training set was used for

model building, and the test set was employed to assess the predictive accuracy and effectiveness of the developed models. Python's existing predictive modules are utilized for all modeling and forecasting tasks.

4.1 Developing ARIMA Model

Data series stationarity is a precondition for building an ARIMA model. In the ARIMA model development, as a first step, we are required to determine the stationarity of our data series. The Augmented Dick-Fuller (ADF) method was employed for this purpose. Table 2 contains the ADF test result for our data series before differencing.

Table 2. ADF test result before differencing

ADF value	*P-value*	*Critical Values*		*Result*
-2.3572	0.1541	-3.491245	@ 1%	Non-stationary
-2.3572	0.1541	-2.888195	@ 5%	Non-stationary
-2.3572	0.1541	-2.580987	@ 10%	Non-stationary

As we can see, the calculated p-value is lower than the significant level (i.e., p-value << 0.05), and the ADF value is higher than any critical value at the level of 10%, 5%, and 1%, respectively. Our series, therefore, is non-stationary. To make our series stationary, we must differentiate it at various time lags and then draw the autocorrelation function (ACF) to ascertain the proper differencing order for our ARIMA model.

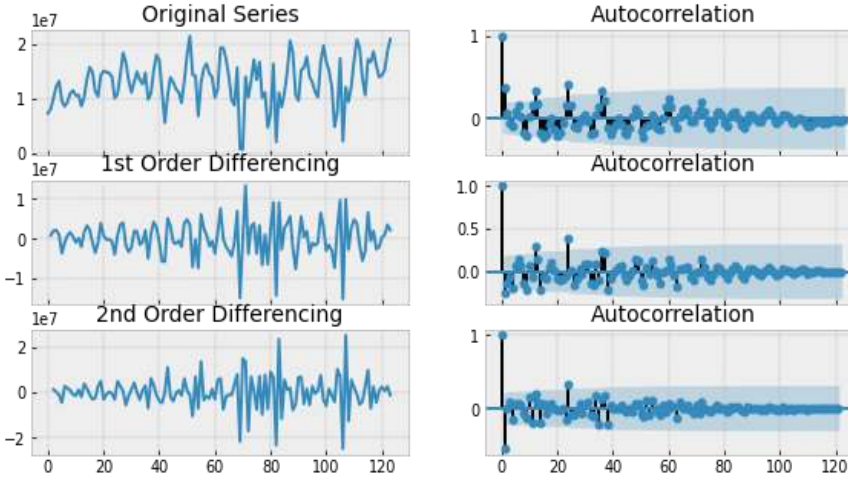

Fig. 3 The ACF plots various order of differencing.

The autocorrelation function plot steadily reached zero in the first order of difference. Also, some of the dotted horizontal lines occurred outside the significant (blue region) area, showing the series might not have been appropriately differenced see Fig. 3. However, in the second order of difference, the ACF plot quickly converged to zero, and the dotted horizontal lines did not cross the significant zone, showing that our series

perfectly transformed to stationary in the second order of difference. To verify this, let us apply the ADF test on our second-order differenced series again.

Table 3. ADF test result after second-order of difference.

ADF Statistics	*P-value*	*Critical Values*		*Result*
-6.952662	0.000000	-3.492401	@ 1%	Stationary
-6.952662	0.000000	-2.888696	@ 5%	Stationary
-6.952662	0.000000	-2.581255	@ 10%	Stationary

The result displayed in Table 3 shows that the p-value is highly significant [<<0.05], and the ADF Statistics value is lower than all the critical values. Hence, we can set the differencing order as 2, depicting parameter d's value in the ARIMA (p,d,q) model.

Next, we determine the value of autoregressive (AR) and moving average (MA) terms, alternatively referred to as parameters p and q in the ARIMA model. The machine learning approach is used for this purpose. Grid search, a popular machine-learning technique for hyperparameter optimization, is used for this purpose. The method tries each combination of p and q from the subsets we provided. Additionally, to determine the ideal combination for parameters p and q, the method requires an objective function that evaluates how perfectly the model fits the data. The Akaike information criterion (AIC) function is commonly used for this purpose. AIC is a statistical measure used to evaluate and compare the ARIMA models in terms of how well they fit the data [14]. The lower the AIC value, the better the model is at forecasting error. Mathematically it can be described as:

$$AIC = -2l + 2K \tag{3}$$

Where l is the log-likelihood of the model's prediction of the observed y-values and k is the number of parameters in the model. Hence, we consider AIC values for optimal ARIMA model selection. So let us use the stats model module in Python to applying the ARIMA model to our consumed electricity data. Initially, we fixed ARIMA's AR and MA terms, each with a value of four. As a result, numerous ARIMA models were developed with different p and q parameter combinations. Table 4 holds the summary of developed ARIMA models having the least AIC value on our data.

Table 4. Development summary of candidate ARIMA models.

Model	*Terms*	*Coefficient*	*P > |z|*	*AIC values*
ARIMA(0,2,3)	ma.L1.D2.kWh	-1.6362	0.000	3672
	ma.L2.D2.kWh	0.2818	0.124	
	ma.L3.D2.kWh	0.3545	0.000	
ARIMA(0,2,4)	ma.L1.D2.kWh	-1.5796	0.000	3576
	ma.L2.D2.kWh	0.2972	0.146	
	ma.L3.D2.kWh	0.1784	0.396	
	ma.L4.D2.kWh	0.1170	0.250	

ARIMA(4,2,2)	ar.L1.D2.kWh	0.4172	0.000	3678
	ar.L2.D2.kWh	-0.0344	0.738	
	ar.L3.D2.kWh	-0.0073	0.943	
	ar.L4.D2.kWh	-0.0783	0.414	
	ma.L1.D2.kWh	-1.9917	0.000	
	ma.L2.D2.kWh	1.0000	0.000	
ARIMA(4,2,2)	ar.L1.D2.kWh	-0.4085	0.000	3682
	ar.L2.D2.kWh	-0.3566	0.003	
	ar.L3.D2.kWh	-0.2664	0.006	
	ar.L4.D2.kWh	-0.3124	0.001	
	ma.L1.D2.kWh	-1.0000	0.000	
ARIMA(0,2,2)	ma.L1.D2.kWh	-1.8857	0.000	3683
	ma.L2.D2.kWh	-0.8858	0.009	

According to the model development summary in Table 4, the ARIMA(0,2,3) model has the lowest AIC values compared to all other developed ARIMA models. The model's parameters p,d, and q have been determined to have values 0,2, and 3, respectively. Also, all MA terms' coefficient sum is less than one. Hence, we can conclude that the ARIMA(0,2,3) model has a high degree of fit compared to all other models constructed on our consumed electricity data (see Table 5).

Table 5. Development summary of the selected ARIMA model

Dep. Variable:	D2.kWh	**No. Observations:**	110
Model:	ARIMA(0, 2, 3)	**Log Likelihood**	-1831.408
Method:	CSS-mle	SD **of innovation**	3853493.588
Date:	Mon, 08 Aug 2022	**AIC**	3672.815
Time:	10:22:57	**BIC**	3686.318
Sample:	2	**HQIC**	3678.292

	coef	*std err*	*z*	*P>|z|*	*[0.025*	*0.975]*
const	-872.4962	1025.473	-0.851	0.395	-2882	1137
ar.L1.D2.Value	-1.6362	0.140	-11.706	0.000	-1.910	-1.36
ar.L2.D2.Value	0.2818	0.183	1.538	0.124	-0.077	0.64
ar.L3.D2.Value	0.3545	0.099	3.571	0.000	0.160	0.54

Next, the ARIMA (3,1,0) model is put through diagnostic testing to ensure it has provided the best fit for the data and that no more pertinent information in our data series is left for extraction. This can be achieved by performing the residual analysis of our best-fitted model. Fig 4. depicts the outcome of the residual analysis of the selected ARIMA(0,2,3) model.

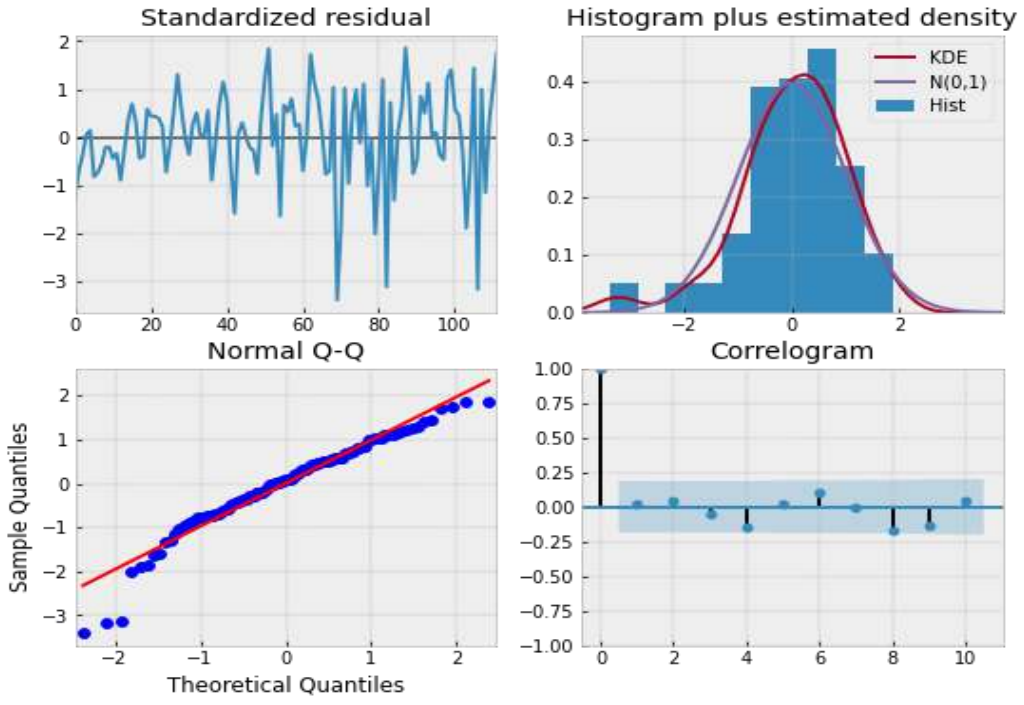

Fig. 4 Illustrates the residual errors, density plot, Q-Q plot of the residual, and ACF plot of the residual.

The model's residual errors, shown in Fig. 4, lack any discernible trend and retain a constant variance along the zero means. Similarly, the density plot illustrated in Fig. 4 implies that the residual errors have a normal distribution with near-zero means. This is verified by the Q-Q plot shown in Fig. 4, which suggests a linear trend for the residual errors of our proposed model. Likewise, the dotted vertical lines in Fig. 4 do not cross the significant threshold, showing no autocorrelation between our model's residual errors and its lagged version. So, from the statistics illustrated in the above figures, we can infer that our proposed ARIMA (0,2,3) model has successfully extracted all the essential knowledge from our consumed electricity data series and residual errors are white noise.

4.2 Developing MLP model

The fundamental structure of the MLP neural network must be defined before we apply the multilayer perceptron algorithm to our consumed electricity data series. We chose a single node in the input layer, eight neurons in a single hidden layer, and a node in the output layer as a preliminary network structure. The Stochastic Gradient Decent (SGD) optimization method is used to get optimal network architecture. Rectified Linear Unit (Relu) activation function is considered a transformation function, and Root Mean Square Error (RMSE) is used as a cost function. For model implementation and model evaluation, Python's open-source 'Keras' deep learning package is employed. The neural

network is trained for 400 epochs, for which we obtain the minimum amount of training and test errors.

After performing an empirical experiment, we found the MLP model with a single input node, two hidden layers each with 12 and 4 neurons, and a node in the output layer to be the best fit for our data series. This indicates that the model predicts electricity consumption demand for time t_4 using the consumed electricity amount of time t_0, t_1, and t_3. Hence, the 1-8-12-1 is the best neural network structure to train the MLP model on our data series. The forecasting accuracy of this proposed MLP model is assessed in the model evaluation and comparison section.

4.3 Model Evaluation and comparison

This research work has considered Mean Absolute Error (MAE) and Mean Absolute Percentage Error (MAPE) to measure and compare the predictive accuracy of developed models (i.e., ARIMA (0,2,3) and MLP). Researchers recommend these metrics when assessing the forecasting accuracy of a model on a single data series [16]. MAE metric measures a model's predictive performance by taking the absolute difference between the forecasted and actual values. Mathematically it can be formulated as:

$$MAE = \frac{\sum_{i=1}^{n} |Y_i - \hat{Y}_i|}{n} \quad (4)$$

In the formula, $\hat{Y}_i$ is the forecasted value, Y_i is the actual value, and n is the overall number of observations in the test set. A model in terms of performance is deemed superior to other models if it has the lowest MAE value. Likewise, the MAPE metric determines the accuracy of a model by taking the mean absolute difference between a forecasted value and an actual value divided by the actual value. The final result is expressed in percentages. A model is considered superior to others if it has a low MAPE. Mathematically it can be described as:

$$\text{MAPE} = \frac{1}{n} \left| \frac{X_i - \hat{X}_i}{X} \times 100 \right| \quad (5)$$

Where $\hat{X}_i$ indicates the predicted value, X_i denotes the actual value, and the letter n indicates the total number of observations in the test set. We can show a model's MAPE value in percentage of accuracy with the equation below:

$$\text{Acc\%} = 100 - \text{MAPE} \times 100 \quad (6)$$

Table 6 shows the predictive performance of MLP and ARIMA models in terms of mean absolute percentage error and mean absolute error on the test set. Likewise, Fig. 5 and Fig. 6 illustrate the ratio of the forecasted and actual value in predicting ARIMA and MLP models.

Table 6. Predictive performance of MLP and ARIMA models.

Model	*MAPE*	*MAE*	*Accuracy (MAPE)*
Multilayer perceptron (MLP)	18.00	11126380000000.0	82.0%
ARIMA	21.50	11724960107369.0	78.5%

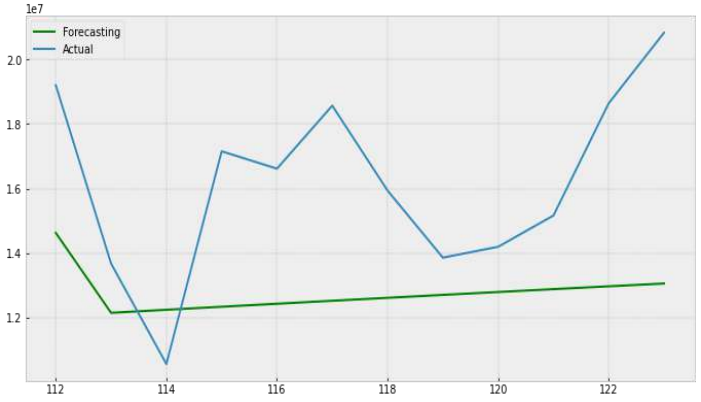

Fig. 5 Actual electricity consumption vs forecasted consumption by ARIMA model.

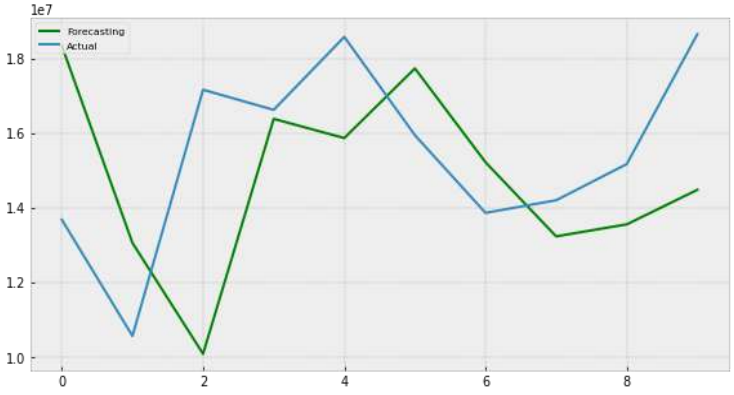

Fig. 6 Actual electricity consumption vs forecasted consumption by MLP model.

In Fig. 5 and Fig. 6, it can be observed that the electricity consumption values predicted by the MLP model are closer to actual consumption values than the prediction made by the ARIMA model. Also, from Table 6, it can be noticed that the MLP model has a lower rate of errors in terms of MSE and MAPE compared to ARIMA Model. In the case of forecasting accuracy, the MLP model has obtained 82%, with the ARIMA being modeled with lower accuracy of 78.5%. In general, from Table 6, Fig. 5, and Fig.

6, we can conclude that the MLP algorithm best fits our data and can be used to predict the electricity consumption demand of Kunduz province for the next three years.

5. Result and Discussion

As discussed previously, the main goal of this research study is to build a model that precisely forecasts the electricity consumption demand in Kunduz province for the next three years. For this purpose, we conducted a time series forecasting analysis on the monthly electricity consumption data of Kunduz province gathered from April 2011 to July 2022. ANN-based multilayer perceptron technique from machine learning and ARIMA model from statistics were employed. First, we implemented the ARIMA model on stationary series, and by considering the AIC criterion for model specification, we found the ARIMA (0,2,3) model best fitted our data. Subsequently, we applied multilayer perceptron on data series. As a result of an empirical analysis, we found a neural network structure with a single input node, two hidden layers each with 12 and 4 neurons, and a node in the output layer as the best MLP model. Next, considering the MAPE and MAE performance metrics, evaluation and comparison were performed between MLP and ARIMA-developed models. As a result, we found that the MLP model outperforms the ARIMA (0,2,3) model in forecasting electricity consumption demand. According to results shown in Table 6 and Figs. 4-5, we can claim that our MLP 1-8-12-1 model has best fitted our consumed electricity data and can be used to forecast the monthly electricity consumption demand of Kunduz province for the next three years. Table 7 and Fig. 7 depict the electricity consumption demand predicted by the MLP model from

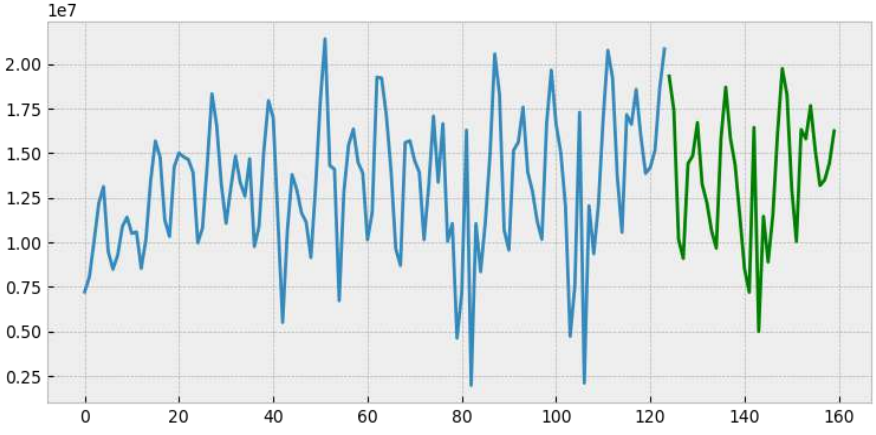

Fig. 7 Forecasted electricity consumption demand in Kunduz Province.

August 2022 to July 2025 in Kunduz province.

In the above plot graph, the x-axis represents the month, and the y-axis indicates the consumed electricity per month. The green curve in Fig. 8 represents the electricity consumption demand for the next three years. The blue curve depicts the previously consumed electricity amounts gathered from April 2011 to July 2022.

Table 7. Predicted monthly consumption demand from 2022 to 2025.

Date	*Consumption demand (kWh)*	*Date*	*Consumption demand (kWh)*
8/31/2022	19314937	2/28/2024	16439771
9/30/2022	17414938	3/31/2024	5005506
10/31/2022	10155868	4/30/2024	11450871
11/30/2022	9097788	5/31/2024	8899191
12/31/2022	14416275	6/30/2024	11523678
1/31/2023	14855235	7/31/2024	16109855
2/28/2023	16713509	8/31/2024	19746326
3/31/2023	13257330	9/30/2024	18268200
4/30/2023	12232078	10/31/2024	13009195
5/31/2023	10640783	11/30/2024	10048901
6/30/2023	9671043	12/31/2024	16318495
7/31/2023	15834149	1/31/2025	15806349
8/31/2023	18693112	2/28/2025	17664622
9/30/2023	15837168	3/30/2023	15160499
10/31/2023	14323535	4/30/2025	13183281
11/30/2023	11458181	5/31/2025	13504001
12/31/2023	8496194	6/30/2025	14425635
1/31/2024	7197085	7/31/2025	16239756

The prediction result reported by our MLP model shows that the electricity consumption demand will tend to have a slightly increasing trend over the proposed period in Kunduz province, as illustrated in Fig. 7 and Table 7. According to the forecasting result, the peak demand for electricity consumption will be in July and August. However, the model marked a decrease in consumption in March and April, probably due to the cool weather we had in these months. Overall, we can conclude that the demand for electricity consumption will somehow have an upward trend in Kunduz province for the upcoming three years. In this contest, we suggest to Kunduz regional electricity organization:

- Adopt more practical policies for electricity energy saving and efficiency.
- Make an effective energy generation strategy for solving the possible electricity supply shortage in the next three years.
- Facilitate investments by establishing a competitive market for generating electricity from other resources.

6. Conclusion

In this research paper, we conducted a time series forecasting analysis on the monthly electricity consumption data of Kunduz province to predict the consumption demand for the next three years. Two well-known forecasting methods, MLP from machine learning and ARIMA from statistics, were employed. Various MLP and ARIMA models were developed on our data series. By considering the AIC criterion for ARIMA and RMSE metrics as a cost function for MLP, we found the ARIMA (0,2,3) and MLP

with 1-8-12-1 neural network structure as the best-fitted models. Next, we assessed and compared the predictive performance of our established MLP and ARIMA models using the MAE and MAPE accuracy criteria. As for the evaluation result, we noted the MLP model with satisfactory forecasting results and can be used effectively to predict the consumption demand for the next three years. The prediction result from our MLP model showed that the electricity consumption demand would tend to have a slightly upward trend in Kunduz province for the next three years. The consumption might increase in July and August and decrease in March and April.

To the best of our literature knowledge, this is the first research work to apply time series forecasting approaches to predict the electricity consumption demand in Kunduz province. We believe that the outcomes of this research work significantly help Kunduz's regional electricity authorities in better energy management and allow them to make effective decisions regarding energy cost and efficiency. Also, the ministry of energy and water of Afghanistan and Kunduz's regional electricity organization can utilize the result of this research work in making effective decisions for short-term load balancing and strategic plans for new energy generation, transmission infrastructure, and preparation of secure power systems. For future research, we recommend that the forecasting models consider info from other predictors such as GDP, population, and indexations of industrial activity in Kunduz province. Also, in this research study, we implemented the conventional time series forecasting techniques. Future research can adopt other practical forecasting approaches, including the Gray model, Long Short-Time Memory (LSTM), and Support Vector Regression (SVR), which might improve the accuracy of consumption demand prediction.

7. References

[1] V. Bianco, O. Manca, and S. Nardini, "Electricity consumption forecasting in Italy using linear regression models," *Energy (Oxf.)*, vol. 34, no. 9, pp. 1413–1421, 2009.

[2] International Energy Agency, "Global Energy Review 2012." [online] Available: https://iea.blob.core.windows.net/assets/d0031107-401d-4a2f-a48b-9eed19457335/GlobalEnergyReview2021.pdf. [Accessed: 24-Jul-2022].

[3] Statistical Review of World Energy. [online] Available at: <https://www.bp.com/content/dam/bp/business-sites/en/global/corporate/pdfs/energy-economics/statistical-review/bp-stats-review-2021-full-report.pdf> [Accessed 24 July 2022].

[4] C. Nichiforov, I. Stamatescu, I. Fagarasan, and G. Stamatescu, "Energy consumption forecasting using ARIMA and neural network models," in *2017 5th International Symposium on Electrical and Electronics Engineering (ISEEE)*, 2017.

[5] S. L. Lai, M. Liu, K. C. Kuo, and R. Chang, "Energy consumption forecasting in Hong Kong using ARIMA and artificial neural networks models," *Appl. Mech. Mater.*, vol. 672–674, pp. 2085–2097, 2014.

[6] J. Miao, "The energy consumption forecasting in China based on ARIMA model," in *Proceedings of the 2015 International Conference on Materials Engineering and Information Technology Applications*, 2015.

[7] C. Hamzacebi and H. A. Es, "Forecasting the annual electricity consumption of Turkey using an optimized grey model," *Energy (Oxf.)*, vol. 70, pp. 165–171, 2014.

[8] A. Bagnasco, F. Fresi, M. Saviozzi, F. Silvestro, and A. Vinci, "Electrical consumption forecasting in hospital facilities: An application case," *Energy Build.*, vol. 103, pp. 261–270, 2015.

[9] S. Mishra and V. K. Singh, "Monthly energy consumption forecasting based on windowed momentum neural network," *IFAC-PapersOnLine*, vol. 48, no. 30, pp. 433–438, 2015.

[10] S. G. Yoo and H.-Á. Myriam, "Predicting residential electricity consumption using neural networks: A case study," *J. Phys. Conf. Ser.*, vol. 1072, p. 012005, 2018.

[11] A. Camara, W. Feixing, and L. Xiuqin, "Energy consumption forecasting using seasonal ARIMA with artificial Neural Networks models," *Int. J. Bus. Manag.*, vol. 11, no. 5, p. 231, 2016.

[12] S. Ozturk and F. Ozturk, "Forecasting energy consumption of turkey by Arima model," *J. Asian Sci. Res.*, vol. 8, no. 2, pp. 52–60, 2018.

[13] A. Jalil Niazai, A. Zahirzada, M. Akbar Shahpoor, and A. Rahman Safi, "Time Series Forecasting of Registered, Recovered, and Death Cases of COVID-19 for

the Next Sixty Days in Afghanistan," *2020 IEEE International Conference on Advent Trends in Multidisciplinary Research and Innovation (ICATMRI)*, 2020, pp. 1-6, doi: 10.1109/ICATMRI51801.2020.9398481.

[14] R. Adhikari and R. K. Agrawal, "An introductory study on time series modeling and forecasting," arXiv [cs.LG], 2013.

[15] X. Fan, L. Wang, and S. Li, "Predicting chaotic coal prices using a multi-layer perceptron network model," *Resour. Policy*, vol. 50, pp. 86–92, 2016.

[16] R. J. Hyndman and A. B. Koehler, "Another look at measures of forecast accuracy," *Int. J. Forecast.*, vol. 22, no. 4, pp. 679–688, 2006.

[17]

Authors Profile:

Abdul Jalil Niazai is an assistant professor at Kunduz University's software engineering department. He got a master's degree in information management from the Asian Institute of Technology (AIT), Thailand, in 2019, and BSc in computer science from Peshawar University in 2015. His research interest lies in data science, machine learning, and computer vision. Abdul Jalil Niazai has been acting as leader of the research committee of the software engineering department since 2020 at Kunduz University.

Mohammad Akbar Shahpoor received a BCS degree in computer science from Nangarhar university in 2012 and an MSC degree in computer science from the Indian Academy Degree College of Bangalore, India, in 2018. Presently, he is working as an assistant professor in the department of software engineering at Kunduz university. His research areas include software engineering, data science, and machine learning.

Abdullah Zahirzada received a B.Sc. degree in computer science from Kunduz University, Afghanistan, in 2016 and an M.Sc. in Information Technology at the School of Information Technology (SIT) from King Mongkut's University of Technology Thonburi, Thailand, in 2022. Presently, he is working as an assistant professor in the department of Information Systems at Kunduz university. His research interests are Data Science, Data Mining, Image Processing, Machine Learning, and Cognitive Computing.

Noor Ahmad Noori is currently a Ph.D. scholar at the National University of Science & Technology, Pakistan. He received an MS in Information Management from the Asian Institute of Technology, Thailand, in 2018 and a BSc degree in Computer Science from Peshawar University, Pakistan, in 2014. His research interests include Data Science, Big Data Analysis, Machine Learning, and Computer Networking. Noor Ahmad has eight years of administrative, teaching, and research experience.

Abdul Rahman Safi received a BCS degree in Information Systems from Kabul University in 2013 and an MS degree in Information Management from the Asian Institute of Technology, Thailand, in 2019. His research areas include software engineering, data science, and artificial intelligence. Presently, he is working as an assistant professor in the department of Information Systems at Kabul university.

KPU International Journal of Engineering & Technology
Volume 2, Issue2, Dec. 2022
e-ISSN:2790-0819, p-ISSN:2790-0800
Date Received: 2022-09-22
Date Accepted: 2022-12-18
Date Published: 2022-12-30

A Case Study of Climate Change Impacts Assessment on Ghowr Pozalich Small Hydro Power, Afghanistan

MUJEEBULLAH MUJEEB*

*Assistant Professor, Department of Natural Resources Management, Faculty of Environment, Kabul University, Kabul, Afghanistan. Email: mujeebmujeebullah1401@ku.edu.af

Abstract

In this study, climate change impacts on Ghowr Pozalich's small hydropower are conducted and this paper downsizes the investigation and centers on water resources for power generation. Small Hydropower (SHP) has developed as an energy source that is acknowledged as renewable, effortlessly created, reasonable, and safe for the environment. As of now, hydropower accounts for nearly 16% of the world's total control supply and is the world's most prevalent (86%) source of renewable electrical vitality. Hence, direct impacts on the sector of hydroelectricity are implied. Although run-of-river SHPs are also going to be impacted by the climatic variations, the research suggests that run-of-river SHPs can generate energy even in cases of declined river discharges and concludes on the slight impacts on power generation under specific water level variations. These highlights have expanded small hydropower improvement in esteem giving rise to a modern slant in the renewable vitality era. The protest of the inquiry is to examine climate alter impacts on energy generation delivered by run-of-river small hydropower plants with the utilization of future stream flow. The deferring impacts depend on such variables as neighborhood hydrological conditions and geographic highlights. There are numerous areas where runoff and hydropower era will increment due to expanding precipitation, but too numerous locales where there will be a decrease.

Keywords: climate change, Ghowr Pozalich, Hydrology, hydropower generation

* Corresponding Author

1. Introduction

Climate change alters is one of the awesome challenges of the 21st century [1]. A community's socioeconomic improvement and living benchmarks are all subordinate to power and the higher the standard of living, the higher the request for power. Power is the primary level of requirement for any financial movement in arrange to carry out generation [2]. The request for electrical vitality is expanding day by day, so the fast increment within the request for hydropower vitality and the perilous issues of worldwide warming and the going increment within the cost of fossil fuel is renewable energy. Renewable energy assets have expanded in cost, so that vitality can be gotten from a source in such a way that, despite being renewable, it has less negative impacts on the environment [3]. Small hydropower plants are one of the renewable energy sources that have maintained their importance because the energy is easily generated from water, it is easy to operate, and it is cheap. And it is an environmentally friendly resource. With these benefits, the demand and implementation of small water power plants are increasing throughout the world [4]. Because the big dams of electricity generation are not completed in the planned time due to the lack of national budget and environmental problems, filling this gap has also played a major role in the increased use and implementation of small hydropower plants, which in developing countries, less investment, less construction period, and harmony with the living environment are considered good. Because of the above advantages, micro-obese power plants have attracted the attention of both groups (developed and developing) of countries [4]. North America and Europe have already taken advantage of the hydroelectric potential. On the other hand, African, Asian, and South American countries have failed to use the existing water energy potential which is shown in Table 1.

Table 1. Installed Capacity of Small Hydropower Projects in the world [1]

Name of the Continent	Capacity in MW	Percentage (%)
Asia	32641	68
Europe	10723	22.3
North America	2929	6.1
South America	1280	2.7
Africa	228	0.5
Australia	198	0.4
Total	**97997**	**100**

Small-scale power plants are a good way to meet the shortage of electricity in developing countries, with China being a good example. China gets its two hundred and sixty-five gigawatts (265GW) of energy from three hundred forty-three thousand (43,000) small hydropower plants, which is a huge amount of energy production [5]. The Ghowr Pozlich Power Generation Project, which has a power generation capacity of 4.05 MW, is located on the river Harirod in Ghowr province and Chaghacharan district. Taking advantage of this economic potential will not only meet the electricity demand but also increase the economy and living standards of the country and especially the region. All in all, the number of small hydropower plants with a production capacity of more than one megawatt is small, and some of them are in serious need of rehabilitation. The Ministry of Water and Electricity should take concrete steps in this regard [6]. The implementation of renewable energy production projects in Afghanistan has many economic and social benefits; working land, access to electricity, social development, and reducing the negative effects of the climate at the international level. The Islamic Republic of Afghanistan is asking for cooperation from the international community so that our country can develop in this area and the next twenty (20) years, ninety-five percent (95%) of the country's energy production will come from renewable energy sources [7]. The Ministry of Water and Electricity has prepared the Law on the Regulation of Electric Energy Services and the Renewable Energy Policy to achieve the strategic goals of Afghanistan, which foresees the main contribution of renewable energy in development programs [8]. This arrangement will be executed in two stages. The primary stage will be actualized between the years 2015 and 2020 and amid this period will make a solid environment for renewable vitality advancement, private sector participation, and investment. In the second phase, which will be implemented between the years 2021 and 2032, renewable energy will be launched in a commercial form based on the experience gained in the first phase. Competitive elements are introduced. Afghanistan needs reliable energy sources for stability and development and fortunately has dedicated sources of renewable energy (hydro, solar, wind, biomass, and geothermal) [9]. Using the country's electric energy is the right of everyone based on the law on the regulation of electric energy services, so the production of electric energy should increase because the goal of renewable energy development is the development of Afghanistan's energy sector. Accordingly, the Ministry of Water and Electricity is the key ministry for the leadership and development of Afghanistan's energy sector to attract the confidence of investors in this sector. It was mentioned in the section on hydropower projects that the three decades of war in Afghanistan have stopped all the infrastructure projects, so the projects of small hydropower plants have also faced a long obstacle. Fortunately, it was said that around the year (2001), work started again in this area and various organizations implemented projects on a small production level in the villages, but still more efforts are needed to

make full use of the available economic potential. Utilizing this financial potential will not as it were meet the request for power, but will moreover increment the economy and living benchmarks of the nation, particularly within the locale [10]. All in all, the number of Small hydropower plants with a generation capacity of more than one megawatt is small, and some of them are in serious need of rehabilitation. The Ministry of Water and Electricity should take concrete steps in this regard. Afghanistan's renewable energy sources with productive capacities are shown in Table 2.

Table 2. Afghanistan's renewable energy sources with a productive capacity [1]

Energy production source	Total generating capacity in MW
Hydropower energy	23,000
Wind power energy	67,000
Solar energy	222,000
Geothermal energy	(3,000 – 3,500)
Biomass energy	4,000

The Ghowr Pozalich power plant project has a power generation capacity of 4.05 MW with an annual energy production of 16.15 GWh.

2. Study Area

2.1. Provincial Profile of Ghowr Pozalich Small Hydropower

The study area is located near Badghab village and sixteen kilometers (16 Km) east of Chaghacharan city [11]. The project consists of a thirty-meter (30 m) high dam located in a narrow valley with a tunnel on the left side, which diverts excess water downstream. The power generation structure is located in the lower part on the right side. The Harirod River flows from west to east and divides the Chaghacharan district into two parts. The Harirud River is located in the Harirud-Marghab river basin, which is one of the five largest river basins in Afghanistan. The tributary area of the project is sixteen kilometers (16 Km) west of Chaghacharan, near Badgah village on the Harirud river [12]. The catchment area is located in a place where there are steep mountains on both sides. While it was mentioned in the project section that three decades of war in Afghanistan have halted all infrastructure projects, ninety small projects have also faced obstacles which are shown in figure1 [12].

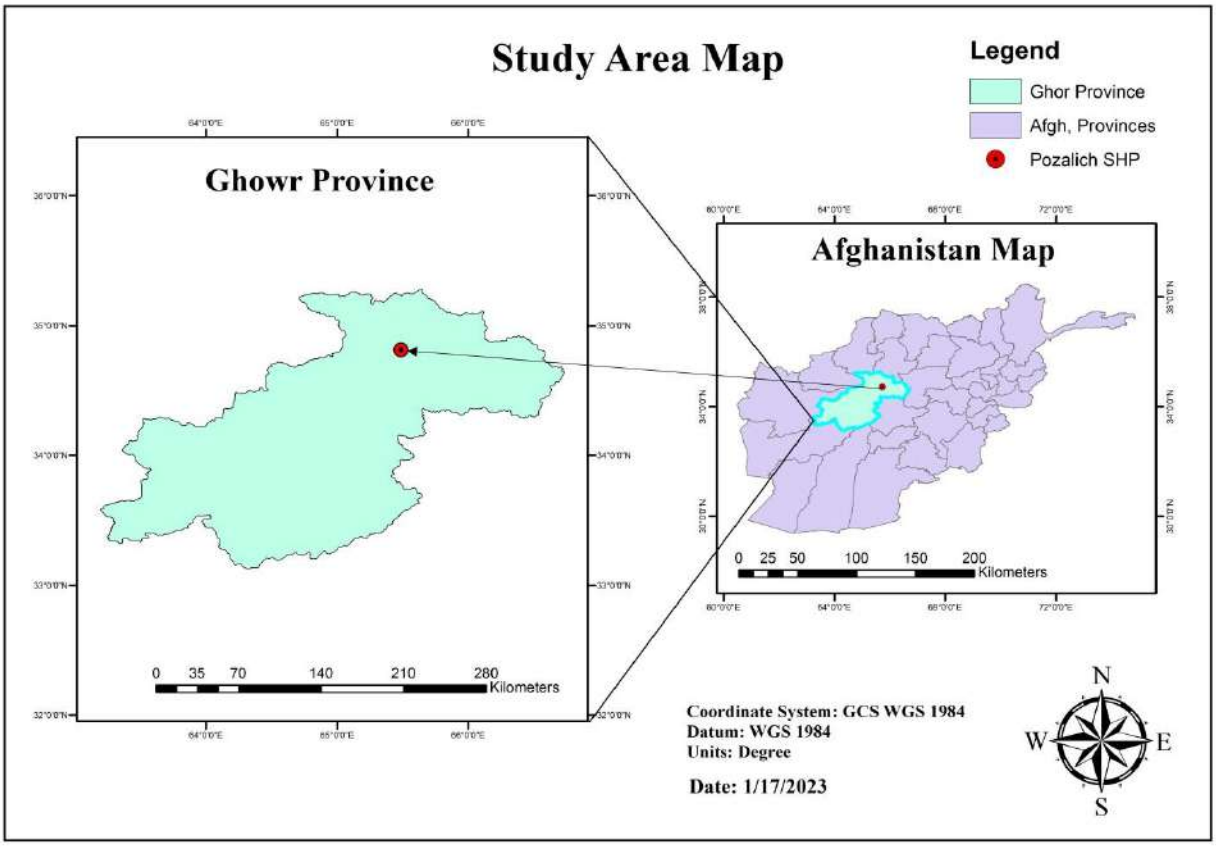

Figure1. Afghanistan Administrative Map and Ghowr SHP Location

3. Methodology

The SHP under investigation is the Ghowr Pozalich run-of-river small hydropower plant. To achieve the objectives, of this study, the literature mostly focused on climate change impacts in a general context and within Afghanistan for over the last 20 years was reviewed. Considering the review policy, authorized database search engines were used to filter the related scientific articles, conference proceedings, books, and reports from peer-reviewed and highly indexed journals. Based on the data from two measuring stations located at the end of the Ghor Pozlich Power Coat Project acquired from the Ministry of Energy and Water (MEW), the hydrological regime of the river can be assessed in different periods. This data is the Annual Mean Water Discharge (m^3/sec) of Chaghacharan Station between 1962-1980.

4. Climate change impact on small hydropower (SHP)

A few inquiries about discoveries distributed around the world include the climate change impacts on hydropower assets [12]. Nearly all of the hydropower ponders displayed in this paper have focused on expensive or medium spatial scales [13]. There are no specialized or financial reasons compelling the advance advancement of huge or medium-scale hydropower, but usually, they are built with a reservoir that would submerge plants and forests, reducing their carbon sequestering ability and then leading to methane emissions [14]. As a result, SHP stations, the larger part of which are runoff sorts without dams and supplies, play a vital role in rustic zap in numerous nations and are generally supported following a prosperous period of large or medium-scale hydropower improvement. See the noteworthy part of the SHP in the vitality framework of the long term, it is vital to pick up a better understanding of the impacts of climate change [15]. Since the centrality of hydropower time and its potential affectability to climate alter has as of now been set up in later time, a few quantitative gages of the specialized potential for hydropower have been established [16]. However, relatively few studies have addressed the specific factors of climate change's impact on hydropower. Based on previous studies, this paper focuses on the causal examination of these impacts and categorizes them as either coordinated or circuitous impacts [17].

4.1. Direct factor of climate change impact on hydropower

Global warming is one of the foremost climate change factors compared with other factors such as humidity, cloudiness, and precipitation. It has an important influence on hydropower generation and water resource supplies. Global warming increases global temperature patterns which then, in turn, alters the precipitation patterns [18]. One consequence of these alterations tends to be earlier spring snowmelt which has direct effects on hydropower generation [18]. It is well-documented that temperatures have been rising across the world and impacting the hydropower resource. Temperature is more likely to affect the operations of high-elevation hydropower reservoirs with low storage capacity [19]. High temperatures lead to more snowmelt and, often, more intense periods of seasonal precipitation. However, precipitation is not independent of rising temperatures which also leads to changes in power generation [19].

4.2. Power/Energy Generation Analysis

The Ghor Pozlich Power Plant Project, which has a 30-meter high dam and is used to generate electricity from stored water, during non-rainy seasons, maximum production is carried out only during peak hours. In the case of case operation, the height fluctuation will be from 15m to 25m. When the sediments fill up to 20 meters (20m) of sediment, the

water pipes will be raised to a height of 20 meters (20m). The designed flow of the project is 20m^3/sec, so during the times when the river flow is less than the designed flow, it only performs maximum production during peak hours and less production during non-peak hours [19]. Three Kaplan turbines with a production capacity of 1.35 MW each and a design flow of 6.67m^3/sec will be used in this project. For the examination of power generation carried out here, the general generation productivity (83%) is expected. Here, for three-seat Kaplan turbines, the upkeep plan ought to be adaptable, so a 2% blackout rate is calculated for the energy generation [19]. It is known that the yearly energy generation is rising to 16,150 MW. When it is raining, the current is added to the outlined current, so the electric coil can create the most extreme introduced control. Monthly energy production varies from 543 MWh in January to 2950 MWh in May. This is clearly shown in Table 3.

Table 3. Average monthly energy production for the SHP under consideration [1]

Mounts	**Jan**	**Feb**	**Mar**	**Apr**	**May**	**June**	**Jul**	**Aug**	**Sep**	**Oct**	**Nov**	**Dec**
Energy in MWH	543	576	2065	2855	2950	2855	1251	661	617	602	605	566
Power factor	0.18	0.22	0.7	1.00	1.00	1.00	0.42	0.22	0.22	0.2	0.21	0.19

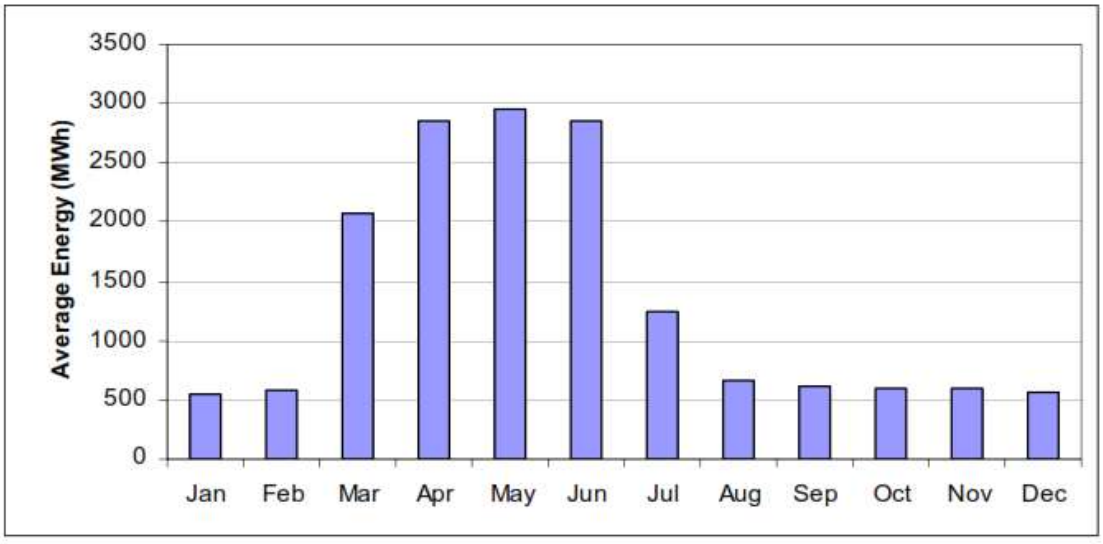

Figure2. Monthly energy production for the Ghowr SHP

5. Results

The Harirud River originates from the central mountains of Afghanistan, which are up to four thousand meters high. Because of the internal wars, there was no hydrological data on the process after 1980, but before that, there were nine hydrological measuring stations in the Harirud-Murghab river basin, seven of which were located in Harirud. Two measuring stations were located at the end of the Ghor Pozlich Power Coat Project. Both of these stations were the stations of Chaghacharan, and the second one was the state government station [1]. The hydrological data from these two stations were available for the years (1962-1980) which are shown in Table 4.

Table 4. Annual average flow (m^3/s) [1]

Year	Annual Discharge (m3/sec)
1962	22.2
1963	19.5
1964	31.8
1965	37.9
1966	14.9
1967	30.6
1968	30.2
1969	62.4
1970	16.6
1971	13.9
1972	30.6
1973	32.7
1974	20.4
1975	46.8
1976	43.8
1977	22.2
1978	27.8
1979	27.5
1980	38.2
Average	30.0

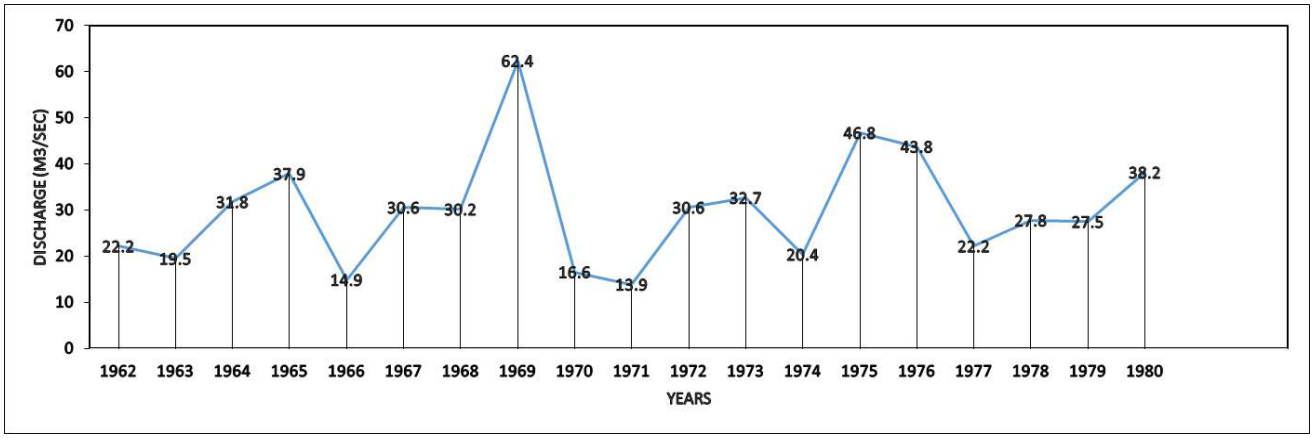

Figure3. Variations in flow discharge throughout the year

The amount of design current depends on the current field current. For projects that operate on the natural flow of a river and are connected to a large power grid, the optimal design flow is taken to be cited to a large power grid, the optimal design flow is taken to be 30% or more of the time flow [19].

5.1. Precipitation and Temperature

There are four meteorological stations in the vicinity of the catchment area, which are shown in Table 5.

Table 5. Metrological stations [1]

Station Name	Latitude (N)	Longitude (E)	Height (m)
Chaghacharan	34° 32˙	65° 15˙	2183
Ghalmin	34° 53˙	65° 18˙	2070
Lal	34° 30˙	66° 18˙	2800
Shahrak	34° 06˙	64° 17˙	2325

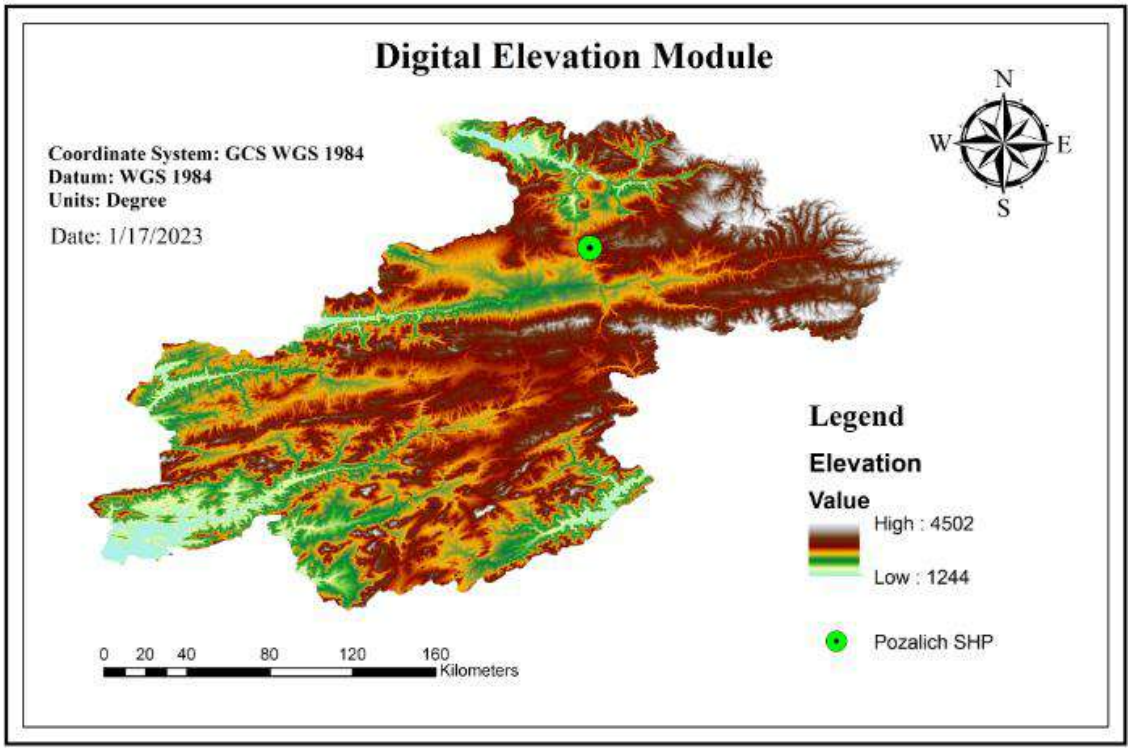

Figure4. The digital elevation module of Ghowr pozalich SHP

The average annual precipitation in four stations is 244 mm, and most of the precipitation is recorded as snow. Table 6 shows that the temperature reaches its lowest point in January and its highest point in July-August.

Table 6. The long-term average precipitation in (mm) [1]

Stations	Jan	Feb	Mar	Apr	May	June	Jul	Aug	Sep	Oct	Nov	Dec
Chaghacharan	36	28	33	41	14	0	0	0	0	6	13	18
Ghalmin	37	35	43	45	20	0	1	0	0	5	11	23
Lal	39	45	51	65	31	2	0	0	1	9	22	24
Shahrak	58	48	53	38	17	2	0	0	0	6	19	35
Average	43	39	45	47	21	1	0	0	0	7	16	25

Station Name	**Chaghacharan**	**Ghalmin**	**Lal**	**Shahrak**
Annual Precipitation	189	220	289	276
Average		**244**		

Precipitation and temperature are very heterogeneous in the Harirod River due to its large range in elevation. The temperature is lowest in January and highest in July-August.

Table 7. The long-term average temperature in (C°) [1]

Stations	Jan	Feb	Mar	Apr	May	June	Jul	Aug	Sep	Oct	Nov	Dec
Chaghacharan	-10.2	-8.1	1.9	8.9	12.9	17.9	19.2	17.8	12.3	6.4	1.2	-4.4
Ghalmin	-7.8	-5.0	3.7	9.4	13.6	17.9	19.8	18.6	13.6	8.5	2.6	-2.8
Lal	-13.2	-10.9	-2.7	4.5	9.2	13.9	13.9	17.8	15.4	4.5	-1.4	-8.54
Shahrak	-12.1	-10.6	0.8	7.9	11.9	11	17.7	16.4	11.9	6.2	6.8	--6.8
Average	-10.8	-8.65	1.9	7.7	11.9	15	18.2	17.1	12.0	6.4	2.3	2.3

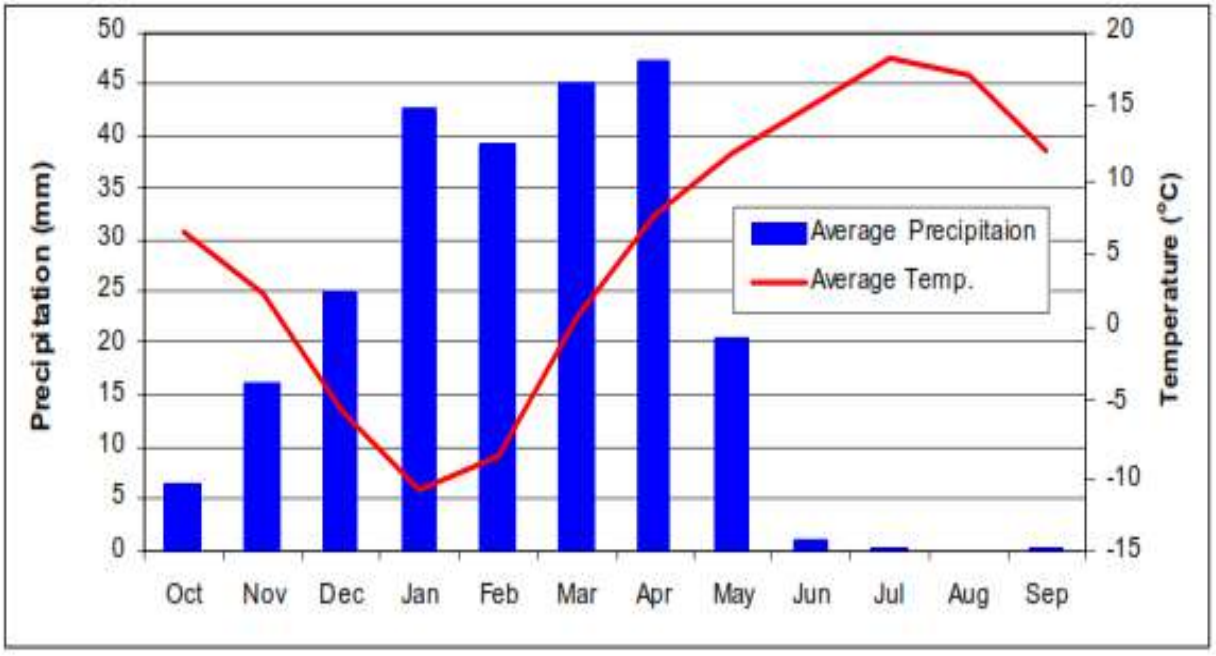

Figure5. The annual average variation in precipitation and temperature

7. Discussion

Both large and small-scale hydropower stations offer significant potential for near and long-term GHG emissions reduction. It is necessary to understand how to sustain and facilitate hydropower production under the adverse effects of climate change impacts. Despite many achievements that have been published on improving the understanding of

and how to cope with the climate change effects on water resources and hydropower, there are still large uncertainties with the dynamic hydrological processes.

Climate change and hydropower development interact with each other in the natural process, so any variation that occurs with one of them will lead to a change in the other. Several problems must still be further investigated. First of all, it is critical to improving the forecast and prediction of changes in the hydrological regime caused by global warming-related climate extreme events. With more spatial and temporal accuracy, these forecasts and predictions will help to make better and more accurate assessments of the hydropower development potential while coping with climate change. Secondly, all of the research presented in this paper was large-scale studies. Most of these studies lacked the unique local hydrographic conditions for project-specific research. Because of the diversity and distinctiveness of each hydropower station, it is extremely difficult to establish universal measures to mitigate climate change impacts. These results may provide more useful idiographic measures for local hydropower generation. In addition to technological efforts, government intervention in hydropower management and regulation should not be ignored. National, regional, and local governments can establish effective measures to promote the implementation of hydropower and other renewable energy projects, regulate and govern hydropower electricity utilization, assist managers with flood-control operations during high flow episodes, and improve water usage procedures during drought periods, and, to ensure the safety of environmental, eco-system, and socio-economic sectors.

With appropriate and feasible mitigation and adaptation strategies, hydropower can promote and enhance the development of local society and communities, and improve the quality of the environment and the socio-economic well-being of society.

8. Conclusion

Both large-scale and small-scale hydropower stations offer significant potential for near and long-term GHG emissions reduction. It is necessary to understand how to sustain and facilitate hydropower production under the adverse effects of climate change impacts. First of all, it is critical to improving the forecast and prediction of changes in the hydrological regime caused by global warming-related climate extreme events. With more spatial and temporal accuracy, these forecasts and predictions will help to make better and more accurate assessments of the hydropower development potential while coping with climate change. With appropriate and feasible mitigation and adaptation strategies, hydropower can promote and enhance the development of local society and communities, and improve the quality of the environment and the socio-economic well-being of society. Hydropower production depends on the available water volume. Climate change projections demonstrate increased stress on surface water resources in terms of

availability, duration of low and high water levels, and timing of seasonal peaks, especially at the end of the 21st century. Hence, direct impacts on the sector of hydroelectricity are implied. Although run-of-river SHPs are also going to be impacted by the climatic variations, the research suggests that run-of-river SHPs can generate energy even in cases of declined river discharges and concludes on the slight impacts on power generation under specific water level variations. It is known that the yearly vitality generation has risen to 16,150 MW. When it is down-pouring, the current is included in the outlined current, so the electric coil can create the most extreme introduced control. Month to month, vitality generation shifts from 543 MWh in January to 2950 MWh in May. Since the net head is twenty-five meters (25m) and the designed flow is 20 m^3/sec, the electromechanical devices for the project include three-digit Kaplan turbines, which are connected to special generators. Has been a typical layout of hydromechanical equipment is shown on the map. In addition to technological efforts, government intervention in hydropower management and regulation should not be ignored.

9. Recommendations

1. National, regional, and local governments can establish effective measures to promote the implementation of hydropower and other renewable energy projects, regulate and govern hydropower electricity utilization, assist managers with flood-control operations during high flow episodes, and improve water usage procedures during drought periods, and, to ensure the safety of environmental, eco-system, and socio-economic sectors.
2. As time passes, climate change impacts hydropower development and hydropower sustainability will increase and place greater stress on the entire energy continuum around the world. With appropriate and feasible mitigation and adaptation strategies, hydropower can promote and enhance the development of local society and communities, and improve the quality of the environment and the socio-economic well-being of society.

10. Acknowledgements

We are grateful to the Department of Hydrology and Meteorology, Ministry of Energy and Water, Afghanistan for providing us with the data on hydrology, meteorology, and electricity generation required for our analysis.

References

[1] "Feasibility study," Small Hydro Power Plant, Ghowr, Afghanistan, Tech. Rep. 11-901-BB, 2007.

[2] A. Eitan, " Promoting Renewable Energy to Cope with Climate Change—Policy Discourse in Israel," *Sustainability.*, vol. 13, no. 6, pages 1-17, March 2021.

[3] G . Bala, K . Caldeira and R . Nemani," Fast versus slow response in climate change: implications for the global hydrological cycle," *Climate dynamics.*, vol. 35, no. 2, pp 423-434, Aug 2010.

[4] C . Skoulikaris and J . Ganoulis, " Multipurpose hydropower projects economic assessment under climate change conditions, *" Fresenius Environmental Bulletin.,* vol.26, pp 5599-607, 2017.

[5] E. F . Moran, M . C . Lopez, N. Moore, N . Müller, and D. W. Hyndman, " Sustainable hydropower in the 21st century, " *Proceedings of the National Academy of Sciences.*,vol.115, pp 11891-11898, November 2018.

[6] H.S . Sachdev, A. K . Akella and N . Kumar," Analysis and evaluation of small hydropower plants: A bibliographical survey *Renew*, " *Renewable and Sustainable Energy Reviews*. vol. 51, pp 1013-1022, November 2015.

[7] O . Paish, "Small hydropower: Technology and current status," *Renewable and Sustainable Energy Reviews*., Vol.6, pp. 537-556, December 2002.

[8] K.M. Odunfa, E.A. Egungbohun, and O.D Owosen, "Hydropower potential of municipal water supply schemes in Osun State: A case study of Okinni Dam, Osogbo, Nigeria, " vol. 7, pp 44-74, June 2022.

[9] L. Berga," The role of hydropower in climate change mitigation and adaptation: a review," *Engineering.*, vol 2, pp 313-318, September 2016.

[10] B.Hamududu and A . Killingtveit," Estimating effects of climate change on global hydropower production," In Hydropower'10, *6th International Conference on Hydropower*, Hydropower supporting other renewables. Tromso, Norway, February 2010, pp13.

[11] M.S. Markoff and A.C. Cullen," Impact of climate change on Pacific Northwest hydropower," *Climatic Change.*, vol.87, pp 469–451, May 2007.

[12] L . Kosnik, " The potential for small scale hydropower development in the US," *Energy Policy*., vol.38, pp 5512-5519, December 2009.

[13] P.J. Robinson," Climate change and hydropower generation," *International Journal of Climatology*., Vol.17, pp 983-996, December 1998.

[14] M.J . Sale and S. C . Kao" Assessment of the effects of climate change on federal hydropower," Oak Ridge National Laboratory, Tech. Rep. 71-210-BB, 2011.

[15] L. B. Zhang, J. L Jin, Z .Y. Zhang, H . Zhang, Y. G. Zhao, " Brief discussion of several issues on the development of hydropower energy under climate change," *Journal of Water Resources Research* ., vol1, pp 501-504, 2018.

[16] A. Tilmant and R. Kelman," A stochastic approach to analyze trade-offs and risks associated with large-scale water resources systems," *Water Resources Research*., vol.43, pp 43, June 2007.

[17] K . Madani and J. R. Lund, "Estimated impacts of climate warming on California's high-elevation hydropower," *Climatic Change*., vol.102, pp 521–538, 2010.

[18] D.O.E," Effects of climate change on federal Hydropower," Congress, US Department of Energy Washington, Tech. Rep.20585- DC, January 2017.

[19] E . Kolokytha and C . Skoulikaris," WRM and EU policies to adapt to climate change- Experience from Greece," *Climate Change-Sensitive Water Resources Management*," *1st ed.*, Ed. London: CRC Press, 2020, pp.1-23.

Author Profile:

Mujeebullah Mujeeb received a B.S. degree in Civil Engineering from Nangarhar University in 2015 and an M.S. degree in Water Resources and Environmental Engineering from the Polytechnic University of Kabul in 2019. Presently, He is working as an Assistant Professor in the Department of Natural Resources Management, Faculty of Environment, Kabul University, Kabul Afghanistan. His areas of research include Natural Resources Management, Applied Hydrology, and Energy Resources.

KPU International Journal of Engineering & Technology
Volume 2, Issue2, Dec. 2022
e-ISSN:2790-0819, p-ISSN:2790-0800
Date Received: 2022-10-10
Date Accepted: 2022-12-22
Date Published: 2022-12-30

A Review on Physical Properties of Nano-Concrete

NOORULLAH ZAHID*

*Assistant Professor, Department of Civil, Engineering Faculty, Shaikh Zayed University, Khost Town, Afghanistan. Email:zahidnoorullah@gmail.com

Abstract

All the properties of concrete are associated with the processes that occur at the nano-scale. In this study, the physical properties of nano-concrete are reviewed. Nano-concrete has nanoparticles (such as Nano SiO2, Nano Al2O3, NanoTiO2, Nano Fe2O3, Nano Fe3O4, Nano Clay, NanoZrO2 carbon nanotubes, nano-fibers, and carbon nano-fibers) as admixtures in small quantities as a percentage of the burden of the cement. Due to its excellent physical properties, nano-concrete is becoming more and more popular in practical engineering. To get a deep understanding of the physical properties of nano-concrete, researchers have done a lot of research in this area. In this review paper, the most common is used. The nanoparticles have effectiveness on concrete's physical performance such as strength, modulus of elasticity, durability, density, abrasion resistance, resistance to permeability, and water absorption and frost resistance. Nanoparticles improve the share of strength and modulus of elasticity with the relevancy of the control mixes. The microstructure of various varieties of concrete is significantly enhanced upon the addition of nanoparticles and as a result durability of concrete increases. The microstructure of concrete with nanoparticles is denser and more uniform than that of conventional concrete. The nanoparticles reduce porosity, increase the density of cement concrete, and thus show an improvement in resistance to permeability and water absorption than conventional concrete, and therefore the frost resistance of concrete is improved. The addition of nanoparticles to concrete mixes showed more abrasion resistance for concrete and mortar. The decrease in workability of concrete with nanoparticles may be compensated by using of superplasticizer in concrete mixes.

Keywords: Nano-concrete; Nanoparticles; Nanotechnology; Physical property.

* Corresponding Author

1. Introduction

Nanotechnology of concrete includes nanometer-scale renovation techniques to form a brand new adequate generation of cementitious composites with ideal physical behavior, with the assistance of which made the concrete with unique properties. The final word goal of concrete nanotechnology is that the studying of concrete at the nano-scale and also the studying of nanoparticles accustomed give better properties to concrete.

Among the changes that nano-cement and nano-cementing materials have brought in concrete technology is the increase in crack resistance, decrease within the curing time, increase in ductility, and also increase in its strength. These positive changes have led to the employment of nano cement in most industries. The nanoparticles like TiO_2, Al_2O_3, ZnO_2, SiO_2, carbon nanotubes, nanofibers, and carbon nanofibers can affect the mechanical and physical properties of cement concrete. When the cement particles mix, the combination is composed of holes from some micrometers to some millimeters, which is one of the explanations for the low strength of cement concrete. the employment of nanotechnology has solved this problem. So well that nano-crystals penetrate within the pores of cement mix and well cover the space between cement particles. This decreases the porosity and permeability which highly affect the standard of the concrete mix and increases its strength and durability [28].

Nanocrystals that fill nanopores will affect and increase their viscosity furthermore. On the opposite hand, nano cement granules and nano-particles are suspended in liquids and water and don't precipitate. This function allows for the preparation of a dense and suitable cement paste with nano-particles and cement. The very dense cement paste will positively affect the physical properties of cement concrete [44].

Nanomaterials such as nano silica, nano-TiO_2, Al_2O_3, ZnO_2, carbon nanotubes, nanofibers, etc. have the capability of improving the properties of concrete. It is clear that nanomaterials are still in their developing stages, and they have many challenges and unsolved complications for their huge commercial and application prospects. The main objective of this article is to study the incorporation of nanostructured materials in concrete mixes, which could improve the concrete's physical properties such as strength, modulus of elasticity, durability, density, abrasion resistance, resistance to permeability and water absorption, and frost resistance. The microstructures of concrete are significantly improved by the inclusion of nanomaterials, as the nanomaterials enhance the hydration process by generating more hydrated products.

2. Nano-concrete

Concrete is a construction material from an acceptable mixture of cement, water, sand, and gravel. Concrete is formed of cement paste (obtained from the chemical action of cement and water) and aggregates (sand and gravel) where the paste acts as a glue and binds the sand and gravel thus receiving concrete. In some cases it's necessary to feature some admixtures that are added to concrete in small quantities as a percentage of the burden of the cement, some part of them are nanoparticles, these nanoparticles are employed in concrete to urge some good properties like increasing strength, density, and durability of concrete. When nanoparticles are added to a concrete mixture as cement replacement in various percentages, this type of concrete is called nano-concrete [17].

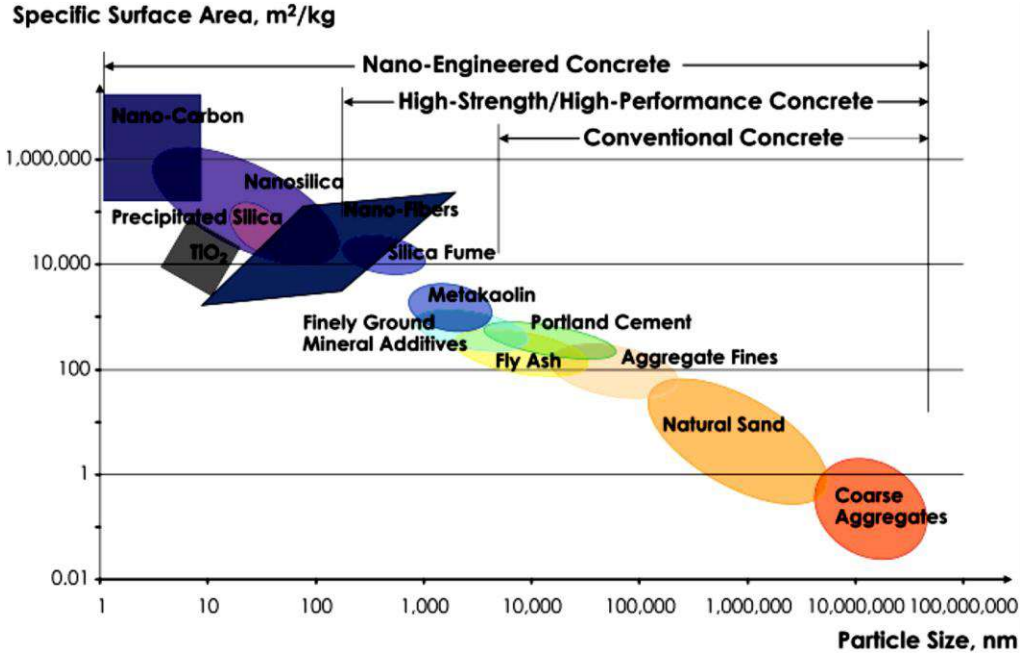

Fig.1 The particle size and specific surface area scale related to concrete materials [39].

2.1. Differing types of nanoparticles used in concrete:

Nanoparticle refers to the ultrafine material with particle size at the nanometer level (1-100nm), which is larger than the atomic cluster (the cluster of atoms but 1nm in length) and smaller than the usual powder, within the transition zone of the cluster to the macroscopic object, a typical mesoscopic system. Because of its small size, large area, and other factors, have subsequent four special effects: size effect, quantum effect, surface effect, and interface effect. These four effects mainly reflect the structural, chemical, and physical characteristics of nanoparticles, which are called "the most promising materials of the 21st century".Nano-mineral powder mainly includes nano-silica, nano-calcium carbonate, and nano-silica powder. In ordinary hydraulic cement within the distribution

of 10-100nmgel pores, the incorporation of nano-powder just fills these gaps and plays a job in improving the permeability of concrete and toughness [44].

There are different types of nanoparticles utilized in concrete. There'll introduce the foremost important and widespread nanoparticles which are employed in cement concrete. These nanoparticles are usually made up of the cement itself, like nano iron, nano corundom, nano silica, etc. these nanoparticles have many advantages and downsides, and therefore the main problem of using these nanoparticles with cement concrete within the world belongs to them is that the economic discussion and their impact on the environment. For this reason, it's important to seek out the optimum and effective amount of those nanoparticles within the concrete and to search out nanoparticles that haven't any harmful effect on the environment [40]. Below are some current research results presented and reviewed. Sun et al, researched to change the impact of nano-silica on the concrete's initial compressive strength in large quantities of ash [40].

The results show that the nanoparticles are incorporated into the concrete, which might effectively improve the mechanical properties like compressive and flexural properties of concrete. The incorporation of nano-silica improves the mechanical properties of concrete much beyond that of nano-calcium carbonate. The explanation is that the volcanic ash activity of silica is far above that of silica fume, and also the incorporation of silica makes the slurry fluidity decrease and therefore the aggregation time is significantly shortened. At the identical time, the incorporation of nano-silica also can significantly improve the concrete early strength. Nano-silica puts into the cement, thanks to its structure, physical and chemical characteristics, and cement during a sizable amount of Ca(OH)2 combined, thereby promoting cement hydration, improving the reaction of the exothermic efficiency so the cement slurry micro-structure to boost the cement more uniform and dense. Nano-calcium carbonate incorporation plays physical and chemical effects, reducing the inner area of cement stone to hurry up the first hydration of clinker speed, reducing porosity, increasing the density of cement concrete, and thus improving the compressive strength of concrete [44].

The study shows that the control cement sample lacking ash and nano-silica had the best compressive resistance. This control sample's strength was 58% cement and a couple of steel,40% ash, and nano-silica. Adding huge quantities of ash, particularly greater than 70%, concrete's compressive strength is drastically decreased. Jalal et al, have also checked out high performance [8].

In the study where samples containing nano-silica showed higher strength than samples containing nano-silica ash [33], [13]. The effect of ash on nano silicone on the compressive strength of high-performance compacted concrete [8].

The results show that the addition of ash decreased the strength and also the addition of nano-silica increased the strength. However, the compressive strength of 15% of ash in concrete at 90 days is slightly increased compared to the control. Rahim et al studied the effect on the compressive strength of cementitious concrete containing wood ash by adding nano-silica [27]. Contains a sample containing 2% nano-silica within the presence of wood ash, the effect of nano-silica is little when young, but resistance increases with age. This increase is because of improved pozzolanic reaction. However, during this study, the optimal amount of nano-silica is 1.5%. Windham and Vapilay also investigated the results of nano silica [43], per their research, increasing nano silica increases compressive strength and so decreases it. Therefore, 1.5% gives the very best compressive strength. The rationale for this increase is that the hydration process of tricalcium silicate (C3S) is quicker within the presence of nano-silica. The use of carbonate nanoparticles has been explored, leading to improved mechanical strength, impact resistance, and flexural strength [25].

Another study by Ehsani et al, combined carbonate particles with a carbon coating and investigated the effect on the compressive strength of concrete [25]. This carbon coating is the result of the soot-burning material being combined with lime milk in solution by the reactor. Supported observations, we discover that his 3-day strength of calcium carbonate-bearing concrete with nanocarbon coating shows a decrease in strength compared to the quality sample, as an example, the tenth amount of cement by weight reduces strength by approximately 15.6%. Studies have shown that as concrete ages, the 7-day strength of concrete increases in compressive strength compared to regular concrete specimens. This increase occurs up to three of the burden of the cement, but as this nano fraction increases, the sample undergoes a process of decreasing compressive strength at 7 days old. In addition to the self-cleaning properties of concrete.

Research has shown that the utilization of titanic oxide nanoparticles improves the hydration rate and shortens concrete curing time [10]. Also, the employment of those nanoparticles increases the flexural strength and compressive strength of concrete showing the effect of adding titanium dioxide nanoparticles to the concrete itself [14], [15]. The addition improves the microstructure of concrete and reduces internal voids in concrete, which improves the mechanical properties and durability of concrete [9].

The addition of alumina nanoparticles to the concrete mixture significantly increases the modulus of elasticity of concrete. Experience has shown that adding 10% aluminum nanoparticles increases the modulus of elasticity of concrete by 153%, but has no significant effect on concrete strength [16]. The theoretical and mathematical effects of the addition of aluminum oxide nanoparticles on the hydration of concrete were investigated, and it had been found that the addition of those particles reduced heat release and accelerated the height release time of that heat [28].

The addition of three by weight of corundum nanoparticles to concrete reduces heat to release the foremost [28]. Theoretically and mathematically, the results of the workability of modified concrete containing 0.5, 1.5, 0.5, and a pair of alumina nanoparticles by weight of cement are studied, and also the results show that increasing the number of alumina oxide nanoparticles decreases the workability of concrete. The samples of concrete-containing nano-silica give better results than samples of concrete-containing nano ferrite with an approximate rate of about 10%. The samples of concrete containing granite give better results than similar-containing dolomite and also the approximate rate of about 10%. The utilization of a superplasticizer was necessary for the concrete mixes to boost workability [18].

Table 1. Effect of some important nano-particles on properties of concrete [39].

S/ No.	***Nanoparticles used***	***Improved property of concrete***
1	Nano-silica	○ Contributes to reduced emissions of CO2, as the addition of 1 kg micro silica reduced almost 4 kg cement, and this can be higher if nano silica is used ○ Offers increased durability to concrete ○ Improves compressive strength ○ Increases the flexural strength, ○ Improves the tensile strength
2	Carbon nanotubes	○ Decreases the concrete's final setting time, ○ Restricts crack development and propagation at early ages, ○ Produces dense concrete, ○ Increased quality of bond interaction between aggregates and cement paste ○ Increases the compressive strength ○ Improves the tensile strength, Young's modulus, flexural strength, and fracture toughness ○ Decreases the required size of concrete structural members ○ Decreases the early and long-term shrinkage of concrete
4	Nano-TiO2	○ Increases the abrasion resistance of concrete ○ Improves compressive strength ○ Increases the durability of concrete structures ○ Increases the flexural strength ○ Speeds up the early-age hydration of ordinary ○ Portland cement ○ Offers self-sensing and self-cleaning properties to concrete structures

5	Nano-Fe2O3	○ Improves compressive strength ○ Increases the flexural strength ○ Improves split tensile strength ○ Reduces the setting time of fresh concrete ○ Decreases the total porosity of concrete ○ Improves concrete's abrasion resistance
6	Nano-Al2O3	○ Increased serviceability ○ Increases the modulus of elasticity of concrete. ○ Reduced heat release ○ Accelerated the height release time of the heat
7	Copper nanoparticles	○ Improves formability ○ Increases corrosion resistance

3. Effect of nanoparticles on physical properties of concrete

Compressive strength: Based on research, it can be said that nano silica (NanoSiO2) is the most commonly used nanoparticle in a cement matrix, but there are other nanoparticles such as NanoAl2O3, NanoTiO2, NanoFe2O3, NanoFe3O4, NanoClay, NanoZrO2, etc. used. Adding 1, 3, and 5% NanoSiO2 and NanoTiO2 to regular concrete showed a 12% increase in compressive strength for the sample containing 1% nano-silica and an 18% increase for the sample containing 1% nano titanium dioxide. [13], [8]. Another study reported that Zr, Fe, Ti, and Al nano-oxides were used at 1.5 wt% of the cementitious material in super-reinforced concrete, with the best improvement in compressive strength of 55% for samples containing nano-alumina [27]. Adding 0.5 to 2% of nano-silica and nano-alumina and curing in both water and lime water showed that in both cases nano-silica performed better than alumina, with similar results for the treated samples [43]. In another study, nano-silica and micro silica were used in proportions of 1, 3, 5, and 7 in aerated concrete, and nano-silica had a much better effect. A sample containing 7% nano-silica showed a 48% increase in compressive strength [38]. The use of nano Fe_2O_3 at a percentage of 1 to 5 provides the greatest improvement in compressive strength (72% increase with 4% by weight) [30]. Nanosilica dioxide and aluminum are used in ordinary concrete. The optimum percentage of these nanoparticles ware 3% by weight of nano-aluminum oxide and 5% by weight of nano-silicon cement to improve the maximum compressive strength of concrete, 8%, and 30%, respectively [5]. Another study used polypropylene (PP) fibers in addition to nano-silica and nano-aluminum, and the highest improvement was associated with 5% nano-silica, using 2% PP fibers by volume of concrete. The amount of improvement was 31%, slightly greater than the improvement of 5% silica without fibers [11]. The addition of nano-silicon dioxide in amounts of 0.3 and 0.9% by weight of cementitious materials increased the compressive

strength of concrete by 9% and 12%, respectively [4]. Another study used 10% by weight nano-silicon cement and showed an approximately 30% improvement in compressive strength [41]. The use of 1% and 2% nano-silica also increased the peak compressive strength of concrete containing 2% nano-silica with a water-to-cement ratio of 0.39 by 11% [3] in a review article [37].

The use of nano-silica in HPC (high-performance concrete) with body ash of 0%, 1%, 3%, 5%, 7%, and 9% and increasing the number of nano-silica up to five improved the compressive strength of the samples up to 22% in 3 days old samples. And for above 5% of nano-silica like with 7% and 9% of nano-silica, this improvement decreases [6]. In an exceeding study on macro and micro characteristics of concrete through the employment of carbon nanotubes of 0.3%, 0.5%, and 0.75% of the cement weight. The results showed that carbon nanotubes could improve compressive strength by 12% [42]. The development of compressive strength of concrete at the age of three,7, and 28 days showed a major increase. At the age of three days, the compressive strength of concrete that contained nano silica increased between 3.82% - 11.84%; whereas, at the age of seven and 28 days, the compressive strength of concrete with nano silica increased respectively by 3.87% - 17.24% and 4.93% - 24.59%. The resulting splitting enduringness ranges between 13.298 MPa – 19.918 MPa. there's a powerful correlation between concrete's splitting lastingness and compressive strength. The splitting enduringness tends to extend together with the rise of concrete's compressive strength [36].

Modulus of elasticity: The development of compressive strength of concrete at the age of three,7, and 28 days showed a big increase. At the age of three days, the compressive strength of concrete that contained nano silica increased between 3.82% - 11.84%; whereas, at the age of seven and 28 days, the compressive strength of concrete with nano silica increased respectively by 3.87% - 17.24% and 4.93% - 24.59% [36]. With the addition of nano-silica and nano ferrite, the improving percentage of flexural strength and modulus of elasticity of concrete reaches an approximate rate of about 23% and 25%, respectively, with relevance to the control mixes. Increasing the number of NS and NF by quite 3% and a pair of by weight degrades the compressive strength, splitting tensile, flexural strength, and modulus of elasticity of concrete [18].

Durability: Nanosilica is capable of improving the durability of concrete. The rise of 10% nano-silica replacement within the resistance to sulfate attack is healthier than that of 0% nano-silica [35]. In a study reviewed the employment of nanoparticle materials in several styles of concrete was discussed, and conclusions are provided that nanoparticles reduce the permeability of cementitious mixtures against chloride ions; thus, lower values of chloride ion penetration are seen with the incorporation of nanoparticles. The inclusion of nano-scaled particles improves the resistance against freezing and thawing. Using 5%

of nano-silica and three nano-alumina reduced the loss of compressive strength by 16.28% and 18.19%, respectively. Various kinds of nanoparticles impose different effects on the shrinkage property of the mixture. The carbonation depth of concrete can obtain different values with differing types of nanoparticles. The microstructure of various varieties of concrete is significantly enhanced by the addition of nanoparticles since nanoparticles improve the hydration process by producing more hydrated products [29]. A study base on experimental results obtained that coal ash concrete containing NS significantly improved the mechanical properties of concrete specimens relative to a bearing concrete (without NS), which was because of the reaction of NS particles with Ca(OH)2 at the ITZ to provide more C-S-H gel and therefore the densification of the microstructure. However, the optimum amount for every mechanical property was different; the splitting durability reached a maximum when the NS replacement level was 2%, and when the NS replacement level was 3%, the compressive and flexural strengths reached their maximums. Adding NS particles can dramatically improve the impact resistance at the primary cracking of the concrete; however, the speed from initial cracking to failure was faster, and therefore the brittleness of the concrete didn't change. After being impacted, the concrete specimens containing NS were divided into two halves along the impact direction, and also the concrete specimens still exhibited brittle failures, as in ordinary concrete. Compared with the control concrete, the low dosage of NS can greatly ameliorate the concrete's chloride penetration resistance and freezing-thawing resistance. At the two replacement levels, uniform dispersion of NS particles was easily achieved. The development of the pore structures within the concrete and also the filling effect of the NS were liable for the reduction within the chloride diffusion coefficient and ameliorated the freezing-thawing resistance of the concrete [26]. The application of nano-based concrete materials is beneficial concerning enhanced engineering properties of cement materials, particularly for the production of sustainable as well as self-healing concretes.

Density: Based on the results of the research conducted on concrete with the addition of nano-silica as cement partial substitute material, the result is summarized that nano-silica is in a position to extend the density and sturdiness of concrete. In an experimental study adding nanoparticles of the dimensions of but 100 nm into the concrete mix. This study evaluated the utilization of varied nanoparticles in concrete and so compared them to standard concrete. Concrete containing nano silica and nano clay was compared to concrete containing silica fume, fly ash, and slag. The results showed that the microstructure of the nano-silica concrete was denser and more uniform than that of the traditional concrete [24]. In an experimental study on mortar by adding TiO2 nanoparticles of 0.5%, 1.0%, 1.5%, and 2.0% of the cement weight were. the common size of TiO2 nanoparticles was 15 nm. The research results at the age of seven days

showed that the nano-TiO2 paste was denser and more compact than that without nano-TiO2 [21].

Abrasion resistance: The use of nano SiO_2, nanoTiO_2, and polypropylene (PP) fibers shows that the lower usage levels of these nanoparticles have better effects on abrasion resistance, and the addition of 1% titanium dioxide was better than 3% and 5%. Improvements of 181%, 148%, and 90% were found, respectively, and the application of 1% nano-silica had a better effect on abrasion resistance than 3% nano-silica, respectively [8]. Another study on Nano SiO_2 and Nano Al_2O_3 used 0.5–2 wt% in water and lime water, and the abrasion resistance of nano silica was better than that of nano alumina. The optimal amount of these materials is 2% by weight of the cementitious material [43]. Different percentages (4%, 8%, and 12%) of nano SiO_2 were added to the colloidal solution, and different amounts (25%-50% at different times and numbers) were also used as sprays 1 to 3 times. Treat with the colloidal solution for 28 days, then test or treat with water and spray onto a clean surface. In each case it contained a higher amount of nano silica of 50% and sprayed 3 times or 12% colloids (showed greater improvement in abrasion tests) Treatment and spraying with colloids containing nanoparticles gave abrasion resistance improvements of 42% and 32%, respectively [33]. The addition of nanoSiO_2 and nano SiC in percentages of 1, 2, and 3 separately and in combination shows that the optimal amount to improve the abrasion resistance in concrete is 2 and 3% by weight of cementitious materials for nano SiO_2 and nano SiC, respectively (49 and 68% improvement, respectively) and the combined mode is the answer better (75% improvement) compared to the separate state [22].Comparison using 40% fine nanoporous material or 5% nano-silica or a combination of 5% nano-silica and 25% fly ash as alternatives to cement. It showed 20%, 16%, and 13% more abrasion resistance for concrete and 82%, 73%, and 68% more abrasion resistance for mortar, respectively [31].

Resistance to permeability and water absorption: The use of silica and titanium nanoparticles and PP (polypropylene) fibers in concrete improved the chloride penetration resistance by 31% and 18% for samples containing 1% nano-titanium dioxide and 1% nano-silica, while PP fibers negatively affected chloride penetration resistance. Also in this study, samples with low levels of nanoparticles showed 1% better improvement than samples with high levels of 3% and 5% against chloride penetration [13]. NZrO_2, NFe_3O_4, NTiO_2, and HPC concrete with 1.5% nanoparticles of NAl2O3, 80% improvement in water uptake from samples containing NFe_3O_4 and NTiO_2 and 70% improvement in chlorinated NZrO2 penetration by NAl2O3 (70%) [27]. In a study on aerated concrete, nano silica by 1%, 3%, 5%, and 7%, and micro silica by 3%, 5%, and 8% were used separately. Micro-silica had a better effect than nano-silica on permeability. The addition of 8% micro-silica showed an improvement of about 25% and the addition of 7% nano-silica also showed a permeability improvement of about 20% [38].

Nanohematite is equivalent to 4%, showing an improvement in water absorption of about 74% [30]. Nanoacids Al_2O_3, Fe_2O_3, Fe_3O_4, and nano clay showed positive effects on the water absorption of cement mortar, and the authors reported different optimal amounts from 0.5% to 4%, depending on the type of treatment and other materials used in the concrete mix [19]. Nano-silica, nano-alumina, and nano-hematite were put into two types of mortar containing fly ash and silica foam separately, and the compound to be used and its permeability and water absorption were investigated. The addition of 1.25% of nano-aluminum oxide in a mortar containing silica foam has improved 29% of the permeability [23]. Using 1.25% of the three mentioned nanoparticles as combinations described in a fly ash-containing mortar increases the water absorption of the mortar by 14% [32]. Using 0.3% and 0.9% Nano SiO_2 also improves water permeability, so adding 0.3% nano-silica increases the permeability of concrete by 56% [4]. In one study, two types of nano silica were used, one with a fine particle size of 15 nm and the other with a large particle size of 80 nm (each with a 4% difference) (0.5, 1, 1.5, and 2) are used. Water permeability was tested and in the long run, larger nanoparticles showed a superior effect in improving permeability (approximately 23% using 2% of the weight of coarse-grained nano-silica cement) but in the short term, the effect of finer nanoparticles has been better [20]. Nano-silica colloids were used in two different ways (spraying or treatment with nano-silica colloids) to improve permeability, which is the best result for the case where samples were applied in colloids containing 12% nano-silica and 31% improvement in water permeability is shown. Also, the spray of a solution containing nano-silica at a concentration of 50% increased the permeability by 12% [33]. In one study, the effects of Nano SiO_2 on the mechanical properties and durability of concrete were examined in various investigations [7]. Colloidal and powdery modes were used, and the addition of 3.8 wt% nano-silica improved the water permeability by 88% [12].

Frost Resistance: Frost resistance is one of the keys to the durability of concrete, and one of the factors that affect the durability of concrete is the cycle of freezing and thawing. Because the strength of concrete is directly associated with the security and performance of the building structure, its mechanical properties are of concern. To make sure the sturdiness of the building structure within the use of the method, frost resistance in the real world is critical. Consistent with the freezing and thawing of M7.5 specimens, the inner structure of the concrete after adding nanometer material was greatly improved, and also the internal structure of the concrete was improved greatly. The pore size of 150mm disappears from the concrete, greatly increases the interior density of concrete, and avoids structural damage caused by hydrostatic theory and force per unit area theory. Xiaolin Ren and Shunkai Li studied the identical similar comparison test. it was found that under the condition of $-10C^0$, 25 times freeze-thawing was allotted, the incorporation of nanometer material was 0.75% concrete strength loss was 3.2%, and also the reference

concrete loss rate was 8.6%, the nanometer material within the concrete, the frost resistance of concrete is improved [36].

4. Discussion

In recent times, advanced nanotechnology has been employed in various sectors for the comfort and welfare of humanity. A majority of the nanostructure-based products applied to date in the concrete sector have numerous advantages. There are several explanations for accepting the fact that nanomaterial usage is rising. Innovative concrete structures need structural components with superior properties, as well as higher durability. The best solution is the incorporation of nanostructured materials in concrete mixes, which could improve the concrete's properties. It should also be noted that nanomaterials are still in their developing stages, and they have many challenges and unsolved complications for their huge commercial prospects.

Nanomaterials such as nano-silica, nano-TiO2, Al2O3, ZnO2, carbon nanotubes, nanofibers, etc. have the capability for increasing the durability of concrete by improving mechanical and thermal properties. The microstructures of various kinds of concrete are remarkably improved by the inclusion of nanomaterials, as the nanomaterials enhance the hydration process by generating more hydrated products. Incorporating various nanomaterials into the concrete mixes decreased the setting time as well as workability, which was due to the stronger reactivity of nanomaterials having a larger surface-to-volume ratio. The decrease in workability of concrete with nanoparticles may be compensated by using of superplasticizer in concrete mixes.

Improvement in compressive strength could be observed with an improvement in the replacement ratio of nanomaterials. This was due to the improved hydration of a more compacted microstructure with the incorporation of finely dispersed nanomaterials. With the incorporation of a nanomaterial such as carbon nanotube (CNT), the concrete compressive strength could be improved to 21%, and also it can result in a decrease in the early as well as long-term shrinking of concrete of 54.0% and 15.0%, respectively. Moreover, the CNT addition to concrete showed 17.0% to 18.0% reduced long-term creep as compared to the concrete with no CNTs. Overall, it was noted that optimum concentrations of nanomaterial incorporation in the concrete could enhance its flexural, tensile, and compressive strength, along with workability and water absorption. With the addition of nano-silica and nano ferrite, the improving percentage of flexural strength and modulus of elasticity of concrete reaches an approximate rate of about 23% and 25%, respectively, with relevance to the control mixes.

Nanomaterials could positively impact the increase in the sustainability and durability of concrete. Nanosilica is capable of improving the durability of concrete. The rise of 10% nano-silica replacement within the resistance to sulfate attack is healthier than that of 0% nano-silica. Different nano-materials could improve the self-healing property of concrete

and will restore the weakened constructions in an advanced manner at a lesser expense, relative to that accomplished by epoxy-containing healing products, therefore attaining ecological sustainability. The reaction of Nano-silica particles with Ca(OH)2 at the ITZ provided more C-S-H gel and therefore the densification of the microstructure could be obtained. The application of specific nanostructured materials could improve the performance of concrete, as well as its life cycle.

Results have been showing that the nano-TiO2 paste was denser and more compact than that without nano-TiO2. The nanomaterial-incorporated concrete could permit the development of ultra-high strength concrete frameworks having higher durability, thereby decreasing the maintenance needs.

It is extremely important to develop an advanced procedure to make sure the appropriate nanomaterial dispersion in commercial-scale field applications. Effective dispersion of nanoparticles is key to achieving the full benefits of adding nanoparticles in a cementitious system.

A rise in the concentration of nanomaterial in the advanced smart nano-based concrete structures greater than the optimum amount was demonstrated to show an adverse impact on the strong performance and durability, which was mostly because of the less compaction, nonuniform dispersion, and development of weaker sections in the concrete. The optimum quantity of incorporated nanomaterials is very important. The optimum addition of appropriate nanomaterial to the concrete can improve mechanical properties such as tensile strength, compressive strength, flexural strength, and durability, etc. of the concrete. For example, the use of nano SiO_2, nanoTiO_2, and polypropylene (PP) fibers shows that the lower usage levels of these nanoparticles have better effects on abrasion resistance. The optimal amount of these materials is 2% by weight of the cementitious material. Freeze–thaw resistance and abrasion resistance of the concrete can also be improved with the addition of nano-silica to the concrete mix. The use of silica and titanium nanoparticles and PP (polypropylene) fibers in concrete improved the chloride penetration resistance by 31% and 18% for samples containing 1% nano-titanium dioxide and 1% nano-silica, while PP fibers negatively affected chloride penetration resistance. Colloidal and powdery modes were used, and the addition of 3.8 wt% nano-silica improved the water permeability by 88%. In a study, it was found that under the condition of $-10C^0$, 25 times freeze-thawing was allotted, the incorporation of nanometer material 0.75% concrete strength loss was 3.2%, and also, the frost resistance of concrete is improved.

Nano-materials can offer concrete structures with self-sensing and self-cleaning abilities. However, the concentration of the nanomaterial present in the concrete should be in a very limited quantity.

5. Findings

The main finding of this paper indicates that the properties of concrete can be significantly improved with the incorporation of various types of nanoparticles.

The application of nano-based concrete materials is beneficial concerning enhanced engineering properties of cement materials, particularly for the production of sustainable as well as self-healing concretes.

It was noted that the nanostructured materials have a higher capability in smart infrastructure applications with superior strength concrete frameworks.

The nanomaterials improve the properties of concrete by the addition of an optimum quantity of incorporated appropriate nanomaterial to the concrete.

6. Future Recommendations

The dispersion of the incorporated nanoparticles is one of the main challenges regarding the use of nanoparticles in the concrete matrix. Thus future studies should focus on finding innovative methods to provide a uniform dispersion of nanoparticles and avoid the formation of agglomerates.

The workability of nanoparticle-induced concrete is recommended. So, research can be performed to obtain the optimum amount of required superplasticizer.

Using nanoparticles in fewer amounts accompanied by waste materials such as plastic aggregates or plastic fibers can be an attractive research study. Further research can be made on the properties of cement-based materials containing both nanoparticles and waste plastic materials to examine long-term properties and improve sustainability. This topic is essential regarding environmental issues due to the accumulation of waste plastic materials.

It is advised to substitute the conventional ordinary Portland cement-based concretes with functional/smart nano-concrete structures for sustainable development.

It was noted that nanomaterials can play an important role in the development of construction materials, and thus proper understanding of these nanomaterials is extremely important. Along with the substantial advancement of nanomaterials in different applications, it should also be noted that nanomaterials are still in their developing stages, and they have many challenges and unsolved complications for their huge commercial prospects. Thus, an investigation can be made to further understand the properties of nano-concretes.

The lack of information on nanomaterial toxicology topics and a tendency to disconnect from prevailing research and development is a significant blockade for its development, to suppress these types of restrictions, organized construction sector-strategic policies should be followed to benefit from the nanomaterials to attain reasonable benefit in particular application extents and the product categories.

7. Conclusion

In this study, the effectiveness of nanoparticles on concrete's performance is discussed, and the following conclusions were drawn:

1) Based on the research, it can be said that nano silica (nanoSiO_2) is the most commonly used nanoparticle in a cement matrix, but there are other nanoparticles such as nano Al_2O_3, nanoTiO_2, nanoFe_2O_3, nanoFe_3O_4, nano clay, nanoZrO_2 carbon nanotubes, nanofibers, and carbon nanofibers.
2) Nano-silica had a much better effect than micro-silica.
3) The nanoparticles improve the strength of concrete. There is a strong correlation between concrete's splitting tensile strength and compressive strength. The splitting tensile strength tends to increase along with the increase of concrete's compressive strength.
4) The addition of nanoparticles to concrete improves the flexural strength and modulus of elasticity of concrete, as with the addition of nano-silica and nano ferrite the improving percentage of flexural strength and modulus of elasticity of concrete reaches the approximate rate of about 23% and 25%, respectively.
5) Nanoparticles are capable of improving the durability of concrete. They increase the resistance to sulfate attack, reducing the permeability of concrete mixtures against chloride ions; improve the resistance against freezing and thawing; reduce the loss of compressive strength; the various types of nanoparticles impose different effects on the shrinkage property and carbonation depth of concrete mixture; the microstructure of different types of concrete is significantly enhanced upon the addition of nanoparticles.
6) Concrete with the addition of nanoparticles as cement partial substitute material showed that the microstructure of the nanoparticles' concrete was denser and more uniform than that of the conventional concrete.
7) Nanoparticles were added to the concrete mixture, they improved its abrasion resistance. The use of nano SiO_2, nanoTiO_2, and polypropylene (PP) fibers shows that the lower usage levels of these nanoparticles have better effects on abrasion resistance.
8) Nanoparticles added to concrete mixtures greatly increase the internal density and resistance to permeability and reduce the porosity of concrete thus the frost resistance and resistance to freezing and thawing are improved. In order ensures the durability of concrete.

References

[1]Balaguru, P. (2005). *Nanotechnology and concrete: Background, opportunities, and challenges.* Paper presented at the Proceedings of the International Conference–Application of Technology in Concrete Design.

[2]Balaguru, P., & Chong, K. Nanotechnology and concrete: research opportunities. *Proceedings of the ACI Session on Nanotechnology of Concrete: Recent Developments and Future Perspectives*. 2006.

[3]Camiletti J, Soliman AM, Nehdi ML. Effect of nano calcium carbonate on early-age properties of ultrahigh-performance concrete. Magazine of Concrete Research. 2013;65:297-307.

[4]Ganesh P, Murthy RA, Kumar SS, Reheman MS M, Iyer N. Effect of nano-silica on durability and mechanical properties of high-strength concrete. *Magazine of Concrete Research*. 2015;68:229-236.

[5]Gopalakrishnan K, Birgisson B, Taylor P, Attoh-Okine N. Nanotechnology in Civil infrastructure, A paradigm shift. Verlag Berlin Heidelberg, Springer, 2011.

[6]Han B, Li Z, Zhang L, Zeng S, Yu X, Han B. Reactive powder concrete reinforced with nano SiO2- coated TiO2. *Construction and Building Materials*. 2017;148:104-112.

[7]Hosseini P, Afshar A, Vafaei B, Booshehrian A, Molaei Raisi E, Esrafili A. Effects of nano-clay particles on the short-term properties of self-compacting concrete. *European Journal of Environmental and Civil Engineering*. 2017;21:127-147.

[8]Jalal M, Pouladkhan R, Harandi O, Jafari D. Comparative study on effects of Class F fly ash, nano silica, and silica fume on properties of high-performance self-compacting concrete, *Construction, and Building Materials*, 2015;94:90-104.

[9]Jalal, M., Fathi, M., & Farzad, M. (2013). Effects of fly ash and TiO 2 nanoparticles on rheological, mechanical, microstructural, and thermal properties of high strength self-compacting concrete. *Mechanics of Materials, 61*, 11-27.

[10] Jayapalan, A., Lee, B., & Kurtis, K. (2009). Effect of nano-sized titanium dioxide on early age hydration of Portland cement *Nanotechnology in Construction 3* (pp. 267-273): Springer.

[11] Khaloo A, Mobini MH, Hosseini P. Influence of different types of nano-SiO2 particles on properties of high-performance concrete. *Construction and Building Materials*. 2016;113:188-201.

[12] Langaroudi MAM, Mohammadi Y. Effect of nano-clay on workability, mechanical, and durability properties of self-consolidating concrete containing mineral admixtures. *Construction and Building Materials*. 2018;191:619-634.

[13] Li G. Properties of high-volume fly ash concrete incorporating nano-SiO2. *Cement and Concrete research*. 2004;34:1043-1049.

[14] Li, H., Zhang, M.-h., & Ou, J.-p. (2007). Flexural fatigue performance of concrete containing nano-particles for pavement. *International Journal of Fatigue, 29*(7), 1292-1301.

[15] Li, H., Zhang, M.-h., & Ou, J.-p. Abrasion resistance of concrete containing nano-particles for pavement. *Wear, 260*(11), 2006. 1262-1266.

[16] Li, Z., Wang, H., He, S., Lu, Y., & Wang, M. (2006). Investigations on the preparation and mechanical properties of the nano-alumina reinforced cement composite. *Materials Letters, 60*(3), 356-359.

[17] Li, Zongjin, *Advance concrete technology*, John Wiley & Sons, INC, New Jersey. 2011.

[18] Mohamed A. and Khaled A., Effect of using different types of nanomaterials on mechanical properties of high strength concrete, *Elsevier, Construction and Building Materials 80,* (2015), pp.116–124

[19] Nazari A, Riahi S, Riahi S, Shamekhi SF, Khademno A. An investigation on the Strength and workability of cement-based concrete performance by using ZrO2 nanoparticles. *Journal of American Science*. 2010;6:29-33.

[20] Nazari A, Riahi S, Riahi S, Shamekhi SF, Khademno A. Influence of Al2O3 nanoparticles on the compressive strength and workability of blended concrete. *Journal of American Science*. 2010;6:6-9.

[21] Nazari A., The effects of curing medium on flexural strength and water permeability of concrete incorporating TiO2 nanoparticles, *Materials, and Structures*, 2011, 44:773–786.

[22] Niewiadomski P, Hoła J, Ćwirzeń A. Study on properties of self-compacting concrete modified with nanoparticles. *Archives of Civil and Mechanical Engineering*. 2018;18:877-886.

[23] Norhasri MSM, Hamidah MS, Fadzil AM. Applications of using nanomaterial in concrete: A review. *Construction and Building Materials*. 2017;133:91-97.

[24] Ozyildirim, Celik, Laboratory Investigation of Nanomaterials to Improvethe Permeability and Strength of Concrete, Virginia Transportation Research Council, 530 Edgemont Road,Charlottesville, VA 22903-2454, www,vtrc,net, 2010. (434) 293-1900.

[25] Parveen S, Rana S, Fangueiro R. A Review on Nanomaterial Dispersion, Microstructure, and Mechanical Properties of Carbon Nanotube and Nanofiber Reinforced Cementitious Composites, *Journal of Nanomaterials*, 2013.

[26] Peng Z., Dehao S., Qingfu L., Shikun Z, and Yifeng L., Effect of Nano Silica Particles on Impact Resistance and Durability of Concrete Containing Coal Fly Ash, *Nanomaterials*, 2021, pp. 1-19.

[27] Raheem A, Ikotun B. Investigation of Workability and Compressive Strength of Wood Ash Cement Concrete Containing nano-silica. *Advanced Materials Research*. 2019;1154:129-136.

[28] Rashad, A. M. A synopsis about the effect of nano-Al 2 O 3, nano-Fe 2 O 3, nano-Fe 3 O 4, and nano clay on some properties of cementitious materials–a short guide for Civil Engineer. *Materials & Design*, 2013, *52*,143-157.

[29] Rawa A. M. and Niyazi U. K., Nanoparticles used as an ingredient in different types of concrete, SN *Applied Sciences*, (2021) pp. 1-17.

[30] Ren J, Lai Y, Gao J. Exploring the influence of SiO2 and TiO2 nanoparticles on the mechanical properties of concrete. *Construction and Building Materials*. 2018;175:277-285.

[31] Ruan Y, Han B, Yu X, Li Z, Wang J, Dong S. Mechanical behaviors of nano-zirconia reinforced reactive powder concrete under compression and flexure. *Construction and Building Materials*, 162, 663-673

[32] Ruan Y, Han B, Yu X, Zhang W, Wang D. Carbon nanotubes reinforced reactive powder concrete. Composites Part A: *Applied Science and Manufacturing*. 2018;1112:371-382.

[33] Said L, Zeidan M, Bassuoni MT, Tian Y. Properties of concrete incorporating nano-silica. *Construction and Building Materials*. 2012;36:838-844.

[34] Saleem, H.; Zaidi, S.J.; Alnuaimi, N.A. Recent Advancements in the Nanomaterial Application in Concrete and Its Ecological Impact. Materials **2021**, 14, 6387. https://doi.org/10.3390/ma14216387

[35] Saloma, Amrinsyah N., Iswandi I. and Mikrajuddin A. Improvement of concrete durability by nanomaterials, The 5th International Conference of Euro Asia Civil Engineering Forum (EACEF-5), *Elsevier*, 2015, pp. 608-612

[36] Saloma, Amrinsyah N., Iswandi I., and Mikrajuddin A., Experimental Investigation on Nanomaterial Concrete, *International Journal of Civil & Environmental Engineering (IJCEE-IJENS)* Vol:13 No:03, June 2013, pp 15-20.

[37] Shaikh FUA, Supit SWM. Mechanical and durability properties of high volume fly ash (HVFA) concrete containing calcium carbonate (CaCO3) nanoparticles. *Construction and Building Materials*. 2014;70:309-321.

[38] Sivasankaran U, Raman S, Nallusamy S. Experimental Analysis of Mechanical Properties on Concrete with Nano Silica Additive. *Journal of Nano Research*. 2019;57:93-104.

[39] Sobolev K. Nanotechnology in Construction. 2015. Nanotechnol Constr. https:// doi. org/ 10. 1007/ 978-3- 319- 17088-6

[40] Sun J, Shen X, Tan G, Tanner. Modification Effects of Nano-SiO2 on Early Compressive Strength and Hydration Characteristics of High-Volume Fly Ash Concrete. *Journal of Materials in Civil Engineering*. 2019;31:04019057.

[41] Uthaman S, Vishwakarma V, George RP, Ramachandran D, Kumari K, Preetha R, *et al*. Enhancement of strength and durability of fly ash concrete in seawater environments: Synergistic effect of nanoparticles. *Construction and Building Materials*. 2018;187:448-459.

[42] Valquíria S, M., José M.F., Calixto, Luiz O., Ladeira, dan Adriano P, Silva, Macro and Micro Characterization of Mortars Produced with Carbon Nanotubes, *ACI Materials Journal*, May-June 2011.

[43] Vandhiyan R, Pillai E.B. Influence of Nano Silica Addition on the Behavior of Concrete and Its Impact on Corrosion Resistance. *Journal of Computational Theoretical Nanoscience*. 2018;15:530-536.

[44] Wei L., Linkai X., Xiaochu W., and Yi R., A Review of Mechanical Properties and Durability of Nano-concrete, *Advances in Engineering Research*, Volume 136, (7th ICADME) 2017, pp. 5-8.

Author Profile:

NOORULLAH ZAHID received the B. Tech. degree in the department of civil engineering from Nangarhar University in 2004, Nangarhar, Afghanistan, and completed the M. Tech. degree in the division of structural engineering of the civil department from the National Institute of Technology Warangal (NITW) in 2012, Warangal, Telangana, India. Currently, He is working as an Assistant Professor in the Department of Civil Engineering at Shaikh Zayed University, Khost, Afghanistan. His areas of research include Civil Engineering.

KPU International Journal of Engineering & Technology
Volume 2, Issue2, Dec. 2022
e-ISSN:2790-0819, p-ISSN:2790-0800
Date Received: 2022-10-11
Date Accepted: 2022-12-23
Date Published: 2022-12-30

Use of Worn Tires as Aggregates Replacement and its Effect on Certain Properties of Concrete

AHMAD MASOUD AHMADYAR[1], SIFATULLAH BAHIJ[2*], SEBGHATULLAH KARIMI[3]

[1]Graduate Student, Department of Civil & Industrial Construction, Kabul Polytechnic University, 5th District, Kabul, Afghanistan. Email: hmdyar@gmail.com

[2*]Assistant Professor, Department of Civil & Industrial Construction, Kabul Polytechnic University, 5th District, Kabul, Afghanistan, and Ph.D. Candidate, Civil Engineering Department, National Institute of Applied Sciences-Strasbourg, Strasbourg, France. Email: sifatullah.bahij@kpu.edu.af

[3]Associate Professor, Department of Civil & Industrial Construction, Kabul Polytechnic University, 5th District, Kabul, Afghanistan. Email: karimi.pharmacy@gmail.com

Abstract

This article aims to investigate the replacement of natural aggregates with worn tires and its effect on certain properties of concrete. Therefore, worn tire aggregates were used as fillers in the concrete mixtures at 5%, 10%, and 15%. The prepared samples were examined for physical properties such as dry density, porosity, and water absorption, ultrasonic pulse velocity (UPV) after 28 days of curing as well as mechanical parameters such as compressive, split tensile, and flexural strengths after 7 and 28 days of curing. The results show that the physical properties of concrete have improved with the incorporation of rubber, and this improvement was more significant for higher percentages of worn tires. In contrast, the mechanical properties have decreased with the increase of rubber content in concrete mixtures, yet rubber concrete exhibited ductile characteristics as opposed to the brittle behaviors of conventional ones. Finally, it was found that the concrete containing rubber has lower sound transmission properties compared to the reference ones.

Keywords: Rubber concrete, ® Worn tires, Mechanical properties, Physical properties, and Ultrasonic pulse velocity

* Corresponding Author

1. Introduction

Recently, people are using their potential to consume more. The result of such consumption is nothing unless a reduction in initial resources and increasing landfill space. Therefore, humans usually try to find broader sources with low prices and ways to get rid of waste. Rubber is one of the significant waste materials in the modern world and causes many environmental problems. Rubber has been used as the most important material in various parts of people's lives, but the most prevalent application is in automobile tires.

Globally, more than three billion tires are produced annually, and roughly 1.5 billion tires reach the end of their service lives each year [1,2]. On the other hand, landfilling, energy recovery, material recovery, retreading, and reuse/export are the most common waste tire management methods [3]. Furthermore, it was reported that around 64% of worn tires were disposed of in landfills, illegally dumped, or hoarded, while just 13% were recycled globally in 2014 [4].

Besides, the Deputy Ministry of Revenues and Customs has reported that a total of 246,713 tons of tires were imported into Afghanistan in 2019 and 2020. The same amount will be wasted once they are used. On the other hand, there is no proper treatment for their waste, and the only solution for waste is landfilling or part of them being used in brick kilns and bathrooms.

Moreover, the researchers have found that the gaseous (CO, NO_2, and SO_2) emissions of waste tires after burning were higher than the permitted limit. For example, the SO_2 emissions were higher than the USEPA's permitted limit (156.74 $\mu g/m^3$). The USEPA-allowable limit for CO due to automobile and truck tires was surpassed (10,285.71 $\mu g/m^3$), while the USEPA-allowable level for NO_2 concentration (56.33 $\mu g/m^3$) was only met by bicycle tires. It shows that open burning of scrap tires (OBST) releases dangerous pollutants that constitute a major threat to both the environment and human health. Therefore, partial replacement of aggregates with worn tire waste will provide the best solution for tire waste consumption, solve problems of lack of aggregates on construction sites, and decrease environmental problems [5].

Several studies were conducted to explore the effect of the incorporation of waste tires as fine or coarse aggregates on different properties of cementitious materials. For instance, experimental work was conducted to study the effect of the incorporation of waste tires into concrete compositions. It was found that the physical properties of rubber-based concrete were improved compared to the normal ones [5–8], while the mechanical properties of rubber concrete had decreased [9]. Furthermore, using scrap tire rubber aggregates in place of conventional aggregates enhanced concrete's permeability, ductility, energy dissipation, damping, and reduced thermal conductivity [9,10]. In addition, waste tires as coarse aggregates were incorporated into concrete mixtures to study various properties of concrete, such as compressive strength, tensile strength, ductility, etc. It was discovered that rubber concrete is lighter and absorbs less water compared to the control ones [11]. Moreover, the density, flexural strength, and compressive strength of double-layer concrete paving blocks were affected, while tire rubber was partially replaced by natural aggregates. The outcomes highlight that it may be possible to create double-layer concrete paving blocks by substituting waste tire rubber

with natural aggregates. Here, the mechanical properties (compressive and flexural strengths) could be balanced with other factors. However, if the percentage of replaced aggregates exceeds 20%, the mechanical strengths will suffer significantly [12]. Contrarily, the incorporation of a higher content of waste rubber in concrete mixtures resulted in the reduction of mechanical strength as well as Young's modulus of elasticity [9,10]. However, the incorporation of mineral admixtures (silica fume) in rubber concrete resulted in the improvement of compressive strength [11]. Additionally, several studies in this area have shown that the incorporation of worn tires resulted in the reduction of concrete's compressive, split tensile, and flexural strengths [13–19].

In conclusion, the literature review presents that several investigations have been carried out in this area, although the majority of them concentered on the mechanical characteristics of rubber concrete. However, this article focuses on the use of worn tires as a partial replacement with coarse aggregates to investigate their effect on the physical, mechanical, and acoustic characteristics of rubber concrete in comparison with the normal ones. The specific tests could be slump value, compressive strength, tensile strength, flexural strength, water absorption, dry density, porosity, and ultrasonic pulse velocity. In addition, this article's focus on Afghanistan's geography and conditions set it apart from earlier ones in another important way.

2. Experimental Work

2.1. Materials

The worn tire used in this experimental study was MILSTAR-HEAVY DUTY, made by Apollo Company, with the specifications as shown in Figure 1.

Figure 1. Worn tires made by Apollo Company

The Ghori Portland Cement used in this study was produced by the Pol-e Khumri factory of Afghanistan following ASTM C150 requirements [20], and it had a specific gravity of 3.034 and a surface area of 2900 cm^2/gr. Additionally, crushed coarse aggregates with a size of 10–25 mm and natural river sand with a maximum particle size of 4.75 mm have also been employed as coarse and fine aggregates. The crumb rubber was ground into various sizes after removing the steel and textile fibers. The difference in the specific gravity of river sand and crumb rubber was taken into consideration while replacing. The size distributions for sand, gravel, and rubber are shown in Figure 2.

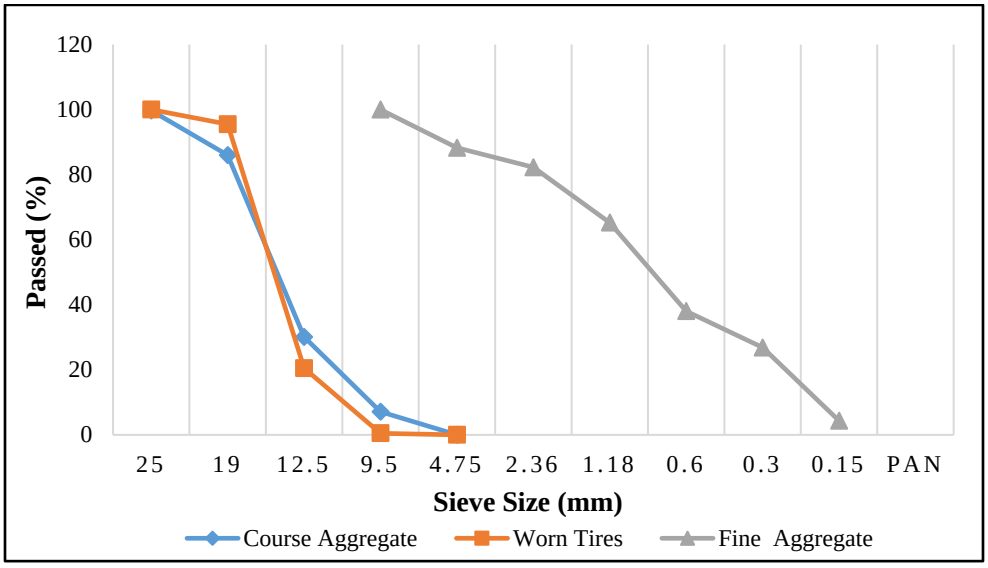

Figure 2. Grading of rubber, coarse and fine aggregates

From particle size analysis, it was observed that crumb rubber contains slightly coarser particles, and has lesser water absorption than fine and coarse aggregates. The low water absorption values add to the quality of concrete. In addition, some physical properties of fine and coarse aggregates and worn tires are presented in Table 1.

Table 1. Physical properties of filler materials

Type of aggregates	***Specific gravity***	***Bulk density (kg/m^3)***
Fine aggregates	2.704	1742.895
Coarse aggregates	2.693	1535.164
Worn tires	1.129	556.870

Moreover, the superplasticizer type G named BEVETOL-SPL, a product of Izomat Company, following EN 934-2 standard considerations [21], was added to the concrete mixture to improve the workability of rubber concrete.

2.2. Methods

Before casting the samples, the molds were oiled for easy demolding. The concrete mixtures were prepared using a tilting drum mixer. Then the concrete was placed in the molds to prepare samples of various shapes and sizes, as shown in ***Table 2***. After that, the samples were kept in the molds for 24 hours before being cured for 7 and 28 days under a temperature of (20 ± 2) C°.

Table 2. Specification of concrete samples

No	*Type of samples*	*Description*	*Conducted tests*
1	Cube 100 mm	Reference	Compressive strength, UPV, water absorption, dry density, and porosity
		5% of worn tires	
		10% of worn tires	
		15% of worn tires	
2	Cylinder (100×200) mm	Reference	Split tensile strength
		5% of worn tires	
		10% of worn tires	
		15% of worn tires	
3	Beam (100×100×500) mm	Reference	Flexural strength
		5% of worn tires	
		10% of worn tires	
		15% of worn tires	

The material proportions were calculated following ACI 291.1 [22], which has a constant w/c ratio of 0.45 and a total binder content of 433 kg/m^3. The mixed proportion of concrete mixtures containing various percentages of worn tires is shown in ***Table 3***. In addition, the dry density, porosity, and water absorption were calculated using ASTM C642-06 [23]. A compression test was performed using the ADR touch SOLO 1500 machine. The pacing rate for the cubic sample compression test was set at 3.0 KN/s to get the compressive strength following ASTM C39 [24]. The split tensile strength test was performed on the same machine according to ASTM C496 [25] with a pacing rate of 0.94 KN/s. The beams were used for flexural testing following ASTM C78 [26]. Finally, the ultrasonic pulse velocity (UPV) test has been conducted on 100 mm cubes utilizing the direct approach and the ELE Pundit Pulse Device according to the ASTM C597 standard [27].

Table 3. A mix ratio of materials for 1m^3 of concrete

Materials	***Weight of materials for 1m^3 of concrete***			
	Percentages of worn tires			
	0%	***5%***	***10%***	***15%***
Water (kg)	195	195	195	195
BEVETOL-SPL (gr)	2.5	3.4	4.2	4.9
Cement (kg)	433	433	433	433
Fine aggregate (kg)	652	652	652	652
Coarse aggregate (kg)	1060	1037.8	1015.6	993.4
Worn tires (kg)	0	22.2	44.4	66.6

3. Result and Discussions

3.1. Workability

The workability of concrete mixtures containing various percentages of worn tires is shown in Figure 3. It was observed that the workability of concrete mixtures had decreased for the samples containing worn tires, and this reduction was more significant for higher percentages. For example, concrete with 0% of worn tires had a slump value of 80 mm, while for concrete mixtures containing 15% of worn tires, only a 5 mm slump was obtained. Therefore, BEVETOL-SPL superplasticizer was added to the concrete mixture according to its technical specifications to improve the workability of the concrete. This reduction could be related to the flaky and flat-surfaced shapes of rubber aggregates, which have a higher surface area compared to natural aggregates. Therefore, such a higher surface of rubber aggregates results in the enhancement of friction, the reduction of inter-particle movement, and finally a reduction in workability.

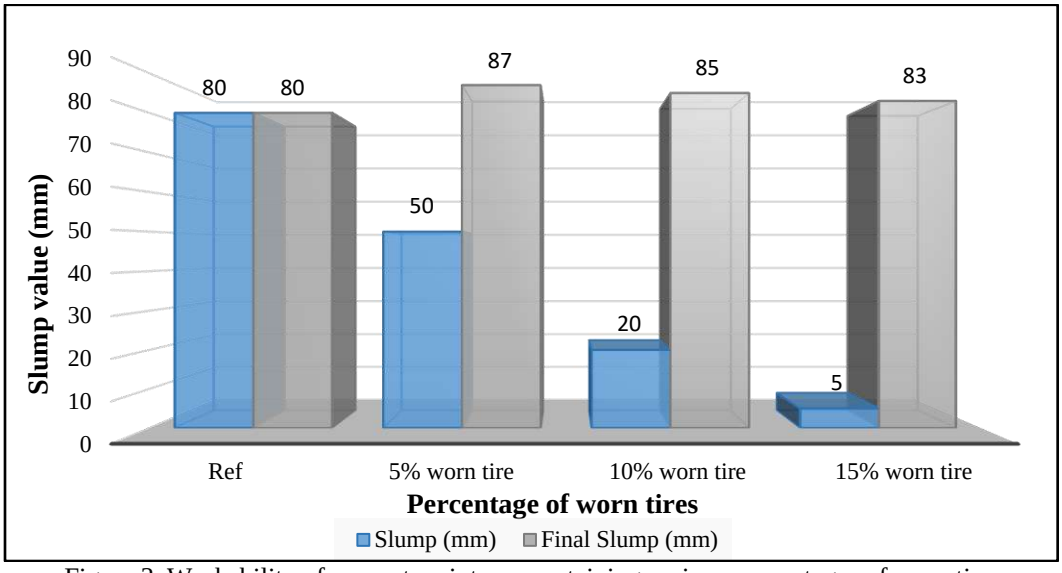

Figure 3. Workability of concrete mixtures containing various percentages of worn tires

3.2. Physical Properties

3.2.1. Dry Density

The dry density of concrete is determined by its mass-to-volume ratio. The dry density was determined after exposing the 28-day hardened cubic specimens to a 110 °C oven for 24 hours. The outcomes of dry density for reference specimens and the ones containing different contents of worn tires are shown in ***Figure 4***. It could be observed that the dry density has decreased with the increase in the percentage of worn tires in concrete mixtures. For instance, the dry density was reduced by up to 8.4% when 15% of the mixture's worn tires were replaced. This could be attributed to the lower specific gravity of rubber aggregates compared to the natural coarse and fine aggregates [28]. In addition, the increase in rubber percentages increases the air content, which results in a further reduction of the dry density.

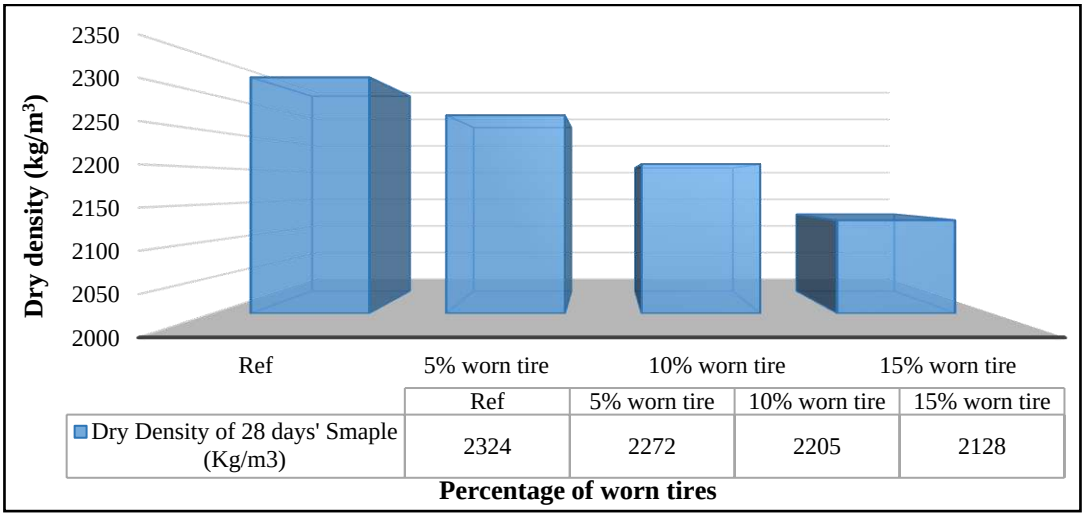

Figure 4. The dry density of concrete mixtures containing various percentages of worn tires

3.2.2. Porosity

The porosity of concrete mixtures containing 0%, 5%, 10%, and 15% of worn tires was measured and their results are shown in ***Figure 5***. The outcomes indicate that the rubber concrete has higher porosity compared to the normal one, and this enhancement was more significant for the mixtures containing a higher content of worn tires. For example, concrete samples with 15% of worn tires had 11.1% higher porosity than the reference. This could be because of weak adhesion between rubber and cement paste, which results in micro-cracks and cavities. In addition, the crumb rubber functioned as an air-entraining agent, which might improve the concrete's porosity [28].

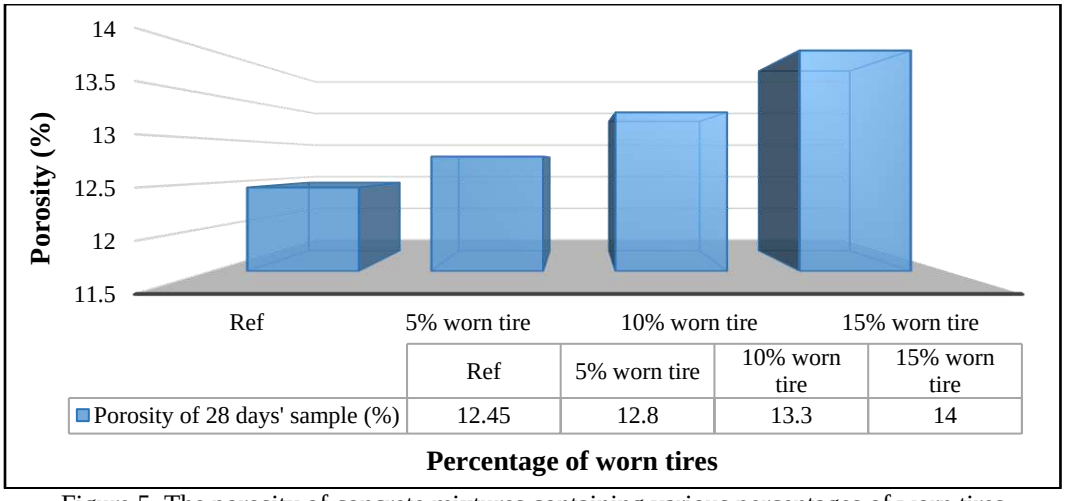

Figure 5. The porosity of concrete mixtures containing various percentages of worn tires

3.2.3. Water absorption

The outputs of water absorption are shown in ***Figure 6***, and it highlights that with the increase of rubber content in concrete mixtures, the water absorption has enhanced as well. The water absorption has increased by 9.7%, 15.3%, and 21.5% for the samples

containing 5%, 10%, and 15% of worn tires compared to the reference concrete, respectively. This is because of the rubber's hydrophobic properties and the porous microstructure of rubber concrete [15].

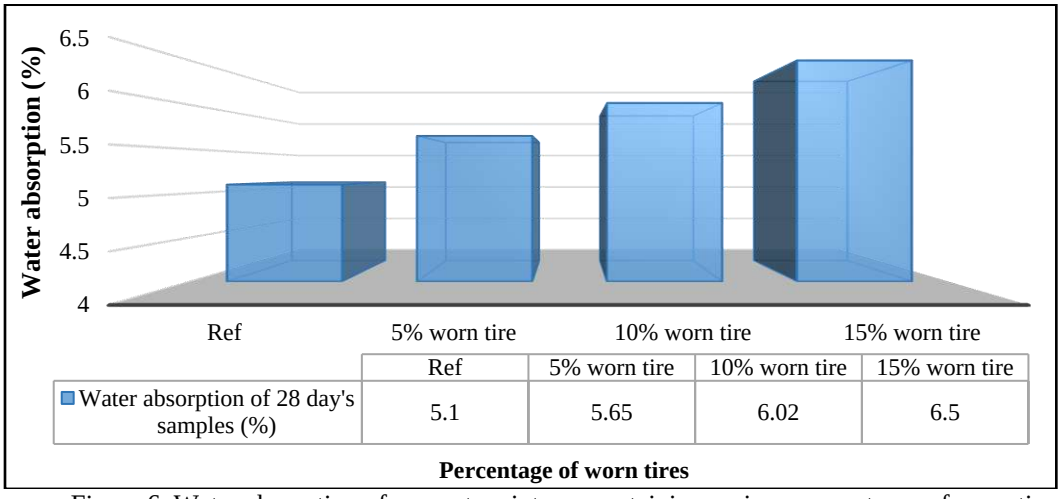

Figure 6. Water absorption of concrete mixtures containing various percentages of worn tires

3.3. Mechanical Properties

3.3.1. Compressive strength

A material or structure's compressive strength refers to its capacity to sustain compressive stresses without breaking or deforming. The compressive strength of concrete specimens observed after 7 and 28 days of curing is shown in Figure 7**,** and the outcomes show that the incorporation of worn tires resulted in the reduction of compressive strength. Specifically, 28 days' compressive strength decreased by 15.0%, 30.9%, and 42.6% with the incorporation of 5%, 10%, and 15% of worn tires compared to the control specimens, respectively. This is because of the rubber's hydrophobic properties and a weak interfacial connection between cement paste and rubber, which reduces the mechanical strength. In addition, rubber particles cause weak spots inside the concrete, where there is a higher concentration of stresses and, as a result, a reduction in the mechanical strengths due to the rubber's lower modulus of elasticity [15].

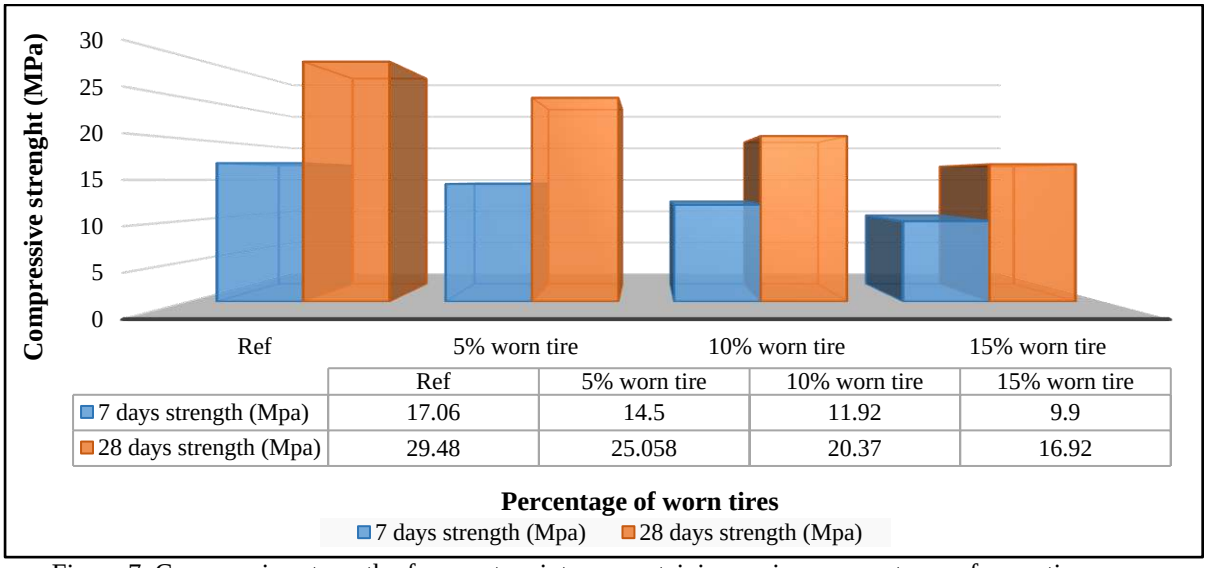

	Ref	5% worn tire	10% worn tire	15% worn tire
7 days strength (Mpa)	17.06	14.5	11.92	9.9
28 days strength (Mpa)	29.48	25.058	20.37	16.92

Figure 7. Compressive strength of concrete mixtures containing various percentages of worn tires

In addition, the reference samples had broken into several pieces when a compressive force was applied. While the specimens containing rubber pieces were not separated into many portions because of the flexible properties of rubber aggregates as shown in Figure 8.

a *b*

c *d*

Figure 8. Cracking pattern after compression test: a) Reference, b) 5%, c) 10%, and d) 15%

3.2.2. Split tensile strength

The split tensile strength is an indirect way of determining the tensile strength of concrete using cylindrical specimens that split across the vertical diameter. Figure 9 shows the findings of split tensile strength obtained for the specimens containing various percentages of worn tires after 7 and 28 days of curing. It demonstrates that replacing natural aggregates with rubber ones did not have a considerable effect on the 7-day split

tensile strength. However, the split tensile strength after 28 days of curing noticeably decreased with the incorporation of rubber waste, and this reduction was more remarkable for higher amounts of worn tires. For example, the 28-day split tensile strength of specimens containing 15% worn tires has been reduced by 40.1% compared to the reference concrete. This is attributed to the weak bond and adhesive properties between cement paste and rubber aggregates. In addition, the weak interface zone between rubber and cement may act as a micro-crack due to weak bonding between the two materials, which accelerates concrete breakdown [13].

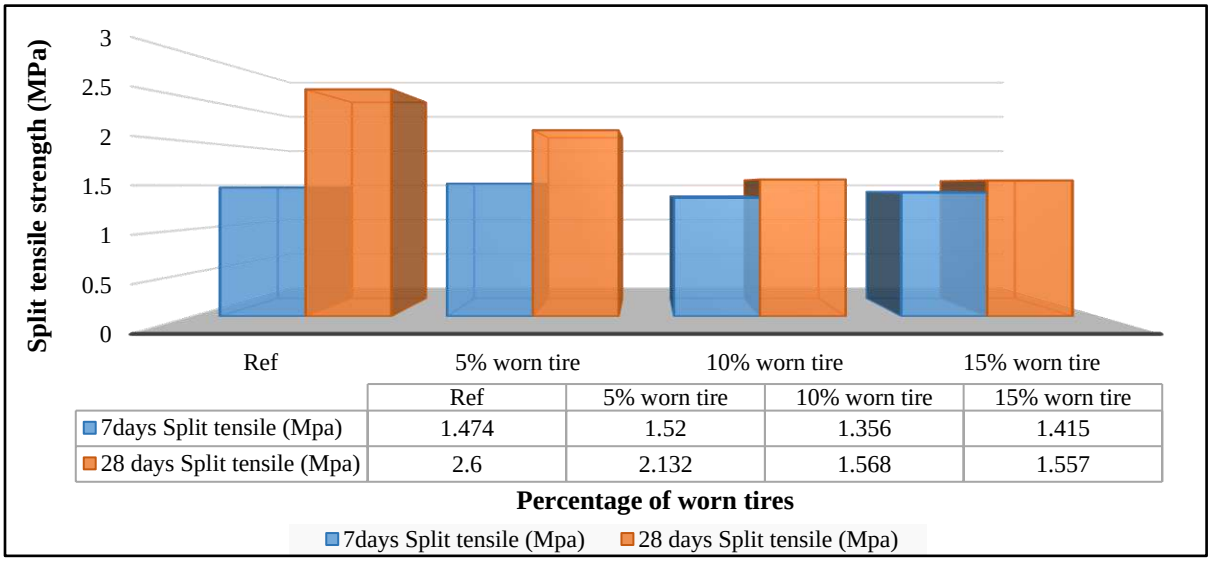

	Ref	5% worn tire	10% worn tire	15% worn tire
7days Split tensile (Mpa)	1.474	1.52	1.356	1.415
28 days Split tensile (Mpa)	2.6	2.132	1.568	1.557

Figure 9. Split tensile strength of concrete mixtures containing various percentages of worn tires

In addition, the samples with 5%, 10%, and 15% worn tires are cracked but not split, but the reference sample under tensile tension is completely divided into two different fragments as shown in Figure 10.

a *b*

c *d*

Figure 10. Cracking pattern after the split tensile test: a) Reference, b) 5%, c) 10%, and d) 15%

3.2.3. Flexural Strength

The outcomes of the flexural strength are displayed in Figure 11. The results demonstrate that the replacement of worn tires with coarse aggregates had a tiny impact on the flexural strength of samples after 7 days of curing. This could be because of the lower adhesion between cement paste and other concrete ingredients and the lower achieved resistance of cement. However, the 28-day samples show a considerable reduction in the flexural strength of the specimens having rubber wastes, and this reduction was more noticeable for a higher volume fraction of worn tires. As a result, a lack of strong bonding between rubber particles and cement paste is a major factor in reducing flexural strengths. It was found that chipped rubber could be easily removed from concrete after the concrete samples were broken for the flexural strength test [13].

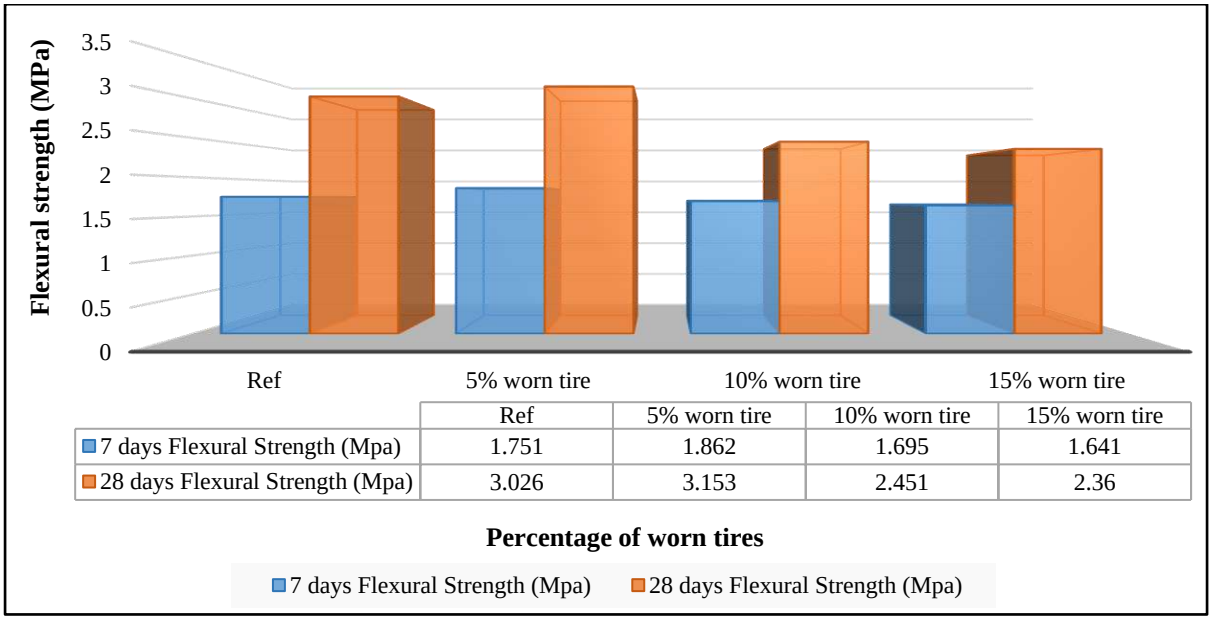

	Ref	5% worn tire	10% worn tire	15% worn tire
7 days Flexural Strength (Mpa)	1.751	1.862	1.695	1.641
28 days Flexural Strength (Mpa)	3.026	3.153	2.451	2.36

Figure 11. Flexural strength of concrete mixtures containing various percentages of worn tires

Additionally, it was noted that the rubberized samples were more flexible while the control specimens showed brittle failure and broke into two pieces when loaded, as shown in Figure 12.

a *b*

c *d*

Figure 12. Beam cracking pattern: a) Reference, b) 5%, c) 10%, and d) 15%

3.3. Acoustic properties

An ultrasonic pulse velocity (UPV) test was conducted on 28-day cubic samples to explore the transit time of ultrasonic pulses from concrete specimens. The UPV value was measured for concrete mixtures without a rubber and with 5%, 10%, and 15% of worn tires. ***Figure 13*** shows the UPV results and indicates that with the incorporation of worn tires, the UPV value has decreased. As a comparison, the samples containing 15% of worn tires transmit sound at a pace that is 1.3 km/s slower than the reference samples. This reduction in the UPV is due to air content and crumb rubber, which entraps air on its surface [29].

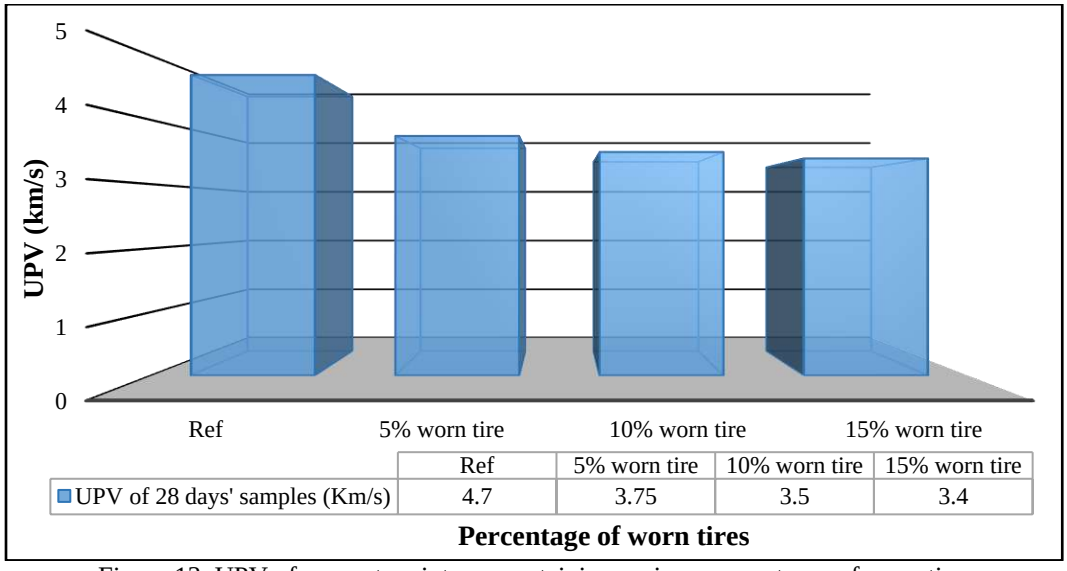

Figure 13. UPV of concrete mixtures containing various percentages of worn tires

4. Conclusions

Overall, the presence of worn tires in the composition of concrete could improve the physical, sound, and flexibility properties of concrete. On the other hand, it can negatively affect its mechanical strength. The key and specific outcomes are highlighted as follows:

- The incorporation of worn tires into concrete mixtures resulted in a decrease in workability, and this reduction was more remarkable for higher percentages of rubber.
- The addition of rubber into concrete mixtures could greatly improve the physical properties, such as water absorption and dry density, of concrete, and this enhancement was more significant for a higher volume fraction of rubber.

- The incorporation of worn tires into concrete has reduced the compressive, tensile, and flexural strengths. It means that higher percentages of worn tires have the lowest mechanical strengths. Meanwhile, it was found that the rubber concrete has more flexibility compared to the control ones.
- The highest UPV value was achieved for the reference samples, while the UPV value significantly decreased with the incorporation of worn tires, and such a reduction was more significant for higher percentages.
- Finally, the partial incorporation of worn tires in cementitious materials results in greener, cheaper, and lighter building materials. In addition, this could be a possible solution for the reduction of rubber waste materials and environmental protection. Moreover, the substitution of fine and coarse aggregates by worn tires reduces or prevents the decrease of natural resources for aggregates.

5. Acknowledgement

The University of Kabul Polytechnic, as well as everyone who assisted the authors, are appreciated.

Reference

[1] H.H. Al-Kayiem, B.A. Bhayo, E. Magaril, P. Ravi, Rudimentary Assessment of Waste-to-Wealth of Used Tires Crumbs in Thermal Energy Storage, Recycling. 7 (2022). https://doi.org/10.3390/recycling7030040.

[2] D. Mentes, C.E. Tóth, G. Nagy, G. Muránszky, C. Póliska, Investigation of gaseous and solid pollutants emitted from waste tire combustion at different temperatures, Waste Management. 149 (2022) 302–312. https://doi.org/10.1016/j.wasman.2022.06.027.

[3] K. Frikha, L. Limousy, J.P. Claret, C. Vaulot, K.F. Pérez, B.C. Garcia, S. Bennici, Potential Valorization of Waste Tires as Activated Carbon-Based Adsorbent for Organic Contaminants Removal, Materials. 15 (2022) 1–26. https://doi.org/10.3390/ma15031099.

[4] S. Kordoghli, M. Paraschiv, R. Kuncser, M. Tazerout, M. Prisecaru, F. Zagrouba, I. Georgescu, Managing the Environmental Hazards of Waste Tires, Journal of Engineering Studies and Research. 20 (2016). https://doi.org/10.29081/jesr.v20i4.52.

[5] L.A. Jimoda, I.D. Sulaymon, A.O. Alade, G.A. Adebayo, Assessment of the environmental impact of open burning of scrap tires on ambient air quality, International Journal of Environmental Science and Technology. 15 (2018) 1323–1330. https://doi.org/10.1007/s13762-017-1498-5.

[6] M. Mrad, R. El Samra, Waste Tire Management : Lebanon Case Study, Journal of Waste Management and Disposal. 3 (2020) 1–13.

[7] U.S.P.R. Arachchige, G.M. Sithari, T.G.A.H.R. Thalagahawaththa, G.M. Tharakie, K.V.H. Tharuka, Environmental pollution by the tire manufacturing industry, International Journal of Scientific and Technology Research. 8 (2019) 80–81.

[8] Z. Jankovská, M. Večeř, I. Koutník, L. Matějová, A case study of waste scrap tire-derived carbon black tested for nitrogen, carbon dioxide, and cyclohexane adsorption, Molecules. 25 (2020) 1–14. https://doi.org/10.3390/molecules25194445.

[9] K. Strukar, T. Kalman Šipoš, I. Miličević, R. Bušić, Potential use of rubber as aggregate in structural reinforced concrete element – A review, Engineering Structures. 188 (2019) 452–468. https://doi.org/10.1016/j.engstruct.2019.03.031.

[10] Y.C. Khern, S.C. Paul, S.Y. Kong, A.J. Babafemi, V. Anggraini, M.J. Miah, B. Šavija, Impact of Chemically Treated Waste Rubber Tire Aggregates on Mechanical, Durability and Thermal Properties of Concrete, Frontiers in Materials. 7 (2020) 1–11. https://doi.org/10.3389/fmats.2020.00090.

[11] I. Alam, U.A. Mahmood, N. Khattak, Use of Rubber as Aggregate in Concrete: A Review, International Research Journal of Engineering and Technology (IRJET). 4 (2015) 92–96. https://www.academia.edu/download/57999767/IRJET-V5I11287.pdf.

[12] J. Euniza, H. Md Nor, P.J. Ramadhansyah, H. Zaiton, Use of Waste Tyre Rubber as Aggregate in Double Layer Concrete Paving Blocks, Advanced Research in Applied Mechanics. 1 (2014) 25–30.

[13] A. Sofi, Effect of waste tire rubber on mechanical and durability properties of concrete – A review, Ain Shams Engineering Journal. 9 (2018) 2691–2700. https://doi.org/10.1016/j.asej.2017.08.007.
[14] R. Irmawaty, H. Parung, N. Md Noor, Experimental study of rubber particles from recycled tires as concrete aggregates, IOP Conference Series: Earth and Environmental Science. 473 (2020). https://doi.org/10.1088/1755-1315/473/1/012130.
[15] F.M. Silva, E.J.P. Miranda, J.M.C. Dos Santos, L.A. Gachet-Barbosa, A.E. Gomes, R.C.C. Lintz, The use of tire rubber in the production of high-performance concrete, Ceramica. 65 (2019) 110–114. https://doi.org/10.1590/0366-6913201965S12598.
[16] G. Etefa, A. Mosisa, Waste Rubber Tires: A Partial Replacement for Coarse Aggregate in Concrete Floor Tile Production, American Journal of Civil Engineering. 8 (2020) 57. https://doi.org/10.11648/j.ajce.20200803.12.
[17] N.R. Pardeshi, D.P. Singh, S.R. Patil, P.J. Gorde, P.P. Janrao, Performance and Evaluation Of Rubber As Concrete Material, International Research Journal of Engineering and Technology(IRJET). 4 (2017) 554–560. https://irjet.net/archives/V4/i1/IRJET-V4I195.pdf.
[18] Y. Tang, W. Feng, W. Feng, J. Chen, D. Bao, L. Li, Compressive properties of rubber-modified recycled aggregate concrete subjected to elevated temperatures, Construction, and Building Materials. 268 (2021) 121181. https://doi.org/10.1016/j.conbuildmat.2020.121181.
[19] A. Mohd Mustafa Al Bakri, S. Fadli, S. Nuzul, M.D.A. Bakar, K.W. Leong, Comparison of Rubber As Aggregate and, 1st International Conference On Sustainable Materials 2007_ICoMS 2007 9-11 June 2007, Penang. (2007).
[20] ASTM C150, Standard Specification for Portland Cement, American Society for Testing and Materials. (2009).
[21] EN 934-2, Admixtures for concrete, mortar, and grout, European Standard. (2012).
[22] ACI 211.1-91, Standard Practice of Selecting Proportions for Normal, Heavyweight, and Mass Concrete, ACI Manual of Concrete Practice, Part 1: Materials and General Properties of Concrete, Detroit, Michigan. (1994).
[23] ASTM C642-13, Standard Test Method for Density, Absorption, and Voids in Hardened Concrete, American Society for Testing and Materials. (2013).
[24] ASTM C39, Standard Test Method for Compressive Strength of Cylindrical Concrete Specimens, American Society for Testing and Materials. (2009).
[25] ASTM C496, Standard Test Method for Splitting Tensile Strength of Cylindrical Concrete Specimens, American Society for Testing and Materials. (2009).
[26] ASTM C78, Standard Test Method for Flexural Strength of Concrete (Using Simple Beam with Third-Point Loading), American Society for Testing and Materials. (2009).
[27] ASTM C597, Standard Test Method for Pulse Velocity Through Concrete, American Society for Testing and Materials. (2009).
[28] R.B.N. Khan, A. Khitab, Enhancing Physical, Mechanical and Thermal Properties of Rubberized Concrete, Engineering, and Technology Quarterly Reviews. 3

(2020) 33–45. https://doi.org/10.5281/zenodo.3852541.
[29] B.S. Mohammed, N.J. Azmi, M. Abdullahi, Evaluation of rubbercrete based on ultrasonic pulse velocity and rebound hammer tests, Construction and Building Materials. 25 (2011) 1388–1397. https://doi.org/10.1016/j.conbuildmat.2010.09.004.

Authors Profile:

AHMAD MASOUD AHMADYAR received his bachelor's degree in civil engineering from Kabul Polytechnic University in 2012, and he obtained his master's degree in structural engineering from the same university in 2022. From 2013 to 2021, he worked on NATO and governmental projects. He is currently engaged in research and plans to pursue his studies at the Ph.D. level. His area of research interest includes concrete and construction materials.

SIFATULLAH BAHIJ received his B.Sc. degree in Civil Engineering from Kabul Polytechnic University in 2012, M.Sc. degree in Civil Engineering from King Fahd University of Petroleum & Minerals, Saudi Arabia, and he is currently a Ph.D. candidate in the Civil Engineering department of National Institute of Applied Sciences, Strasbourg, France. He is a faculty member of the Civil and Industrial Construction Department of Kabul Polytechnic University, Kabul, Afghanistan. His research interests include concrete and construction materials, ultra-high performance fiber reinforced concrete (UHFRPC), green concrete and newly generated concretes, cementitious materials with plastic and rubber wastes, finite element modeling (FEM), destructive, non-destructive, SEM, interferometry, and microscopic analysis, and retrofitting of concrete elements with various cementitious and FRP materials.

SEBGHATULLAH KARIMI received his B.Sc. degree in Civil Engineering from Kabul Polytechnic University in 2007, and his M.Sc. degree in Construction Management from the University of Brighton, UK in 2012. He was a faculty member of the Civil and Industrial Construction Department of Kabul Polytechnic University, Kabul, Afghanistan from 2008 to 2021. His research interests include concrete and construction materials and construction project management.

KPU International Journal of Engineering & Technology
Volume 2, Issue2, Dec. 2022
e-ISSN:2790-0819, p-ISSN:2790-0800

Date Received: 2022-08-15
Date Accepted: 2022-12-20
Date Published: 2022-12-30

The Evolution of Mosque Architecture: A Case Study of Mosques in Kabul, Afghanistan

NOORULLAH HASHEMI[1*] ABDUL HALIM HAKIMI[2], MOHAMMAD AYOUB AWWAB[3], HASIBULLAH SAKHA[4]

[1*]Graduate Student, Department of Architecture, Construction Faculty, Kabul Polytechnic University, Kabul, Afghanistan. Email: noorullahhashemi199@gmail.com

[2]Associate Professor, Department of Islamic Studies, Construction Faculty, Kabul Polytechnic University, Kabul, Afghanistan. Email: halim.hakimi52@gmail.com

[3]Associate Professor, Department of Islamic Studies, Construction Faculty, Kabul Polytechnic University, Kabul, Afghanistan. Email: Ayoub.Awwab1@gmail.com

[4]Graduate Student, Department of Architecture, Construction Faculty, Kabul Polytechnic University, Kabul, Afghanistan. Email: Sakhahasibullah@gmail.com

Abstract

Mosque is a place for worshiping Allah and prostration. It serves numerous other purposes for Muslims in addition to its religious ones. Islam has a very old history with mosques. It is impossible to imagine an Islamic society without mosques. The Quba Mosque, Al-Aqsa Mosque, and Nabawi Mosque were the first mosques built in Islam, and have undergone several renovations and transformations since then. Muslims ruled the world and conquered a vast area in the first Hegira century, they conquered Afghanistan and built the country's first mosque, known as Noh Gonbad situated in the Balkh province. After occupying Kabul, Afghanistan's capital. They built the first mosque there by the name of Shah Do Shamshira. Following this, numerous mosques were constructed in Kabul and other parts of Afghanistan, which also underwent a great deal of change during this time. In this study, we employed a historical-descriptive methodology. We have employed the library, case studies, and field research. studied the three well-known and historic mosques Shah Do Shamshira, Pol Kheshti, and Pakhta Froshi to learn more about how mosques were altered throughout this time. We get to know that; these mosques' architecture has been affected during this period. at first, it was just a place to worship but periodically, it has been used for other purposes too such as education, colonies, counseling centers, Social center, the court of justice, and so on. Shah do Shamshira mosque's interior and exterior show the decorations of Indian- Mughals which were affected by abroad architecture but then mosques architecture used the modern way. Mosques have been divided into two sections winter and summer because of the heating system. But the latest mosques which have been built in Afghanistan were modern and in one General hall.

Keywords: Mosque Architecture, Kabul City, Islamic Architecture

* Corresponding Author

1. Introduction

Muslims congregate and pray in mosques, which are also known as places of prostration. A mosque has a social, political, educational, and judicial purpose for Muslims in addition to its religious use. The majority of these tasks still exist today. The Quba mosque is the first-ever mosque in the world of Islam. Al-Aqsa mosque, Al- Nabawi constructed after this. These mosques had undergone many changes in different periods. The first attack of Muslims on northern Afghanistan was in the first century of Hijri during the caliphate of Prophet Usman, under the leadership of Ahnaf son of Qais, after the conquest of northern Afghanistan, which is today's Balkh, Arab Muslims held prayers and based the foundation stone of the first mosque called Nine Domes (Noh Gonbad). Under the leadership of Lis son of Qais, who fought with two swords and was martyred in this fight, Arab Muslims assaulted Kabul, the capital of Afghanistan. Later, a mosque was built in this location and was given his name (Lis son of Qais). Following that, Kabul saw the construction of numerous mosques that heavily incorporated Islamic architectural ornamentation. There is no background research on this topic. Mosque has a very special place in afghan society. Afghanistan is a country that does not follow an exact style of architecture. In early mosques, foreign architecture and culture had an impact on the architecture of these constructions. And it had been built very traditionally. In this article, an effort has been made to explore the architectural evolution of renowned mosques in Kabul from the time of their creation to the present.

2. Background Research

An Islamic city is inconceivable without a mosque. Mosque has a unique place among religious structures in cities. Mosque is the most notable architectural component of Islam and has existed in society since the beginning of this religion's civil manifestation. it is a hub for religion, culture, and society that is inextricably linked to the fabric of society and the urban environment. Since their founding, mosques throughout the Islamic world have undergone numerous changes and transformations. These changes and transformations are the results of a variety of factors, but the fundamental components and characteristics of these structures have remained constant, and they are followed by all mosques worldwide.

2.1. Quba Mosque

The Quba Mosque, which is located in a village with the same name outside of Medina, is the earliest in the Islamic world. During his quick visit to this region in the first year of the hegira, the Prophet Muhammad (PBUH) constructed this mosque. The Holy Prophet (PBUH), whom himself engaged in this mosque, contributed to the construction of this building. This mosque features a relatively straightforward layout, an unpaved courtyard, and walls built of unfired clay with a grid of arches. Palmwood was utilized to build the foundation as well as to cover the prayer area. There are three entrances to this mosque,

located in the east, west, and south. The Muslim qibla at that time pointed toward Jerusalem on its north side. Its southern gate was moved to the north as the qibla moved to Mecca. During the Caliphate of Usman son of Affan, the Quba Mosque was extended and repaired. The Quba Mosque's second restoration dates back to the time of Omar, the son of Abdul Aziz, who constructed the mosque's original minaret. Abu Yali al-Husseini restored it after him and added the altar. Jamal al-Din Isfahani Zangian minister in Mosul, gave the order to construct it in 555 A.H. Some areas underwent extensive restoration and renovation in the eighth and ninth century A.H. It was enlarged and its territory grew during the Ottoman rule and notably during the Saudi era. Currently, there are multiple naves in this mosque, and each one has a unique dome. [1]

Figure 1 (Simple moquette of Quba Mosque) [2]

Figure 2 (Current building of Quba Mosque) [3]

2.2. Al-Aqsa Mosque

Al-Aqsa Mosque, which is referred to as the first Qibla of Muslims, is the second mosque in the Islamic world. It was constructed in Jerusalem, Palestine, on a peak known as Moriah. Muslims see this mosque as a sacred site. This mosque measures 281 square meters in size from the south, 310 square meters in the north, 462 square meters in the east, and 491 square meters in the west. Unlike the Haram Mosque and the Prophet's Mosque in Makkah and Medina, which have both undergone historical development, these specifications have not changed since this location was built as a mosque for prayer. Architecture from the Roman, Byzantine, and Greek periods is combined and displayed in one form in the Al-Aqsa Mosque. When someone enters the mosque from the north side, they are greeted by a sizable portico that was constructed under the tenure of King Essa, the ruler of Damascus (634 AH), and later refurbished. Al-Aqsa Mosque is situated in the southern portion of the courtyard of Haram. The women's mosque entrance is situated on the southwest side of the mosque, which has two porticoes. 53 meters from the west side, these two porticoes link to the Magharba Mosque. On the northwest side, there is also a sizable, magnificent porch known as Zakaria's Altar. Nine domes were built in various eras all around the Al-Aqsa Mosque. [4]

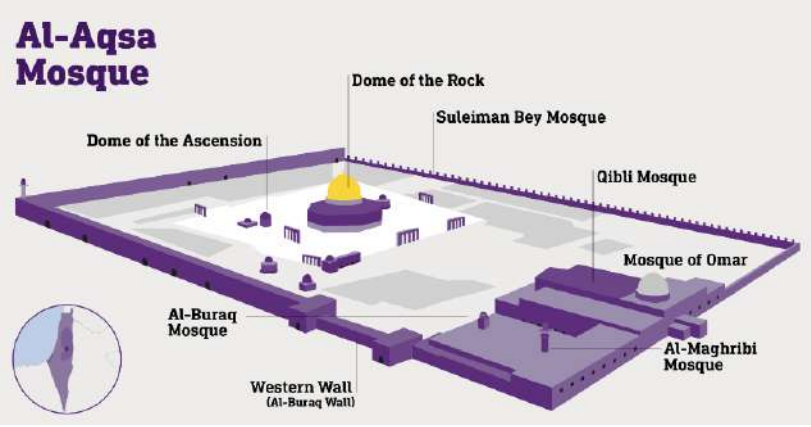

Figure 3 (Site plan Model of Al-Aqsa Mosque) [5]

2.3. Al-Nabawi Mosque

The Prophet Mohammad Mosque, which is in Medina, Saudi Arabia, where the holy Prophet's shrine is also located, is the third mosque in the world. The structure of this mosque has undergone numerous modifications, and it now has a rectangular layout with two levels. Al-Nabawi Mosque has twenty-four rotating domes and a paved roof. These domes have been drilled with holes to provide for the proper lighting of the mosque's interior. This mosque's roof can be used for prayer during peak hours. One of the twenty-four domes of this mosque is larger and taller than the others, and it is also known as the Prophet Mohammad's (PBUH) dome. The Prophet's companions Abu Bakr, Omar, and Usman are the owners of other domes. This mosque has seen numerous additions and modifications over the years.

Up until the time of Fahd, the son of Abdul Aziz, this mosque has undergone a great deal of renovation. Its area and space have increased by 50% after the most recent restoration. This mosque features ten minarets and 41 doorways. The Nabawi Mosque's existing structure included a square layout with two floors and a prayer hall that was bent to the south. The first floor is found in the main prayer hall. The modern mosque is 100 times larger than the original structure that the prophet Mohammad erected (PBUH). This mosque can accommodate 500,000 people at once. [6]

Figure 4 (Al-Nabawi Mosque Model) [7]

2.4. Al-Haram Mosque

Al-Haram Mosque, also known as the Muslims Kaaba is one of the oldest and holiest mosques in the entire Muslim world. Rectangular is the fundamental shape of this mosque's planning in terms of architecture. The shape of a rectangle represents steadiness, solidification, and perseverance. This leads to a final dome shape, a circle, and a representation of the sky. The Al-Haram Mosque is unique in that has the holy Kaaba and does not adopt any other mosques' architectural styles. However, it does contain the typical indications, traits, and components of a mosque. In addition to using the inner space well, architects tried to utilize the outside area of this revered mosque to the fullest extent possible. [8]. The most significant and numerous events, modifications, renovations, and developments that have occurred during the history of this Collective Mosque are listed below:

2.4.1. Pre-Islamic period

The Kaaba's surroundings were known as Masjid al-Haram before Islam, and it had roughly defined limits.

Except for the Kaaba, the mosque had no walls, fences, or other structures until the advent of Islam. It is only indicated in narrative sources that the current location of Masjid al-Haram for the construction of the Kaaba was chosen before the creation of man and that it was built by angels, but there is no historical documentation regarding when that region was chosen as a mosque.

Ibrahim (A) is credited with constructing this mosque in a narration from the Holy Prophet (PBUH). The oldest mosque in the world, according to this account is Masjid al-Haram.

2.4.2. Caliphs' period

During the rule of the second Caliph, the mosque's location underwent its first alteration. He purchased some nearby homes and combined them with the mosque. He also built a small wall around the mosque and had lights installed on the wall to illuminate the area around the mosque at night.

The third caliph created a portico and a covered area for the mosque because there were so many pilgrims visiting the Collective Mosque that he had to demolish the nearby homes and incorporate them into the mosque.

2.4.3. Umayyad period

Walid, the son of Abdul Malik Umayyad (rule: 86–96 A.H.), restored the mosque and expanded the Collective Mosque's floor space by 1725 square meters. He constructed porches around the mosque and opulent pillars to support them. These columns were exquisitely ornamented. Walid also constructed the gold-encased gutter of the Kaaba which is also recognized by that name now.

2.4.4. Abbasid period

The mosque's size was doubled by Mansour, the second caliph of the Abbasids who also built porticoes around it and added almost 5000 square meters to the north and west of the mosque. Along with adding more ornamentation to the walls and columns, Mansour constructed a few minarets on the mosque's western side.

In 161 AH, Mehdi Abbasi son of Mansour (reign: 158-169 AH) took the nearby homes and incorporated them into the mosque's plot of land. In this way, the mosque gained 8380 square meters, and several doors were opened all around it. The mosque, however, remained unchanged for centuries. In 164 AD, Mahdi Abbasi gave the order to build a square area in the southern part of the mosque where the Kaaba would be placed. Consequently, the mosque's area was enlarged to 6560 square meters, porticoes were constructed and columns were created. These columns are still standing, and they still bear the Mahdi Abbasid period's inscription.

2.4.5. Saudi Period

The mosque's area reached 160861 square meters when King Abdul Aziz Al Saud ordered its development in 1368 AH/1328 SH. Construction on the project began in 1375 AH/1335 SH. Over 300,000 people were expected to attend prayers, so this space was taken into consideration. In addition, there are 64 mosque doors now.

King Fahd started an enormous expansion of this collective mosque in the year 1409 A.H. Since 1403 AH, this concept has been studied and some nearby properties have been purchased. This Collective Mosque has never seen a rise quite like this one. The mosque's west side received an addition of 76,000 square meters. In that area, two large minarets of 89-meter heights were constructed. The middle of the added level, which was supported by four columns, had three substantial domes erected into it.

The Collective Mosque currently houses about one million worshipers in a very big complex that spans more than 88,000 square meters. The third floor of Masjid al-Haram, which comprises three floors, is a very huge space. [9]

2.4.6. Holy Kaaba

In Mecca, there is a famous cube-shaped building called the Kaaba that is situated between two mosques. For Muslims, the Kaaba is the Qibla and the most significant location of worship. Any Muslim who has completed the Hajj rite and the ritual of worship is required to visit it once in their lifetime, if certain requirements are met, such as having the financial means to do so. [10]

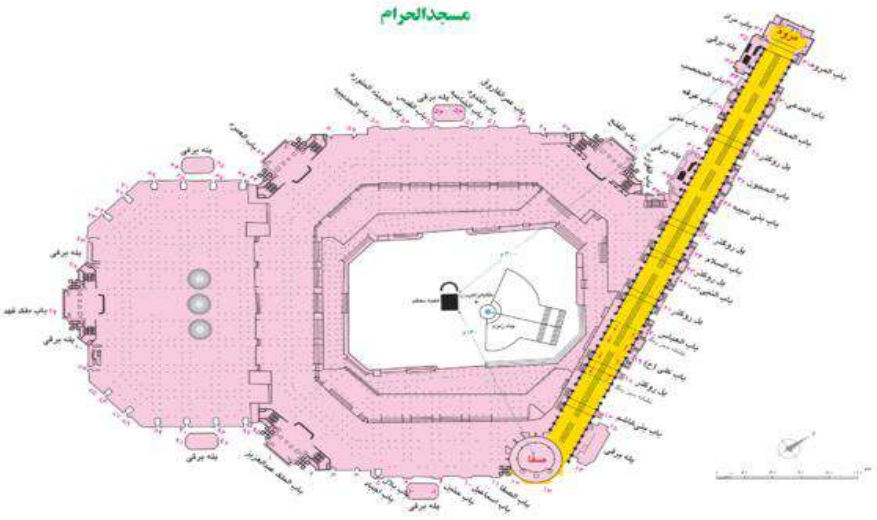

Figure 5 (Al-haram Mosque) [10]

3. Mosques in Afghanistan

3.1. Noh Gonbad Mosque

One of the nations in the globe where the majority of people are Muslims in Afghanistan. In this nation, the place of worship and prayer is extremely significant and priceless. The Noh Gonbad mosque, which lies three kilometers from Balkh city, was the first mosque to be erected in Afghanistan. The first Muslim attack on Afghanistan occurred in the year 652 A.H. During the Sasanian era in the second half of the eighth century, this mosque was constructed. This mosque originally had nine domes and six substantial columns with concave Islamic ornamentation and motifs that were inspired by various creative schools and styles. Currently, only four of the mosque's foundations are still in place, and others have collapsed. The Islamic school of art is represented by these four pillars and their breathtakingly magnificent arches. [11]

Figure 6 (Noh Gonbad Mosque) [11]

Figure 7 (Noh Gonbad Mosque) [11]

3.2. Shah Do Shamshira Mosque

Lis son of Qais was one of the Arab Muslims' leaders when they prepared the initial assault on Kabul during the period of Prophet Usman. Lis fought valiantly and was martyred during this conquest. According to this, Muslims performed their first prayer in Kabul after the city was conquered, and they laid the foundation stone for a mosque there and gave it the name "King of Two Swords" in honor of the warrior who used both hands in battle. The current structure of this mosque, which adds to its beauty and majesty, was rebuilt in 1306 by the mother of Shah Amanullah Khan Ghazi. This mosque has undergone development and reconstruction throughout history. [12]

Figure 8 (Shah Do Shamshira Mosque View) [12]

3.3. Pol Kheshti Mosque

The center of ancient Kabul is where you'll find this mosque. The minaret and dome of this mosque, which has a very long history, are visible from several locations in Kabul. According to stories, this mosque was built on the foundation of a temple that had been demolished. Its structure was finished as a one-story structure with three hallways, seven porticoes, and twenty-one domes. They hung a large clay-burning light, which was moved up and down by chain anchors, in the center of each dome. At that time, these lights exuded a unique splendor. Around the exterior wall of the mosque, the verses of the Holy Qur'an are inscribed in Kufi and Sols script for a distance of 88 meters. The mosque's courtyard has been carpeted with common stone slabs that have been polished to resemble marble stones and the carpet within the mosque has been painted. The current mosque has a 62-meter-tall minaret and an 18-meter-tall green dome. Three thousand devotees can congregate here at once. The Pol Kheshti Mosque's new structure is composed completely of translucent marble. [13]

Figure 9 (Pol Kheshti Mosque View)

4. Problem Statement

Afghanistan is an Islamic nation with 99% Muslims in its population. Each region and city in Afghanistan have a large number of these constructions. However, lack of information about the design and architecture of early Muslim mosques and their evident similarities, mosques in Afghanistan do not adhere to any specific architectural guidelines. In early mosques, architects made an effort to take all of the rules and principles of architecture into consideration when building and designing the mosque, but the mosques were built later based on arbitrary plans. It has eroded the basis and guidelines for them. In this article, we discuss the methods and specifics related to elements of the early mosques and their evolution in the current mosques of Kabul which have no historical background research.

5. Methodology

This research utilized a descriptive-historical method. This article draws on field research, case studies, and library studies. To comprehend the evolution of mosques in our country, we first read historical writings that covered the origins, development, and history of mosques throughout various historical eras. After that, every aspect of the building's architecture including its size, style, and beauty as well as its reconstruction and modifications have been thoroughly examined in library and digital research. After conducting fieldwork, we visited both old and new mosques in Kabul, photographed each of their components and historical features, and recorded every last detail, including plans, site plans, images, and information. Different historical eras and architectural styles have different aspects and traits, which have been discovered and explained. The oral history told by the village elders has also been employed in this research due to a lack of historical documentation. It is helpful to know the history of each mosque, its components, its evolution, and other vital factors. In this field study, the questionnaires have been explained to the surrounding people and the results have been included in this

research. Then we will get to know the evolution of the early and new mosques in Kabul city.

6. The evolution of mosque Architecture in Afghanistan

6.1. Shah Do Shamshira Mosque

There is a building that stands out in the middle of Kabul's town, surrounded by both new and old structures, in an area crowded with people and vehicles. This is the earliest mosque in Kabul city. The large dome with the two golden minarets adjacent to it offers a good view of the surrounding city. The Shah Do Shamshira Mosque is a historically significant location that highlights Kabul's magnificence and was unharmed by recent wars and internal strife in Afghanistan. This mosque was formerly a pilgrimage site but was later transformed into a mosque. Kabul residents utilize it today as a place of prayer and devotion. A signboard with verses from the Qur'an is placed on the right side of the mosque entrance. A wheat cluster with two plaster-carved swords that cross one other is located in the southern section and at the top of the mosque entrance. Shah Do Shamshira Mosque has undergone many changes during its history. This is the location of the first Muslim martyrs during the takeover of Kabul. In 36 A.H. Muslims struck Bast Bastan for the first time before advancing on Kabul. Lis son of Qais, one of the army's commanders, entered Kabul after the city's defenses were breached by catapults and were slain following a protracted battle in the current location of the Shah Do Shamshira Mosque, which bears his name. Throughout its history, this mosque has undergone numerous ups and downs and has been demolished multiple times. But it was built for the last time by Shah Amanullah Khan's mother and according to another narration by " Shah Amanullah's wife Queen Surya" in 1306 AH. This mosque is significant culturally and exhibits the elegance of the 20th-century architecture. This mosque is a symbol of the refinement of recent construction and has cultural significance. The architects from the Chardehi region completed the mosque's dome and other finishing touches. This mosque, which was designed by Turkish architects based on a mosque in Turkey, features the largest wooden dome in Kabul, measuring 12 meters in diameter.

Figure 10 (Shah Do Shamshira Mosque View) [Source: Authors]

The Shah Do Shamshira mosque is two stories tall, with four clay pillars supporting the first floor's dome. These columns have very lovely carvings on the ends and are miniature versions of actual green columns. The altar on this floor is likewise miniature and has a highly intricate carving in addition to the heads of the columns, which are painted in green and gold hues. Beautiful miniatures that once adorned the walls of the mosque's columns have been lost as a result of the locals' understanding and the mosque's periodic painting. However, during the most recent restoration of this mosque, which was completed by the Ministry of Urban Development and Lands in collaboration with the Presidency's National Development Administration, some of these delightful paintings and miniatures that were once inside the mosque have been brought back to life.

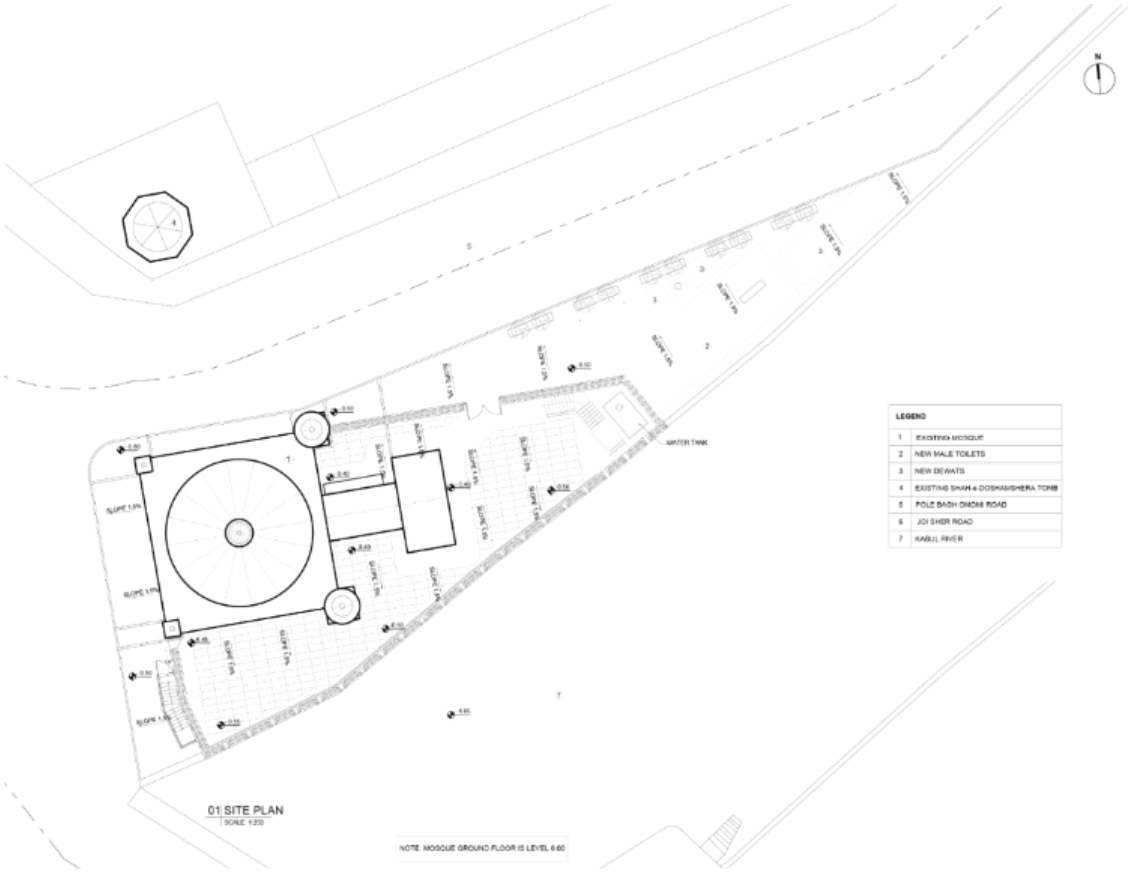

Figure 11 (Site plan of Shah Do Shamshira Mosque) [Source: Authors]

A staircase that continues rotating to the mosque's end of minarets is located on the first floor of the mosque's entrance side. This stairway inside the minarets continues up to the roof of the mosque and above that to the end of the minarets, which ends at a terrace that had been used to call for prayer previously. The mosque's second level has a wooden carpet on it and is made up of a dome above a floor without columns. A lamp hangs in the center of this 12-meter-diameter wooden dome, which also has a 12-meter diameter.

An iron curtain surrounds the mosque's roof from the outside, preventing rain from entering the structure. Pigeons abound around the mosque, adding to its picturesque surroundings. The National Development Administration of the Presidency worked with the Ministry of Urban Development and Lands to rebuild this mosque lately. Additionally, this mosque will be renovated and a modern underground ablution hall with muezzin and mullah chambers will be constructed for it. [Source: Authors]

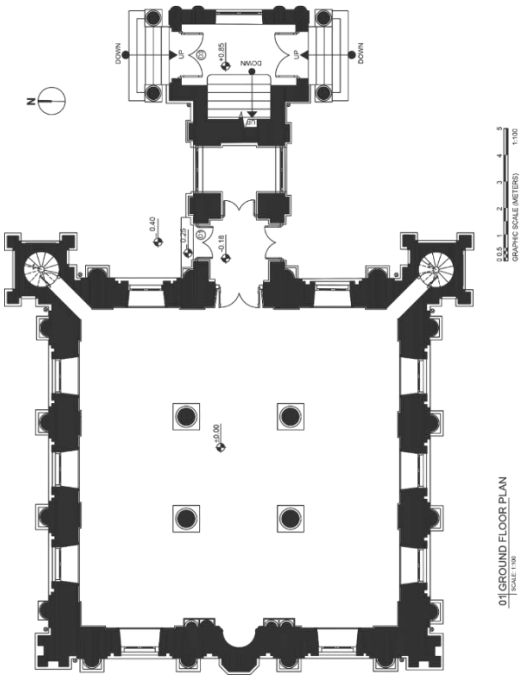

Figure 12 (Ground Floor plan) [Source: Authors]

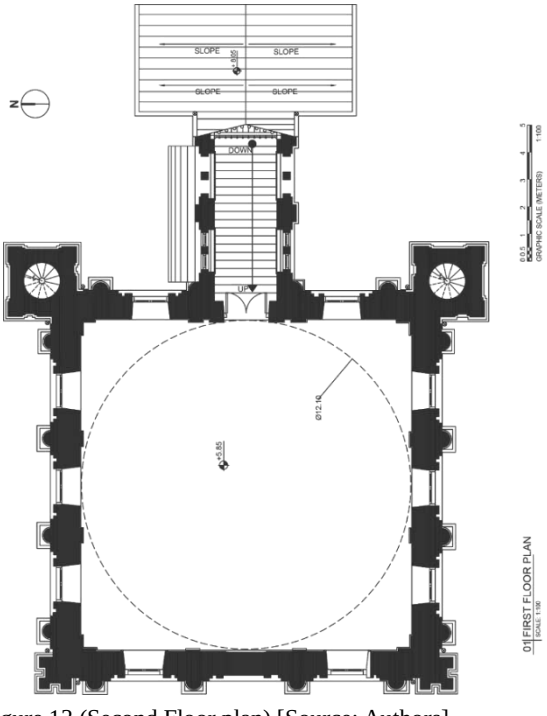

Figure 13 (Second Floor plan) [Source: Authors]

Figure 14 (Shah Do Shamshira Mosque- Interior) [Source: Authors]

Figure 15 (Minaret) [Source: Authors]

6.2. Pol Kheshti Collective Mosque

One of the biggest and most historic mosques in the nation and splendor of all time is Pol Kheshti Mosque, formerly known as Lab Darya Mosque. This mosque boasts a towering minaret and a huge dome that is visible from a great distance. The three-thousand-year-old Pol Kheshti Mosque is thought to have served as Prophet Suleiman's (AS) place of worship. The Pol Kheshti Mosque is thought to have originally been a temple that was transformed into a mosque after Muslims invaded the area. The initial Foundation's stone was kept in both the new mosque's Foundation and the altar of the previous mosque. It was also preserved in the new altar's Foundation. The main construction of this mosque started in 1187, under the reign of Timor Shah Durrani. Due to disagreements among the ministers, it was never finished. In 1213 AH, Timor Shah's son Shah Zaman finished the building of the Pol Kheshti Mosque. A bridge made of baked clay and plaster was constructed over the Kabul Sea during the reign of Timor Shah Durrani close to the Collective Mosque, also known as Pol Kheshti Mosque by the local populace. Following that, another structure with three corridors, seven porticoes, and twenty-one domes was constructed in the middle of the previously mentioned mosque under the reign of Abdul Rahman Khan in 1271 AH. Amid each dome, there was a big lamp in which the kerosene was burning. Sandalwood was used for the mosque's inside carpet, while plain stone slabs were used outside. These slabs were polished out to match the marble stones. The mosque's plastering was regarded as one of the era's greatest architectural achievements. This mosque had three gates, including a massive gate that faced the market and was topped by an octagonal dome that was long and broad and featured ornamented porticoes. The mosque's azan site was positioned above the gate and used to say the azan there.

Figure 14 (Pol Kheshti Mosque View*)* [Source: Authors]

Amanullah Khan gave the order to construct a new school for children in this mosque, perform necessary maintenance on the mosque, and establish a comfortable residence and ablution hall there in 1303 A.H.

The previous mosque was destroyed and a new mosque was constructed in 1334 AH, during the reign of Muhammad Zaher Shah. This mosque boasts a 62-meter-tall minaret and a dome that rises 18 meters above the floor and can hold 3000 people at once. The dome is ornamented with blue-green tiles, while the first and second levels' walls, corridors, and porticos are all made of translucent marble. A massive lamp, weighing 1,600 kilograms, is situated in the center of the main dome.

Its rehabilitation and reconstruction, which was the responsibility of the Ministry of Urban Development and Housing, have now been finished and put into use.

The second level of the Pol Kheshti Mosque is entirely composed of domes and arches, which allows for a smooth flow between the rooms. A pond is positioned inside the ablution area, which enhances its beauty and fosters a pleasant ablution experience. [Source: Authors]

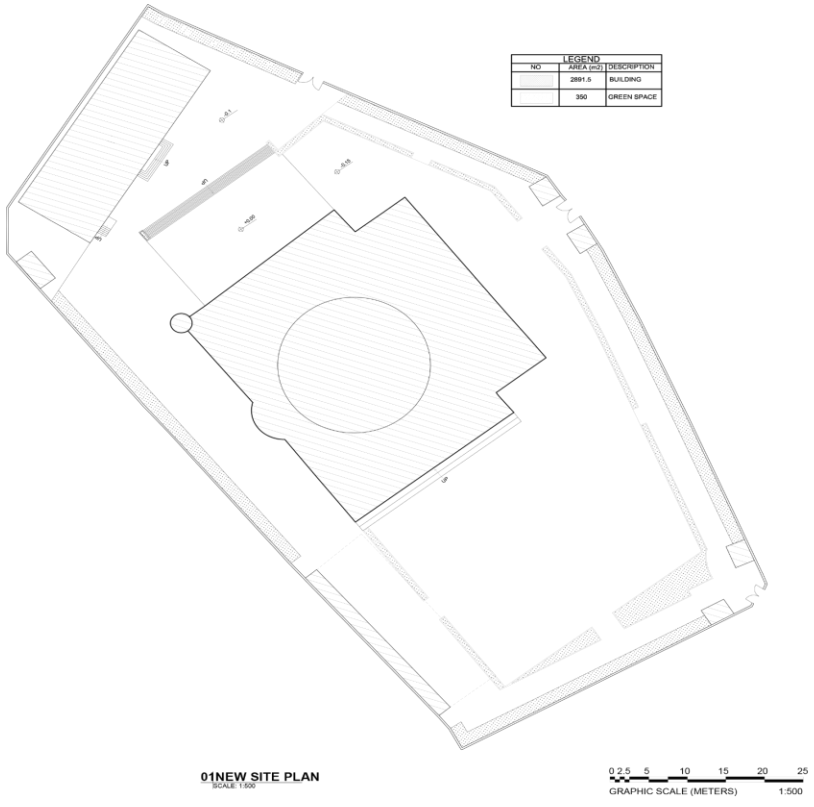

Figure 15 (Site plan of Pol kheshti Mosque) [Source: Authors]

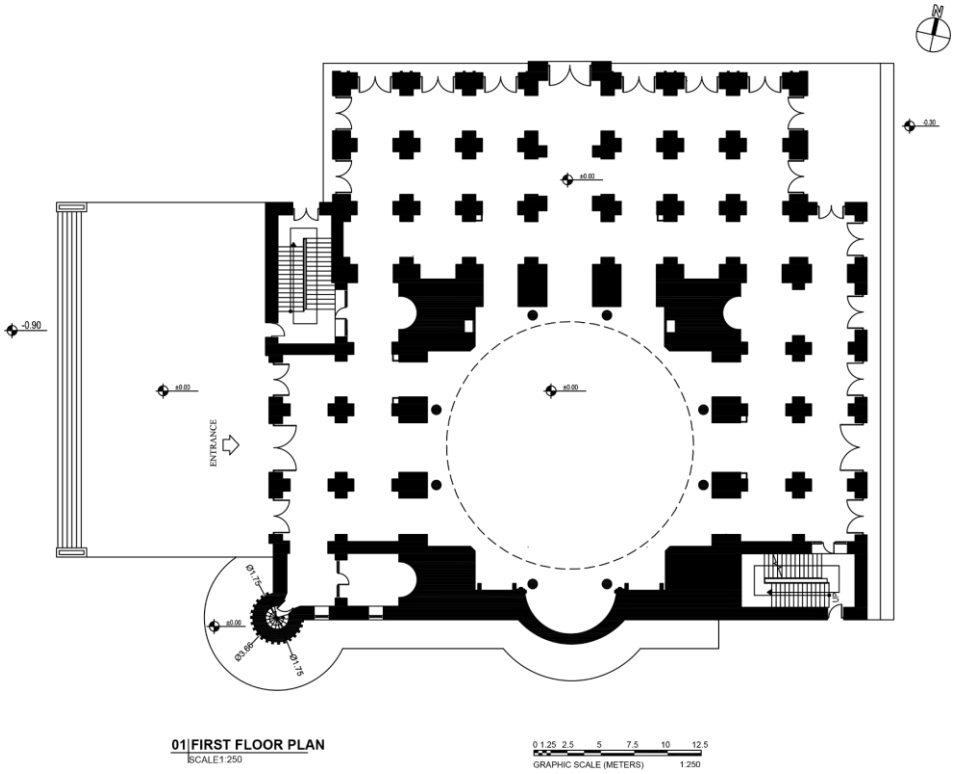

Figure 16 (First-floor plan of Pol Kheshti Mosque) [Source: Authors]

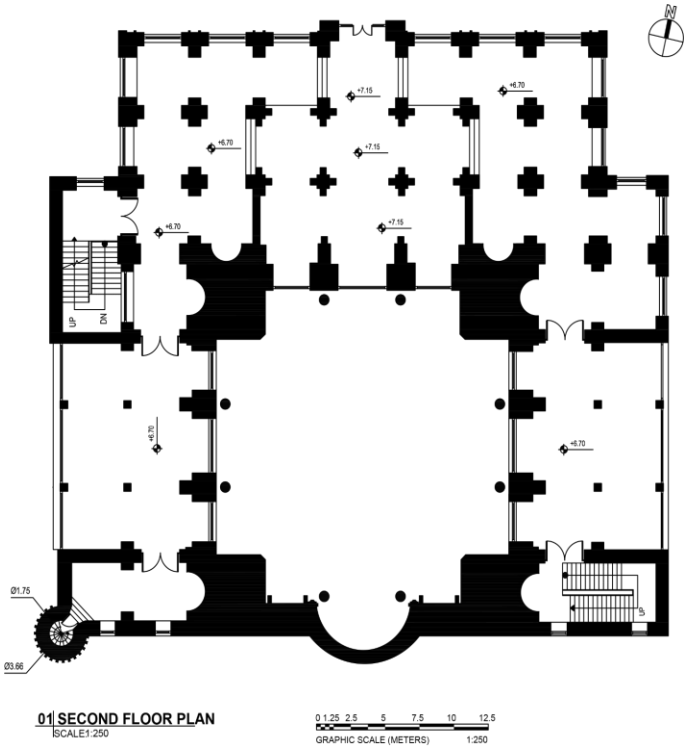

Figure 17 (Second Floor plan of Pol Kheshti Mosque) [Source: Authors]

Figure 18 (Pol Kheshti Mosque Interior) [Source: Authors]

Figure 19 (Pol Kheshti Mosque Ablution area) [Source: Authors]

Figure 20(Mosque Interior) [Source: Authors]

6.3. Pakhta Froshi Collective Mosque

During the reign of Shah Durrani, the initial construction of the Chub froshi mosque, Noor al-Islam Collective Mosque, or Pakhta froshi Mosque in the historic city of Kabul took place. About 25,000 rupees were spent on the building's development and repair, most of which went into re-creating the domes, arches, and porticoes. People claim that during the reign of this king, the winter mosque was constructed in the courtyard of the Collective mosque. To maintain this magnificent mosque, Abdul Rahman Khan constructed a religious school inside of it. Mullah Abu Bakr Akhundzada from Kandahar, Qazi Pashdi from Laghman, Maulvi Palch from Ghazni, and Maulvi Ghulam Jan from Logar are some of the religious experts who instruct pupils there.

Figure 21 (Pakhta froshi Mosque View) [Source: Authors]

Figure 22 (Roof of P.F.M) [Source: Authors]

During the reign of Abdul Rahman Khan, Ghulam Nabi Khan worked to restore and renovate the Noor al-Islam Mosque, which had been constructed using 200 tons of iron, clay, plaster, stone, wood, and lime.

The explosion of the gunpowder storage of the stores next to the mosque, which took place in 1341 AH, might be listed among the other historical occurrences that occurred above the stated mosque, according to the longtime residents of this neighborhood. Due to the recklessness of one merchant, the gunpowder shops close to this mosque were set on fire, resulting in a tremendous explosion that caused significant financial damage to the locals.

Due to its proximity to the wood shops, the mosque in question was formerly known as the Chub Froshi Mosque. Shah Zaman renamed it the Shahi Mosque during the renovation, and people continued to refer to it by this name under the reign of Abdul Rahman Khan.

Because of its white exterior and interior decorations, it was formerly known as the White Mosque and could be found in the Wood Store Pass, next to the till Shop Pass and the Book Store Pass. The Agha Khan Foundation renovated the Pakhta froshi Mosque in 2004 after it was devastated during the civil wars. The Department of Mosques of the Ministry of Urban Development and the Afghan Construction Authority have recently begun restoration work as of 2018 A.H. The Pakhta froshi Collective mosque measures 80 meters in length and 23 meters in width. It is situated in the center of the mosque's courtyard. This mosque contains 31 domes, including a sizable dome in the middle. All of the mosque's domes are constructed of clay, each measuring 20 cm in length and width, together with lime for the adhesive and other materials. Iron is used to cover the main mosque's roof as a defense against environmental elements.

The mosque's main entrance is a gate with two minarets around it that is located at the entrance to the courtyard. The mosque's main minaret, which includes a decorative

element, is situated next to the enclosure wall. The water from a pond created in the mosque's courtyard is utilized for ablution. The Winter Mosque, as well as the muezzin and mullah's apartments, is located in the northern section of the Mosque courtyard. Some sources claim that these two were constructed during the reign of Shah Abdul Rahman Khan. The eastern portion of the winter mosque contains a firehouse that is used to heat the mosque throughout the winter.

The winter mosque, which is located in the northern section of the mosque, is 17 meters long and 15 meters broad. It has a lovely altar that is entirely covered with flowers, and the hall of the mosque has 12 columns supporting the ceiling, each 50 cm long and wide. Clay is the main component of these columns.

The pan of the house below the mosque, which has a carpet-clay floor, heats the space. On chilly winter days, people pray in this mosque.

The school is situated in the rear of the Collective Mosque; a portico from the southern corner mosque separates it from the mosque's main structure. The courtyard's central school structure is surrounded by other buildings and rooms. All of its chambers have dome-shaped, baked clay roofs. Each room features an oven-shaped fireplace that serves as the room's heat source throughout the winter. The Holy Quran and other religious texts have been studied and memorized at different times in this school.

The Pakhta Froshi mosque's entrance is marked by a two-story tower that was constructed to ring out the call to prayer. A 180-degree spiral staircase in this building ends on the roof of the next-door businesses. Pigeons are currently residing in a hole with a covered head in the gloom. An iron curtain that covers the dome's roof prevents the Abdul Rahman Collective Mosque roof from leakage. [Source: Authors]

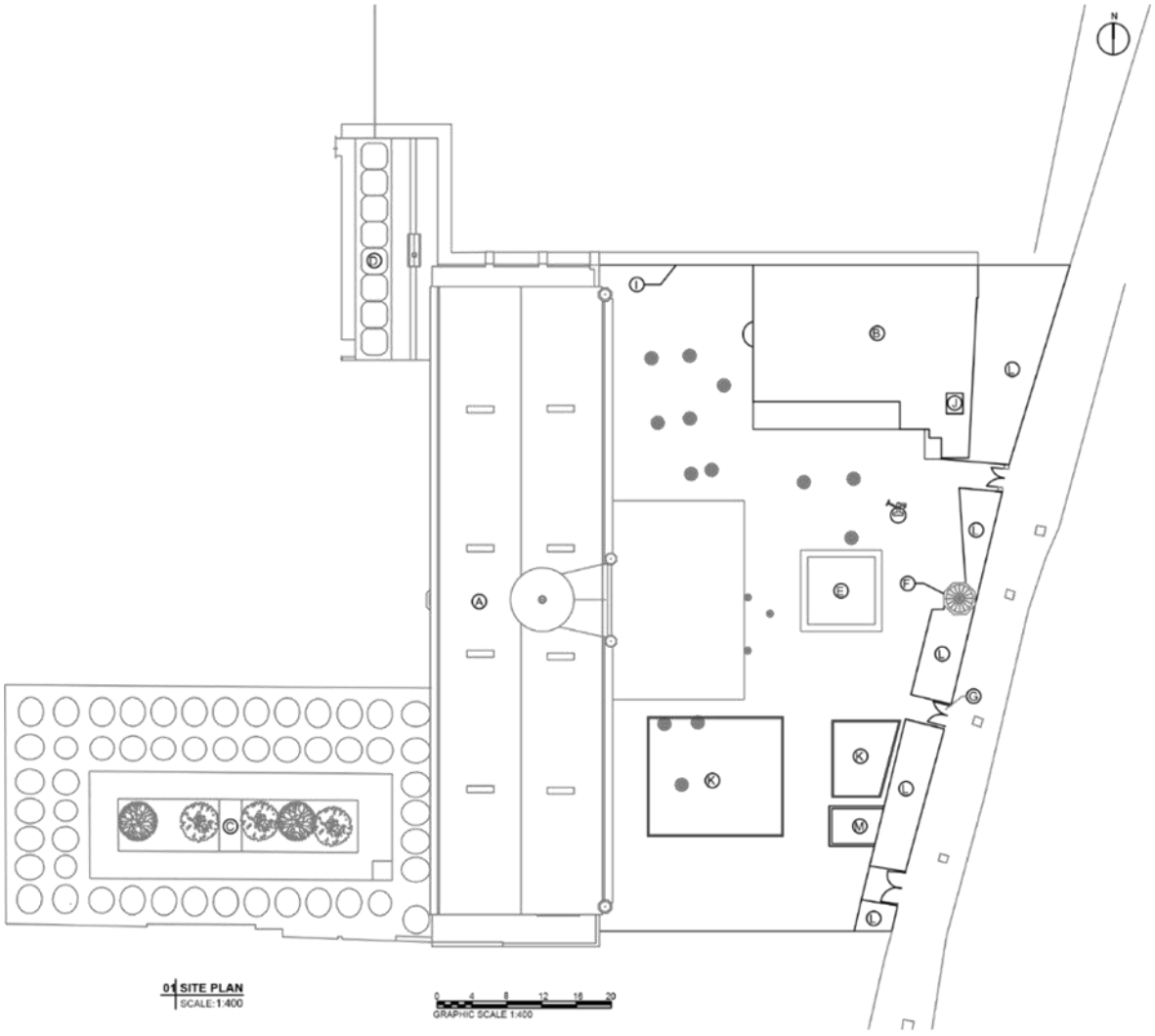

Figure 23 (Site plan of Pakhta froshi mosque) [Source: Authors]

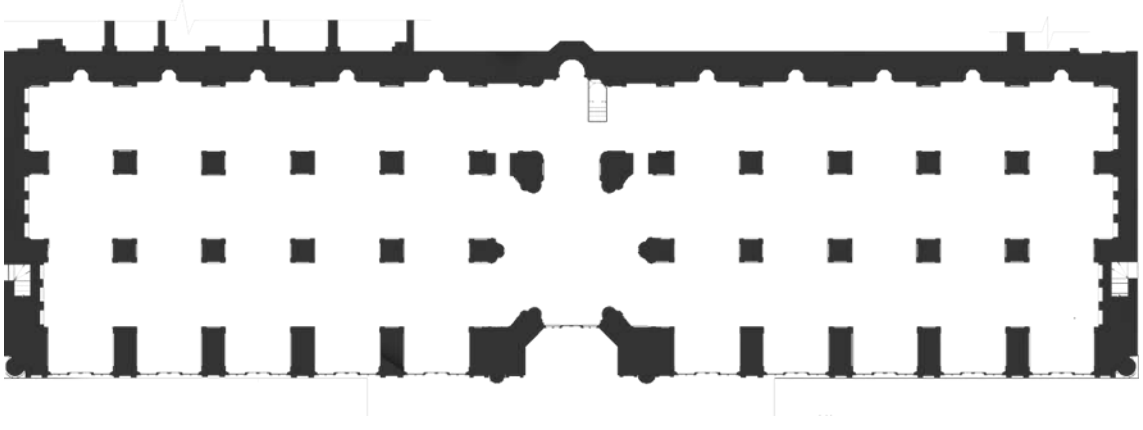

Figure 24 (Pakhta froshi Mosque Ground Floor Plan) [Source: Authors]

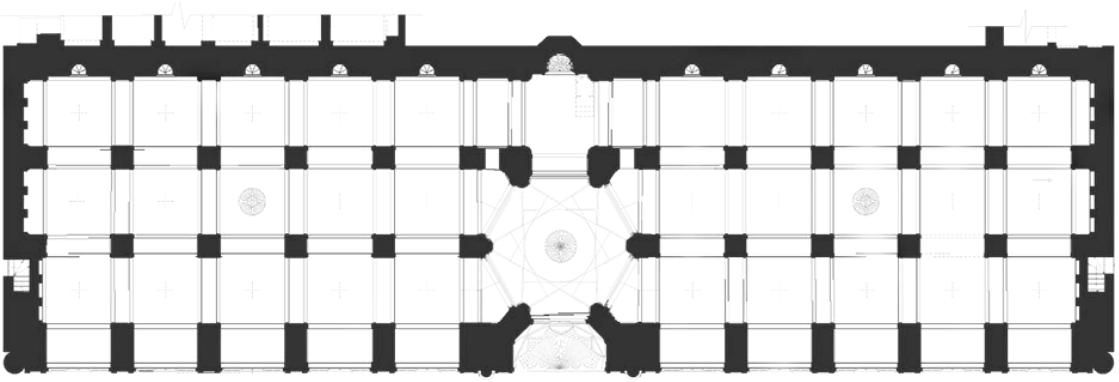

Figure 25 (Pakhta froshi Mosque Second Floor Plan) [Source: Authors]

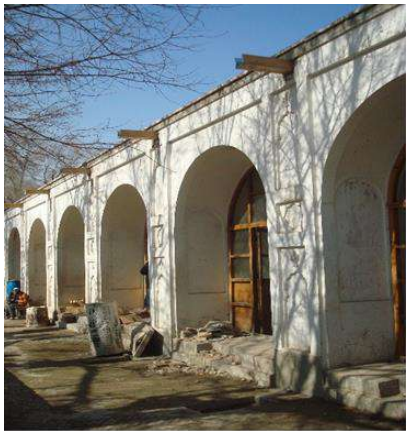

Figure 26 (Pakhta Froshi Mosque View) [Source: Authors]

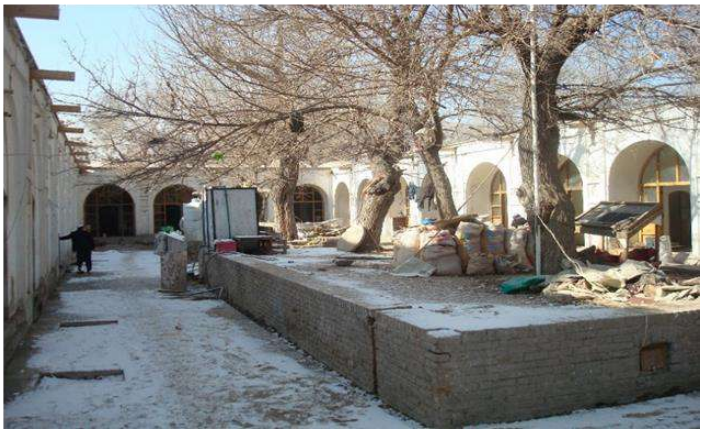

Figure 27 (Courtyard of P.F.M) [Source: Authors]

5.4. Abdul Rahman Khan Mosque

Enormous, stunning mosques have existed in Afghanistan for a very long time.

The "Abdul Rahman Khan" mosque in Kabul is among the largest and most recent of them. This mosque, which was constructed in Kabul's business district and close to "Zarnegar" park, can accommodate 10,000 worshipers.

This mosque was constructed at the beginning of 2001 by Haji Abdul Rahman Khan, one of Kabul's well-known businessmen. This mosque bears his name, Abdul Rahman Khan, and was constructed by him with the best amenities. An Afghan architect named "Mir Hafiz Ullah Hashemi" was responsible for the creation of the Abdul Rahman Khan Mosque. Although the Abdul Rahman Khan Mosque's construction was finished in 2009, it wasn't inaugurated until 2012. The opening ceremony of the Abdul Rahman Khan Mosque was attended by Hamid Karzai, the former leader of Afghanistan, and several other dignitaries.

The Abdul Rahman Khan Mosque has two minarets and 14 domes. Some individuals estimate that there are 20 domes. The minarets are approximately 62 meters high, and each one has a water supply for the ablution of worshipers.

The Abdul Rahman Khan Mosque's walls, minarets, and domes are adorned with Quranic verses and Islamic symbols. The mosque has a unique beauty because of these lines and patterns, which are characteristic of Afghan art. Everybody's soul is polished by the Holy Qur'anic verses that are displayed around the mosque.

The basement portion of the Abdul Rahman Khan Mosque has 1,600 square meters of ablution space. The simultaneous capacity of this restroom is 500 people.

The Abdul Rahman Khan Mosque's men's section is 900 square meters in size, while the second level, which is for women only, is 500 square meters.

In addition to a library, Abdul Rahman Khan Mosque has a school. Its library comprises two male and female reading rooms and 150 000 boo allows worshipers and readers the opportunity to study and learn alongside their devotion, this library is tremendously beneficial to both groups. the dome being invaded by natural elements. As previously reported, the gunpowder storehouses caught fire, destroying this minaret, which was later rebuilt. This is evident from the materials utilized in the minaret's construction. [13]

Figure 28 (Abdul Rahman khan Mosque [Source: Authors]

7. Result

After studying those 4 well-known mosques in Afghanistan, we find out that these mosques have undergone many adjustments and alterations. Shah do Shamshira mosque has a lot of decoration and designs which has been inspired by Moghul architecture and decorations. This mosque just has a small prayer hall with two stories tall with different miniature. A lot of local construction materials such as wood. Its dome and carpets have been built of wood which shows the impact of local architecture.

As we mentioned that mosque is an inseparable element of afghan society, and most afghans are sending their children to the mosque for education and Islamic studies. So, the culture of the society affected the architecture of this mosque. Pol-kheshti mosque besides its religious use has a school for kids and a separate ablution area.

The heating of the mosque is a little difficult during the winter. lots people had a place in their house by the name of Taba Khana which has a basement with the necessary equipment for heating the home. This element has been used in the Pakhta froshi mosque too. So, the mosque has two summers and a winter prayer hall. This shows how custom and tradition affect the architecture of the mosque. Wood, clay, and iron are the local construction materials that had been used in this mosque.

Abdulrahman mosque is one of the earliest mosques which has been built in Kabul. They have used modern architecture in composition with Islamic architecture. The miniature and decoration in the exterior parts of this construction show the beauty of Islamic architecture. This mosque has a broad ablution area and restrooms with a facility for education that provides a library for people.

8. Conclusion

We find out that the culture and tradition of people in the society have affected Afghanistan's architecture especially mosque architecture. Early mosques have been affected by foreign architecture, Moghul Miniatures, and Patterns. Mosques have been evaluated from time to time. Society, People's morals, and Construction materials had the most impact on this evaluation. Society customs ,traditions, and demands have been utilized in these mosques such as Taba Khana, Religious schools, and so on. According to our study, most of the present mosques do not have the basic elements of the standard mosque. Most of them have been built arbitrarily. Mosque is a historic and ancient base of Islam and as Allah (SWT) said the Religion is completed 1400 years ago and there is no change possible on that, similarly society doesn’t want change and alterations in the base and basic elements of mosques, lots of afghans want those ancient architectural elements in today’s mosques. Such as winter and summer prayer halls, and the religious use of mosques in society.

Reference

[1] A. A. M. a. T. Aryanti, "The Domes: El Wakil's Traditionalist Architecture," *IOP Conference Series: Materials Science and Engineering,* 2017.

[2] "Islami City," Islami City, 2013. https://www.islamicity.org/7942/the-form-of-the-prophets-mosque/.

[3] D. A. Khalil, Atlas of the Qur'ān: Places, Nations, Landmarks.

[4] H. F. Al.Ratrout, "The Second Mosque in the Earth that Islamic Jerusalem Forgot revealing the ancient Al-Aqsa Mosque," *Journal of Islamic Jerusalem Studies,* pp. 23-52, 2013.

[5] H. Fayyad, "Middle East Eye," [Online]. Available: www.middleeasteye.net.

[6] H. M.Al-Ahmadi, S. Wael and R. H. Malkawi, "Statistical analysis of the crowd of dynamic in Masjid al-nabawi in the city of Medina, Saudia Arabia," *International Journal of Crowd Science,* pp. 52-62, 2018.

[7] S. Faruqui, "Muslim Hands," muslimhands.org.uk.

[8] S. a.-h. Riyaz, "Spatial analysis of Masjed al-haram," *Journal of interdisciplinary studies in humanities,* vol. 4, no. 3, pp. 61-87, 2012.

[9] A. H. Noqrakar, "Holy Kaaba Fundamental design of desirable places of worship," *Islamic architectural research,* vol. 1, no. 1, pp. 25-41, 1392.

[10] H. Alhawasli and M. R. Bemanian, "THE IMPACT OF HOLY KAABA CUBIC SHAPE ON THE INCORPOREAL," *JOURNAL OF ISLAMIC ARCHITECTURE,* pp. 103-110, 2018.

[11] C. Gimondi, The Ancient Noh Gonbad Mosque, THe study and Consideration Of an Early Islamic Monument at Balkh, BOLIS EDIZIONI, 2016.

[12] A. W. Ayoobi and H. G. Demirkol, "An evaluation of architectural monuments in," *JOURNAL OF DESIGN FOR RESILIENCE,* vol. 2, no. 1, pp. 64-85, 2021.

[13] E. Knobloch, The archaeology and architecture of Afghanistan, 2002.

[14] A. (. (2011)., " Asian Historical Architecture," https://www.orientalarchitecture.com/.

Authors Profile:

Noorullah Hashemi born in Kabul, Afghanistan. He graduated from school in 2016 and received his Bachelor's Degree in Architectural Engineering from Kabul Polytechnic University in 2022. His area of interest are including Islamic Architecture, Sustainability, and Modern Architecture.

Abdul Halim Hakimi has a Master's Degree in Islamic Studies his Field of Research includes Islamic Studies. He is currently working as head of the Islamic Studies Department of Kabul Polytechnic University.

Mohammad Ayuob Awwab was born in 1351. He graduated from Imam Bukhari Secondary School in 1371. He received his bachelor's degree in Islamic studies from Kabul University in 1375. He joined Kabul Polytechnic University Islamic Studies Department in 1377. He is interested in Islam and science, Quran, and contemporary sciences.

Hasibullah Sakha born in Kabul, Afghanistan. He graduated from school in 2016 and received his Bachelor's Degree in Architectural Engineering from Kabul Polytechnic University in 2022. His area of interest are including Islamic Architecture.

KPU International Journal of Engineering & Technology
Volume 2, Issue2, Dec. 2022
e-ISSN:2790-0819, p-ISSN:2790-0800
Date Received: 2022-10-03
Date Accepted: 2022-12-22
Date Published: 2022-12-30

Mapping and Evaluating Land Suitability Using a GIS-Based Model: A Case Study in the Abyek Area, Qazvin, Iran

MARHABA SAHBANI[1], FEREYDOONS ARMADIAN[2*], MOHAMMAD DAUD HAIDARI[3]

[1]Department of Soil Science and Irrigation, Kabul University, Kabul, Afghanistan, Email: sahbani50400@gmail.com

[2*]Department of Soil Science, Faculty of Agricultural Engineering and Technology, College of Agriculture and Natural Resources, University of Tehran, Karaj, Iran, E-mail: fsarmad@ut.ac.ir

[3]Department of Soil Science and Irrigation, Kabul University, Kabul, Afghanistan, Email: m.daud.haidari@gmail.com

Abstract

Land suitability is an important strategy for optimal and sustainable use of land and stabilization of its performance. The area covers 5,215 hectares and consists mostly of cultivated land. The objective of this study was to evaluate the available land resources and produce a land suitability map for irrigated wheat. For an assessment of the study area, a total of 32 representative soil profiles were used for collecting soil samples. They were also used as input to the model. The conditioned Latin Hypercube Sampling (cLHS) method was used for determining sampling points. Covariates for running the model were elaborated from remote sensing data. The suitability classification for irrigated wheat crops was determined using a parametric method. The random forest model of SAGA GIS software was used to predict suitability classes. For preparing the final map of land suitability, firstly the raster map related to the parameters affecting land suitability was prepared in the ArcGIS environment, and secondly, this raster file was stacked in the random forest model with auxiliary variable layers and the final map was obtained. The results showed that about 52.68% (2747.5 ha) of the studied area was found to be highly suitable (S1), 44.1% (2295.4 ha) was moderately suitable (S2), and 2.96% (154.8 ha) was marginally suitable (S3). In addition, 0.33% (17.4 ha) of the total area was classified as currently unsuitable. The main limiting factors for land suitability were texture, depth, alkalinity, and the presence of coarse fragments in the soil. It was also found that with the help of environmental variables and GIS, making the framework for the optimum use of land become very easy and provided significant advantages in terms of time and economic aspects.

Keywords: Land suitability, Wheat, Variables, Parametric method, Random forest model

* Corresponding Author

1. Introduction

Land evaluation is the process of relating the specific type of land use to the features of land resources, using scientific standards and techniques. Users and planners can use the findings as a reference to find alternatives to other land uses [1]. Land can be utilized for a variety of purposes, such as entertainment, agriculture, industry, housing, fishing, and the preservation of nature. An adequate framework for land management and appropriate land use is provided by the evaluation of a specific area. Any choice about land use in the initial step requires land evaluation of resources and technology available. The efficient utilization of available land resources for sustainable agricultural crop production necessitates land evaluation. Farmers and policymakers will be able to identify the most suitable places for different plant production and management options and establish sustainable agriculture using the results produced from the creation of a geographical soil map and land assessment [2]. Land suitability analysis is a method of land evaluation that identifies the main limiting factors of a particular plant. In addition, it assists in the creation of a suitable crop management system to increase land productivity through options. Land suitability evaluation is a method that can be used for growing plants resistant to unfavorable environmental conditions [3-4].

GIS is a very useful tool for preparing thematic maps. The integration of geological and topographical maps with digital elevation models is done much more accurately and quickly by GIS. It also greatly reduces the time required for data entry and output [5]. Different machine learning models are used to discover patterns in data and to make predictions and have a great potential to improve land suitability evaluation [6]. The random forest model, which use to predict soil classes, was introduced by Breiman in 2001 as an extension of the CART model to improve the efficiency of the model estimation [7] and it has been mainly used in remote sensing studies; random forest model can consider several environmental variables simultaneously [8].

According to several recent studies, the availability of remotely sensed data and Geographic Information Systems (GIS) allows the combining knowledge from various sources to improve land suitability evaluation [3-4-6-9-10-11-12-13] and the current study was conceptualized using these research findings.

Cereals are an important part of dietaries; they are a significant source of energy, protein, vitamins (vitamins A and C), and minerals (potassium and calcium) [14]. Wheat (*Triticum aestivum* L) is the most widely grown cereal crop in the world - an estimated, wheat covering about 237 million hectares annually [15]. The main objective of this research was to perform the land suitability evaluation and carry out suitability mapping for the wheat crops by integrating different information using GIS tools for areas in the eastern

part of the Qazvin province of Iran. In addition, the main factors limiting the proper growth of wheat in the study area will also be identified.

2. Methods and Materials

2.1. Study area

The study area is approximately 5215 ha and is located between latitudes 36° 2′-36° 8′ N and longitudes 50° 20′-50° 20′ E in Abyik County of Qazvin province of Iran (fig. 1). Its altitude extends between 1163 -1379 m.a.s.l and its temperature and moisture regimes are thermic and xeric. According to the Bagh-e-Kowsar Meteorological Station, The amount of annual rainfall is 278.43 mm and the annual average temperature is 13.88 °C. The month with the most rain was March, with 52.2 mm of rainfall, and the month with the least rain was September, with 0.18 mm of rainfall. Temperatures averaged 21.47 °C for the highest and 6.07 °C for the lowest. In terms of topography, the area is mainly flat, and the majority area has fertile farmland for cultivation.

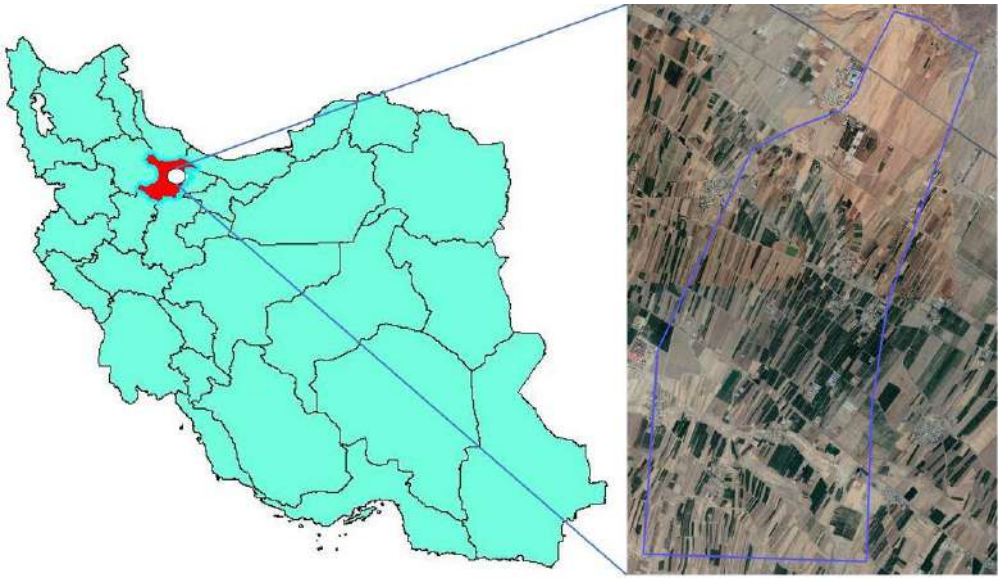

Figure 1. Study area

2.2. Soil sampling and analysis

The soil sampling scheme was performed by applying the conditioned Latin Hypercube Sampling algorithm (cLHS) [16]. The distribution of 32 locations acquired by cLHS is illustrated in Figure 2. The method presented is a stratified randomized design that with the help of multivariate distribution causes effective sampling of the study area. Regarding environmental variables and the geological map of the study area, R Software was used to perform the conditioned Latin Hypercube Sampling (cLHS) approach. The

geological map of the study area has been obtained from the geological Survey and mineral exploration of Iran. Digital elevation model ASTER GDEM with the 30-meter spatial resolution was obtained from Aster Global Digital Elevation Map (http://gdex.cr.usgs.gov/gdex/) and a satellite image of the study area belonging to Sentinel-2 was downloaded from Copernicus Open Access Hub. Variables such as Slope, Slope length, Wetness Index (WI), Multi-resolution Valley Bottom Flatness Index (MrVBF), and Multi-resolution Ridge Top Flatness Index (MrRTF), were extracted from DEM using SAGA GIS and ArcMap software. Normalized Difference Vegetation Index (NDVI) was extracted from satellite images using ERDAS IMAGINE and SNAP software. The selected variables were entered into the conditioned Latin Hypercube Sampling technique, and the algorithm divided the data into n values with the same probability, after applying the Latin square condition (one sample in each dimension a and b) the layers are combined and the algorithm starts it repeats the process until the objective evolution function reaches stability. 50 thousand iterations were used to run the model and obtain the objective function (Figure 3).

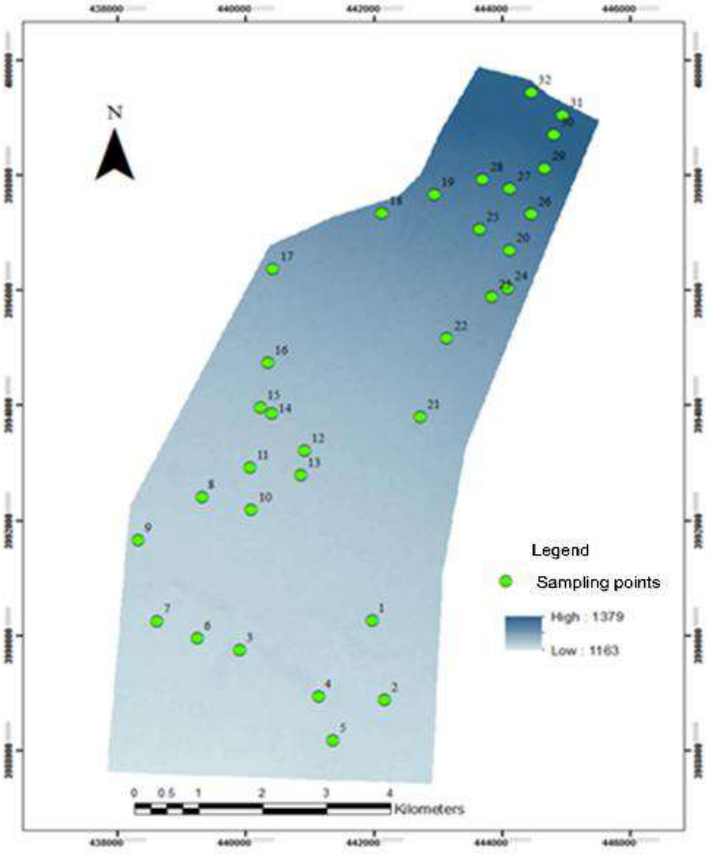

Figure 2. Soil sample point

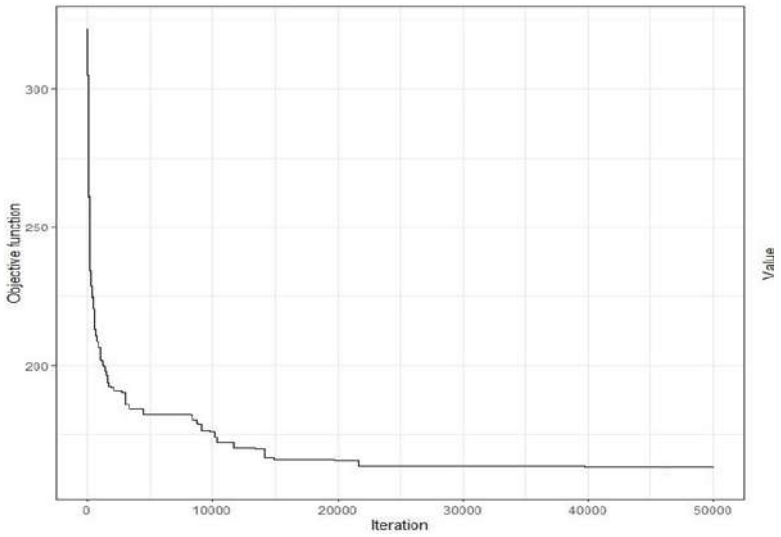

Figure 3. Evolution of the objective function

The Global Positioning System (GPS) was used to determine the geographical locations of all sampling points (profiles) and then profiles were excavated. Profiles were defined using the Field book for describing and sampling soils [17], and samples were collected from all of their genetic horizons and sent to the laboratory for regular physicochemical analyses. Soil samples were air dried and then crushed with mortar and pestle and passed through a 2-mm sieve for separating the coarse fragments (<2mm). The fine particles were stored in separate containers and used for physicochemical analysis. The calcium carbonate contents of the soil were determined using back-titration methods [18]. The organic carbon content was determined by the modified Walkley and Black method described by Jackson [19]. The amount of gypsum was measured using the Acetone method [20]. The soil pH and Electrical conductivity (EC) were measured in extracted saturated soil. The soil texture was determined using the hydrometer method [21].

2.3. Land Suitability evaluation

A parametric approach (Square Root method) [22] was utilized for 32 profiles to assess land suitability for irrigated wheat. The most important factors in land evaluation are topography, soil, and climate. These factors, particularly topography (including relief/ slope and elevation) and soil, have a considerable impact on the land unit determination. Relief and elevation are closely related to plant requirements as relief effect land management and erosion risk, while elevation affects heat and sunlight.

In this study, firstly, important information about the research area's land features was collected. Some of the data were obtained from the results of soil studies (laboratory

analyses and field observation) and climatic data (minimum and maximum temperatures, number of sunshine hours, amount of rainfall, relative humidity, and wind speed) used in land evaluation for various purposes (specifying plant growth period, cultivation date, and so on) were obtained from the Bagh-e-Kowsar meteorological station.

Eight parameters have been used in this work to study land suitability for irrigated wheat. These parameters are soil calcium carbonate, depth, EC, pH, organic carbon, texture, coarse fragments, and gypsum. The average weight of these parameters, including climate (criteria used to determine land suitability), for each profile up to the root depth, was calculated. As our targeted plant is irrigated wheat, an annual crop, of up to 100 cm was calculated. Then, the land limitation (in terms of soil and topography) of each map unit was determined by matching the characteristics of each soil profile with the criteria of the plant demands table [23-24].

The parametric approach (Square root method) uses the following formula to calculate the final land index:

$$I = Rmin \times \sqrt{\frac{A}{100} \times \frac{B}{100} \times \frac{C}{100} \times \ldots}$$

Where I is the index, Rmin is the minimum rating, and A, B, C, … are other ratings besides the minimum rating [25].

Rainfall was eliminated using data from the Bagh-e-Kowsar meteorological station to determine climatic appropriateness, considering the assumption that irrigated wheat water requirements are met by irrigation. Other environmental parameters for the growth cycle [23] were determined using 22-year meteorological data from the Bagh-e-Kowsar synoptic station.

After identifying the climatic parameters needed to assess the climate of the study area, the values were compared with the table of wheat climatic requirements, and the final climatic class for wheat was obtained by using the parametric approach (Square Root method).

The land index was then calculated using the parametric method based on the degree of suitability of the climate elements. After that, considering soil [24] and climatic [23] limitations, the final class of land suitability was determined according to the numerical values of the land index for different classes of land suitability. Finally, the map of land suitability for irrigated wheat production was prepared.

2.4 Modeling to create a digital map of land suitability assessment

To model the land suitability assessment, all land suitability classes were recognized and coded based on the parameters such as soil organic carbon, texture, pH, EC, calcium carbonate, depth, gypsum, and coarse fragments.

Google Earth was used to detect all soil profiles by knowing their geographical coordinates and then saving them as a single KMZ layer. After that, ArcMap software was used to convert the specified layer to a shape file. In the next step, the prepared shape file along with the layer related to the digital elevation model for sampling from land suitability classes and preparing the latest file related to the land suitability classes to introduce it for the desired model was entered into ArcMap software. This method was used to prepare and store the final shape files of land suitability classes.

The digital elevation model (one of the primary indicators of land characteristics) was used to determine the terrain components, which were derived from the ALOS satellite with a spatial resolution of 12.5 meters. After digital elevation model derivation and changing the coordinate system to the UTM coordinate system, five indexes: Wetness (humidity) Index (WI), Multi-resolution Valley Bottom Flatness Index (MrVBF), Multi-resolution Ridge Top Flatness Index (MrRTF), land shapes, and morphometric Features) were calculated and derived using SAGA software. Sentinel-2 images with a spatial resolution of 10 meters from 2017, 2018, and 2019 were utilized to derive the Normalized Difference Vegetation Index (NDVI). Finally, a shape file of land suitability classes along with prepared environmental variables was provided to the random forest model in SAGA software. The model is implemented using 500 trees, with each node containing five different features (mtry).

3. Results and Discussion

The land suitability evaluation procedure was set based on Food and Agriculture Organization's (FAO) 1976 general framework in terms of land suitability [26]. According to the findings of the climate assessment in the study area, the climate does not impose any restrictions on its cultivation and therefore the climate class was obtained as S1. Table 1 shows the land suitability classes for irrigated wheat in each land unit. Figure 4 displays the digital map of the land suitability classes for irrigated wheat, and Table 2 shows the area devoted to the land suitability classes for irrigated wheat. The soils of these regions have mainly less than 2% slope. Generally, cereal crops require slightly sloping land for smooth and easy tillage practices. In addition, the soils have suitable depth; root penetration will stop with soil depth limitation because of a physical barrier or unsuitable chemical properties [27]. The results of the land suitability analysis showed that the large parts of the studied area were classified as highly suitable 52.68% (2, 2747.5

ha) (Table 2) and is located mostly in the central part of the studied area (Figure 4). Because of a physical barrier such as coarse fragments and soil texture, 23.58% of the studied area was classified as S2s (Table 2), The S2s land units are located in the north and south parts of the studied area (Figure 4). Due to the soil alkalinity, 20.43% and 2.65% of the studied area were classified as S2n and S3n (Table 2); these are low lands, located in the south part of the studied area with gypsum-containing soils (Figure 4). However, 0.31% and 0.33% of the studied area (Table 2), located in the north part of the studied area (Figure 4) were classified as N1s and S3s, due to soil texture limitations and the presence of coarse fragments.

The findings show that the accuracy of the results obtained with the square root method is high and revealed to be more realistic in comparison with other methods' results. Bagherzadeh and Mansouri Daneshvar (2011) used different methods, including the square root method, to evaluate land suitability for wheat cultivation in Iran [28]. He fined that texture/structure, coarse fragments, OC, CEC, and pH are the most significant limiting factors for irrigated wheat. Zeinodini (2003) evaluated the land suitability for wheat crops in Iran. The land suitability classification results based on the parametric method show that the land suitability classes are various from S1 to S3. This author found that the dominant limiting factors for wheat cultivation are gypsum, texture, and soil structure [29]. Baqer Zadeh et al. (2012) reported that the Storie method's results were very strict and far from reality, whereas the square root represented more balanced results for the determination of land suitability classes [30].

Table 1: Land suitability classes in each land unit using a parametric approach (square root method) for irrigated wheat

Land suitability unit	Land index	suitability class	Land suitability unit	Land index	suitability class
1	60	S2n*	17	16	N1s
2	61	S2n	18	40	S3s
3	65	S2s*	19	62	S2s
4	58	S2s	20	61	S2s
5	83	S1	21	83	S1
6	66	S2n	22	59	S2s
7	88	S1	23	79	S1
8	41	S3n	24	55	S2s
9	56	S2n	25	77	S1
10	81	S1	26	63	S2s
11	94	S1	27	37	S3s
12	89	S1	28	58	S2s
13	91	S1	29	58	S2s
14	83	S1	30	57	S2s
15	89	S1	31	55	S2s
16	88	S1	32	58	S2s

*n and s show soil alkalinity and soil physical (properties) limitations

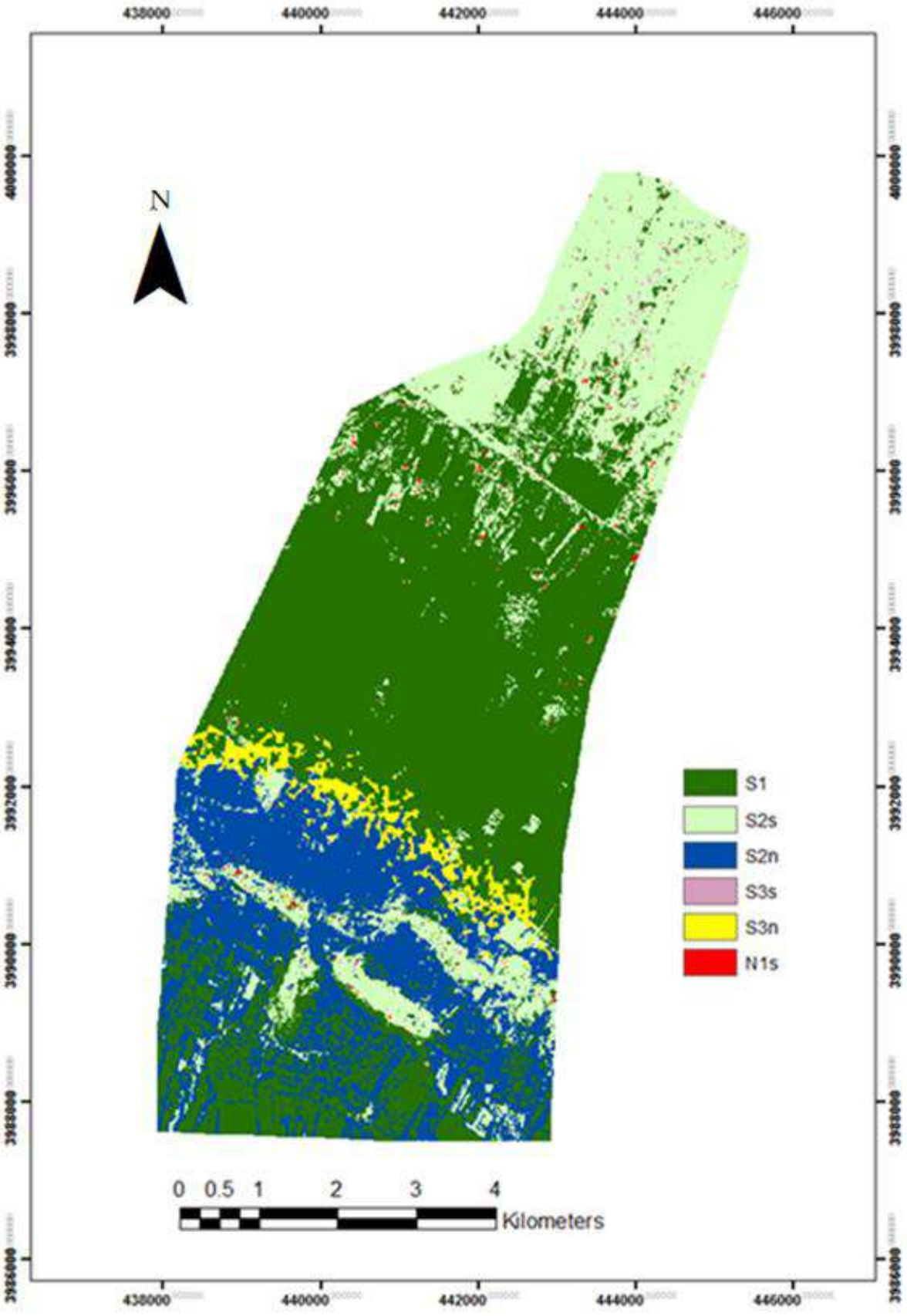
438000
440000
442000
444000
446000
N
S1
S2s
S2n
S3s
S3n
N1s
0 0.5 1 2 3 4
Kilometers

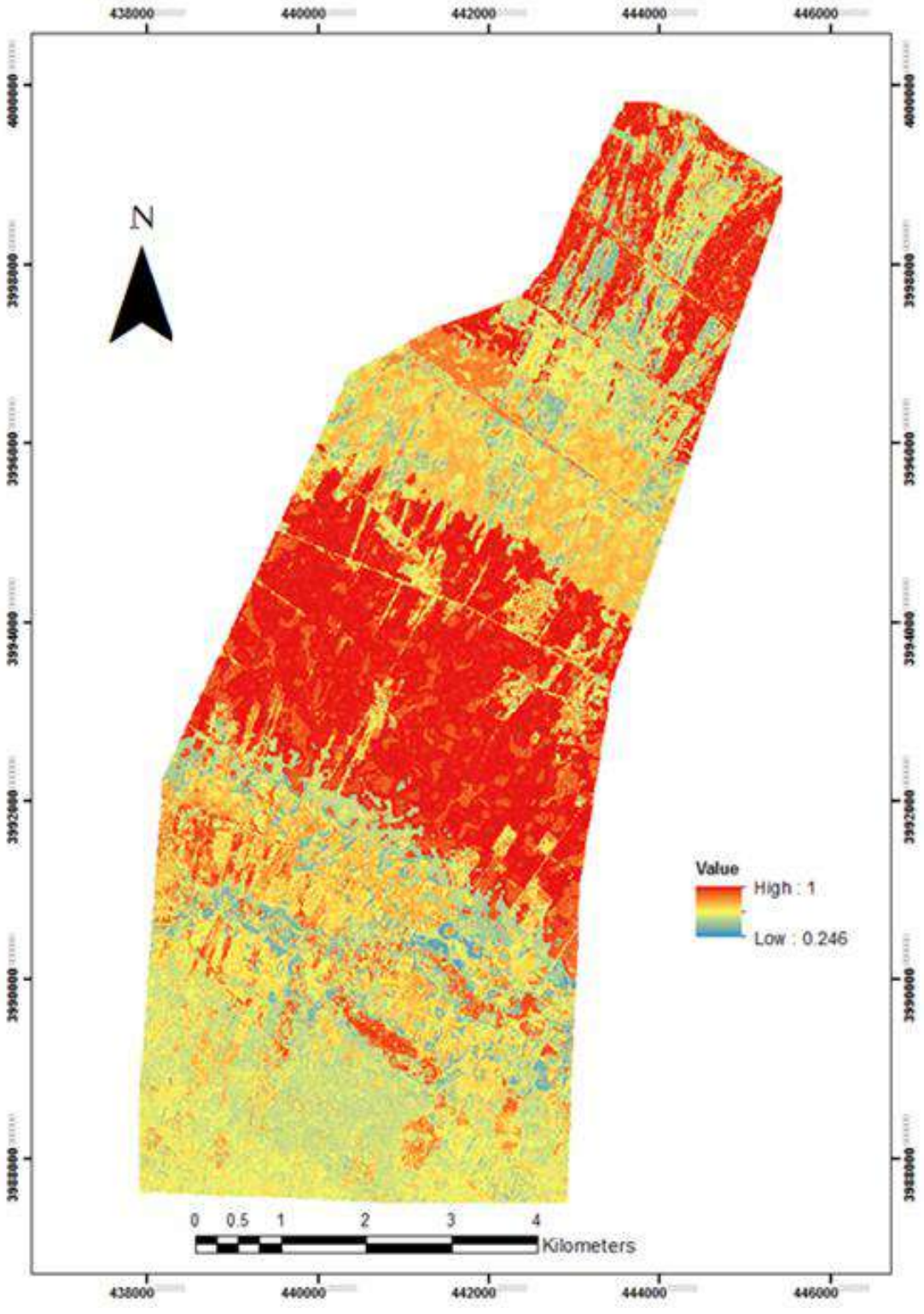

Figure 5. Probability map of land suitability classes for irrigated wheat

According to the probability map of land suitability, the central and northern parts of the study area have the highest accuracy. The estimation accuracy was low in some parts, such as those between the northern and central parts, and it was very low in the southern parts of the study area. Obtaining a probability map, which helps to interpret the map, is a good achievement. The probability map was obtained based on a digital map of land suitability.

Table 2: Area related to land suitability classes for irrigated wheat

land suitability class	Area (ha)	Area (%)
S1	2747.5	52.68
S2s	1229.8	23.58
S2n	1065.6	20.43
S3s	16.3	0.32
S3n	138.5	2.65
N1s	17.4	0.34

4. Conclusions

The purpose of this study was to perform the land suitability evaluation and carry out suitability mapping for the irrigated wheat crops by integrating environmental auxiliary variables, using GIS tools. The parametric method (square root formula) was used to evaluate the suitability. Land suitability analysis of the studied area indicated that 2747.5 ha (52.68%) had no restrictions for wheat cultivation and were classified as highly suitable S1. About 2294.4 ha (44.01%) of the studied area was classified as moderately suitable (S2) due to the soil alkalinity and soil physical properties restrictions, for irrigated wheat cultivation. Due to the soil alkalinity and soil physical properties restrictions, the remaining 3.31% were classified as marginally suitable (S3) and currently not suitable (N1). In preparing a land suitability map for irrigated wheat, variables such as the Normalized Difference Vegetation Index, Inverted-red Edge Chlorophyll Index, Digital Elevation Model, Multi-resolution Valley Bottom Flatness Index, and Multi-resolution Ridge Top Flatness Index, all of these variables had the greatest influence on soil changes and the creation of a digital map of land suitability classes for irrigated wheat.

Acknowledgments

The authors would like to thank all members of the soil science laboratory, Department of Soil Science, Faculty of Agricultural Engineering and Technology, College of Agriculture and Natural Resources, University of Tehran, for providing the facilities to carry out this work and for their suggestions.

References

[1] S. Ritung, F. Agus, and H. Hidayat, "Land suitability evaluation with a case map of Aceh Barat District," 2007.

[2] B. H. J. Massawe, "Digital soil mapping and GIS-based land evaluation for rice suitability in Kilombero Valley, Tanzania," The Ohio State University., 2015.

[3] A. A. El Baroudy, "Mapping and evaluating land suitability using a GIS-based model," Catena., vol. 140, pp. 96-104, 2016.

[4] B. Harms, D. Brough, S. Philip, R. Bartley, D. Clifford, M. Thomas, and L. Gregory, "Digital soil assessment for regional agricultural land evaluation," Global Food Security., vol. 5, pp. 25-36, 2015.

[5] M. Liengsakul, S. Mekpaiboonwatana, P. Pramojanee, K. Bronsveld, and H Huizing, "Use of GIS and remote sensing for soil mapping and for locating new sites for the permanent cropland-A case study in the highlands of northern Thailand," Geoderma., vol. 60, pp. 293-307, 1993.

[6] Y. Ostovari, A. Honarbakhsh, H. Sangoony, F. Zolfaghari, K. Maleki, and B. Ingram, "GIS and multi-criteria decision-making analysis assessment of land suitability for rapeseed farming in calcareous soils of semi-arid regions," Ecological Indicators., vol. 103, pp. 479-487, 2019.

[7] M. Wiesmeier, F. Barthold, B. Blank, and I. Kögel-Knabner, "Digital mapping of soil organic matter stocks using Random Forest modeling in a semi-arid steppe ecosystem," Plant and soil., vol. 340, no. 1, pp. 7-24, 2011.

[8] Y. Zhang, B. Sui, H. Shen, and L Ouyang, "Mapping stocks of soil total nitrogen using remote sensing data: A comparison of random forest models with different predictors," Computers and Electronics in Agriculture., vol. 160, pp. 23-30, 2019.

[9] S. Hamzeh, M. Mokarram, and S. K. Alavipanah, "Combination of Fuzzy and AHP methods to assess land suitability for barley: Case Study of semi-arid lands in the southwest of Iran," Desert., vol. 19, no. 2, pp. 173-181, 2014.

[10] A. Mishelia, and E. M. Zirra, "Application of Geographic Information System (GIS) in evaluating suitable areas for wheat cultivation in Adamawa State Nigeria," Int. J. Sci. Knowl., vol. 6, pp. 14-22, 2015.

[11] R. B. Zolekar, and V. S. Bhagat, "Multi-criteria land suitability analysis for agriculture in the hilly zone: Remote sensing and GIS approach," Computers and Electronics in Agriculture., vol. 118, pp. 300-321, 2015.

[12] G. Ayalew, and Y. G. Selassie, "Land suitability evaluation for cereal and pulse crops using geographical information system in East Amhara region, Ethiopia," Research Journal of Agriculture and Environmental Management, vol. 4, no. 3, pp. 141-148, 2015.

[13] A. H. Rabia, "A GIS-based land suitability assessment for agricultural planning in Kilte Awulaelo district, Ethiopia," In The 4th International Congress of ECSSS, EUROSOIL., p. 1257, 2012.

[14] U. G. A. S. SIsmaila, A. S. Gana, N. M. Tswanya, and D. Dogara, "Cereals production in Nigeria: Problems, constraints, and opportunities for betterment," African Journal of Agricultural Research., vol. 5, no. 12, pp. 1341-1350, 2010.

[15] O.G. Olabanji, M. U. Omeje, I. Mohammed, W. Ndahi, and I. Nkama, "Wheat: In Cereal Crops of Nigeria: Cereals: Principles of production and utilization," NU., vol. 4, pp. 230-249, 2004.

[16] B. Minasny, and A. B. McBratney, "A conditioned Latin hypercube method for sampling in the presence of ancillary information," Computers & geosciences., vol. 32, no. 9, pp. 1378-1388, 2006.

[17] P. J. Schoeneberger, D.A. Wysocki, and E. C. Benham, E, "Field book for describing and sampling soils," Government Printing Office., 2012.

[18] D. W. Nelson, and L. P. Sommers, "Total carbon, organic carbon, and organic matter. Methods of Soil Analysis: Part 2 chemical and microbiological properties," vol. 9, pp. 539-579, 1983.

[19] M. L. Jackson, "Soil Chemical Analysis," Constable and Co. Ltd. Prentice Hall of India Pvt. Ltd., New Delhi., pp. 10–114, 1973.

[20] L. A. Richards, "Diagnosis and improvement of saline and alkali soils," vol. 78, No. 2, p. 154, 1954.

[21] G. W. Gee, and J. W. Bauder, "Particle size analysis. Methods of Soil Analysis, Part 1. Physical and Mineralogical Methods," Soil Science Society of America. Inc., Madison, WIS, USA, 1986.

[22] Ir. C. Sys, E. Van Ranst, and J. Debaveye, "Principles in land evaluation and crop production calculations," Land Evaluation Part I, Agricultural publication., 1991.

[23] Ir. C. Sys, E. Van Ranst, J. Debaveye, and F. Beernaert, "Crop requirements," Land Evaluation Part III, Agricultural publication., 1993.

[24] J. Seyedmohammadi, F. Sarmadian, A. A. Jafarzadeh, M. A. Ghorbani, and F. Shahbazi, "Application of SAW, TOPSIS and fuzzy TOPSIS models in cultivation priority planning for maize, rapeseed and soybean crops," Geoderma., vol. 310, pp. 178-190, 2018.

[25] S. M. Khiddir, "A Statistical Approach in the Use of Parametric Systems Applied to FAO Framework for Land Evaluation," Doctoral dissertation, Ghent University., 1986.

[26] Framework, FAO. “A Framework for Land Evaluation. Food and Agriculture Organization of the United Nations,” Rome, Soils Bulletin., No. 32, 1976.

[27] G. Debesa, S. L. Gebre, A. Melese, A, Regassa, and S. Teka, “GIS and remote sensing-based physical land suitability analysis for major cereal crops in Dabo Hana district, South-West Ethiopia,” Cogent Food & Agriculture., vol. 6, pp. 1-19, 2020.

[28] A. Bagherzadeh, and M. R. Mansouri Daneshvar, “Physical land suitability evaluation for specific cereal crops using GIS at Mashhad Plain, Northeast of Iran,” Frontiers of Agriculture in China., vol. 5, pp. 504-513, 2011.

[29] A. Zeinodini, “Land suitability evaluation for wheat in Kerman provinces,” In Proceeding of the 8th Iranian Soil Science Congress., vol. 26, p. 29, 2003.

[30] R. BaqerZadeh, A. BagherZadeh, and J. Moinrad, “Analysis of parametric methods for assessing the quality of Nishabur plain land suitability for wheat (*Triticum aestivum* L),” Journal of Agricultural Ecology., vol. 4, no. 2, pp. 121-130, 2012.

Authors Profile:

Marhaba Sahbani received his BSc degree from plant science Department of Alberoni University in 2010. He got his MSc degree in soil science from College of Agriculture and Natural Resources, University of Tehran, Karaj, Iran in 2019. Presently he is working as assistant professor in Soil science and Irrigation Department, Kabul University, Kabul Afghanistan. His area of research includes Pedology and Land Evaluation.

Fereydoon Sarmadian received his PhD in soil science from College of Agriculture and Natural Resources, University of Tehran, Karaj, Iran in 1992. From 1989 up to present, he is working as professor in Soil science Department, University of Tehran, Karaj, Iran. His area of research includes Pedology and Land Evaluation.

Mohammad Daud Haidari received his BSc degree from Agronomy Department of Kabul University in 2006. He got his MSc in soil science and agricultural chemistry from University of Agricultural Sciences (UAS), Bangalore, India in 2011. In 2012, he obtained his PhD in soil science and plant nutrition from Tokyo University of Agriculture and Technology (TUAT), Tokyo, Japan in 2017. Presently he is working as assistant professor in Soil science and Irrigation Department, Kabul University, Kabul Afghanistan. His area of research includes Soil chemistry and plant nutrition.

KPU International Journal of Engineering & Technology
Volume 2, Issue2, Dec. 2022
e-ISSN:2790-0819, p-ISSN:2790-0800

Date Received: 2022-10-06
Date Accepted: 2022-12-19
Date Published: 2022-12-30

Determination of A Suitable Operating Method For Gas Wells From Jurassic Reservoir Rocks in The Khwaja Gogerdak Gas Field, Northern Afghanistan

SADAF JALAL[1*], MOHAMMAD WALID OMID[2], ABDUL SHUKOOR DAWAR[3]

[1*]Assist. Professor, Department of Oil and Gas Mines Engineering, Kabul Polytechnic University, KPU campus, 5th District, Kabul, Afghanistan. Email: sadafjalal_92@yahoo.com

[2]Assist. Professor, Department of Oil and Gas Mines Engineering, Kabul Polytechnic University, KPU campus, 5th District, Kabul, Afghanistan. Email: walid.omid99@gmail.com

[3]Professor, Department of Oil and Gas Mines Engineering, Kabul Polytechnic University, KPU campus, 5th District, Kabul, Afghanistan. Email: ab.shukoordawar@gmail.com

Abstract

The technological regime (method) for gas exploitation from wells is the determination of the appropriate flow rate for gas wells, considering the physical and mechanical properties of reservoir rocks and formation pressure, which can provide normal gas exploitation during good operation. The objective of this scientific research paper is to determine a suitable gas extraction method to maximize well flow. By adjusting and choosing a suitable operating method, we will be able to foresee and stop various problems. These problems include the formation of water tongue and water penetration into the wells, confinement of the gas within the formation, factors that may damage the production intervals, and rapid reduction of the formation pressure. Finally, determining and choosing an appropriate gas exploitation method can help us increase the rate of gas flow and extend the life of the well. This scientific-research work is a mix of field and library work and is based on the figures measured in the head and bottom of well No. 3. The measured figures and information collected from this well are: daily gas production, amount of formation, wellhead pressure, and well bottom pressure, Parameters and characteristics of the productive formation, like the gas compression capability coefficient, the filtration resistance coefficient, and the permeability coefficient, have been determined using formulas and graphs, both analytically and graphically. The question is: Which exploitation regime (method) should we use to minimize the exploitation problems and maximize the amount of gas production? This scientific research work is a mixture of field and library works and is based on the data collected from the head and bottom of well no. 3 of the Khwaja Gogerdak gas mine. The measurements, data, and information gathered from the above-mentioned well include the production rate of gas per day, the amount of pressure of the formation, and the wellhead. In addition, the parameters and characteristics of the productive formation, like the coefficient of compression capacity of the gas, coefficient of resistance to filtering, and coefficient of impermeability are determined by formulations and graphs, both analytical and graphical. The question is: What operating regime (method) should we use to minimize exploitation problems and maximize gas production? In this article, problems with the gas exploitation process are well identified, and reasonable solutions are predicted. As a result, without determining an appropriate technological exploitation regime, it is not possible to extract gas properly from the wells.

Keywords: Suitable gas exploitation regime, daily discharge, well testing, reservoir rocks, gas mine.

* Corresponding Author

1. Introduction

To extract gas from mines, it is necessary to determine a suitable technological regime for the exploitation of gas. If a suitable operating regime is not selected, the operating process will face serious problems such as the destruction of the area around the bottom of the well (productive interval), formation of sand barriers, accumulation of water on the bottom of wells, rusting of production equipment, formation of water tabs (uneven progression of the gas contour), entrapment of gas in reservoir rocks, etc.

To avoid the problems mentioned previously during the process of exploiting Jurassic reservoir rocks, we must determine an appropriate exploitation regime for well No. 3 and all other wells drilled in the Khwaja Gogerdak Gas Field. Hydrodynamic testing has incredible scientific and economic value. We can select a suitable technological gas exploitation regime by analyzing, interpreting test results, and obtaining various productive layer parameters.

The main purpose of this research paper is to determine the maximum permissible and favorable gas flow rate from the Jurassic formation of the Khwaja Gogerdak Gas field based on the formation pressure, the pressures at the head and bottom of the well, and well discharges under different operating regimes.

Furthermore, parameters such as porosity, permeability, saturation, and thickness of the gaseous layers are determined with the help of field studies, comprehensive calculations, and analyses using formulas, graphs, figures, and tables. Finally, the necessary parameters are arranged, and appropriate technological gas exploitation regimes are chosen for the exploitation of gas from wells.

In this study, we are focusing on the following point.

1. Determination of an appropriate technological gas exploitation regime (method) for wells.
2. Identification of important parameters of production formation (porosity, permeability, formation pressure, etc.)
3. Determination of an appropriate operating regime for gas production to maximize the allowable flow rate (discharge rate) of wells.
4. Evaluation of the productivity of wells and associated fluids.

2. The structure map of the Jurassic

The structure of the Khwaja Gogerdak Mines field is located in the north part of Afghanistan, 23 kilometers east of the city of Sheberghan, Jawzjan, Afghanistan. This is one of the most gas-rich parts of northern Afghanistan. In the Khwaja Gogerdak Gas Mining field, gas reservoirs are proven in upper Jurassic limestones, dolomite, sandstones, and, to some extent, Cretaceous calcareous sediments. Gas production started from this mine with the cooperation of the Soviet Union in October 1967 (2.6 billion cubic meters per year). Until now, most of the gas reserves have been depleted from the Getrif, Albian, and Aptian reservoirs in the Khwaja Gogerdak gas field. The extracted gas

was then transported by pipeline to the former Soviet Union and Mazar-e-Sharif fertilizing and the electric planet. Currently, gas is depleted from the Getrif sediments of the Khwaja Gorgerdak Mining field. However, the reserve of Jurassic sediments, which amounts to about 10.6 billion cubic meters, is still intact and has been completely opened by wells No. 3, 41, and 43. In this mining field, no gas has been extracted from the Upper Jurassic mine, because of its location at a greater depth and the sourness of its gas (containing hydrogen sulfide). Preventing future exploitation problems requires determining optimal exploitation regimes and maximum allowable flow rates from these wells.

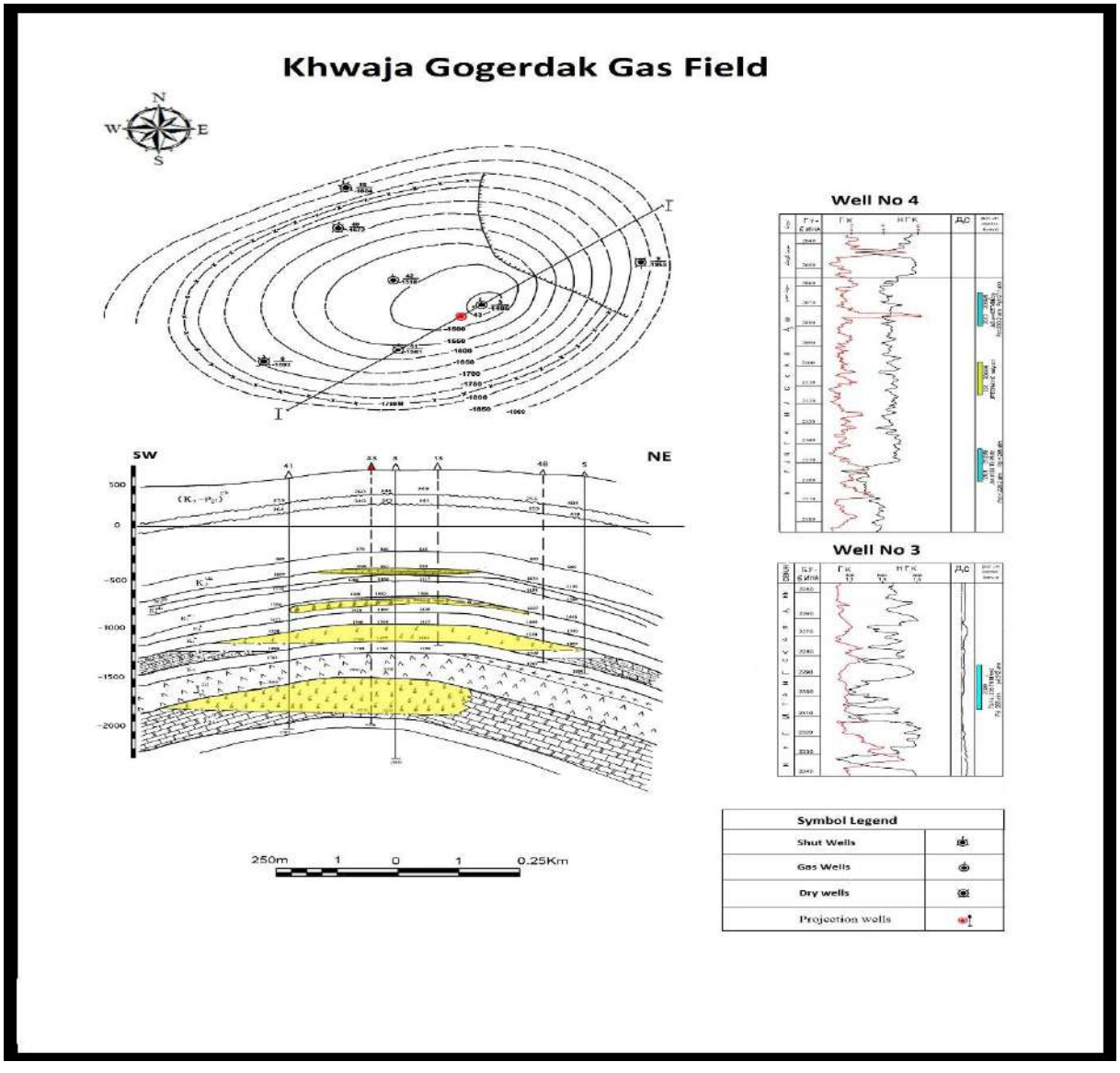

Figure 1: The structural map of the Khwaja Gogerdak gas field

Well No.3

Well, No.3 is drilled on the top of the anticline for evaluation and exploitation of the Khwaja Gogerdak gas field. The depth of the well is 2800 m.

The characteristics of the well according to the basic information Measured in the field:

- The average depth of wells — L_{av} = 2309m
- Relative density of gas — $\bar{\rho}$ = 0,66
- Stratum heat — $T_{lay} = 368k^{\circ}$
- Stratum pressure — P_{lay} = 318 atm
- The diameter of exploitation column — D = 127mm
- The thickness of the productive layer — h = 51m
- Gas viscosity — μ= 0,02CPz
- Feed meter radius — 2δ = 750,Rk = $\frac{750}{2}$= 375m
- Depression — ΔP=54at

3. Methodology

The current research was done through both library-based methods and field surveys. The first part was performed by reviewing the existing literature, but the second part was carried out with a distributed questionnaire along the studied route.

The data used in this research paper are collected from wells during gas production and other scientific research reports from the Jawzjan Hydrocarbon Survey Directorate and the Afghan Gas Directorate. Subsequently, information and field data were analyzed and evaluated by reliable scientific sources and international scientific experiments. Based on that, an appropriate method for gas production from the wells, layer filtration resistance coefficient, the permeability coefficient of the layer, physical-mechanical characteristics of the rocks, pressure, and temperature of the upper Jurassic production interval of the Khwaja Gogerdak gas field was determined.

In this research, gas well number (3) of the Khwaja Gogerdak gas field was tested with the constant regime method. And the well was debited by the DUKT CTDM consumption meter, and the figures were measured. Pressure and temperature under different working regimes are written in table 1.

T*able 1: The price of gas exploitation parameters that are measured in the wellhead*

Gas heat in the wellhead $T_{mou,}$ k^o	Choke coefficient C	Static pressure $P_{mou.\ st}$, atm	Dynamic pressure P_{mou}, atm	Choke diameter in mm	Regime Number
315	62.244	105	100	19.05	1

320	46	125	120	15.85	2
321	35.44	138	128	12.7	3
322	25.245	169	145	11.13	4
318	16.917	175	170	9.51	5

4. Determination of an appropriate operating system for the Khwaja Gogerdak Jurassic wells:

The wells are tested using different gas-producing methods. There are two common methods to test oil and gas wells:

1. Well testing during constant operation (constant fluid flow rate).
2. Well-testing in static operation (variable fluid flow rates).

The hydrodynamic testing of the well involves determining the necessary parameters for the well, and the production layer during the filtration of the gas from the bottom of the well and from the bottom of the well to the surface. Research on the hydrodynamics of oil and gas wells and the analysis and interpretation of their results are important parts of the oil and gas production process. [3]

Gas wells were tested during constant operation in this study, and the good flow rate was measured several times by installing and removing different chokes into the X-mass tree outlet line. At each flow rate, wellhead and bottom pressures were measured. The equipment used in the data collection of this research is illustrated in the figures below.

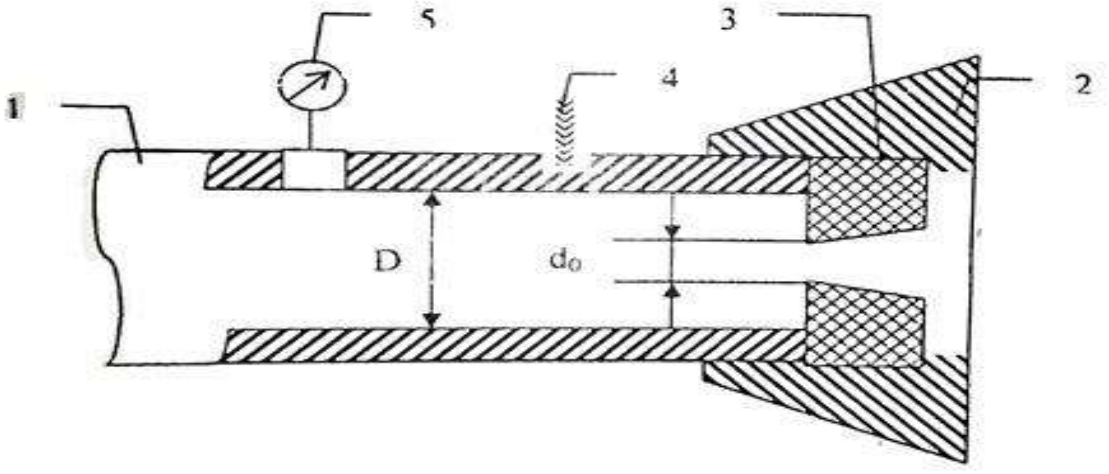

Figure 2: Critical flow rate diaphragm measuring tool

During the investigations, a special gas consumption measurement device (wellhead monitor and critical flowmeter) is installed on the wellhead outlet lines. The structure of this device is illustrated in Fig (4). This device is composed of a body (1) and a choke (2), which is connected to the body through a joint (3). The choke has cone-shaped canals with specific diameters. In addition, in the unit of measurement, special channels are installed for connecting the manometer, the duck (5), and the thermometer. [3] [2]

In the study of gas wells, the gas passes through the measurement device and is released into the atmosphere. Simultaneously, the gas pressure in the measuring device (dynamic pressure), the pressure in the back space of the tubing (static pressure), and the gas temperature are measured. Subsequently, the operating regime of the well is changed by changing the diameter of the choke. For this purpose, the well is shut down for a short period (10-15 minutes) and the valves are measured by the instruments. After installation of the new choke, the good flow rate changes, causing pressure changes at the wellhead after a period of (2-3) hours or more. Pressure and temperature are measured twice.

Basic formulas for performing calculations:

Gas compressibility coefficient calculation formulas:

$Z = F(P_{acou}, T_{acou})$…… ……..…..……..1

$P_{cri} = 49.5 - 3.7 \cdot \bar{\rho}$ ……..…...2

$T_{cri} = 93 + 176 \cdot \bar{\rho}$ …….3

$P_{acou} = \frac{P}{P_{cri}}$…….4

$T_{acou} = \frac{T}{T_{cri}}$…….……..5

c. The formula to determine a gas well's 24-hour flow rate:

$Q = \frac{C_1 \cdot P_{m \cdot din}}{\sqrt{Z_1 \cdot T \cdot \bar{\rho}}}$ m^3/24h……6

d. Formula to determine the pressure at the bottom of the well concerning the static pressure of the well.:

$P_w = P_{m \cdot st} \cdot e^s$……..…7

e. Formula to determine the pressure at the bottom of the well using the dynamic pressure of the wellhead.:

$P_w = \sqrt{P_{m \cdot din} \cdot e^{2S} + \theta q^2}$, KGF/cm2……..8

f. The gas flow equation of the downhole production interval.:

$P_{lay}{}^2 - P_w{}^2 = Aq + Bq^2$……..9

g. Formula for the determination of the permeability factor of the production film.:

$$K = \frac{116 \cdot mg \cdot z \cdot P_0 \cdot T_{lay} \cdot \ln \frac{K_k}{R_w}}{\prod \cdot K \cdot h \cdot T_0} \text{.....10}$$

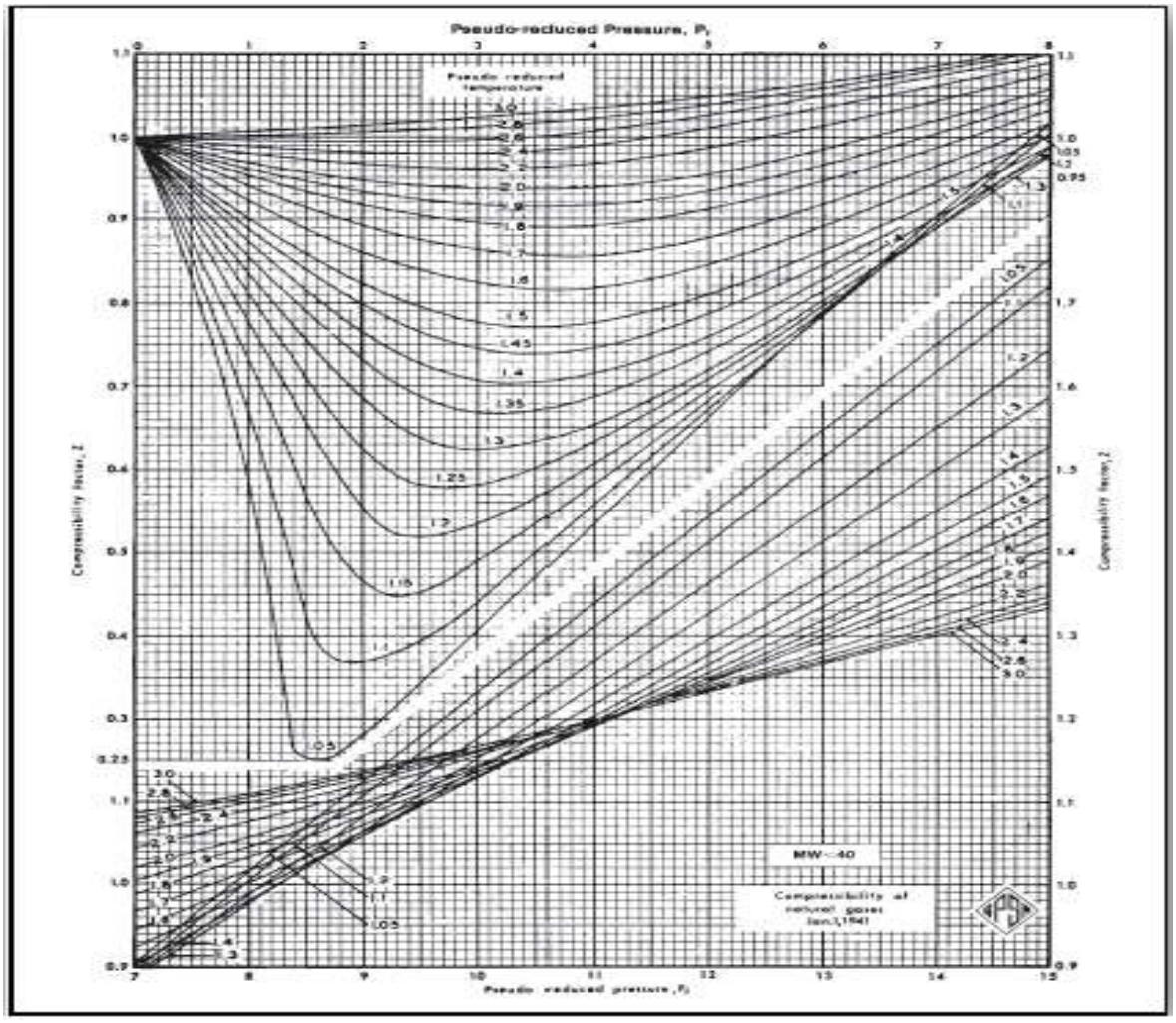

Figure 3: Determination of the gas compressibility coefficient based on the calculated pressure and heat.

4.1.The sequence of calculations:

Well Flow Rate Calculation: After testing the well, we calculate the flow rate of the well in each gas extraction regime as follows:

$$Q = \frac{\mathrm{C} \cdot P_{m \cdot din}}{\sqrt{\mathrm{Z} \cdot T \cdot \bar{\rho}}} \qquad \mathrm{m3/24h}$$

Here: $P_{m\cdot din}$ dynamic pressure before choke, Z gas compressibility coefficient, T Gas temperature in Kelvin, $\bar{\rho}$ relative density of gas and C is the choke coefficient.

To obtain the flow rate, the coefficient of compressibility for each regime is defined. First, the value of the critical pressures P_{cri}, critical temperature T_{cri}, calculated pressure P_{acou}, calculated temperature T_{acou}, and the value of the compression coefficient is defined using the above diagram.

Regime 1:

$T_{cri}=93+176\bar{\rho}$ =93+176·0,66=93+116,6=209,160k

$P_{cri}=49{,}5-3.7\bar{\rho}$ =49,5-3,7·0.66 =47,06at

$T_{acou1}=\frac{T_{mou1}}{T_{\text{cri}}}=\frac{315}{209{,}16}=1{,}5$

$$P_{acou1}=\frac{P_{m\cdot din1}}{P_{\text{cri}}}=\frac{100}{47{,}06}=2{,}12$$

$$Z_1=0{,}84$$

Using the above prices and formulas, the well debit will be calculated as follow:

$$Q_1=\frac{C_1\cdot P_{m\cdot din}}{\sqrt{Z_1\cdot T\cdot\bar{\rho}}}=\frac{62{,}244\cdot 100}{\sqrt{0{,}84\cdot 315\cdot 0{,}06}}=\frac{6224{,}4}{13{,}2}=471{,}5T\cdot M^3/24h$$

Regime 2:

$T_{acou2}=\frac{T_{mou2}}{T_{\text{cri}}}=\frac{320}{209{,}16}=1{,}53$ $P_{acou2}=\frac{P_{m\cdot din2}}{P_{\text{cri}}}=\frac{120}{47{,}06}=2{,}55$

$$Z_2=0{,}82$$

$$Q_2=\frac{C_2\cdot P_{m\cdot din}}{\sqrt{Z_2\cdot T\cdot\bar{\rho}}}=\frac{46\cdot 120}{\sqrt{0{,}82\cdot 320\cdot 0{,}62}}=\frac{5520}{13{,}16}=419{,}45T\cdot M^3/24h$$

Regime 3:

$T_{acou3}=\frac{T_{mou3}}{T_{\text{cri}}}=\frac{321}{209{,}16}=1{,}53$ $P_{acou3}=\frac{P_{m\cdot din3}}{P_{\text{cri}}}=\frac{128}{47{,}06}=2{,}72$

$$Z_3=0{,}8$$

$$Q_3=\frac{C_3\cdot P_{m\cdot din}}{\sqrt{Z_3\cdot T\cdot\bar{\rho}}}=\frac{35{,}44\cdot 128}{\sqrt{0{,}82\cdot 321\cdot 0{,}66}}=\frac{4536.3}{13.18}=344{,}1T\cdot M^3/24h$$

Regime 4:

$T_{acou4}=\frac{T_{mou4}}{T_{\text{cri}}}=\frac{322}{209{,}16}=1{,}54$ $P_{acou4}=\frac{P_{m\cdot din4}}{P_{\text{cri}}}=\frac{145}{47{,}06}=3{,}08$

$$Z_4 = 0{,}8$$

$$Q_4 = \frac{C_4 \cdot P_{m\cdot din}}{\sqrt{Z_4 \cdot T \cdot \bar{\rho}}} = \frac{25{,}245 \cdot 145}{\sqrt{0{,}79 \cdot 322 \cdot 0{,}66}} = \frac{3660.5}{12{,}95} = 282.6T \cdot M^3/24h$$

Regime 5:

$\mathrm{T}_{acou5} = \frac{T_{mou5}}{T_{\mathrm{cri}}} = \frac{318}{209{,}16} = 1{,}52 \quad P_{acou5} = \frac{P_{m\cdot din5}}{P_{\mathrm{cri}}} = \frac{170}{47{,}06} = 3{,}6$

$$Z_5 = 0{,}78$$

$$Q_5 = \frac{C_5 \cdot P_{m\cdot din}}{\sqrt{Z_5 \cdot T \cdot \bar{\rho}}} = \frac{16{,}917 \cdot 170}{\sqrt{0{,}78 \cdot 318 \cdot 0{,}66}} = \frac{2875{,}89}{12{,}9579} = 255T \cdot M^3/24h$$

Calculation of bottom-well pressure P_w: For each gas regime, we determine the bottom-hole pressure P_w with the help of the following formula:

$$P_w = P_{m\cdot st} \cdot e^s$$

Here: $P_{(m\cdot st)}$ is static pressure on the back of the tubing, e, the base of the natural logarithm which is equal to 2.7182, and the price of S can be obtained from the following formula:

$$S = \frac{L_{av} \cdot \bar{\rho}}{T_{av} \cdot Z_{av}}$$

In this formula: L_{av} is the average depth of the well, $\bar{\rho}$ is the relative density, and T_{av} and Z_{av} are the average temperature and compressibility coefficient of the gas. The average temperature in the good column is obtained as follows:

$$T_{av} = \frac{\mathrm{T}_{lay} + \mathrm{T}_m}{2}$$

$$P_{av} = \frac{P_{lay} + P_w}{2} \ atm$$

In the above formula, the bottom well pressure value is not known, so its price is estimated to be higher than the static pressure.

Regime 1:

95+273=3680k $\quad T_{av} = \frac{\mathrm{T}_{lay}+\mathrm{T}_m}{2} = \frac{368+315}{2} = 341,5 \quad {}^0k$

$$T_{acou1} = \frac{T_{av}}{T_{cti}} = \frac{341{,}5}{209{,}16} = 1{,}63 \qquad T_{cri} = 209{,}16$$

$$P_{av} = \frac{105 + 113}{2} = 109 \qquad P_{cri1} = \frac{P_{av}}{P_{cri}} = \frac{109}{47{,}06} = 2{,}3$$

$Z_{av1} = 0{,}88$

$\frac{L_{av} \cdot \bar{\rho}}{T_{av} \cdot Z_{av}} = \frac{2500 \cdot 0{,}66}{341{,}5 \cdot 0.88} = 5{,}5 \qquad e_1^s = 1{,}2066$

$P_{w1} = P_{m \cdot st \cdot 1}. e_1^s = 100 \cdot 1{,}2066 = 126{,}7at.$

Regime 2:

$T_{av2} = \frac{368 + 320}{2} = 344 \qquad P_{av2} = \frac{125 + 133}{2} = 129$

$T_{acou2} = \frac{344}{209{,}116} 1{,}64 \qquad P_{acou2} = \frac{129}{47{,}06} = 2{,}74$

$Z_{av2} = 0{,}87$

$\frac{L_{av} \cdot \bar{\rho}}{T_{av} \cdot Z_{av}} = \frac{2500 \cdot 0{,}66}{344 \cdot 0.87} = 5{,}5 \quad e_2^s 1{,}2066$

$P_{w2} = P_{m \cdot st \cdot 2}. e_2^s = 125 \cdot 1{,}2066 = 150{,}8at.$

Regime 3:

$T_{av3} = \frac{368 + 321}{2} = 344{,}5 \qquad P_{av3} = \frac{138 + 146}{2} = 142$

$T_{acou3} = \frac{344{,}5}{209{,}16} = 1{,}65 \qquad P_{acou3} = \frac{141{,}5}{47{,}06} = 3$

$Z_{acou3} = 0{,}86$

$\frac{L_{av} \cdot \bar{\rho}}{T_{av} \cdot Z_{av}} = \frac{2500 \cdot 0{,}66}{344{,}5 \cdot 0.86} = 5{,}57 \quad e_3^s = 1{,}2107$

$P_{w3} = P_{m \cdot st \cdot 3} \cdot e_3^s = 138 \cdot 1{,}2107 \quad P_{Z3} = 167at$

Regime 4:

$T_{av4} = \frac{368 + 322}{2} = 345 \qquad P_{av4} = \frac{169 + 177}{2} = 173$

$T_{acou3} = \frac{345}{209{,}16} = 1{,}65 \qquad P_{acou3} = \frac{173}{47{,}06} = 3{,}67$

$Z_{acou4} = 0{,}86$

$\frac{\bar{\rho} \cdot L_{av}}{Z_{av4} \cdot T_{av4}} = \frac{0{,}66 \cdot 2500}{0{,}86 \cdot 344{,}5} = 5{,}56 \quad e_4^s = 1{,}2066$

$$P_{w4} = P_{m \cdot st \cdot 4}. e_4^s = 1{,}2066 \cdot 169 = 204at$$

Regime 5:

$$T_{av5} = \frac{368 + 318}{2} = 343 \qquad P_{av5} = \frac{175 + 183}{2} = 179$$

$$P_{acou5} = \frac{179}{47{,}06} = 3{,}8 \qquad T_{acou3} = \frac{343}{209{,}16} = 1{,}64$$

$$Z_{acou5} = 0{,}85$$

$$\frac{\bar{\rho} \cdot L_{av}}{T_{av5} \cdot Z_{av5}} = \frac{0{,}66 \cdot 2500}{343 \cdot 0{,}85} = 5{,}68 \qquad e_5^s = 1{,}2107$$

$$P_{w5} = P_{m \cdot st} \cdot e_5^s = 175 \cdot 1{,}2107 = 211{,}87at$$

4.2.Calculation of good pressure and flowrate parameters:

The function between good pressure and flow rate is: $f(Q) = P_{lay}^2 - P_w^2$. If the line for this function crosses the point where the two lines of the above graph intersect, the calculations are performed using the following formula: [8]

$$f(Q) = \frac{P_{lay}^2 - P_w^2}{Q}$$

If this line does not cross the intersection point of the above graph, then the next function is used for calculations:

$$f(Q) = \frac{P_{lay}^2 - P_w^2 - C}{Q}$$

1) $\frac{P_{lay1}^2 - P_{w1}^2}{Q_1} = \frac{262^2 - 126{,}7^2}{471{,}5} = 111{,}54$

2) $\frac{P_{lay2}^2 - P_{w2}^2}{Q_2} = \frac{262^2 - 150{,}8^2}{419.45} = 109{,}4$

3) $\frac{P_{lay3}^2 - P_{w3}^2}{Q_3} = \frac{262^2 - 167^2}{299{,}7} = 135{,}98$

4) $\frac{P_{lay4}^2 - P_{w4}^2}{Q_4} = \frac{262^2 - 204^2}{271{,}5} = 99{,}55$

5) $\frac{P_{lay5}^2 - P_{w5}^2}{Q_5} = \frac{262^2 - 211{,}87^2}{255} = 105{,}6$

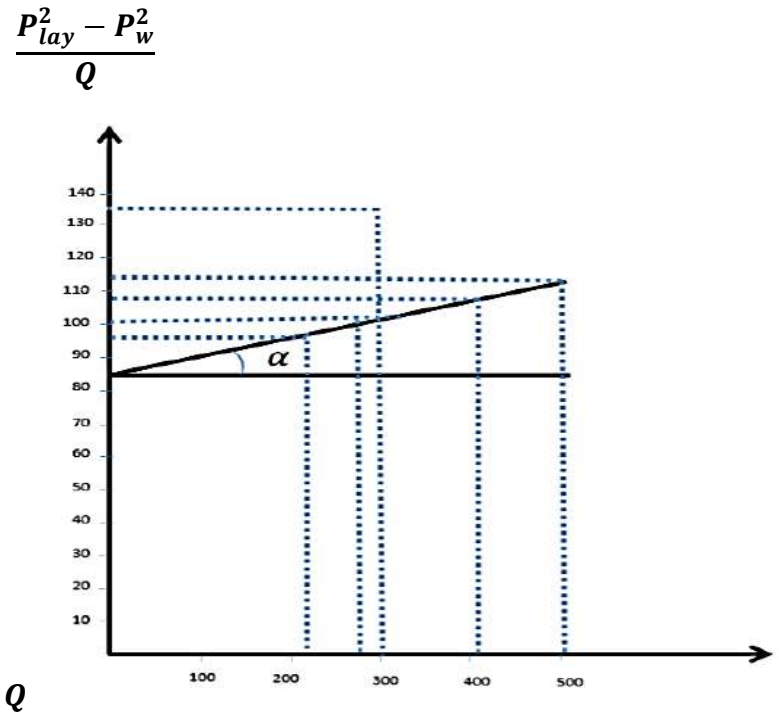

Figure 4: The graph determining the coefficients of filtration power

4.3. Assessment and Finalization of Gas Well Calculations:

The result of the parameters measured for well No. 3 of the Jurassic mines in the Khwaja Gogerdak gas field is illustrated in the figure above. Most of the points take place in a straight line. This status shows that the calculation was performed correctly. We connect the mentioned points and continue the resulting line to the intersection of the order axis. Finally, we will get the price for the coefficient (∝). [3]

$$t_g \propto = \mathrm{B} = \frac{\frac{P_{lay}^2 - P_w^2}{Q}}{Q} = \frac{111.54 - 84}{471.5} = 0{,}058$$

Factors A and B are coefficients of filtration resistance, which are created as a result of the movement of gas from the floor to the well. By placing the coefficients referred to in the gas flow from the reservoir rocks to the well, we obtain the following equation: [1] [3]

$$P_{lay}^2 - P_C^2 = AQ + \mathrm{B}Q^2 = 84Q + 0{,}058Q^2$$

Based on the figures calculated, the permeability coefficient for the stratum (K) is obtained with the following formula.

$$K = \frac{116 \cdot \mu_\Gamma \cdot Z \cdot P_0 \cdot T_{lay} \cdot \ln \frac{R_K}{R_w}}{\Pi \cdot \mathrm{A} \cdot h \cdot T_0}$$

Here: μ_Γ is the gas viscosity in centipoise, h is the stratum diameter on the meter, K is the permeability coefficient, R_K is the radius in meters, and R_C is the radius of the well in meters.

The coefficient of gas compressibility (Z) in productive interval conditions is equal to:

$$T_{acou} = \frac{T_{lay}}{T_{cri}} = \frac{368}{209{,}16} = 1{,}76$$

$$P_{acou} = \frac{P_{lay}}{P_{cri}} = \frac{318}{47{,}06} = 6.75$$

$$Z = 0{,}905$$

According to the above formula, the permeability coefficient is equal to:

$$K = \frac{116 \cdot \mu_\Gamma \cdot Z \cdot P_0 \cdot T_{lay} \cdot \ln \frac{R_K}{R_C}}{\Pi \cdot A \cdot h \cdot T_0} =$$

$$= \frac{116 \cdot 0{,}03 \cdot 0{,}905 \cdot 10^5 \cdot 368 \left(\ln \frac{375}{0{,}1}\right)}{3{,}14.84 \cdot 51 \cdot 273} = K = 0{,}70576 darcy$$

$$K = 0{,}70576\ darcy = 705.76\ m\ darcy$$

The permeability coefficient of the stratum indicates the movement of fluids in the stratum which varies from a few millidarcys to a few thousand millidarcys (mD). As much as the permeability factor of the stratum is high, the flow rate of the wells is also higher. [3]

$$A = 84\ \frac{KgF/cm^2 \cdot 24h}{1000m^3}$$

$$B = 0{,}058 \frac{KgF/cm^2 \cdot 24h}{1000m^3}$$

Free Debit: The absolute free debit is obtained by the following formula:

$$Q_{ab} = \frac{\sqrt{A^2 + 4B\left(P_{lay}^2 - 1\right)} - A}{2B}$$

$$Q_{ab} = \frac{\sqrt{84^2 + 4 \times 0.058(318^2 - 1)} - 84}{2 \times 0.058} = 781.8\ \times 10^3\ \frac{m^3}{day}$$

If the filtration of the production interval is done according to Darcy's Law and there are no barriers in the well. The free flow of the well is equal to $781.8 \times 10^3 \frac{m^3}{day}$.

The maximum allowable flow rate of the well is the favorable well flow rate which indicates the proper production regime where gas production is constant and with no complications. The favorable well discharge is determined by the following formula: [1]

$$q = \frac{-A + \sqrt{A^2 + 4B.\Delta P\left(2P_{lay} - \Delta P\right)}}{2B}$$

$$q = \frac{-84 + \sqrt{84^2 + 4 \times 0.058 \times 54(2 \times 318 - 54)}}{2 \times 0.058}$$

$$q = 308.4 \times 10^3 \frac{m^3}{day}$$

The favorable flow rate of gas is: $308.4\times 10^3 \frac{m^3}{day}$. By choosing this amount of flow rate, we can avoid the following problems: the destruction of the productive interval, corrosion of installed columns and production pipes, gas entrapment at the production interval, and the formation of water tabs. [7]

$$P_{lay}^2 - P_w^2 = \mathrm{A}Q + \mathrm{B}Q^2 = 84Q + 0{,}058Q^2$$

$$P_{lay}^2 - P_w^2 = 84(308.4) + 0{,}058(308.4)^2$$

$$P_w = 264.0\ atm$$

The bottom pressure of a well is gained 54 atmospheres, which is less than the pressure of the productive layer. The reason for the pressure reduction at the bottom of the well is related to the permeability coefficient of the production interval and its porosity. Based on the calculations of the gas flow rate equation, the favorable flow rate from the well was found to be appropriate. The calculated price for the well bottom pressure corresponds perfectly to the real price obtained by experience.

5. Results and Discussion

After analysis of the data, the physical and chemical properties of the hydrodynamic gas, and study of the geology of the minefield of a good number (3) from the Jurassic mine in the Khwaja Gogerdak mining field, the following results have been achieved:

1. The appropriate flow rate for gas extraction is determined by defining the following parameters: gas compression coefficient, maximum gas flow rate, the quantity of pressure at the head and bottom of the well, and quantity of dynamic and static pressure in the wellhead in different extraction regimes.

2. Using the function graph $f(Q) = \frac{P_{lay}^2 - P_w^2}{Q}$ the filtration resistance factors are obtained (A=84, and B=0.058) which are created when the gases are filtered through the production layer.
3. Based on the calculations, the permeability coefficient of the productive layer is obtained at 705.76 mD(millidarcy)
4. The total daily production of the Jurassic reservoir rocks in the Khwaja Gogerdak gas field is calculated (at $781.8 \times 10^3 \frac{m^3}{day}$), which is the highest flow rate for a gas well.
5. The maximum permissible discharge from well No (3) in the Khwaja Gogerdak mining field is $308.4 \times 10^3 \frac{m^3}{day}$. If the flow rate and pressure difference of this well is adjusted based on our calculations, the gasification coefficient of the production layer will be much higher.
6. The gas should only be extracted via tubing pipes, and the diameter of these pipes should be chosen in which the gas velocity in the wellhead should be received at approximately (10m/s), otherwise, the industrial equipment will rust.
7. To avoid rust in the good casing and other equipment, the inhibitor needs to be pumped at the production interval.

A series of calculations are carried out using data obtained from the test of wells No. 3, 41, and 43 from the Khwaja Gogerdak minefield, using different choke diameters. Finally, the wells debit, the pressure of the wells head and bottom, and the value of the function $\frac{P_{lay}^2 - P_w^2}{Q}$) are obtained which are listed in Tables 2 and 3.

Table 2: Basic parameters of gas exploitation

$\frac{P_{lay}^2 - P_w^2}{Q}$	Gas debit 1000 $M^3/24h$	Downhole (Well bottom) pressure Atm	Protective layer pressure Atm	Choke diameter Millimeter	Regime number
111.54	471.5	126.7	318	19.05	1
109.4	419.45	150.8	318	15.85	2
135.98	344.1	167	318	12.7	3
99.55	282.6	204	318	11.13	4
105.6	255	211.87	318	9.51	5

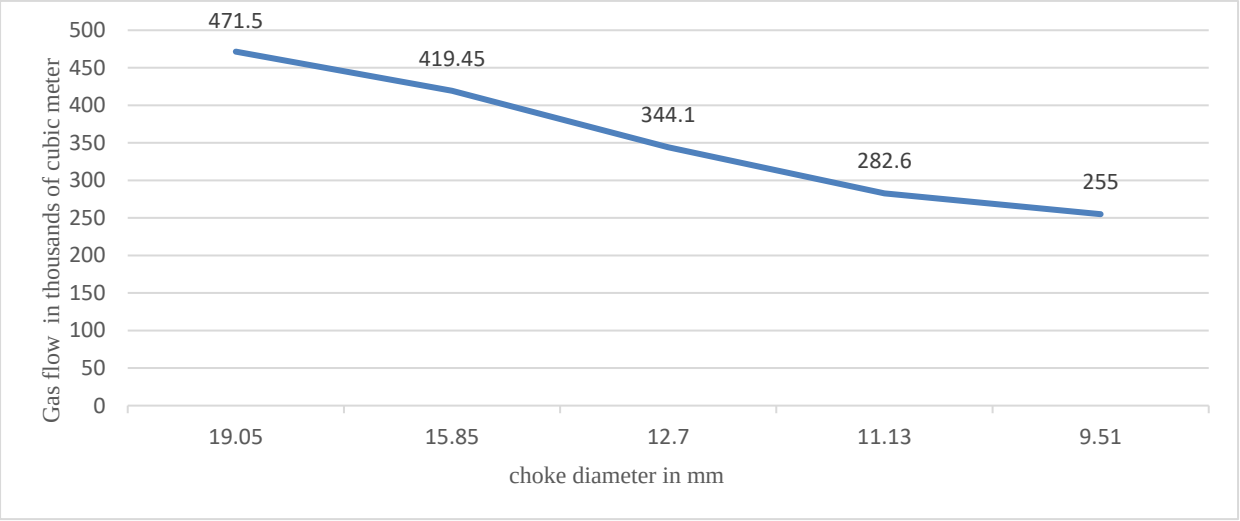

Figure 5: Gas flow graph according to chokes diameters

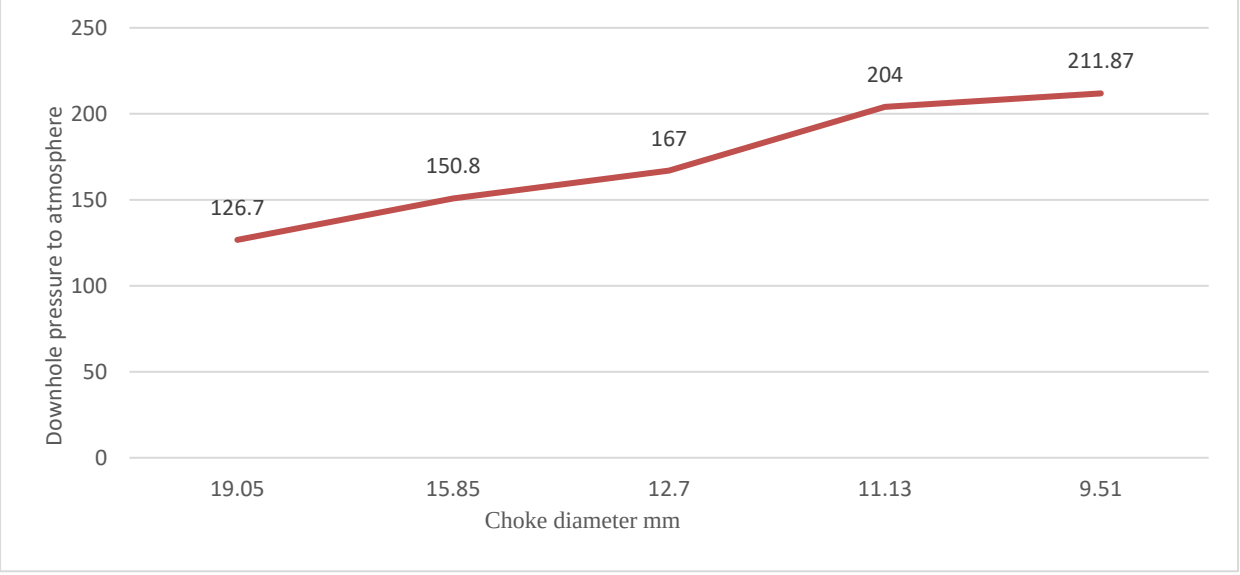

Figure 6: Well bottom pressure graph in different chock diameters.

Based on the above descriptions and results, the following can be suggested:

1. Gas reserves should be calculated through pressure reduction.
2. The acidification of the calcareous production layer is suggested at the beginning of the exploitation process to increase the flow rate.
3. To pump special anti-rust materials (inhibitors), a special valve must be installed at the bottom of the tubing.
4. Anti-rust materials (inhibitors) must be continuously injected into the well at the back of the pipes.

5. The chemical composition of the Jurassic production layer gas of the Khwaja Gogerdak gas field is very different from that of the Heterevien production layer gas. In this regard, gas extraction should be arranged in separate tubes and transferred to the gas collection points of the Yatim Taq gas field.
6. The packers must be used when installing tubing to separate the two different production intervals from each other.

Table 3: Baic parameters of gas exploitation of well No. 3, Khwaja Gogerdak Mining field

Regime number	$\frac{P_{lay}^2 - P_C^2}{Q}$	The pressure of the bottom of the well (PZ)				Well debit		
		Z_{av}	$\frac{\bar{\rho} \cdot L_{av}}{Z_{av} \cdot T_{av}}$	e^S	Downhole pressure P_W	Coefficient C	Coefficient Z	Well debit $1000M^3/24h$
1	111,54	0,88	5,5	1,2066	126,7	62,244	0,84	471,5
2	109,44	0,87	5,5	1,2066	150,8	46	0,82	419,45
3	135,98	0,86	5,57	1,2107	167	30,44	0,8	299,7
4	99,55	0,86	5,56	1,2066	204	24,245	0,79	271,5
5	105,6	0,85	5,68	1,2107	211,8	16,917	0,78	225

7. Conclusion

Based on data on the upper Jurassic layer in the Khwaja Gogerdak field, and the findings highlighted in this research paper, the following conclusions are drawn:

1. The Jurassic production layer gas in the Khwaja Gogerdak mining field is composed of 3.2% hydrogen sulfide and 7% carbon dioxide. The presence of these gases causes the production equipment to rust at high pressure and temperature, increasing expenses.
2. The good flow rate should be adjusted to $308.4 \times 10^3 \frac{m^3}{day}$ following the technological regime defined for the production of wells.
3. Stainless steel casing must be installed into the well during drilling and completion to avoid rust.
4. During operation, inhibitors must be pumped into the production interval to prevent rust.
5. Special valves for pumping inhibitors into the well shall be installed in the stainless steel tubing with the S-75 marking.

Reference

[1] H. Devold, An introduction to oil and Gas production, transport, refining and petrochemical industry, Oslo, 2013, p. 152.

[2] B. Guo, Petroleum production engineering, a computer-assisted approach, Elsev, 2011.

[3] Byars, H.G; corrosion control in petroleum production (pp. 29-30), Houston : TX: NACE International, 1999.

[4] Mehrad, A.T; Zvolinski, V.P; Kapralova, D.O; Niazmand, M.A; "Assessment of oil and gas resources of northern Afghanistan and their impact on energy security in the country," *IOP Conference Series: Materials Science and Engineering(Vol. 976, No. 1, P. 012038),* no. IOP Publishing, 2020 December.

[5] Carroll, J; Natural gas hydrates: a guide for engineers., Gulf Professional Publishing, 2020.

[6] W. Lyons, Working guide to petroleum and natural gas production engineering, Gulf professional publishing, 2009.

[7] M. Zemenkova, Y. Zemenkov, A. Pimnev, and E. Kurushina, "System of controlling the reliability of hydraulic machinery in oil and gas facilities," *In IOP Conference Series: Materials Science and Engineering (Vol. 127, No. 1, p. 012055),* no. IOP Publishing, 2016 April.

[8] D. Green and G. Willhite, Enhanced oil recovery, 2018.

[9] "recovery of different types of oil in Petroleum reservoirs," *Proc. Schl. Eng. Tokai Univ.,,* Vols. pp 53-58, no. ser, p. E41.

[10] N. Malik, "Energy resources in Afghanistan and measures to improve for sustainable development," *Journal of Sustainable Energy,* 2011.

Authors Profile:

Sadaf Jalal received a BSc degree in Oil and Gas Mines Engineering Department from Kabul Polytechnic University in 2010 and completed his MSc degree in Geological Engineering and Exploration of mines in 2018. Presently, she is working as Assist. Prof. in the Department of Oil and Gas mines Engineering, Kabul Polytechnic University, Kabul Afghanistan. His areas of research include Petroleum production and fluid mechanic

Mohammad Walid Omid received a B.Sc. degree in Oil and Gas Mines Engineering from Kabul Polytechnic University in 2014, and MTech (Master of Technology) degrees in Earth Sciences with a specialization in Petroleum Geoscience from the Indian Institute of Technology Bombay (IIT Bombay), Mumbai, India in 2020. He is working as an Assist. Prof. at the Department of Oil and Gas Mines Engineering, Geology and Mines Faculty, Kabul Polytechnic University, Kabul Afghanistan. His field of research includes Active Tectonics, Geology, Geophysics, Remote Sensing, and GIS.

Abdul Shukoor Dawar completed his B.S. and M.S. degrees in Oil and Gas Mines Engineering Department from Kabul Polytechnic University in 1986. Presently, He is a Professor in the Department of Oil and Gas mines Engineering, at Kabul Polytechnic University, Kabul Afghanistan. His field of research is Oil and Gas well drilling and Oil and Gas Well Testing and completion.

KPU International Journal of Engineering & Technology
Volume 2, Issue2, Dec. 2022
e-ISSN:2790-0819, p-ISSN:2790-0800
Date Received: 2022-10-06.
Date Accepted: 2022-12-20
Date Published: 2022-12-30.

Landslide and Rockfall Susceptibility Mapping in Kabul-Jalalabad Road by Analytic Hierarchy Process (AHP) & Weighted Overly Mapping (WOM) Method in GIS

KHAIRUDDIN RASIKH [1*], ZAFAR KHAN SAEEDI [2]

[1*] Teaching Assistant, Department of Geology and Mine, Science Faculty, Nangarhar University, Daronta, Afghanistan. Email: 77rasikh@gmail.com

[2] Teaching Assistant, Department of Geology and Mine, Science Faculty, Nangarhar University, Daronta, Afghanistan. Email: eng.zafar91@gmail.com

Abstract

Landside and Rock falls are known as the most destructive natural hazards that threaten the inviolability of Human communities and infrastructures such as houses, Dames, Tunnels, Roads, etc. Roads in the mountainous area are known more vulnerable because of different factors like route cute disturbing and mass imbalances. Kabul-Jalalabad highway is a major part of Afghanistan's transitional route that connects the central regions to the eastern part of the country. The transportation system of this route is threatened by mass movement and rockfall events. This *study used nine conditional factors including slope, lithology, (TWI), road distances, LU/LC, Curvatures, slope direction (aspect), precipitation, and fault distance. two modules (Analytic hierarchical process (AHP) and Weighted overly mapping (WOM)) are used in this study, Finally, the Landslide Susceptibility Map(LSM) of both modules is Classified into five zones(very high, high, moderate, low and very low) of susceptibility in Arc GIS 10.8; after pairwise comparison in spice-logic 4.1.4 software; slope, lithology, slope direction, precipitation, and fault distance respectively identified as effective factors in landslides and rock fall susceptibility, final (LSM) of both methods shows that high and very high levels sensitivity zones Covers 21.35%, 8.43% for AHP and 40.16%, 10.72% for WOM modules respectively, Accuracy assessment of both module done based on 101 locational denoted landslides, (ROC) curve and AUC index are used to classifiers accuracy evaluation; finally AHP module known as much better than (WOM) one because of its (AUC) value that shows 0.923(Excellent) greater than 0.845(very good) (AUC) index of (WOM) module.*

Keywords: Landslide, rock fall, susceptibility, AHP, WOM, Kabul-Jalalabad highway, ROC.

[*] Corresponding Author

1. Introduction

Landslides and rock falls are known as one of the most common Natural hazards that threaten human civilization and welfare in many parts of the world.[1]. These phenomena are defined as mass (soil and rocks) movement in an unstable condition which often led massive damage to humanity as much as economic loss, financial cries even injuries or Causalities [2]. In human civilization, roads are one of the most important infrastructures which bring facilities for transportation and as well as economic trades that play a great role in the welfare of society, economic growth, and development of communities. The financial budget spent for the construction of roads in different geographical locations depends on the variety of environmental, climatic, and other natural conditions that requires for its construction, as well as its maintenance and safety. At the same time, the majority of landslides occur along the roads [3].it means protection of this national capital is necessary for the long-term suitable use of them.

Kabul-Jalalabad highway is one of the busiest and most important routes in Afghanistan; this route is characterized by a large exposure to slope instabilities and landslides, rock fall threatening roads according to climatic and physiographic conditions. The dominant topographic features result from active tectonic events; they are mainly high in its western parts and extend to, depressions, and deep valleys in the central (Laghman province) and eastern (Nangarhar province) parts. Landslide susceptibility mapping is a novel attempt in Afghanistan; it can be used as an efficient tool that gives additional efforts in landslide mitigation in a different part of the country. This phenomenon also causes a lot of damage and many problems, and along with that, that increases the cost of road construction, the cost of maintenance, repairs, and reconstruction, meanwhile such unexpected accidents disrupt transportation and increase traffic risks; therefore Identifying the effective factors in the occurrence of landslides in an area and zoning its risk is one of the basic tools to achieve solutions to control this phenomenon and select the most appropriate and practical option.

Landslide and rockfall mitigation are one of the contemporary attempts in the survey, construction, and maintenance of roads, and its potential susceptibility mapping is accomplished by different methods all across the world. Landslide susceptibility methods and modules are developed by researchers and experimented accord to various conditions in different parts and points of the earth; one of the much more sophisticated and more advised modules for different natural hazards mitigating like flood hazard and areal potential sensitivity evaluating method that based on probabilistic approach is analytic hierarchy process (AHP) that widely used and experimented at different causes by researchers like C Other methods have also been recommended and used including the

frequency ratio logistic Regression (LR)by researchers like [4,5] and weights of evidence (WoE) used by [6,7].

This study aimed to provide and develop a probabilistic-based approach that was completed on landslide and rock fall susceptibility assessment along the Kabul- Jalalabad highway by applying two methods. The first one is the analytic hierarchy process which is a multi-parametric method that was originally developed [7]. The second one is Completely GIS-based methods that call weighted overly mapping (WOM) algorithms, that widely used by many researchers all across the world and produce landslide susceptibility maps in a quite unpretentious manner [8,9,10].

2. Geographic and Natural Characteristics of Rout of interest (ROI)

The studied route was the Kabul-Jalalabad highway. This highway with a length of 104 km was put into operation in 2010. A large part of the route passes through mountainous areas with a narrow structure and is located in parts close and parallel to the Kabul and Alingar rivers. Often the road is built as a trench in the heart of the mountain and in some places, it is accompanied by tunnels and passes over embankments or bridges at the valley's intersection points. The project starts from the center of Kabul city, crosses the Mahipar and its heights, and faces the soroby plains. Crossing the vicinity of Daronta Dam, it leads to Jalalabad city. The highest height of the studied route is 2514.76 meters above sea level.

The western part of the road specified with high elevation, steep slope, and mountainous physiography mainly surrounded by different types of sedimentary (polyester calcites and Dolomites, conglomerate, etc.) and highly jointed and fractured metamorphic and igneous (schist, Gneiss, marble, Amphibolite, Granite Diorite, etc.) Rocks. At the area near the soroby suburb area of Kabul, this road passes from hill shaped and relatively plate area containing Cenozoic Clastic sedimentary rocks. After that road extends to a valley continued parallel to the Kabul river, which is familiarly known by the name of Silk valley, that is characterized by a steep slope and highly faulted and fractured metamorphic and igneous rocks that end in the patented area mainly composed by sedimentary fasces.

The studying portions of the road end at approximately 1 km extended with a steep slope and unstable state jointed Granodioritic rocks which causes rock fall events often more.

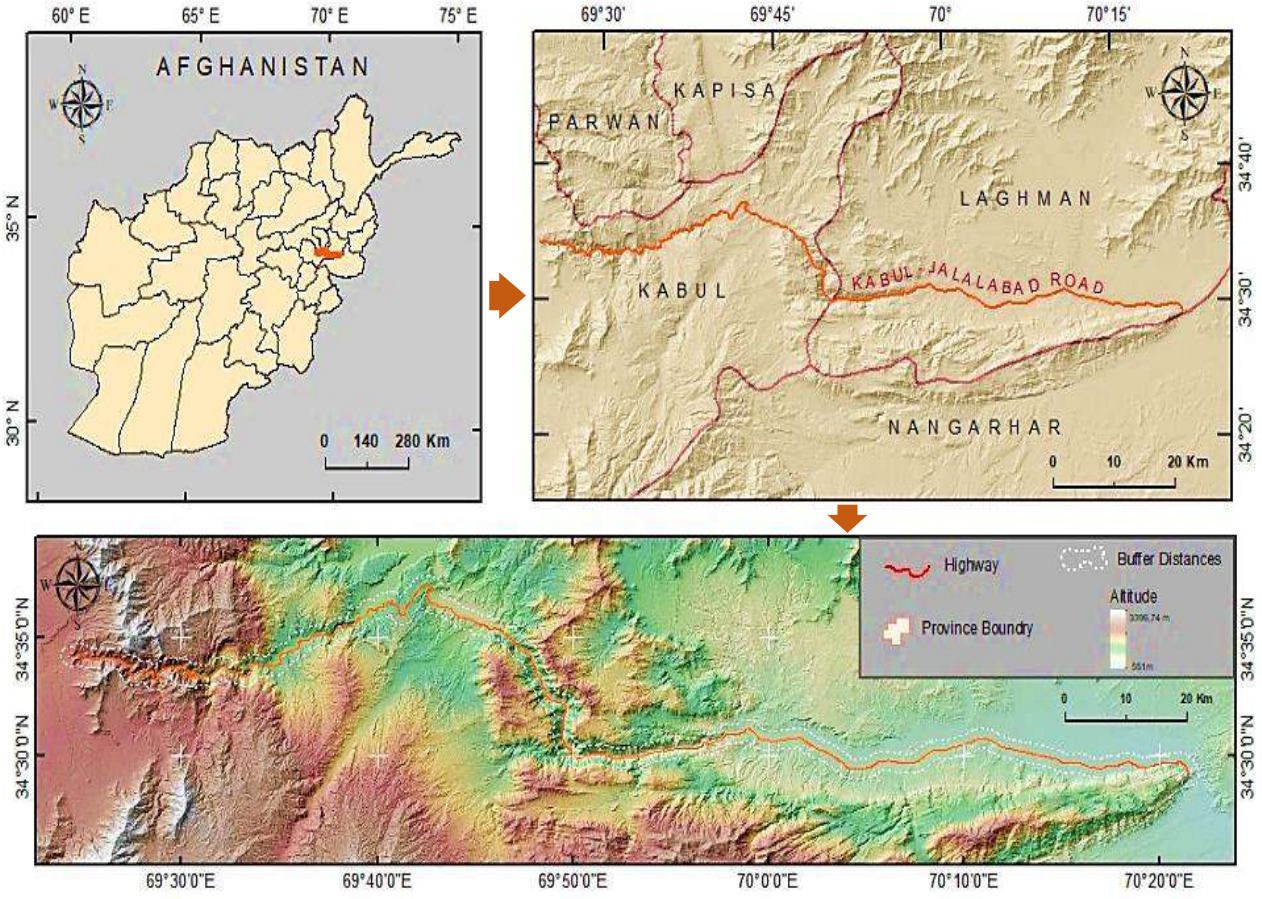

Fig. 1: Map of studying Road.

The eastern point of the road is ended at the Daronta subarea of Jalalabad city. Due to the difference in height, which can be seen in the studied route, from (586m) to (2514.76m) with different climatic varieties. As in the western parts of this route, the rainfall amount and temperature are relatively high than the temperature during the year in the eastern regions. The beginning of the route has a latitude of 34˚ 34′ 02″ North and a longitude of 64˚ 24′ 17″ East, and the end of the route passes through the latitude of 34˚ 29′ 08″ north and a longitude of 71˚ 21′ 34″ east (Fig.1).

3. Materials and Methods

Landslide is the result of static imbalances, especially in man-made disrupted areas. The stability of slopes is controlled by various natural and human interrupting factors. Recognition of these factors is so important for determining the affecting causes of the occurrence of landslides [9]. Therefore, in the first stage, spatial information was collected, according to a similar previously conducted Approaches, based on reviewed

literature at all (9) factors are considered for preparing a landslide sensitivity map in the area the selected factors including the type of lithology, land use, and Land cover, road distances, faults distance, Curvatures, topographic wetness index (TWI), precipitation, aspect (Slope direction), which described respectively as follows and concluded in the table (1).

3.1.Lithology:

The lithology is the most important factor in the analysis of natural hazards and many morphological features of lands and land surface characteristics depend on its type [10]. The lithological information used in this research was extracted from the 1: 100000 scale map of Afghanistan lithology shape file and after experimental interpretation, classified in to (6) classes as Class_1, 2 ,3 ,4,5,6 which Categorized respectively like ;Class_1(Mica, biotite, biotite-amphibole, garnet-biotite, garnet-sillimanite-biotite, pyroxene-amphibole gneiss, plagiogneiss, and schist, migmatite, quartzite, marble, amphibolite; Class_2 (Limestone, dolomite, marl, Mica, biotite, biotite-amphibole, and garnet-biotite gneiss, plagiogneiss, migmatite, quartzite, marble, amphibolite, Granodiorite, Alas kite, Granosyenite, Granite, Granite), Class_3 (Limestone, marble, quartzite, metasandstone, mica chist), Class_4 (Dunite, Peridotite, Serpentinite Limestone, dolomite, marl, conglomerate, sandstone, siltstone, shale, bauxite and bauxite-bearing rocks Sandstone, siltstone, mudstone, carbonaceous shale marl, conglomerate, weathered acid and mafic volcanic rocks), Class_5 (Gray conglomerate, gravel stone, sandstone, siltstone, clay, limestone, marl, gypsum, salt, acid and mafic volcanic rocks Shale, phyllite, mafic volcanic rocks, limestone), Class_6 (Conglomerate, shingly sediments, gravel, sand, siltstone, breccia, limestone, gypsum, clay, loam; andesite, dacite and their tuffs (Dashtinovar Group); phonolite and soevite) which thematically Spatial extend shown in (Fig.2b) and table (2 & 5).

3.2. Tectonic Fault distances:

The fault distance layer from tectonic failures is also considered one of the potential factors for landslide occurrence and mass movement phenomenon. This issue is considered significant because of its localization in a new and relatively active tectonic setting of Afghanistan which is characterized as areas with strong topographical relief, which know as a result of continuous fractures in this route and the erosion of the Kabul River. Tectonic liniments were extracted from the 1:100,000 tectonic map of Afghanistan and after the essential correction Zoned in 5 Buffering distances as shown in, Table (5) and (Fig .2d).

3.3.Land cover and land use

(Lc/Lu: Land use and land cover (Lc/Lu) are crucial factors in the occurrence of landslides because they considerable impact on slope stability [11]. The importance of this component is determined by the amount of rainfall and the slope of the ground. Landslides are more likely to occur naturally in areas with steep slopes, moderate vegetation, and heavy rainfall [12]. ; land use and land cover map along the studded route was taken from a 1: 100000 scale Shapefile of Afghanistan's land cover map, which was divided into five Classes as Class_1 (Guardian and fruit trees,) Class_2 (Plate irrigational and Cultivation area), Class_3 (Marshland Permanently inundated lands), Class_4 (Rangeland) and Class_5 which contain Rock Outcrop and Bare Soil that represented in (Fig. 2c) and table (5).

3.4.Slope:

The slope has an essential role in controlling material slippage by increasing the Slope angle, the instability of materials (soil and rock) also increases. To extract this variable DEM data with a spatial resolution of (30m*30m) was used and its thematic map was provided by the use of the Slope algorithm under the Spatial Analysis tools of ArcGIS10.8 program. The slope of the study area varies from (0) degrees to (>72.4) degrees and was classified into (5) equal interval-based division Classes as shown in table (5) and (Fig.2g) .This factor is considered as one of the most important indicators in the study of hazards and natural processes (landslides, rock fall, soil erosion, groundwater potentiality detection, location of agricultural areas, etc.).For landslide risk zoning slope used widely by researchers like [12, 13] that Slope factor has been considered the most important one.

3.5.Aspect:

Aspect or slope direction is also considered a very important factor in the analysis of environmental hazards and the preparation of landslide susceptibility maps [13, 14]. which controls the amount of humidity and diversity of vegetation with the proportional absorption of light and solar energy [15] aspect classification is done in ArcGIS 10.8 software environment by using a Digital elevation model (DEM) (with a cell size of 30m x 30m) table (1) which used for other factors like Slope and curvature, Aspect of studying road classified into five Classes (Plate area, North, East, south, and west) as mentioned in Table (5) and (Fig. 2f) thematic layer.

3.6.Topographic Curvature:

The Topographic Curvature provides influential information about the land surface stability its role in landslides is its ability to concentrate and disperse surface water currents, which therefore plays a key role in water infiltrations and their extent [16]. The Topographic Curvature is the convexity and concavity of a surface using consecutive topographic distances, this factor is produced in Arc GIS10.8 by the use of DEM data with similar resolution as slope and aspect, Curvatures done by the Curvature algorithm of Spatial Analyze tools, Curvature values vary from (-22.3 to +22.4) so that the positive values represent a convex and the negative values concaves and areas with zero values shows flat areas this variable were classified into 3 Classes based on the above characteristics. (Fig 2e).

3.7.Topographic wetness Index (TWI):

This index is one of the important factors in landslide risk assessment analyses. TWI is introduced by Beven and Kirkby [17] and is considered in most landslide research. The topographic wetness index is defined by (Eq.1).

$$TWI = \ln\left(\frac{S}{tan \propto}\right) \qquad \text{(Eq. 1)}$$

Where, S; is the specific area of the water basin, α; is the Slope of the area. This index was analyzed using (30m*30m) resolution DEM data in the ArcGIS10.8 program, and values vary from (3.75 to 24.3) and classified into 4 classes with manual intervals as shown in Table. (5).and (Fig. 2h).

3.8.Annual precipitation:

rainfall is the most important factor in natural disaster assessment such as landslides, rock Falls, mass movements, vegetation varieties and distribution, plant type and density, lithology (type of rocks), and know one of the most important factors in landslide occurrences, it is considered that it would be wrong to address issues such as landslides without considering it. The role of rainfall is mentioned in the works of [18,19] specified as an important and effective factor, which is more diagnostic and important. The average rainfall information of the study area, after being found from the site [20] and then interpolated with IDW method converted to Raster format, which shows the difference between the average rainfall in the study area from (572.01 to 701.17) mm/year, which was classified into 4 classes by manually interval manner in Arc GIS 10.8 as mentioned in Table (5) and (Fig. 2a).

3.9.Road distances:

The road distance is one of the most important human interrupt factors of natural hazards that leads to the instability of the slopes and leads to slipping and crawling of the slopes, which is due to the extension of the road from high to low slopes due to disturbance of the static balance of areas, and vibrations caused by crossing heavy vehicles and trucks which considered as a potential cause of landslides; The distance from the road factor can be mentioned in the works [21]. The road used in this study includes the main portion of (Kabul-Jalalabad road) which after its geometric correction by equidistance's algorithm under the Spatial Analysis tools road distance zoned in <150m,(150-300)m, (300-450)m,(450-600)m,(600-750)m that mentioned in Table (5) and (Fig. 2i).

Table 1: Data sources and their resolutions.

Data type	Sours	Scale / Resolution
Lithology	Afghanistan Geology Map Shapefile from. USGS spatial Data catalog.	1:100000
Land use and land cover	Afghanistan Geology Map Shapefile from. USGS spatial Data catalog.	1:100000
Fault distances	Afghanistan Geology Map Shapefile from. USGS spatial Data catalog.	1:100000
Road distances	Extracted on Google earth.	
Precipitation	https://pps.gsfc.nasa.gov	
Slope	Based on DEM data received from the Earth Explorer site.	30m*30m
Aspect		
Curvatures		
Topographic wetness index (TWI)		

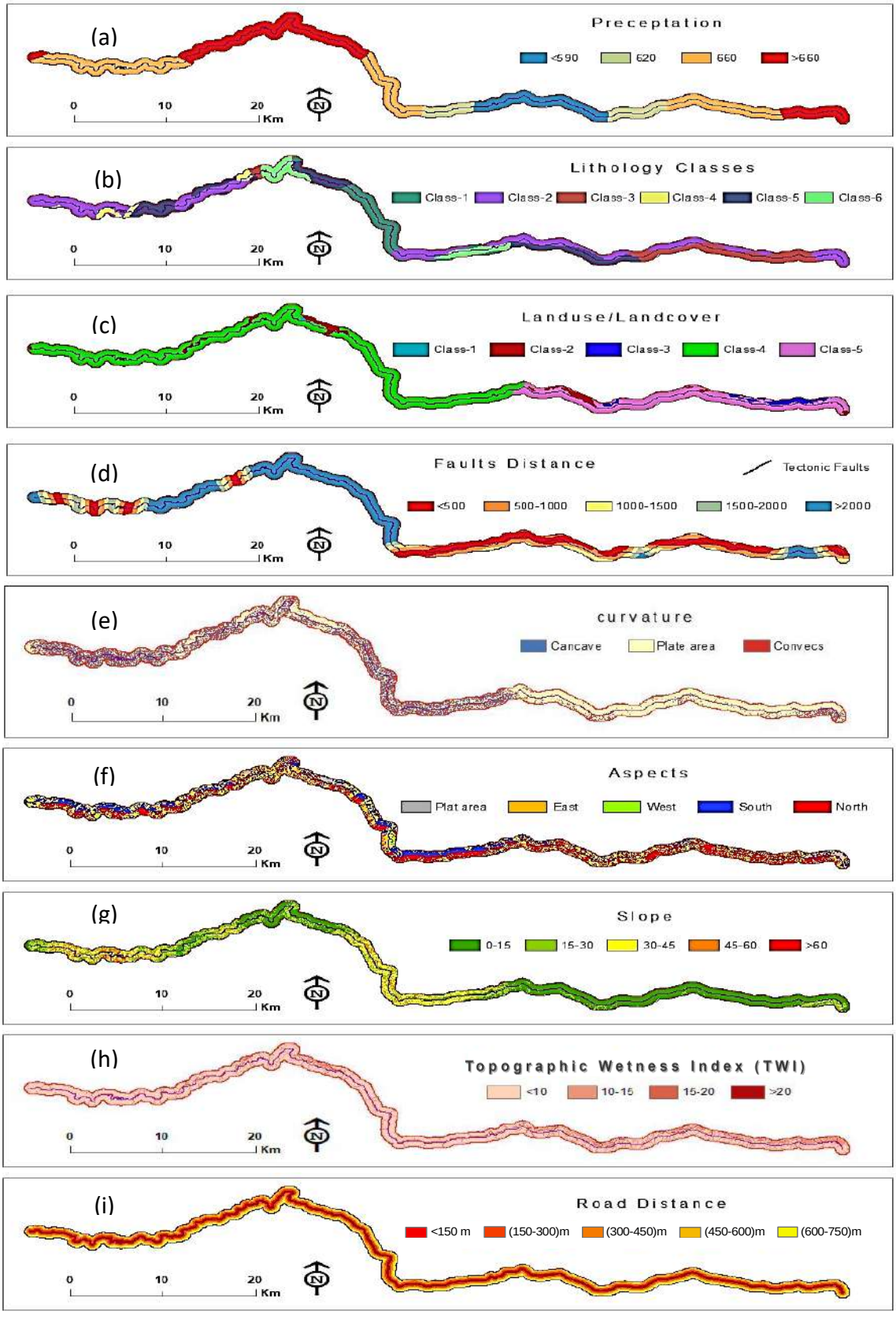

Fig. 2: Classified thematic map of all criteria; (a) precipitation, (b) Lithology, (c) Land cover and Land use, (d) Fault distance. (e) General Curvature, (f) Slope Aspect, (g) Slope (h) Topographic Wetness Index (TWI), (i) Road distances.

4. Methodology

A natural disaster like landslides, flood hazards, and rock falls Susceptibility analysis depends on several factors, identifying the influence role of factors that affect the occurrence of such a natural disaster is the first essential step to their assessments. In this study, to receive the most influential factors and phenomenon, by reviewing the necessary sources and references, formal and valuable information bases such as Afghanistan Natural Disaster Management (ANDM), land transport service departments, and scientific sources of landslide information were collected.

To enrich the spatial information sources, landslides, and rock fall along the studied route field visits and interviews with professionals and people living in the nearby area of the study route have been done and all this information is stored in a suitable database stored in a GIS environment. to identify the role of influence factor of landslide, referred to similar works of researches through Google Scholar, research gate, Science direct, and after receiving information and selecting the decision-making method and identifying the facility of ArcGIS to weight overly mapping (WOM) after all over special judgment carried out in Arc GIS 10.8 and also used analysis hierarchy Process (AHP) method. After analyzing the role of risk factors for landslides and rock falls susceptibility along the Kabul-Jalalabad route in the GIS environment, spatial analysis was performed with

Table 2: Pairwise Comparison table of main factors.

	(X1)	(X2)	(X3)	(X4)	(X5)	(X6)	(X7)	(X8)	(X9)	Weight
Lithology(X1)	1	1/2	5	3	5	3	5	5	1/2	**0.191**
Slope(X2)	2	1	7	5	3	3	5	6	2	**0.276**
land cover(X3)	1/5	1/7	1	1/3	1/2	2	2	3	1/3	**0.056**
Precipitation(X4)	1/3	1/5	3	1	4	2	3	2	1/2	**0.106**
Fault distances(X5)	1/5	1/3	2	1/4	1	2	2	2	1/2	**0.069**
Road distances(X6)	1/3	1/3	1/2	1/2	1/2	1	2	2	1/4	**0.052**
TWI(X7)	1/5	1/5	1/2	1/3	1/2	1/2	1	1/3	1/6	**0.030**
Curvatures(X8)	1/5	1/6	1/3	1/2	1/2	1/2	3	1	1/4	**0.040**
Aspects(X9)	2	1/2	3	2	2	4	6	4	1	**0.181**
* Consistency Ratio	0.066									

overlay and Raster calculator function of spatial analysis tools; overall configuration and essential steps of this research are shown in (Fig .3).

Form of this study is divided into three main stages; First stage is defining the length and wide range of the studding route in this case long portion of the Kabul-Jalalabad road is considered as long as 104 km and buffered by 750m for each side road's center line second stage is the selection of criteria and sub-criteria that have influence role on the occurrence of landslides and rock falls. In the third stage, the pairwise comparison is done based on the analytic hierarchy process (AHP) due to more flexibility and facilitates The spice-logic 4.1.4 software is used to extract the weight of criteria and in the third stage weight of all criteria and sub-criteria defined for their relevant thematic layers, finally according to (Eq.7) AHP method defined to graphic form of statistic representation and spatial distribution.

4.1. AHP Method

The analytic hierarchy process (AHP) is a method for prioritizing criteria that extracts scaled weight of influence factors through the expert judgment of the problem and pairwise judgment of criteria and sub-criteria [21].

This module uses in hierarchically organized decision-making issues that contain a limited number of elements at different levels [22] (Fig.3). The hierarchical structure measures and combines different factors in complex decision-making processes and simplifies the combination of different components of factors into a common whole matrix of rational values [23].

AHP is considered a decision-making and forecasting method that plays the role of decision factors and criteria in terms of the factors that affect it, which can be used if the decision hierarchy is defined [24]. In performing pairwise comparisons, factors (criteria) preference intensity assessment or relative importance which extract after pairwise comparison by numerical values scaled from 0 to 9 (Table .3)

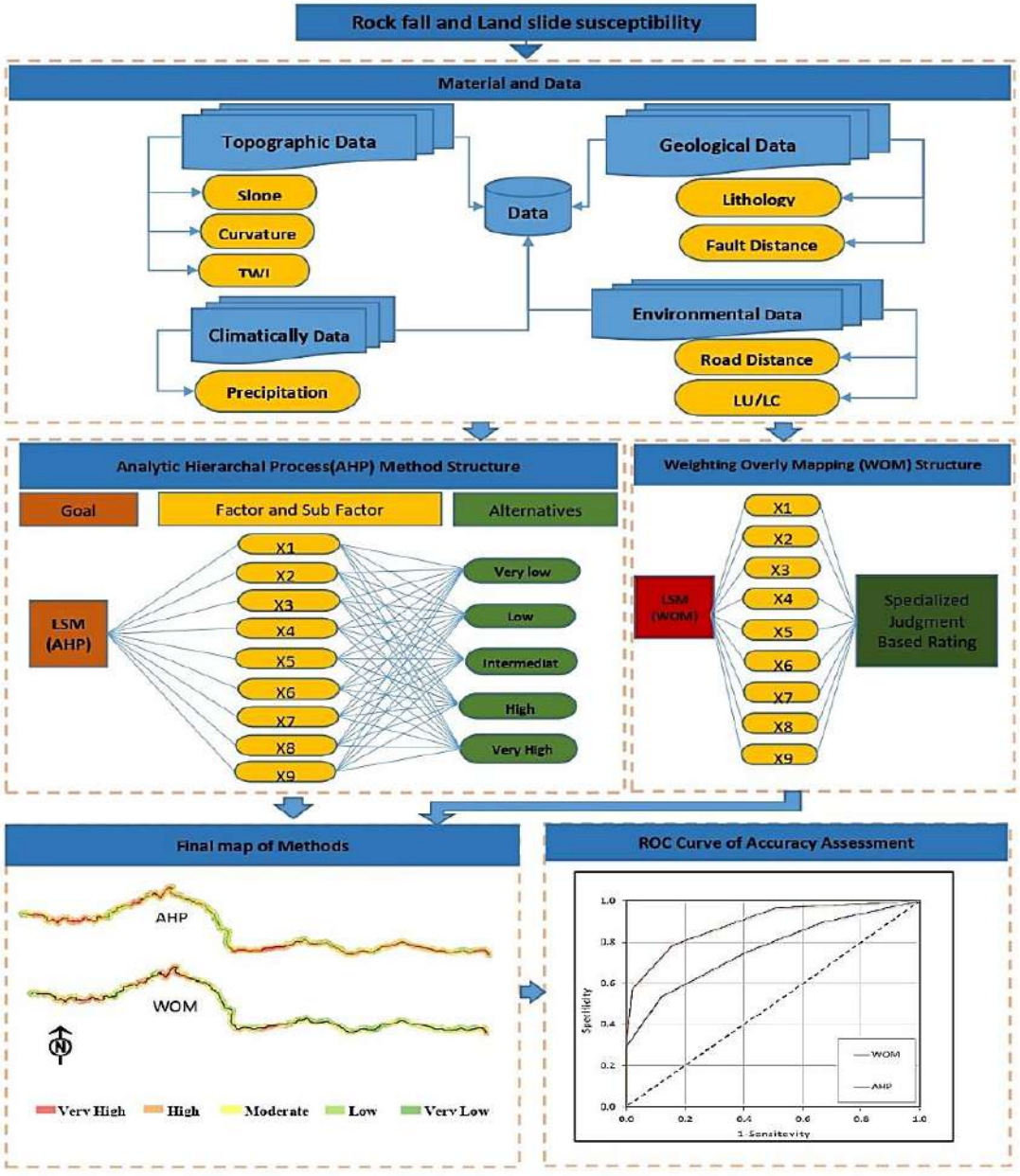

Fig. 3: Flow chart and essential steps of conducted research methods.

Table 3: Numerical scaled value for pairwise comparison [25].

Scale	Degree of preference	Explanation
1	Equal importance	Contribution to the objective is equal
3	Moderate importance	The attribute is slightly favored over another

5	Strong importance	The attribute is strongly favored over another
7	Very strong importance	The attribute is very strongly favored over another
9	Extreme importance	Evidence favoring one attribute is of the highest possible order of affirmation
2,4,6,8	Intermediate values	When compromise is needed

A comparison matrix like Table (2) is then constructed with the results of the preferred intensity evaluation and the values are compared accordingly to solve the principal eigenvalue λ therefore, the total information value in a grid cell j is computed using (Eq. 2)

$$\lambda_* = \sum_{i,j=1}^{n} C_i \, v_j \qquad \text{(Eq. 2)}$$

Where λ_* is the matrix values of compatibility vectors obtained from the sum of the multiplication between each specific vector element and the normalized relative weight considered parameters; C_i is the normalized weight of I Criterion; v_j is the standardized score of j Criterion; i and j are consecutive digit numbers (1, 2, 3…n) [26].

An important condition in a hierarchical decision-making problem is to avoid inconsistencies that should be avoided in the decision-making process using the AHP method. Despite this inconsistency should not exceed a certain threshold that defines as (Eq.3) [27].

$$CR = \frac{C\,I}{RI} \qquad \text{(Eq .3)}$$

Where CR is the consistency Ratio; CI is the consistency Index which obtains from (Eq.4).and RI is the Random consistency index that depends on the degree of comparison matrix and is obtained from the table (4).

$$CI = \frac{\lambda_{max} - n}{n - 1} \qquad \text{(Eq. 4)}$$

Table 4: Degree of matrixes-based incontinency ratio determination [24].

n	2	3	4	5	6	7	8	9	10
RI	0	0.58	0.9	1.12	1.24	1.32	1.41	1.45	1.51

The Consistency Index will be equal to the number of comparisons considered (n), so the CI will be equal to zero to ensure the compatibility ratio (CR) ensures that the original preferential ratings are consistent. In calculating CI, the normalized relative weights and the normalized principal vector, and the principal specific value (λ) is first calculated. λ is simply the mean of the eigenvalues of the comparison matrix [28]. According to [29].The Nature of AHP is a solution to an eigenvalue problem that involves cross-matrix comparisons.

The above processes are run to extract prioritizing values for each factor this method can be summarized in the main steps as follows:

1. Problem recognition for decision
2. Creating a hierarchical structure of the problem at the three levels of purpose, criteria, and options.
3. Perform pairwise comparisons between criteria using the intensity scale and determine the weight of the criteria in order.
4. Calculate the maximum specific weight, compatibility ratio, and normalized values for each criterion/alternative.
5. For an unacceptable CR value, i.e. > 0.10, the comparison must repeat his judgment in pairwise comparisons until the CR value is at an acceptable level [30].
6. Defining the weighted value of each class suitably, and running conclusive formula of module like (Eq.5)

AHP gained its importance, especially in decision-making, due to its interactive graphical user interfaces, automatic calculation of priorities and variables, and sensitivity analysis [31]. Perhaps one of its main advantages is that it provides the ability to measure the consistency of decision-makers preferences and to manipulate quantitative and qualitative criteria [32]. However, the final decision made using the AHP method is based on subjective assessments, especially during pairwise comparisons [33]. In this manner rock fall and landslide susceptibility map (LSM) was finalized by the use of all already weighed criteria and sub-criteria in (Eq.5)

$$LSM = \sum_{i=1}^{n} R_i \times W_i \qquad \text{(Eq. 5)}$$

Where R_i is the rating score of each layer and W_i is the weights for each of the landslide conditioning factors [34].

These observations are confirmed by [35] that decision-makers in any decision problem can be subjective and uncertain about their level of priority, mainly due to

incomplete and uncertain knowledge or information in the decision environment. Therefore, their preferences are subjective and their choices are influenced by sufficient information. In addition, in a decision-making process [36] described the term “mental uncertainty" as scientific ignorance, measurement uncertainty, inability to verify or observe, censorship, or other knowledge deficiencies.

4.2.Weighted Overlay Mapping (WOM) Method

The weighted overlay mapping (WOM) method is a simple and direct tool of Arc GIS to produce a susceptibility map [37, 38]. Many researchers used WOM to produce landslide susceptibility maps [39,40,41]. We used an overlay of raster layers of all controlling factors to prepare a susceptibility map. Raster layers of each controlling factor were reclassified and weighted according to their importance determined by AHP (Table 2 & 5). The cumulative weight of all 9 inputting layers was maintained at a total of 100. All layers were combined by using a weighted overlay tool based on the following (Eq.5).

$$S = \sum W_i S_{ij} / \sum W_i \qquad \text{(Eq. 6)}$$

Where W_i is the weight of the i^{th} factor, S_{ij} represents the subclass weight of the j^{th} factor and S is the spatial unit of the final map. The completion of this process resulted in the ultimate production of a landslide susceptibility map of the Highway (Fig. 4a).

Factors	Classes	Caparison matrix						Weight
		Class_1	Class_2	Class_3	Class_4	Class_5	Class_6	
Lithology	Class_1	1	1/2	1/4	1/4	1/9	1/9	0.033
	Class_2	2	1	1/2	1/3	1/4	1/3	0.069
	Class_3	4	2	1	1/3	1/3	1/3	0.102
	Class_4	4	3	3	1	1/2	1/3	0.172
	Class_5	9	4	3	2	1	1/2	0.268
	Class_6	9	3	3	3	2	1	0.356
CR = 0.037								
		0-15	15-30	30-45	45-60	>60		
Slope	0-15	1	1/3	1/4	1/7	1/9		0.040
	15-30	3	1	1/2	1/3	1/4		0.099
	30-45	4	2	1	1/2	1/2		0.173
	45-60	7	3	2	1	1/2		0.278
	>60	9	4	2	2	1		0.409
CR = 0.011								
		Class_L1	Class_L2	Class_L3	Class_L4	Class_L5		
Landover	Class_L1	1	1/3	1/2	1/6	1/9		0.045
	Class_L2	3	1	1/2	1/2	1/4		0.104
	Class_L3	2	2	1	1/2	1/7		0.117
	Class_L4	6	2	2	1	1/2		0.231
	Class_L5	9	4	7	2	1		0.503
CR = 0.038								
		<590	590-620	620-660	>660			
Precipitation	<590	1	1/3	1/3	1/5			0.078
	590-620	3	1	1/3	1/3			0.156
	620-660	3	3	1	1/2			0.299
	>660	5	3	2	1			0.466
CR = 0.049								
		Concave	Plat area	Convex				
Curvatures	Concave	1	2	1				0.376
	Plat area	1/2	1	1/4				0.149
	Convex	1	4	1				0.474
CR = 0.046								

.... Continued of table 5.

		<500m	500m-1000m	1000m-1500m	1500m-2000m	>2000m	Weight
Fault distances	<500m	1	6	2	4	9	0.517
	500m-1000m	1/6	1	2	2	2	0.167
	1000m-1500m	1/2	1/2	1	2	3	0.164
	1500m-2000m	1/4	1/2	1/2	1	2	0.095
	>2000m	1/9	1/2	1/3	1/2	1	0.057
CR = 0.065							
		<10	10-15	15-20	>20		Weight
TWI	<10	1	1/3	1/3	1/4		0.090
	10/15/2022	3	1	1/2	1/2		0.204
	15-20	3	2	1	1		0.342
	>20	4	2	1	1		0.364
CR = 0.017							
		<150	150m-300m	300m-450m	450m-600m	>600m	Weight
Road distances	<150	1	2	4	5	3	0.402
	150m-300m	1/2	1	3	6	6	0.326
	300m-450m	1/4	1/3	1	3	3	0.140
	450m-600m	1/5	1/6	1/3	1	2	0.070
	>600m	1/3	1/6	1/3	1/2	1	0.062
CR = 0.077							
		Plate Area	North	South	West	East	Weight
Aspects	Plate Area	1	1/6	1/3	1/3	1/9	0.048
	North	6	1	2	3	2	0.369
	South	3	1/2	1	2	2	0.239
	West	3	1/3	1/2	1	1/2	0.117
	East	9	1/2	1/2	2	1	0.228
CR = 0.06							

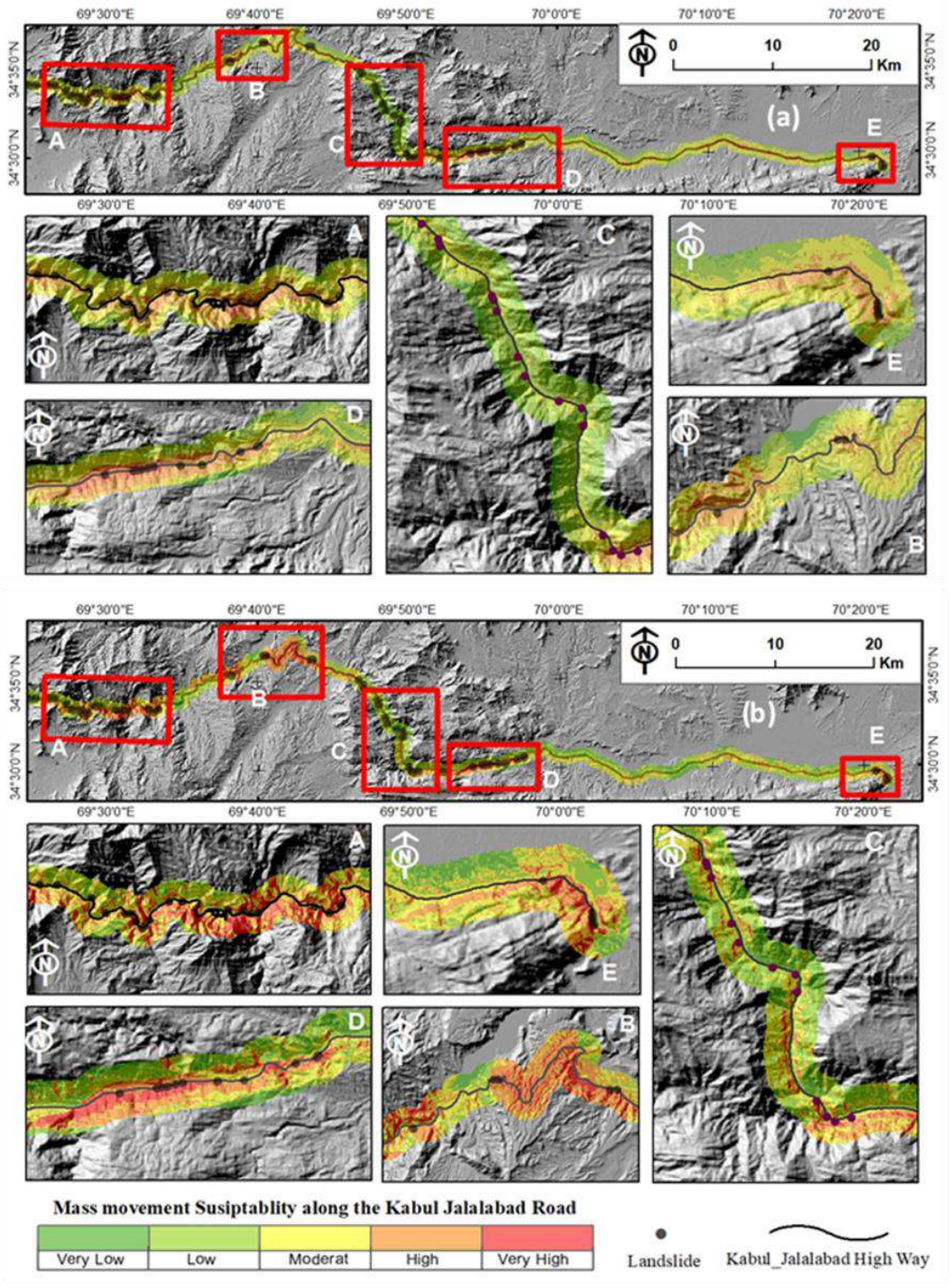

Fig. 4: Rockfall and landslide susceptibility map of Kabul –Jalalabad road; the (a) weight of Overly Mapping (WOM), (b) Analytic hierarchy process (AHP) method approaches.

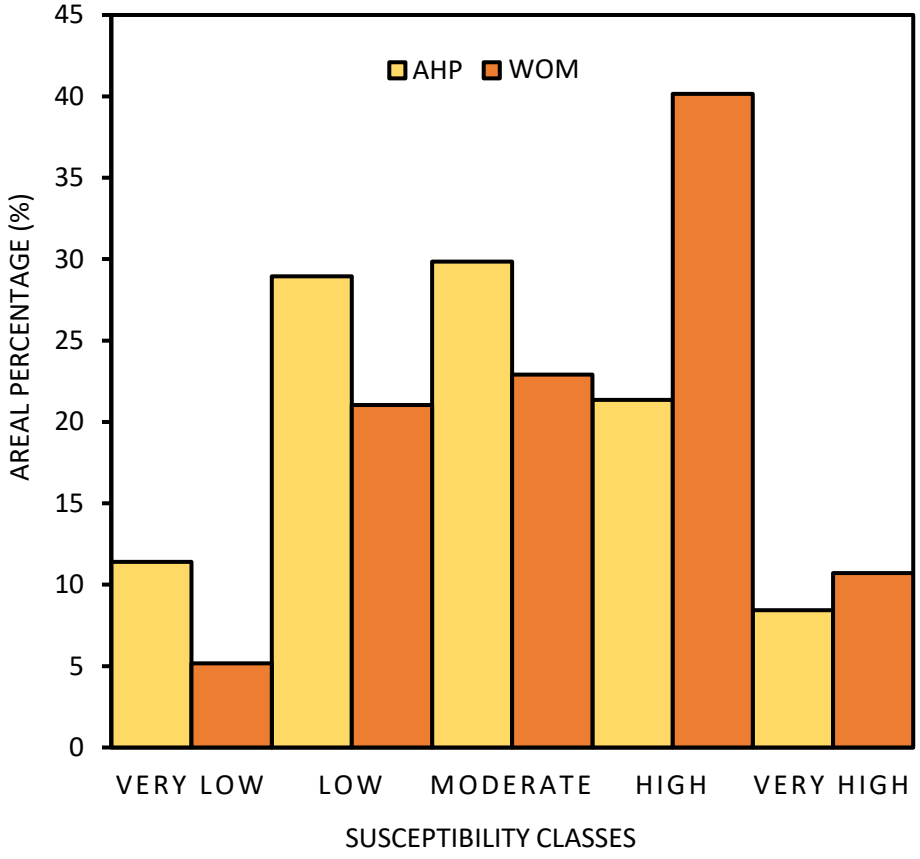

Fig. 5: Areal percentage of rock fall and landslide susceptibility for Kabul –Jalalabad road.

5. Evaluation of research results

Accuracy evaluation of natural disaster susceptibility mapping is one of the basic steps in assessing the susceptibility of the module that overlaps with the landslide sensitivity map and its distribution in this cause receiver operating characteristic curve (ROC) is used to evaluate and compare the accuracy of results. Because of the non-influence rule landslides occurred Rock falls which were detected by different methods mentioned in the methodology were denoted around 101 points of landslide and rock fall evidence all across the studied portion of Kabul-Jalalabad highway as a consequence of filed observation and Google Earth traces. The receiver operating characteristic (ROC) curve is one of the most desirable tools for graphically assessing the accuracy of classifiers for rock fall and landslide susceptibility zoning [42]. In addition, the area under the curve (AUC) index indicates the precision of classifiers, it is quantitative values vary from 0 to 1, that (0.9-1) is excellent, (0.9 - 0.8) very good, (0.8-0.7) good, (0.7 - 0.6) average and

(0.6 - 0.5) is weak [43].The closer area under the curve to 1, represents the best accuracy of classifiers. After finalizing the susceptibility map of methods characterized the accuracy of either and (AUC) index values gain in Microsoft Excel that shows 0.923 and 0.845 for AHP and WOM respectively with graphical representation in (Fig.6)

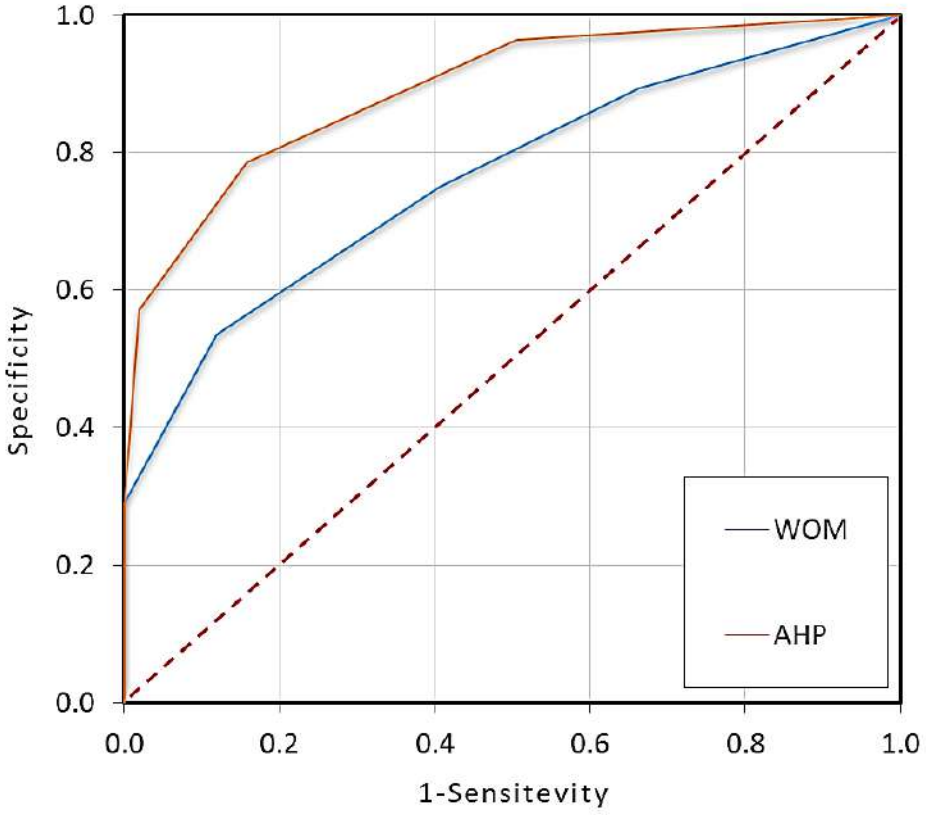

Fig. 6: Graphical Represent of methods accuracy assessment by (ROC) curve.

6. Discussion and results

Respectively after applying (Eq.5 &.6) landslide susceptibility of the area obtained for both studying methods of studying as a form of susceptibility maps which is known as a good tool for recognition of areas prone to landslides of rock fall, these maps are also known as a good source of information in the management of natural disasters like issues titled in this study. Landslide susceptibility zoning maps also show the spatial distribution that confirms all the factors involved in the potential risk of landslides and rock fall. However, this map is not able to predict the amount of displacing materials and its exact time. Nevertheless, predictive models can be valued for regional planning for landslide risk reduction and prevention assistance [44,45]. In this study to Clarify the relationship

between landslide impact factors and their influence role after a Specialistic in judgments and pair wised comparison for main and sub-criteria shown in table (2, 5) weight of all Criteria and their relevant classes vary from (0.033 of lithology's Class_1 to 0.517 of Fault distances <500m Class), Slope, lithology, slope aspects, precipitation, fault distances, and land cover defined as a most influenced factor with 0.276,0.191, 0.181,0.106,0.069 and 0.056 influence weight respectively. The influence weight of slope classes increases continually with an increase of slope gradient then the highs value of slope class is obtained for >60 degrees, and the high value of influence weight of lithology is defined for Class_6 which is shown in table (5) contains Conglomerate, shingly sediments, gravel, sand, siltstone, breccia, limestone, gypsum, clay, loam; andesite, decide and their tuffs, and For aspect classes, North, south, and east has more high values than others as shown in table (5). The AHP module was finalized by defining the main Criteria values as an implication of (Eq.5), which define in expanded form in (Eq.7) Susceptibility map of both methods (AHP and WOM) classified into five Sensitivity and susceptibility levels as (Very low, Low, Medium, High and very high) that frequency of all zones for both methods are represented in (Fig .5), High and very high levels sensitivity zones Covers 21.35%, 8.43% for AHP and 40.16%, 10.72% for WOM respectively. Both methods related (LSM) shows five regions as much more susceptible than another area along the Kabul Jalalabad road and similarly has a high correlation with occurred Landslide and rock fall detected point, which indicates the rational accuracy of methods that five areas recognized with high, slope, positive relief and much weathered and sensitive Rock types. landslide susceptibility map (LSM) of (WOM) produced by the user of (Eq.6) and as shown in (Fig.4a) and areal percentage of each one shown in (Fig.5), which shows many similarities for Very Low, Low and Very High zone of susceptibility With (AHP), that means this method has more relatively high uncertainty than (AHP) modules, because of un running pairwise comparison to priorities all influencing factors. to evaluate the accuracy of each classifier receiver operating Characteristic (ROC) curve and AUC index used to assess the precision of each module Finally AHP module is known as a much better tool than (WOM) one because of their (AUC) value which shows 0.923 for (AHP) that is greater than 0.845 (AUC) of (WOM) module and specified in Excellent and very good Classes respectively. AHP module this ability of prediction is known as high-level experiment judgments between Criteria and their relevant classes, which depends on the level of experts' applicable experience and knowledge to comparing judgments.

$$LSM = 0.867 * X1 + 0.269 * X2 + 0.059 * X3 + 0.104 * X4 + 0.071 * X5 + 0.054 * X6 + 0.030 * X7 + 0.042 * X8 + 0.181 * X9 \quad \text{(Eq.7)}$$

7. Conclusion

This study is based on the probabilistic method as analytic Hierarchy processed (AHP) and weighted overly mapping (WOM). AHP is one of the hierarchy comparison influences of parameters and their prioritizing method for zoning the risk of landslides and other natural disasters, which has recently been used widely by researchers in various parts of the world and denoted with high interest by many researchers. advantages of this method are the use of a small amount of information (influence factors), spatial independence of information in estimating the weight of each factor (variable) on the occurrence of landslides; Non-generalizability, uniqueness of the event, the accuracy of preconditioned information on pre-existing landslides and inflexibility in small geographical constraints are the main disadvantages of the method. Weight of the event; Understanding the factors contributing to landslides is very complex and sometimes unconventional, while the underlying factors contributing to landslides can be identified even in field visits to aerial photography facilities, in which case some factors are neglected to be. Also, in this research, the weighted overlay mapping (WOM) method is used to increase the accuracy of the final results to detect the most susceptible locations, accordingly, the final similarity between the results of these two methods that have a close relation to that. Occurred landslides events distribution and more sensitive influence Factors, the factors affecting the occurrence of Rockfall and landslides in Kabul-Jalalabad road in this research by considering (9) criteria and their thematic maps were provided by the use of ArcGIS10.8 facilities. This study shows about the 5 portions of the road has high association and spatial coordination for rock fall and landslide susceptibility. Spatial distribution of high and very high sensitivity for the AHP method from very high and high potential is (8.43%) and (21.36%) of the study area, respectively, which shows (10.72%) and (40.16%) in WOM; both of these methods have a close relationship between more susceptible area and invented points of Rockfall and landslides. Slope changes, lithological varieties, annual average precipitation, and slope aspect were determined as the most effective factors.

The accuracy of approaches comparatively Assessed by the use of ROC curves shows that AHP is much more valid because of its high (0.923) value of the (AUC) index than the (0.845) of the WOM method.

References

[1] Anbalagan, R. (1992). Landslide hazard evaluation and zonation mapping in mountainous terrain. *Engineering geology*, *32*(4), 269-277.

[2] Bachri, S., Shrestha, R. P., Yulianto, F., Sumarmi, S., Utomo, K. S. B., & Aldianto, Y. E. (2020). Mapping landform and landslide susceptibility using remote sensing, gis, and field observation in the southern crossroad, Malang regency, *East Java, Indonesia. Geosciences*, 11(1), 4.

[3] Basharat, M., Shah, H. R., & Hameed, N. (2016). Landslide susceptibility mapping using GIS and weighted overlay method: a case study from NW Himalayas, Pakistan. *Arabian Journal of Geosciences*, 9(4), 1-19.

[4] Baeza, C., & Corominas, J. (2001). Assessment of shallow landslide susceptibility through multivariate statistical techniques. *Earth Surface Processes and Landforms: The Journal of the British Geomorphological Research Group*, *26*(12), 1251-1263.

[5] Beven, K. J., & Kirkby, M. J. (1979). A physically based, variable contributing area model of basin hydrology/Un modèle à base physique de zone d'appel variable de l'hydrologie du bassin versant. *Hydrological sciences journal*, *24*(1), 43-69.

[6] Chabuk, A., Al-Ansari, N., Hussain, H. M., Knutsson, S., Pusch, R., & Laue, J. (2017). Combining GIS applications and multi-criteria decision-making (AHP) method for landfill siting in Al-Hashimiyah Qadhaa, Babylon, Iraq. *Sustainability*, *9*(11), 1932.

[7] Chowdhuri, I., Pal, S. C., Arabameri, A., Ngo, P. T. T., Chakrabortty, R., Malik, S., ... & Roy, P. (2020). An ensemble approach to developing landslide susceptibility map in landslide dominated Sikkim Himalayan region, India. *Environmental Earth Sciences*, *79*(20), 1-28.

[8] Emami, S. N., Yousefi, S., Pourghasemi, H. R., Tavangar, S., & Santosh, M. (2020). A comparative study on machine learning modeling for mass movement susceptibility mapping (a case study of Iran). *Bulletin of Engineering Geology and the Environment*, *79*(10), 5291-5308.

[9] Das, G., & Lepcha, K. (2019). Application of logistic regression (LR) and frequency ratio (FR) models for landslide susceptibility mapping in Relli Khola river basin of Darjeeling Himalaya, India. *SN Applied Sciences*, 1(11), 1-22.

[10] Dou, J., Tien Bui, D., P. Yunus, A., Jia, K., Song, X., Revhaug, I., ... & Zhu, Z. (2015). Optimization of causative factors for landslide susceptibility evaluation using remote sensing and GIS data in parts of Niigata, Japan. *PloS one*, *10*(7), e0133262.

[11] Gigović, L., Pamučar, D., Božanić, D., & Ljubojević, S. (2017). Application of the GIS-DANP-MABAC multi-criteria model for selecting the location of wind farms: A case study of Vojvodina, Serbia. *Renewable energy*, *103*, 501-521.

[12] Conoscenti, C., Ciaccio, M., Caraballo-Arias, N. A., Gómez-Gutiérrez, Á., Rotigliano, E., & Agnesi, V. (2015). Assessment of susceptibility to earth-flow landslide using logistic regression and multivariate adaptive regression splines: a case of the Belice River basin (western Sicily, Italy). *Geomorphology*, *242*, 49-64.

[13] Hosseini, S.A., Lotfi, R., Lotfalian, M., Karina, A., Parsakhoo, A. (2011). The effects of terrain factors on landslide features along a forest road. *African Journal of Biotechnology*, 10(64): 14108-14115.

[14] Intarawichian, N., & Dasananda, S. (2010). Analytical hierarchy process for landslide susceptibility mapping in lower mae chaem watershed, northern Thailand. *Suranaree journal of science & technology*, 17(3).

[15] Kayastha P, Dhital MR, De Smedt F (2013) Application of the analytical hierarchy process (AHP) for landslide susceptibility mapping: a case study from the Tinau watershed, west Nepal. *Comput Geosci* 52: 398–408

[16] Kulkarni, J. R., Kulkarni, S. S., Inamdar, M. U., Tamhankar, N. M., Waghmare, S. B., Thombare, K. R., ... & Kumar, V. (2022). "Satark": Landslide Prediction System over Western Ghats of India. *Land*, *11*(5), 689.

[17] Lee, G. K., & Chan, E. H. (2008). The analytic hierarchy process (AHP) approach for assessment of urban renewal proposals. *Social indicators research*, *89*(1), 155-168.

[18] Lee, S. and J. Choi. 2004. Landslide susceptibility mapping using GIS and the weight-of-evidence model. Intl. J. Geograph. Inform. Sci. 18(8): 789-814.

[19] Maharaj, R. J. (1993). Landslide processes and landslide susceptibility analysis from an upland watershed: a case study from St. Andrew, Jamaica, West Indies. *Engineering Geology*, *34*(1-2), 53-79.

[20] Mallick, J., Singh, R. K., AlAwadh, M. A., Islam, S., Khan, R. A., & Qureshi, M. N. (2018). GIS-based landslide susceptibility evaluation using fuzzy-AHP multi-criteria decision-making techniques in the Abha Watershed, Saudi Arabia. *Environmental Earth Sciences*, *77*(7), 1-25.

[21] Nyeko, M. (2012). GIS and multi-criteria decision analysis for land use resource planning.

[22] Juliev, M., Mergili, M., Mondal, I., Nurtaev, B., Pulatov, A., & Hübl, J. (2019). Comparative analysis of statistical methods for landslide susceptibility mapping in the Bostanlik District, Uzbekistan. *Science of the total environment*, *653*, 801-814.

[23] Neuhäuser B, Terhorst B (2007) Landslide susceptibility assessment using Bweights-of-evidence^ applied to a study area at the Jurassic escarpment (SW-Germany). *Geomorphology 86(1)*:12–24

[24] Nyeko, M. (2012). GIS and multi-criteria decision analysis for land use resource *planning*.

[25] Oh, H. J., & Pradhan, B. (2011). Application of a neuro-fuzzy model to landslide-susceptibility mapping for shallow landslides in a tropical hilly area. *Computers & geosciences, 37(9)*, 1264-1276.

[26] Pradhan, B. and S. Lee. 2010. Landslide susceptibility assessment and factor effect analysis: backpropagation artificial neural networks and their comparison with frequency ratio and bivariate logistic regression modeling. *Environmental Modeling and Software 25(6)*: 747-759.

[27] Pourghasemi, H. R., M. Mohammady and B. Pradhan. 2012a. Landslide susceptibility mapping using the index of entropy and conditional probability models in GIS: Safarood Basin, Iran, *Catena*. 97: 71–84.

[28] Pourghasemi H. R., B. Pradhan, C. Gokceoglu and K. Deylami Moezzi. 2012b. A comparative assessment of prediction capabilities of Dempster-Shafer and weights-of-evidence models in landslide susceptibility mapping using GIS. Geomatics, *Natural Hazards, and Risk*. doi:10.1080/19475705.2012.662915.

[29] Pourghasemi, H. R., Pradhan, B., & Gokceoglu, C. (2012). Application of fuzzy logic and analytical hierarchy process (AHP) to landslide susceptibility mapping at Haraz watershed, Iran. *Natural hazards*, *63*(2), 965-996.

[30] Poudyal CP, Chang C, Oh HJ, Lee S (2010) Landslide susceptibility maps comparing frequency ratio and artificial neural networks: a case study from the Nepal Himalaya. Environ Earth Sci 61(5):1049– 1064

[31] Radhan B, Lee S (2010) Delineation of landslide hazard areas on Penang Island, Malaysia, by using frequency ratio, logistic regression, and artificial neural network models. *Environ Earth Sci 60(5):*1037– 1054

[32] Regmi, N. R., J. R. Giardino and J. D. Vitek. 2010. Modeling susceptibility to landslides using the weight of evidence approach: Western Colorado, USA, *Geomorphology 115*: 172-187.

[33] Razandi, Y., Pourghasemi, H. R., Neisani, N. S., & Rahmati, O. (2015). Application of analytical hierarchy process, frequency ratio, and certainty factor models for groundwater potential mapping using GIS. *Earth Science Informatics*, *8*(4), 867-883.

[34] Rotigliano, E., Agnesi, V., Cappadonia, C., & Conoscenti, C. (2011). The role of the diagnostic areas in the assessment of landslide susceptibility models: a test in the Sicilian chain. *Natural hazards*, *58*(3), 981-999.

[35] Saaty, T. L. (1980). The Analytic Hierarchy Process Mcgraw Hill, New York. *Agricultural Economics Review*, *70*.

[36] Saaty, T. L., & Vargas, L. G. (1991). *Prediction, projection, and forecasting: applications of the analytic hierarchy process in economics, finance, politics, games and sports* (pp. 11-31). Boston: Kluwer Academic Publishers.

[37] Saaty, T. L. (2008). Decision-making with the analytic hierarchy process. *International journal of services sciences*, *1*(1), 83-98.

[38] Sharir, K., Roslee, R., Ern, L. K., & Simon, N. (2017). Landslide Factors and susceptibility mapping on natural and artificial slopes in Kundasang, Sabah. *Sains Malaysiana*, 46(9), 1531-1540.

[39] Sharir, K., Rodeano, R., & Mariappan, S. (2019, November). Flood Susceptibility Analysis (FSA) Using Analytical Hierarchy Process (AHP) Model at The Kg. Kolopis area, Penampang, Sabah, Malaysia. In *Journal of Physics: Conference Series* (Vol. 1358, No. 1, p. 012065). IOP Publishing.

[40] Shit, P. K., Bhunia, G. S., & Maiti, R. (2016). Potential landslide susceptibility mapping using weighted overlay model (WOM). *Modeling Earth Systems and Environment*, 2(1), 1-10.

[41] Song, W., Ming, X., & Wu, Z. (2013). An integrated rough number-based approach to design concept evaluation under subjective environments. *Journal of Engineering Design*, *24*(5), 320-341.

[42] Silalahi, F. E. S., Arifianti, Y., & Hidayat, F. (2019). Landslide susceptibility assessment using frequency ratio model in Bogor, West Java, Indonesia. *Geoscience Letters*, 6(1), 1-17.

[43] Sweets, J. A. 1988. Measuring the accuracy of diagnostic systems Science 240: 1285-1293.

[44] Umar, Z., Pradhan, B., Ahmad, A., Jebur, M. N., & Tehrany, M. S. (2014). Earthquake-induced landslide susceptibility mapping using an integrated ensemble frequency ratio and logistic regression models in West Sumatera Province, Indonesia. *Catena*, *118*, 124-135.

[45] Van Western, C. J. 2002. Use of weights of evidence modeling for landslide susceptibility mapping 1-21.

Authors Profile:

Khairuddin Rasikh received his BSc. Degree in Geology and Earth Science from Kabul University in 2015 and 2018,he completed his MSc. degree in Geology and Mine Exploration Engineering from Kabul Polytechnic University. Currently, He is working as a teaching assistant in the Department of Geology and Mine at Nangarhar University, Daronta Afghanistan. His area of interest includes remote sensing and field observational Base study of slope Failures and Geological structures.

Zafar Khan Saeedi has gote his BSc. Degree in Oil and Gas from the Engineering Department of Kabul Polytechnic University in 2014 and 2018, he completed his MSc. degree in Geology and Mine Exploration Engineering from Kabul Polytechnic University. Currently, He is working as a teaching assistant in the Department of Geology and Mine Department at Nangarhar University, Daronta Afghanistan. His field of interest is the Geochronological study of carbonatic sedimentary formations.

VISIT US AT: KPU Campus, 5th District, Kabul City, Afghanistan.
www.kpu-ijet.af AND www.kpu-ijet.com

Submit your article @ ijet@kpu.edu.af / kpuijet2@gmail.com